Fluid evolution and characterisation of mineralising solutions in the Central African Copperbelt

Lynnette Natasha Greyling

School of Geosciences
University of the Witwatersrand

Thesis submitted to the Faculty of Science, University of the Witwatersrand, Johannesburg, South Africa, in fulfilment of the requirements of the Degree of Doctor of Philosophy in Science.

Johannesburg, 2009

Declaration

I declare that this research is my own work. It is being submitted for the degree of Doctor of Philosophy in the University of the Witwatersrand, Johannesburg, South Africa. It has not been submitted before for any degree or examination in any other University.

Lynnette Natasha Greyling

---------- day of ---------- 2009

Abstract

The reconstruction of the fluid evolution of the Zambian Copperbelt is presented, where extensive stratiform copper-cobalt mineralisation is hosted in the metasediments of the Katanga Supergroup located in the Lufilian Arc in the Democratic Republic of the Congo and Zambia. Fluid inclusions are characterised from three different tectonic settings at selected deposits within the Zambian Copperbelt in terms of basinal, early orogenic, and late orogenic settings.

Fluid inclusion microthermometry, Raman microspectroscopy, laser ablation inductively coupled plasma mass spectrometry, and stable isotope analysis are used to investigate the nature of basinal, early orogenic, and late orogenic fluids.

NaCl-$CaCl_2$, $MgCl_2$-KCl brines are found to have circulated the sedimentary pile immediately after stratiform copper mineralisation and are the earliest fluids documented from the Copperbelt. $MgCl_2$-KCl brines were also trapped together with CO_2-CH_4-N_2 fluids during these times. Basinal fluids were trapped under minimum pressure temperature conditions of 350 bar and 120°C.

Four distinct early orogenic fluids are found at the Chambishi, Nchanga, and Nkana deposits and consist of NaCl-$CaCl_2$-$MgCl_2$-KCl, $CaCl_2$-KCl, NaCl-CO_2-CH_4-N_2, and pure carbonic fluids. It is seen that these fluids at pressures of 550-800 bar and temperatures of 153-260°C which corresponds to depths of ~5.6-8.2 km.

Late orogenic fluids from the Mufulira and Nkana deposits are the hottest and most complex fluids documented during this study and contain mixtures of hypersaline NaCl-$CaCl_2$-$MgCl_2$ ± KCl and NaCl-$CaCO_3$-saturated ±N_2 brines. Fluids were trapped at minimum temperatures of 240°C and 1750 bar pressure. In addition to these fluids, a low salinity $CaCl_2$-$MgCl_2$-CO_2-CH_4 fluid is also present during late orogenesis. Minimum depth estimates for late orogenic fluids are around 6.61 km. The highest salinities of all three fluid types are found within these late orogenic fluids in addition to the highest levels of Pb, Zn, Cu, Co and Sr. This indicates the prolonged presence and equilibration of these fluids with the host rock. Moreover, late orogenic fluids are also more oxidised compared to relatively more reduced basinal fluids.

A key to the widespread and paragenetically complex nature of the Copperbelt ores may be related to the longevity of fluid flow and the progressive ability of fluids to transport metals. The marked increase in Pb and Zn in later fluids may be relevant to the formation of regional epigenetic Pb-Zn deposits further afield of the Copperbelt, such as

at Kabwe and Kipushi. The late orogenic fluids seen in the Copperbelt compare favourably with mineralising fluids of the epigenetic Pb-Zn Kabwe deposit in terms of metal composition, temperature and moderate salinities.

It is envisaged that early stratiform mineralisation is followed by continuing fluid circulation in the basin whereby metals are scavenged by hotter fluids which continue to act as mineralising agents.

Acknowledgements

The National Research Foundation of South Africa provided funding for this research, and is thanked together with the School of Geosciences at the University of the Witwatersrand, the Centre National de la Recherche Scientifique, the French Embassy in South Africa and the Hugh E. McKinstry Student Research Award from the Society of Economic Geologists Foundation.

My supervisors at Wits University, Laurence Robb, Yong Yao and Sharad Master are thanked for their support, patience, encouragement and guidance. A special note of thanks goes to Laurence whose involvement is greatly appreciated. Marie-Christine Boiron and Michel Cathelineau are thanked for their great hospitality and direction during my time in France. Thérèse Lhomme performed the Raman analysis at the UMR7566, G2R, Université de Henri Poincaré, Nancy, France. Initial Raman microspectroscopy was conducted at the Department of Physics, Wits University. Thank you very much to David Banks at Leeds University for help with the laser ablation analysis, and for finding time to encourage. Linda Forbes is also thanked for her help with the laser ablation analysis. Chris Harris and Jodie Miller are thanked for facilitating the stable isotope analysis at the University of Cape Town. Jan-Marten Huizenga is thanked for constructive suggestions.

Non-Ferrous Metal Plc is thanked for access to the Chambishi open pit, and Konkola Copper Mines Plc for access to the Nchanga and Konkola mines. Mopani Copper Mines is thanked for allowing access to the Mufulira underground and Nkana drill core. Julian Verbeek is thanked for his hospitality during my second field trip based in Chingola, and Mr. Chakraborty at Mufulira mine.

The staff and students at the Department of Geology at Wits University and the Economic Geology Research Institute are thanked, especially Carl Anhauesser for reminding me that the end is near, Judith Kinnaird, Dalena Blithenthall, Safia Cannell, Matt Kitching. Christine Rainaud for being a great friend, Robyn Pickering (for friendship, sushi and coffee), Charlie Seabrook, Louise Coney, Cristiano Lana and Paula Ogilvie.

Cécile Fabre, Audrey Jeanningros, Nicolas Jacquemet, Donatienne Derome, Yacouba Coulibaly, Laurent Richard and Charlotte Mear are thanked for great times in France.

I thank my family and friends for their continuous support, especially the Millsons for their interest. My mom, Letitia and Chris are thanked for their unwavering encouragement, together with Chris Millson for his proof reading, support and patience.

TABLE OF CONTENTS

LIST OF FIGURES

LIST OF TABLES

LIST OF ABBREVIATIONS

aq	aqueous
bn	bornite
BSSL	Banded Sandstone Lower (Nchanga)
BSSU	Banded Sandstone Upper (Nchanga)
BSS	Banded Sandstone (Nchanga)
CAC	Central African Copperbelt
car	carbonic
ccp	chalcopyrite
CL	cathodoluminescence
clath	clathrate
DRC	Democratic Republic of the Congo
FIPs	fluid inclusion planes
IOB	Intermediate Orebody (Nchanga)
l/liq	the liquid phase in a fluid inclusion
LA-ICP-MS	laser ablation inductively coupled plasma mass spectrometry
LBS	Lower Banded Shale (Nchanga)
LOB	Lower Orebody (Nchanga)
NOP	Nchanga open pit
PQ	Pink Quartzite (Nchanga)
py	pyrite
s	the solid phase in a fluid inclusion, including daughter minerals
SM	Shale Marker (Nchanga)
SOB	South Orebody (Nkana)
SSC	sediment-hosted stratiform copper (deposits)
Td	temperature of decrepitation
Te	eutectic point; temperature of initial melting
TFQ	The Feldspathic Quartzite (Nchanga)
$ThCO_2$	temperature of CO_2 homogenisation
Tht	temperature of final homogenisation
Tm	final melting temperature; marked by the dissolution of a solid phase
Tmclath	temperature of clathrate melting, normally given as a range
Tmhalite	temperature of melting of halite
Tmhh	temperature of melting of hydrohalite
v	the vapour phase in a fluid inclusion
UBS	Upper Banded Shale (Nchanga)
UOB	Upper Orebody (Nchanga)
ZCCM	Zambian Consolidated Copper Mines

Chapter 1

INTRODUCTION

1.1 Locality

The sediment-hosted stratiform copper deposits of the Central African Copperbelt extend along the border of Zambia and the Democratic Republic of the Congo (DRC) in an arcuate fold belt, known as the Lufilian Arc (Figure 1.1). The major stratiform copper deposits are found in a region of about 500 km x 50 km along this belt, and are hosted by the metasediments of the Proterozoic Katanga Supergroup.

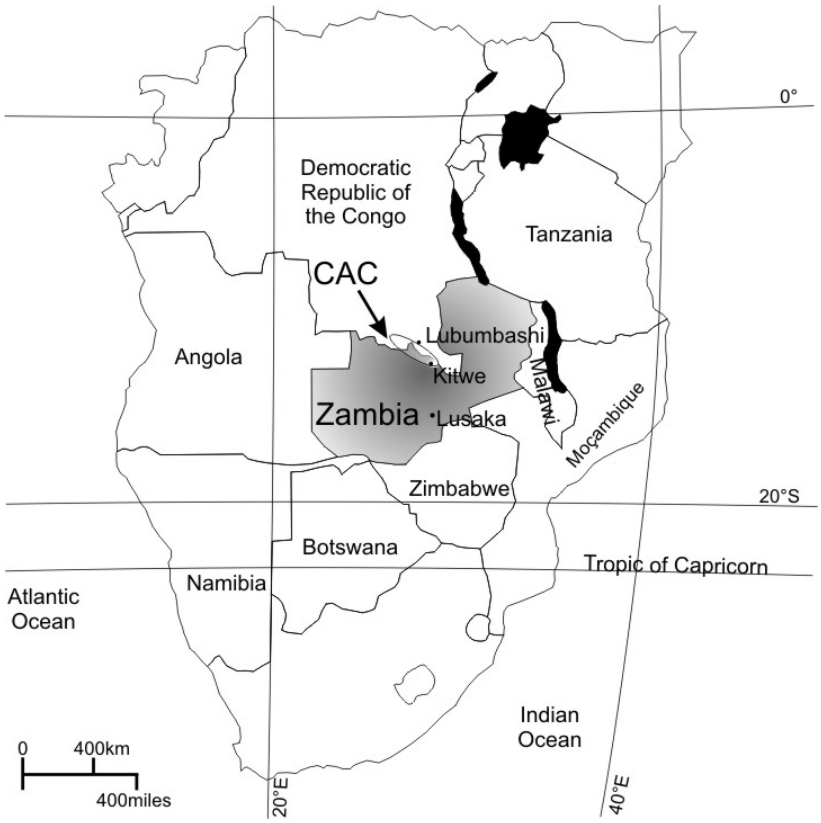

Figure 1.1. Map of Southern- and Central Africa showing the location of the Central African Copperbelt (CAC), situated on the border of the Democratic Republic of Congo and Zambia in the arcuate shape of the Lufilian fold belt. East African rift lakes are indicated by black shading. Azimuthal equal-area projection.

1.2 Motivation

The stratiform ores of the Central African Copperbelt contain about 34% of global cobalt reserves, and more than 10% of global copper reserves (Mbendi, 2005). Zambia supplies 20% cobalt to the world market, making it the second largest global supplier of this metal. Zambia is also the sixth largest producer of copper, of which China currently demands the largest portion of global copper production. Production and reserves of the

Copperbelt in the DRC and Zambia total ~ 190 Mt Cu (Hitzman *et al*., 2005, Selley *et al*., 2005). World copper prices increased to a record-high of US$8,940 a metric ton in July 2008 (I-NET Bridge).

Artisanal mining in the Copperbelt started several centuries before the arrival of Europeans and prospecting commenced in Zambia (then Northern Rhodesia) during the 1890's. Commercial mining started during the 1910's with production at the then Roan Antelope mine (now Luanshya). Several mines currently operate in Zambia and the DRC, and world class deposits include the Bwana Mkubwa, Nchanga, Konkola, and Mufulira occurrences. Moreover, the presence of a variety of epigenetic ores such as the Kansanshi Cu-Au, Lumwana Cu-Co-Au-Ag±U, Shinkolobwe U, Mwezi FeOx-Cu-Au, and Kabwe, Kipushi Zn-Pb-Cu-Ge-Ga deposits within the Katanga metallogenic province illustrates the scale and complexity of mineralisation styles hosted in this region.

Theories on the origin and mechanism of mineralisation of the stratiform deposits have been debated for decades and have ranged from syngenetic (Garlick, 1961a; Sweeney and Binda, 1994) to epigenetic (McGowan *et al*., 2003). Epigenetic stratiform mineralisation, due to the infiltration of magmatic fluids, has been discredited with the discovery of the unconformable relationship of the Katanga Supergroup to the basement (see Chapter 3). Evidence does persist, however, of localized epigenetic occurrences within the Copperbelt, particularly at the Nchanga deposit (McGowan *et al*., 2003). The prevailing generally accepted model currently is that ore genesis is indicated by syngenetic – early diagenetic processes (Cailteux *et al*., 2005a), early- or late diagenetic bacterial reduction of sulphate (Bartholomé *et al*., 1973; Garlick and Fleischer, 1972), and multi-stage diagenetic to early orogenic mineralisation (Selley *et al*., 2005). Recently, Dewaele *et al*., (2006a) indicate a multiphase mineralising Cu-Co system in the western part of the DRC where mineralisation is seen to have started during early diagenesis, continuing after burial. The subsequent enrichment of Cu-Co mineralisation is implicated by crosscutting lineaments (Dewaele *et al*., 2006a).

Fluids have played an important part, not only in the early stratiform mineralisation, but also in the remobilisation thereof, and subsequent epigenetic mineralisation in the Central African Copperbelt. A detailed fluid inclusion study is a means to directly study fluids preserved in certain host minerals both during and after mineralisation. By documenting the *P-T-υ-X* conditions of these fluid inclusions and their relationships to ore minerals, structures and textures, controversies on ore genesis may be better understood. In order to constrain the evolution of palaeo-fluid circulation in the basin-wide mineralisation process, this study investigates the nature (in terms of composition, temperature, and pressure) of various fluid populations from selected deposits in the Zambian Copperbelt.

1.3 Project Objectives

This study investigates the role and character of palaeo-fluid populations preserved in the metasediments of the Zambian Copperbelt by using a dual-scale approach; firstly using a basin-wide scale to regionally classify and compare these fluids by geological mapping and sampling, and secondly to illustrate on a micro-scale the characteristics of fluids at individual deposits involved during stratiform mineralisation, subsequent remobilisation and alteration during deformation. This will be attained by the following:

i. documenting the geological, tectonic, and structural setting of mineralised horizons and the degree of overprinting during regional metamorphism
ii. identifying various fluid inclusion populations representative of different tectonic stages
iii. determining the detailed compositions of fluid inclusions representing each tectonic stage
iv. determining the pressures, temperatures and densities of fluid inclusion groups
v. establishing the link between stratiform mineralisation and fluid inclusions that may record this fluid(s); and fluids present during epigenetic mineralisation
vi. determining the stable oxygen and deuterium isotopic signatures of fluids
vii. determining the palaeo-fluid compositions in terms of trace and major element abundances
viii. comparing the local fluid characteristics for each deposit and placing it in a regional context

Five deposits were selected for this study based on location, mineralisation styles, and metamorphic grades in the Zambian Copperbelt, namely the Chambishi, Nchanga, Nkana, Mufulira and Konkola deposits.

1.4 Layout of the thesis

Chapter 1

The motivation and aim of the study is discussed followed by the layout of the thesis. This chapter also briefly reviews stratiform copper deposits and fluid flow associated with these deposits.

Chapter 2

This chapter illustrates the methodology employed during the course of this study with emphasis on the basic component fluid systems generally found and studied during a fluid inclusion study focused on hydrothermal-sedimentary deposits.

Chapter 3

A look at the regional geological setting is given. Notably, the varying metamorphic grade across the Copperbelt is discussed which impacts directly on the types of fluids associated with individual deposits.

Chapter 4

Detailed geological characteristics of the five individual deposits are documented in terms of geological setting, mineralisation, and the detailed setting of the fluid inclusion samples (related to the regional tectonic framework).

Chapter 5

The P-T-υ-X characteristics of fluids trapped during the early stages of burial stage *prior to the onset of regional deformation* are documented in this chapter from inclusions of the Chambishi, Nchanga, and Konkola deposits. Microthermometry and Raman results are presented.

Chapter 6

Inclusions from the Chambishi, Nchanga, and Nkana, deposits are described as representative of fluids present during the *early stages of basinal deformation*, possibly due to regional compressive metamorphism. The microthermometric and Raman microspectroscopic results are given.

Chapter 7

Fluids trapped during the *peak metamorphism* are documented by microthermometry and Raman microspectroscopy in this chapter, and are recorded from samples of the Nchanga, Nkana, and Mufulira deposits.

Chapter 8

Results of laser ablation inductively coupled plasma mass spectrometry of inclusions documented by microthermometry in the previous three chapters are presented.

Chapter 9

This chapter presents stable oxygen and hydrogen isotope analysis of selected samples of the five deposits, with emphasis on the Chambishi, and Nchanga deposits.

Chapter 10

The results obtained from the fluid inclusion-stable isotope study are discussed and the varying trapping conditions of earlier vs later fluids are discussed.

The appendices to the thesis include relevant raw data, and publications presented during the course of the study, and include details on the microthermometry measurements, Raman microscopic data and laser ablation data.

1.5 Sediment-hosted stratiform copper deposits – a global perspective

Sediment-hosted stratiform copper (SSC) deposits are the world's second largest supplier of copper ore after porphyry copper type deposits, and the world's largest producer of cobalt. Some of these deposits are also known to produce Ag, Au, Pb, Zn, U, and PGEs (Kirkham, 1989; Robb, 2005). Well-known SSC deposits include the Dzhezkazgan region in Kazakhstan, the Kupferschiefer deposits in Poland and Germany, White Pine in Michigan, Spar Lake in Montana, the Dongchuan and Yimen regions in China, and the Central African Copperbelt.

Stratiform copper deposits occur in sequences of oxidised beds, and are generally associated with rift-related environments in intracontinental basins, where oxidation-reduction reactions have controlled metal precipitation (Jowett, 1989; Kirkham, 1989, Brown, 2006, and references therein). The maturation of host beds is an important factor in the genesis of stratiform copper deposits, where host sediments may not have initially been deposited as red beds. The red bed sequence is a product of diagenesis whereby some metals are mobilised during diagenesis (Rose, 1989). As the basinal sediments evolve during diagenesis, the Eh-pH conditions change according to balance reactions (see section below).

These deposits generally consist of disseminated sulphides hosted in anoxic marine or lacustrine sedimentary rocks, immediately overlying typically oxic (red), continental clastic sedimentary rocks. Evaporites are present within the sedimentary sequence, and deposition of the host sediments generally formed within 20-30° N and S of the palaeo-equator in arid and semi-arid regions (Kirkham, 1989). Early deposition of such sequences occurred under oxidizing conditions, or where sediments were rapidly oxygenated immediately after deposition (e.g., during early diagenesis). Subsequent to this early depositional phase, a marine transgression followed, resulting in a more reducing environment, marked by overlying shales, carbonates and evaporites (Jowett, 1989). SSCs may be divided into two subtypes according to Kirkham (1989):

- red-bed type: sulphides are precipitated in localised reduced areas among sediments that were deposited as oxidized continental red-beds in a desert-type environment;
- Kupferschiefer-type: sulphides are precipitated in paralic, anoxic, shallow marine sequences and oxidized red-bed sediments stratigraphically underlie the ore zone.

The method of ore genesis of sediment-hosted stratiform copper deposits has remained a contentious subject. Theories include the syngenetic hypothesis (with sulphide precipitation resulting directly from anoxic seawater), epigenetic hypothesis (late hydrothermal or related to magmatic intrusions), and diagenetic hypothesis – the vast

majority of these deposits are generally viewed as early- or late diagenetic in origin. The process of diagenesis is preferred as the ore-forming mechanism due to evidence which concludes that copper mineralisation predates cementation, occupies original porosity, and the fact that mineralisation is generally conformable within the host rocks. A multi-staged view of mineralisation at the shale-hosted copper White Pine deposit, in Michigan, United States, is also of interest. Mauk *et al*., (1992) proposed that ore formation resulted due to an early expulsion of copper-bearing pore fluid due to compaction of a rifted sequence, followed by additional expulsion during thrust-induced compression (Garven and Raffensperger, 1997).

The sediments in the Zambian Copperbelt have been overprinted during metamorphism to greenschist and amphibolite facies grades, therefore, understanding ore genesis in this area requires the 'removing' of later fabrics. Typically, mineralisation in SSCs is comprised of disseminated, zoned sulphides such as chalcopyrite, bornite, and chalcocite in stratiform horizons. Later, crosscutting veins are also found at some deposits which indicate the remobilisation of early stratiform mineralisation.

1.6 Fluid flow in sediment-hosted copper deposits

The nature of fluids responsible for stratiform copper deposit formation have generally been accepted as oxidised brines capable of transporting metals through oxic red bed sequences (Jowett, 1989). Mineralisation generally occurs when metals are precipitated from solution when encountering anoxic barriers e.g. black shales. Transportation of metals may be in the form of chloride complexes, which maintain metal solubilities at relatively low temperatures (< 100°C; Rose, 1976, 1989). The presence of Na-Ca-Cl fluids have been described for deposits in the Kupferschiefer district in Poland (Jowett, 1989), and Ca-Na-Cl-CO_2 + hydrocarbon-rich fluids of the White Pine deposits (Kelly and Nishioka, 1985).

Brine composition

A simplification of the generation of fluids capable of transporting copper is illustrated in Figure 1.2, which considers the evolution of saline fluids in a closed basin system. According to Jowett (1989), common constituents in saline lakes include Na - CO_3 - Cl-SO_4, Na - Cl - SO_4, Na - Mg - Cl - SO_4, and Ca - Mg - Na - Cl. The fluid composition of fluids entering the basin is dependant on the composition of source waters flowing into the basin, e.g., a basaltic, rhyolitic, or granitic provenance would result in ingressing waters enriched in Ca, Na, Mg, HCO_3^-, SiO_2 at near neutral pH conditions.

Modification of the original brine composition may occur through a variety of factors, such as by precipitation of calcite and gypsum (producing a residual Mg-rich fluid), and clay precipitation and dolomitisation (e.g. producing a residual Mg-depleted fluid). The concentration of certain salts in solution is also governed by the solubility of these salts as a function of temperature (Figure. 1.3). Solubilities of the majority of salts in solution increase with increasing temperature.

For salts such as $CaCl_2$, an initial increase in temperature causes the solubility to increase accordingly. With continued temperature increase though, the solubility of $CaCl_2$ increases dramatically. It follows that fluids are able to carry significant amounts of $CaCl_2$ in solution with only slightly increasing temperatures. This may be important in the carrying capacity of fluids to transport certain metals in solution. Conversely, for NaCl (and to a lesser extent, KCl), a rise in temperature will lead to a slight increase in solubility, but as can be seen from the relatively flat slope of the curve in Figure 1.3, an increase in NaCl solubility will result from a marked increase in temperature.

Moreover, an increase in salinity of an ore fluid would lead to a more rapid pH decrease for monovalent alkali cation-brines than for divalent cation-brines (Yardley, 2005). It follows that a Na-dominated brine of a high salinity has a greater ore-carrying capacity than a Ca-dominate brine of the same salinity (Yardley, 2005). High fluid salinities may be generated by evaporation, and whether fluids originated from evaporate-dissolution or evaporative processes may be investigated using Cl-Br experiments (Carpenter (1978) in Heijlen *et al.*, (2001)).

Cl/Br, Na/Br ratios may be plotted to distinguish between fluids derived from seawater and continental brines. Moreover, $\delta^{37}Cl$ isotope values may also be used to shed light on the nature of source waters as having a seawater or meteoric origin (Banks *et al.*, 2000). Depending on the original composition of the fluid, a solution at a given temperature may dissolve more $CaCl_2$ than NaCl. Brine migration may be triggered by several factors, including thermal anomalies as a result of orogenesis, or due to convection flows.

Metal concentration in fluids

The metal-carrying capacity of a fluid is not only determined by the major cations in solution and the corresponding salinity, but also by the ligand complexing of these cations along with temperature, pressure, pH and fO_2. It follows that the relationship between these factors is important in achieving the equilibrium state at which metals are transported and precipitated from solutions to form orebodies.

During the course of brine development, copper may become available either in the brine or in cements due to the presence of cupriferous mafic minerals in volcanic detritus, (Jowett, 1989), or may be scavenged from granites, felsic granites, and granodiorites (Rickard, 1974). A contributing factor to the metal precipitation potential of fluids is the redox potential of those fluids.

Generally, metals with higher standard reduction potentials (Eh_o) are more susceptible to reduction (Figure 1.4a). This being said, red bed sequences become increasingly oxidised during diagenetic evolution as the basin is progressively infiltrated by descending meteoric waters (Brown, 2006). For fluids carrying both Cu and Co in solution, progressive reduction will firstly result in the precipitation of Cu, followed by Co (Figure 1.4b).

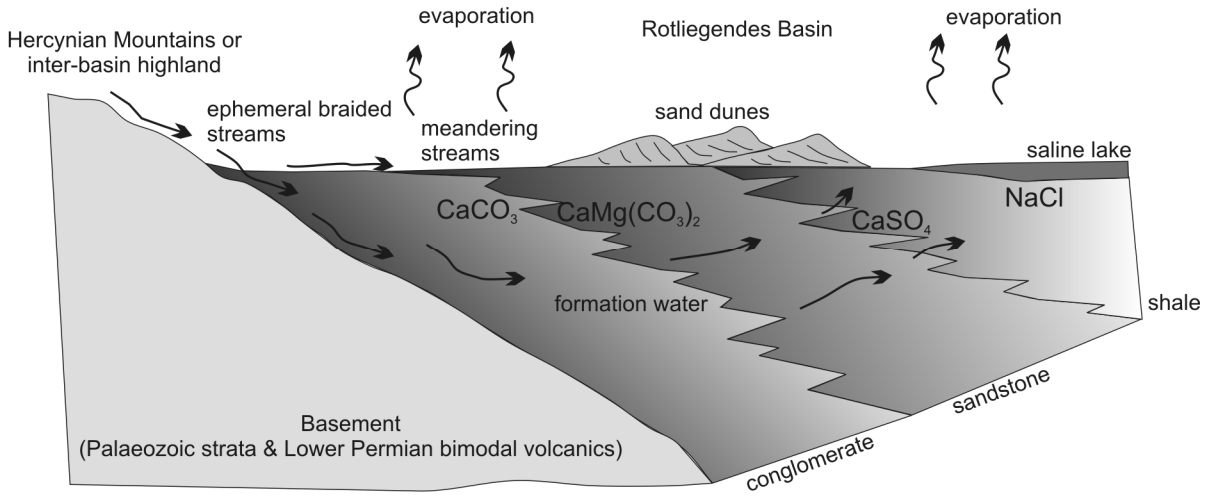

Figure 1.2. Basinal brines are generated by the concentration of certain cations (commonly Na, Ca, K) from modified fresh groundwater. Groundwater becomes enriched during early diagenesis in Na-Ca-Cl, derived from constituents such as calcite, dolomite, gypsum, and clay (after Jowett, 1989; Hardie and Eugster, 1970; Lerman, 1970).

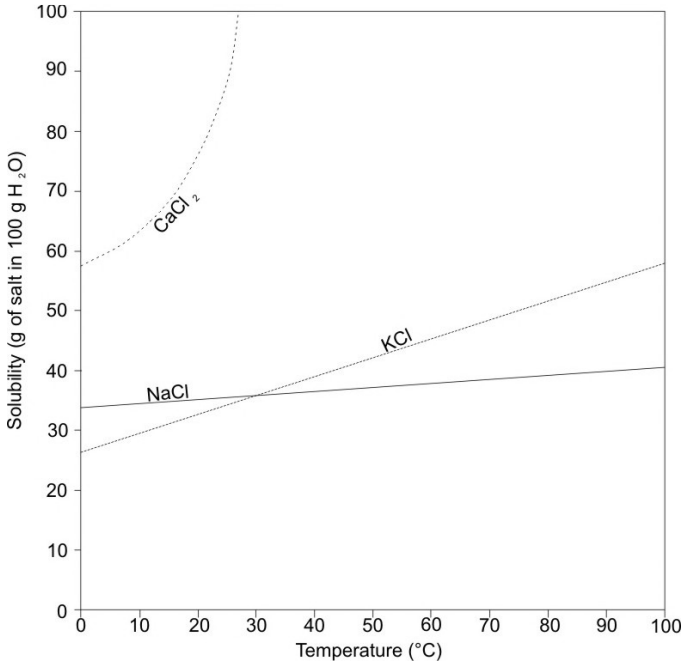

Figure 1.3. Solubility curves for selected cation complexes showing the amount of salt dissolved in a solution of 100g H_2O as a factor of temperature. (Source: www.scidiv.bcc.ctc.edu/wv). See text for details.

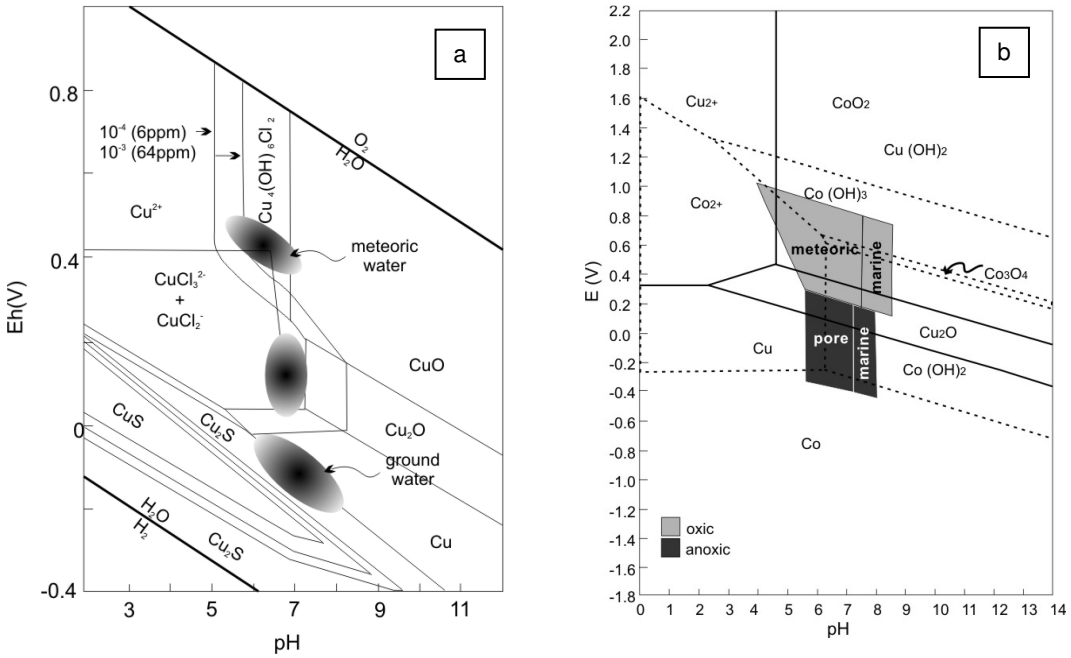

Figure 1.4 (a) Eh-pH stability fields for copper chloride complexes at 25 °C (modified after Rose, 1976; Brown, 2006). (b) Plot of solubilities for selected Cu- and Co-complexes as a function of reduction potential (Eh) and pH (after De Zoubov et al., 1980; Deltombe and Pourbaix, 1980, Brown, 2006). An increase in Eh will increase a solution's potential to oxidise a new species, and conversely, a lower Eh will tend to reduce a new species by losing electrons to the new species. See text for details.

Copper sources may be found in several terrestrial and hydrological reservoirs. Compared to seawater and freshwater, the most important source of copper in the hydrosphere is subsurface waters. Moreover, Rickard (1974) indicates that the solubilities of covellite, chalcocite, chalcopyrite, and bornite in the presence of chloride in hydrothermal environments (T<300°C) are suitable to generate copper ore deposits. Significant terrestrial copper reservoirs are mafic igneous and metamorphic rocks, with minor copper contained in sediments. Solutions capable of transporting copper may be found in oxygenated, chloride-rich pore fluids that have evolved from descending meteoric waters (Brown, 2006). These meteoric fluids would have become increasingly saline after the interaction with evolving evaporites.

Chapter 2

METHODOLOGY and ANALYTICAL PROCEDURES

2.1 Introduction

This chapter reviews the methodology and analytical techniques employed during the investigation into the nature of basinal fluids present in the Zambian Copperbelt. Figure 2.1 illustrates the procedure and sequence of investigation during the study. Emphasis is placed on the fluid inclusion methodology, techniques, basic principles and assumptions.

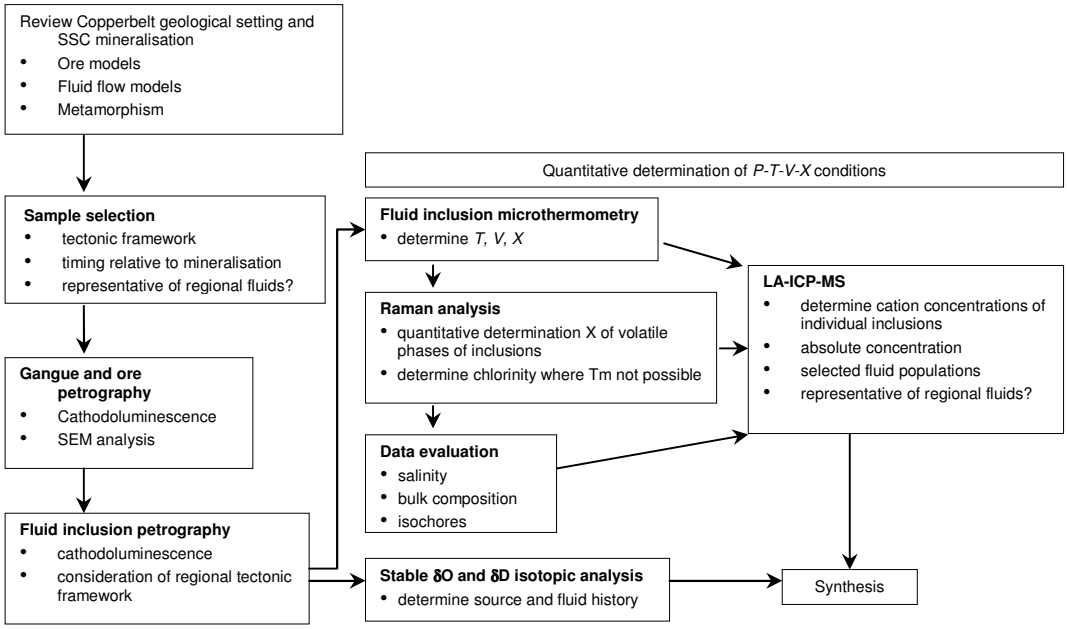

Figure 2.1 Schematic presentation of chronology employed during the course of this study.

2.2 Field work

Field work consisted of the mapping of selected outcrops and logging of particular diamond drill cores during December 2001 and June-July 2002. Samples were collected from underground workings at the Nchanga, Konkola, and Mufulira mines, and from open pit workings at the Chambishi and Nchanga deposits. Samples of diamond drill were collected from the Konkola, Nchanga, Chambishi and Nkana deposits, housed either at the respective mines, or at the Zambia Consolidated Copper Mines (ZCCM) core yard at Kalulushi. List of samples available in Appendix I.

2.3 Ore and gangue mineral optical petrography

Polished thin- and ore sections were prepared at the School of Geosciences, University of the Witwatersrand. Double polished wafers were prepared at the Council for

Geosciences, Pretoria, South Africa. Optical transmitted- and reflected light microscopy of polished thin- and ore sections were conducted at the School of Geosciences, University of the Witwatersrand using an Olympus Vanox petrographic light microscope, and a Leitz petrographic light microscope with mounted Leica DC100 digital camera, and at the UMR CNRS Géologie et Gestion des Ressources Minérales et Energétiques (G2R) 7566 – CREGU at the Université Henri Poincaré, Nancy, France.

Optical transmitted light microscopy was conducted on fluid inclusion double polished wafers (>200µm thickness) at the School of Geosciences at the University of the Witwatersrand and at UMR CNRS G2R 7566 – CREGU at the Université Henri Poincaré, Nancy, France.

2.4 Fluid inclusions

2.4.1 Background

Fluid inclusions are small pockets of fluid trapped in certain minerals either during, or subsequent to, crystal growth (Roedder, 1984; Shepherd *et al.*, 1985; Goldstein and Reynolds, 1994). The relationship between individual inclusions, and amongst inclusions and growth zones, indicates the relative timing of entrapment. Based on petrographic observations, fluid inclusions and fluid inclusion assemblages may be identified as primary, secondary, or pseudo-secondary (Roedder, 1984; Goldstein and Reynolds, 1994). Assuming that no leaking or resetting has occurred during metamorphic events, earlier fluids (late diagenetic) are interpreted to exist either as isolated inclusions (as primary inclusions), or as inclusions occurring along poorly defined planes (as pseudo-secondary inclusions before the termination of the crystal growth). Conversely, fluid inclusions in well-defined fluid inclusion planes (FIP's) have trapped fluids present during (and to some extent after) cracking and annealing of the host crystal, as secondary fluid inclusions.

We assume that inclusions represent isoplethic and isochoric systems, i.e., that no change has occurred to inclusions in terms of chemical composition and volume, over geological time (Goldstein and Reynolds, 1994). The key to determining representative fluid inclusion populations is to document sufficient inclusions of a particular fluid inclusion assemblage (Goldstein and Reynolds, 1994).

The objective of any fluid inclusion study is to constrain the P-T-υ-X conditions of a particular fluid(s), and this is done using a variety of analytical techniques, some which are mentioned below. These analytical methods are constrained by several factors, and

limitations exist with each technique, be it from the inclusion, the inclusionist, or technological advances. In general, fluid inclusions are either studied on an individual basis, e.g., microthermometry, Raman, LA-ICP-MS, and/or using bulk methods, such as isotope analysis, crush-leach analysis (Banks *et al*., 2002). Below follows a brief outline of the techniques used during the course of this study. Temperatures are given in °C in this thesis unless otherwise stated.

Fluid inclusion petrographic classification

Fluid inclusions were identified either as isolated occurrences or in fluid inclusion trails or planes. Inclusions were attributed to these assemblages (Goldstein and Reynolds, 1994; Goldstein, 2001) in order to maintain consistent documentation of assemblages between deposits. Generally, isolated inclusions were classified as primary, whilst inclusions found in trails or planes (FIPs) were accordingly described as secondary (Roedder, 1984; Shepherd *et al*., 1985; Bodnar, 1994; Goldstein and Reynolds, 1994). One of the limitations of fluid inclusion research is the identification of the paragenetic sequence of fluid inclusion assemblages. The identification of isolated inclusions as primary is an over simplification since isolated inclusions may only unequivocally be viewed as primary if they occur within growth zones (Goldstein and Reynolds, 1994). In the absence of growth zones, due to observation difficulties, or massive host material, it is best to state that inclusions are "possible primary inclusions" Shepherd *et al*., (1985). Inclusions in this thesis have been classified as either primary or secondary, but it should be stressed that in the absence of growth zones throughout Chapters 5-7, primary inclusions are actually "possible" primary inclusions.

Fluid inclusion types are also described according to the nomenclature used by Boiron *et al*. (1992)*. Inclusions are classified based on their final homogenisation ($T_{h\,total}$) behaviour, as either 'L' when final homogenisation is to the liquid phase, or as 'V' when final homogenisation is into the vapour phase. Inclusions are further categorised based on the presence of dominant aqueous (w) or carbonic (c) species (Boiron *et al*., 1992).

The determination of P-T-υ-X properties of fluid inclusions was achieved by the integration of microthermometry, Raman microscpectroscopy, laser ablation inductively coupled plasma mass spectrometry and stable isotopes. In addition to optical microscopy, cathodoluminescence microscopy was used during the petrographic investigation to determine the presence of growth generations of quartz veins and quartzites. Cathodoluminescence microscopy may aid in the classification of inclusions into

* see List of Abbreviations

assemblages. The working-conditions of CL microscopy are listed below, also see Boiron *et al.* (1992), and Van den Kerkhof and Hein (2001)

Raman microspectroscopy was used to confirm and quantify the gaseous compositions in aqueo-carbonic and gaseous inclusions (Dubessy *et al.*, 1989; Burke, 2001). Some inclusions proved problematic to measure using microthermometry due to their small size, depth in samples, inclusion shapes etc. Chlorinity of inclusions was determined for inclusions where microthermometric measurements were impeded. This analytical method is relatively new and determines the concentration of chloride in aqueous solutions using the υ(OH) stretching vibration of water (Dubessy *et al.*, 2002). Refer to section 2.4.3 below for more detail on this method.

2.4.2 Fluid inclusion systems

The analytical techniques listed above aid in the determination of fluid *P-T-υ-X* properties. Below is a brief summary of common fluid inclusion systems, focussing on fluids found in the Copperbelt during the course of this study.

Aqueous inclusions

Aqueous fluids are commonly found within the earth's crust and may consist of a variety of cation-ligand complexes. Chlorides, and sulphates to a lesser extent, are the most common ligands in natural fluids due to the availability of chlorides in the crust and because of the stabilities of many metal-chloride solutions in hydrothermal fluids (Yardley, 2005). Ions most commonly dissolved in fluids in inclusions include Li^+, Na^+, K^+, Ca^{2+}, Mg^{2+} and Cl^- (Boiron and Dubessy, 1994). For details on selected aqueous fluid systems, refer to Bodnar *et al.* (1985), Schiffries (1989), Bodnar (1993), Bodnar and Vityk (1994), Boiron and Dubessy (1994), Oakes *et al.* (1990), and references therein.

The determination of the aqueous fluid composition is by the measurement of the temperature at which eutectic melting occurs. For this study, the initial melting of aqueous phases observed during heating is interpreted as the eutectic point, and this temperature is referred to as the eutectic temperature (T_e). Refer to Table 2.1 for a list of general eutectic temperatures with corresponding chemical compositions of the aqueous phase. The system commonly implicated during the course of this investigation is that of $CaCl_2$ - NaCl - H_2O, and eutectic point, melting of hydrohalite, and ice, obtained from microthermometry is plotted to illustrate fluid composition (Figure 2.2).

Table 2.1. Eutectic melting of aqueous phases may indicate the presence of the following compositions (after Davis et al., 1994; Goldstein and Reynolds, 1994).

Te (°C) observed at:	Composition
-35 to -28, and -21.1	NaCl - H_2O
-85 to -70, and -53 to -47	NaCl - $CaCl_2$ - H_2O
-80 to -70, -50 to -45, and -40 to -33	NaCl - $MgCl_2$ - H_2O
-23.4 to -23.0	NaCl - KCl - H_2O
-57	NaCl - $CaCl_2$ - $MgCl_2$ - H_2O

Salinities of aqueous inclusions are determined by the temperature at which final ice melting occurs ($T_m$ice) (Bodnar and Vityk, 1994). For fluids of the H_2O-NaCl system, this salinity is expressed in wt.% NaCl, and for solutions where other cations are present, salinity is expressed as wt.% $NaCl_{equivalent}$ (Bodnar and Vityk, 1994).

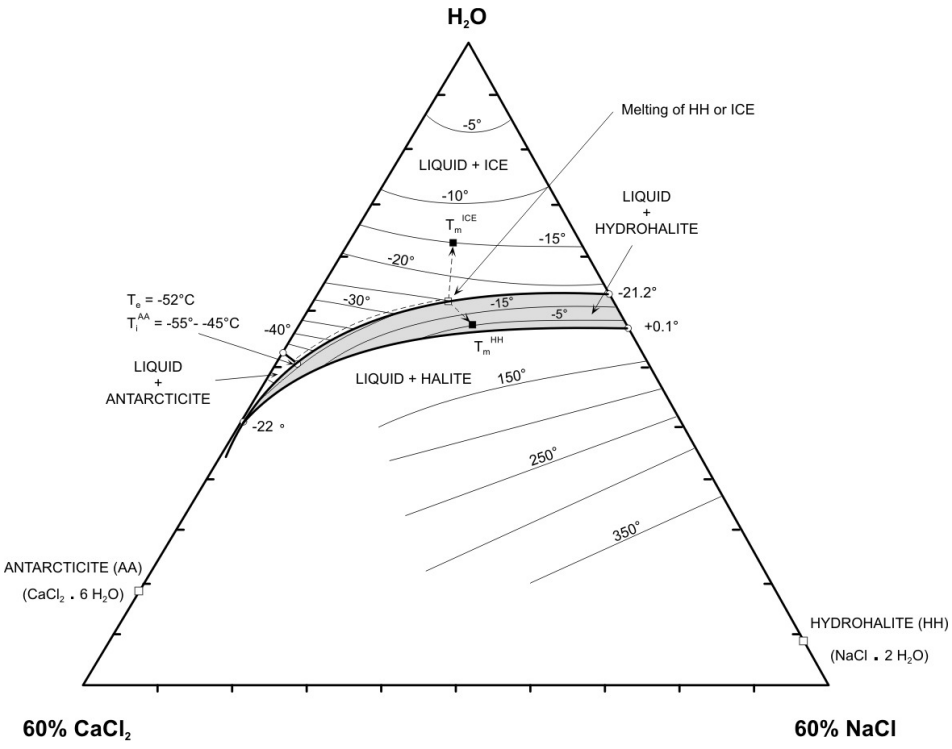

Figure 2.2 Ternary phase diagram for inclusions with a composition of $CaCl_2$ - NaCl - H_2O (modified after William-Jones and Samson, 1990). Cotectic curves are indicated in solid black lines, with isotherms (°C) indicated in dashed lines.

Aqueo-carbonic inclusions

Volatile-aqueous inclusions are frequently trapped during hydrothermal processes, and may be mixtures of aqueous fluids of a range of salinities together with gaseous phases such as CO_2, CH_4, N_2, H_2S. This section briefly reviews the H_2O-CO_2 system, as aqueous fluid inclusions with CO_2 as the major gaseous component constitute the dominant type found in the Copperbelt samples during the course of this study. In addition to aqueo-carbonic inclusions, aqueous-N_2 inclusions are also described in Chapter 7. Several authors have devoted numerous publications to the topic of the nature of aqueous-volatile inclusions and the reader is referred to Burruss (1981), Sterner and Bodnar (1991), Diamond (1994, 2001), Bakker and Thiéry (1994), Huizenga (2001) and references therein.

CO_2 and H_2O possess dissimilar attributes considering the respective triple points and critical points, and are at temperatures below 265 °C and 2.2 kbar, immiscible (Diamond, 2001). Phase relationships are illustrated in Figure 2.3 in terms of P-T-X. The phases represented in the diagram are solid CO_2, clathrate, ice, vapour, carbonic liquid, and aqueous liquid. CO_2 and H_2O may naturally occur in inclusions in various ratios, but the common ratio of high XH_2O and low XCO_2 is further discussed here since this inclusion type is abundant in inclusions studied from the Copperbelt during this investigation.

CO_2 - H_2O inclusions often found in low- to medium grade metamorphic rocks are generally those with high XH_2O, low XCO_2 compositions, which show two or three phases present at room temperature in inclusions as liq_{aq} – liq_{car} (or vap_{car}) or, liq_{aq} – liq_{car} – vap_{car} (Diamond, 2001). The bulk volume of such inclusions according to Diamond (2001) may vary between 5 to > 98 vol.% aqueous liquid. Considering the phase behaviour for an inclusion with a modal composition of ~ XH_2O = 0.9 and XCO_2 = 0.1, trapping of the homogeneous inclusion at a certain P-T determines the bulk molar volume of the inclusion (black hexagon in Figure 2.3). As cooling of the inclusion occurs along the isochore (not drawn in Figure 2.3), the miscibility boundary of the bubble surface is intersected (indicated by filled black hexagon with white circle in Figure 2.3).

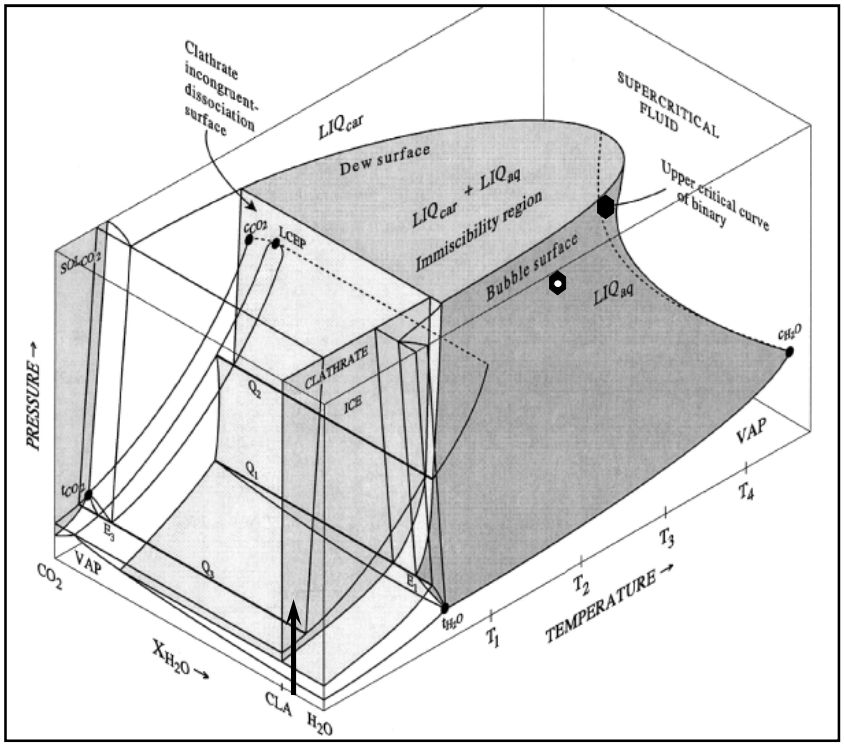

Figure 2.3. Stability equilibrium phases for the H_2O-CO_2 system (Diamond, 1994, 2001). Shaded areas indicate regions of liquid-liquid immiscibility, clathrate dissociation surface, and solid CO_2 composition planes. Fields are not to scale. t_{CO2} = triple point of CO_2 at -56.6 °C, 5 bar; t_{H2O} = triple point of H_2O at 0.01 °C and 0.006 bar; c_{CO2} = critical point of CO_2 at 31.1 °C, 74 bar; c_{H2O} = critical point of H_2O at 374 °C, 221 bar. The arrow indicates a composition of high XH_2O, low XCO_2 which is typical of fluids found in low grade metamorphic rocks. See text for details.

A bubble of carbonic liquid forms when the inclusion reaches the miscibility boundary, where after the inclusion is comprised of two phases and phase behaviour during cooling is predicted by equilibrium phase compositions along tie lines (Figure 2.4a). The composition of the carbonic liquid (L_{car}) is given by the point at which the solvus is reached, and the composition of the aqueous liquid (L_{aq}) is given by the equilibrium point along the tie line at a given temperature (Figure 2.4a).

A comparison with other volatile compositions is given in Figure 2.4b and shows the liquid - liquid miscibility behaviour of fluids composed of $H_2O \pm CH_4$, O_2, N_2, H_2, and Ar (Diamond, 2003). Diamond (2003) notes that critical point compositions for these fluid mixtures are enriched in H_2O at 1 kbar pressure which indicates that H_2O dominates the phase behaviour in such mixed systems, enabling the extrapolation from modelled binary systems into these mixed multivolatile-H_2O systems.

As the temperature of the inclusion continuously decreases after intersection of the dew surface where the coexisting phases are liq_{aq} + liq_{car} + vap, the bubble of carbonic liquid becomes larger consuming the aqueous liquid. A carbonic vapour bubble nucleates during further cooling (along the isochore) within the carbonic liquid phase when the inclusion reaches the three-phase surface point (corresponding to Th_{car} at heating).

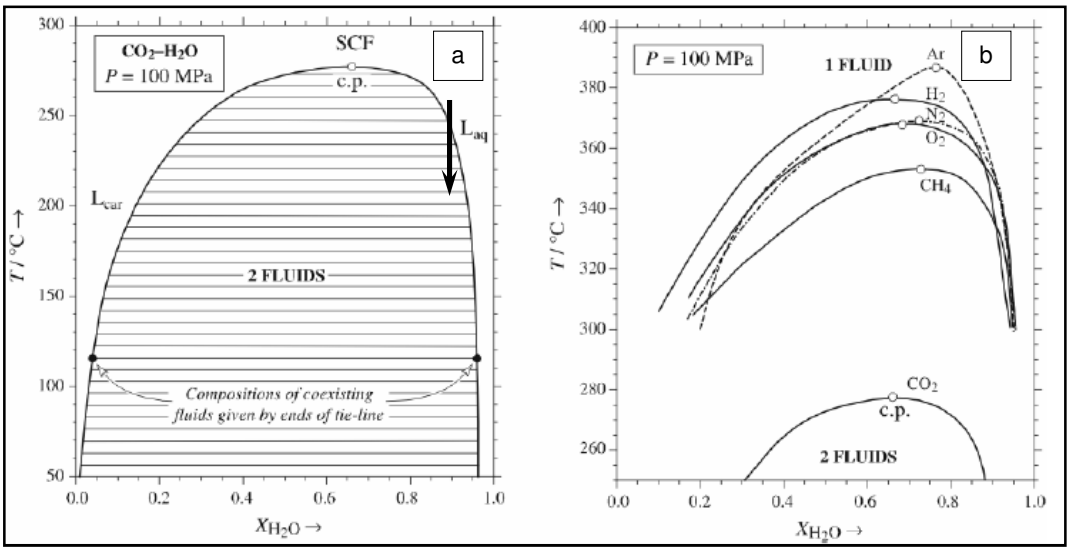

Figure 2.4. Immiscibility boundaries for the (a) H_2O-CO_2 system at 1 kbar, and (b) for selected gaseous-aqueous systems at 1 kbar along an isochoric path (Diamond, 2003). The arrow in (a) indicates an inclusion containing a bulk composition of ~ 0.9 XH_2O, and 0.1 XCO_2 which is referred to in Figure 2.3. SCF: supercritical fluid, c.p.: critical point. Source references are given in Diamond, 2003.

Clathrate crystallisation occurs with continued cooling, usually observed after reaching the crystallisation temperature due to metastability. Ice crystallisation is reached with ongoing cooling in the presence of the carbonic liquid and carbonic vapour. It follows that aqueo-carbonic fluid inclusions may consist of up to four phases at low temperatures, namely liq_{car} + vap_{car} + $solid_{aq}$ + clathrate. According to Diamond (2001), the presence of four phases over a temperature interval in a binary system may be explained by the presence of clathrate which forms a physical diffusion barrier between carbonic and aqueous phases.

With continued cooling, the crystallisation temperature of CO_2 is reached in the presence of vapour + clathrate + ice. Notably, the reader is reminded that microthermometric measurements are conducted during heating of inclusions, whereby the temperatures of phase transitions are measured occurring at their individual equilibrium temperatures,

even though the assemblages are metastable (Diamond, 2001). Temperatures observed during inclusion heating are the melting of the carbonic phases (T_mCO_2), ice melting (T_mice) in the presence of solid clathrate or in the presence of liquid CO_2 where $T_mice \neq$ eutectic T_mice, temperature of homogenisation of the carbonic phases (T_hCO_2), and temperature of final homogenisation (T_htot) where the carbonic fluid dissolves into the aqueous liquid.

Carbonic inclusions

CO_2 may be found in metamorphic rocks along high grade deformation- and shear zones, in rocks were the selective disappearing of aqueous fluids occurred due to post-metamorphic annealing in rocks that initially had some CO_2 present (Touret, 2001). CH_4 may be sourced from the breakdown of organic material (Killops and Killops, 1993), or from the re-equilibration during retrograde metamorphism (Van den Kerkhof and Thiéry, 2001). N_2 may be sourced from banded iron formations (Touret, 2001), and has been recorded in eclogites along with aqueous fluids (Andersen *et al*., 1989).

The phase transition behaviour of carbonic inclusions is well documented by Van den Kerkhof and Thiéry (1990, 2001). Phase behaviour of inclusions is related to fluid composition and molar volumes, and therefore is an essential observation during microthermometric measurements. Transitions in the CO_2 - CH_4 - N_2 system are illustrated in Figure 2.5.

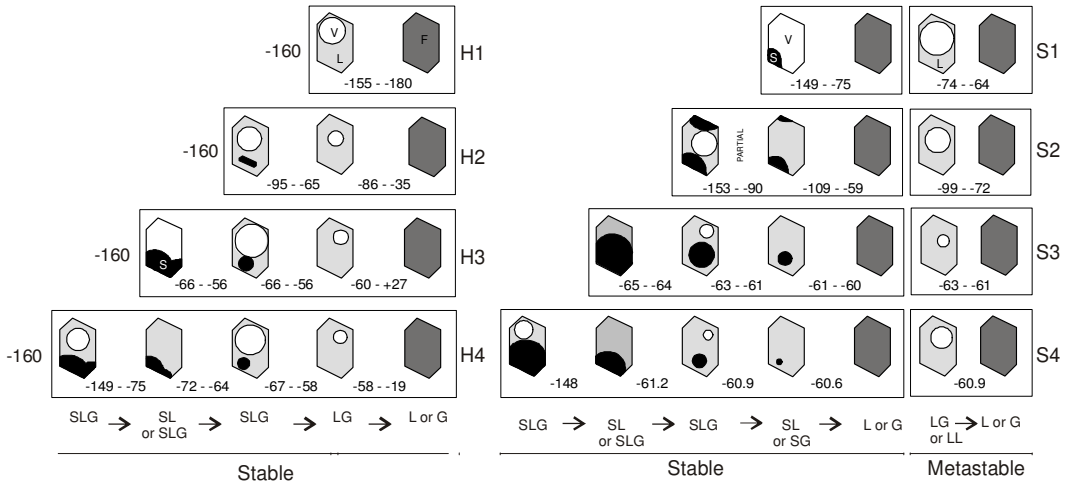

Figure 2.5 Sequence of phase transitions for the system CO_2-CH_4-N_2 between -160 and 31 °C. Final homogenisation behaviour is shown on the left, and final sublimation behaviour on the right. L: liquid, G: gas. Black: solid CO2, light grey: liquid, dark grey: supercritical fluid (simplified after Van den Kerkhof and Thiéry, 2001).

The type of phase behaviour identified and the number of transitions is related directly to the composition of the inclusion, e.g., H1-type inclusions are generally composed of CO_2 - poor fluids, while H2-type behaviour is generally typical of CO_2 - CH_4 fluids. For further details on phase behaviour, refer to Van den Kerkhof and Thiéry (1990, 2001).

2.4.3 Fluid inclusion microthermometry

Fluid inclusion microthermometry was initially conducted using a Linkam TH600 heating-freezing stage mounted on an Olympus Vanox transmitted light microscope at the University of the Witwatersrand. Measurements were done using the 50x objective long-working distance lens. Samples were polished on both sides (double polished) to 200-300 µm thickness. The heating-freezing stage has a temperature range between -196°C and +600°C, and is connected to a liquid nitrogen pump (LNP 2) and TP92 programmable thermal control unit, allowing heating and cooling rates of between 0.1°C and 90°C per minute. Inclusions were cooled to -130 to -190°C, and phase transitions were measured during heating. The stage was calibrated using pure CO_2 inclusions (composition confirmed with Raman analyses) in quartz from the Harare-Bindura greenstone belt, Zimbabwe, at the triple point of CO_2 (-56.6°C), and homogenisation temperatures of synthetic H_2O inclusions in quartz (SynFlinc, supplied by FluidInc) for calibration up to 0°C. Low temperature phase transitions (<10°C) are estimated to have a precision of 0.2 °C, and homogenisation measurements of H_2O inclusions a precision of 5°C.

Fluid inclusion microthermometry was also performed at the UMR CNRS G2R 7566 – CREGU at the Université Henri Poincaré, Nancy, France, using a Linkam MDSG600 motorized heating-freezing stage with MDS motor controller, mounted on an Olympus BX optical light microscope. The stage is controlled with a TMS94 temperature programmer and liquid nitrogen pump, connected to a PC computer using Linksys 32 temperature control software. The microscope is fitted with a CCD camera. The temperature range for the stage ranges between -196°C and +600°C, and has cooling and heating rates between 0.1°C and 90°C per minute. The stage was calibrated using synthetic CO_2 inclusions in quartz (supplied by FluidInc), at the triple point of CO_2 (-56.6°C), and homogenisation temperatures of synthetic H_2O inclusions in quartz (SynFlinc, supplied by FluidInc) for calibration up to 0°C. Low temperature phase transitions (<10°C) are estimated to have a precision of 0.2 °C, and homogenisation measurements of H_2O inclusions a precision of 4°C. Estimation of the volumes of volatile phases at room temperature was done using the volumetric estimation chart of Roedder (1972). Phase transitions in inclusions were measured upon heating.

The following temperatures were measured during microthermometry experiments[1]:

- final melting of gaseous (CO_2, CH_4, C_2H_6) $\pm N_2$ $\pm H_2S$ inclusions; T_m (sol + liq + vap = liq + vap)
- homogenisation of gaseous $\pm N_2$ $\pm H_2S$ inclusions; T_h (liq + vap = fluid)
- first melting of aqueous inclusions; T_e (sol + vap = sol + liq +vap)
- melting of hydrates (e.g., hydrohalite $NaCl \cdot 2H_2O$); $T_m$hh (sol + liq + vap = ice + liq + vap)
- final melting of aqueous inclusions; T_m (sol + vap + liq = liq + vap)
- melting of clathrate (e.g., $CO_2 \cdot 6H_2O$); $T_m$cla (liq_{aq} + $fluid_{car}$ + sol_{cla}+ vap = liq_{aq} + $fluid_{car}$ + vap). A variety of molecules such as H_2S, CH_4, C_2H_6 may be trapped within the clathrate structure (Roedder, 1984).
- homogenisation of aqueous inclusions; $T_h$aq (aq_{liq} + vap = aq_{fluid}).
- dissolution of solid phases (e.g., halite); $T_m$halite (liq_{aq} + sol_{halite} + vap = liq_{aq} + vap)

Unless otherwise indicated, Thaq is also total homogenisation of the inclusion, and corresponds to the minimum trapping temperature. Due to observation difficulties when measuring Te, and hydrate melting in the presence of ice, the uncertainty of some of these measurements may reach 5°C.

2.4.4 Raman microspectroscopy

A Jobin-Yvon Raman microspectrometer was used to quantitatively determine the gaseous compositions and chlorinity of fluid inclusions at UMR CNRS (G2R) 7566 – CREGU at the Université Henri Poincaré, Nancy, France (Dubessy *et al*., 1989, 2002). The Raman microspectrometer is connected to an Olympus BH2 petrographic light microscope. An ionized Ar-laser supplied the 514.5 nm excitation source. The laser was focused on the sample by 80x long working distance objective lens. Additional detail on the working conditions is documented in Dubessy *et al*., (1992, 2002).

The Raman effect (or scattering) is observed due to energy changes as a result of inelastic collisions between vibrating polyatomic molecules or molecular groups when an incident beam of monochromatic light is focussed on a sample (Rosasco and Roedder, 1979; Dubessy *et al*., 1982; Burke, 2001). This observed scattering is related to known compositions. The quantitative determinations of compositions by Raman analysis have for decades only been possible for polyatomic gas species. However, recent advances have enabled the determination of chloride concentration in aqueous solutions by the

[1] see List of Abbreviations

Raman spectrometric analysis of the stretching vibration (υOH) of water in the 2800-2800 cm^{-1} region of the Raman spectrum (Mernagh and Wilde, 1989; Dubessy *et al*., 2002). This technique compliments microthermometric analysis and allows for the determination of bulk ion content (Dubessy *et al*., 2002).

2.4.5 Salinity calculations

Aqueous inclusions

Salinities for the aqueous inclusions were calculated from T_{mice} using the equations in Bodnar and Vityk (1994).

Fluids with <23.2 wt.% NaCl (Bodnar, 1993):

$$\text{Salinity (wt.\%)} = 0.00 + 1.78\,\theta - 0.0442\,\theta^2 + 0.000557\,\theta^3$$

where θ = the freezing point depression measured in °C (T_{mice})

Fluids with >26.3 wt.% NaCl (Sterner *et al*., 1988):

$$\text{Salinity (wt.\%)} = 26.242 + 0.4928\,\Psi + 1.42\,\Psi^2 - 0.223\,\Psi^3 + 0.04129\,\Psi^4 + 6.295 \times 10^{-3}\,\Psi^5 - 1.967 \times 10\text{-}3\,\Psi^6 + 1.1112 \times 10^{-4}\,\Psi^7$$

where Ψ = halite dissolution T (°C)/100

Aqueo-carbonic inclusions

The practise of calculating salinities from final ice melting temperatures may not be applied to aqueo-carbonic fluids due to some of the aqueous phase being locked up in gas hydrates (clathrates), which would lead to overestimation of salinities based on T_{mice} values. Therefore, salinities for aqueo-carbonic inclusions were calculated using degree of fill, T_hCO_2 and T_mclath by using the equation of state in Bodnar (1983) and Brown and Lamb (1986, 1989) in the *Linkam Scientific PVTX* software programme for Fluid Inclusions, V 2.1.

Salinity determination using chlorinity values

Chlorinity determination by Raman microspectroscopy was also used to calculate salinities using the measured Cl^- concentration in mol/kg H_2O of individual inclusions. This method proved invaluable for salinity calculations where the observation of phase changes were hampered due to size, shape, degree of fill or depth in host minerals.

Average content of solutions deduced from microthermometry: Na/Ca = 5

$$\text{NaCl wt.\% equiv.} = \frac{m\text{NaCl} \times 58.4}{(1000 + m\text{NaClequiv.}) \times 58.4}$$

2.4.6 Bulk composition and density

Bulk densities of aqueous inclusions are determined by the final ice melting temperature ($T_m$ice) in NaCl-bearing fluid inclusions (Boiron and Dubessy, 1994) using the computer programme *Bulk*, version 01/03 (Bakker, 2003). Bulk densities of aqueo-carbonic inclusions were calculated from the densities of the aqueous phase and of the gaseous phase. When considering the amount of CO_2 dissolved in the aqueous phase, the molar volume is determined from the bulk density and composition. The density of the aqueous phase is also corrected for the overestimation of the density of the non-aqueous phase which is due to the volume discrepancy between ice and water (Boiron and Dubessy, 1994).

Isochores (lines of constant volume) were calculated and plotted using *Isochor* version 13/03/96 (Bakker, 1997) and *Isoc* version 01/03 (Bakker, 2003). Relevant equations of state were used to model inclusion properties and are referred to in the individual chapters.

Measured homogenisation temperatures provide the minimum temperatures at which inclusions were trapped. In order to obtain the maximum trapping temperature for a fluid inclusion assemblage the values of certain variables are needed. These variables are the fluid pressures, densities, temperature and compositions. The true trapping temperature may be gained from the homogenisation temperature and the trapping pressure in addition to considering fluid compositions. Compositions are determined from microthermometry and Raman microspectroscopy and are related to simplified systems such as H_2O, CO_2, CH_4, CO_2-CH_4, H_2O-NaCl, and H_2O-NaCl-CO_2. According to Roedder and Bodnar (1980), and Shepherd *et al*. (1985), the methods commonly used to calculate fluid pressures from microthermometric data are:

- vapour pressures at T_h
- independent geothermometers
- intersecting isochores of co-existing fluids
- daughter mineral dissolution temperatures

Using these methods requires knowledge about the assumptions made during the estimations and inherent limitations of each method.

2.4.7 Laser ablation inductively coupled plasma mass spectrometry (LA-ICP-MS)

The in situ quantitative analysis of fluid inclusions in terms of major, minor, and trace elements, is made possible by laser ablation inductively coupled plasma mass spectrometry (Günther *et al.*, 1997, 1998). The analyses were performed at the School of Earth Sciences, Leeds University, Leeds, in the United Kingdom. Inclusions are ablated with a 193nm ArF Lambda Physik Excimer laser, in a Geolas Q Plus laser ablation system (Allan *et al.*, 2005). Ablation occurs in a He stream and the ablated material is analysed in an Agilent 7500c ICP-MS with an Octopole Reaction Cell. The sample chamber design has been optimised along with the mixing of a carrier gas with a make-up gas to give a smooth signal and to spread the peak derived from a single laser shot over at least several seconds. The ICP-MS is operated with no gas in the reaction cell for most elements, but for elements such as Ca and Fe where the Ar from the plasma causes interference on the principal isotope (^{40}Ar overlaps ^{40}Ca and ArO overlaps ^{56}Fe) H_2 is introduced into the reaction cell.

After initial ablation with a 25µm diameter incident beam (diameter depending on the size of the individual inclusion), the inclusions were ablated again with a larger diameter beam to ensure excavation of the inclusion cavity for best reproducibility of element ratios. Calibration graphs of counts per element relative to counts per Na versus the weight to weight ratio of the element relative to Na were determined from standard reference materials NIST610, NIST612, and synthetic solutions of known composition. Na was the reference for calibration, with salt solutions of various compositions. Absolute element concentrations in ppm were calculated from the product of elemental weight ratios and known Na concentrations determined by microthermometry. Refer to Appendix II for details on calculations.

2.5 Cathodoluminescence microscopy – modified cold stage

Cathodoluminescence (CL) is the emitted visible radiation when a sample is bombarded under vacuum by an electron beam that stimulates electron energy level transitions (Marshall, 1988; Pagel *et al.*, 2000). CL microscopy of polished thin sections and double polished sections was conducted at the School of Geosciences, University of the Witwatersrand, using an Olympus BH-2 light microscope fitted with a CITL Mark 3a

Cold Cathode stage, connected to a vacuum pump. The microscope with stage is connected to a Leica DC100 digital camera.

The advantage of studying fluid inclusion petrography coupled with CL has been documented by Boiron *et al.* (1992), and Van den Kerkhof and Hein (2001). In order to study CL in quartz sections for fluid inclusion petrography, a modified sample holder was submerged in liquid nitrogen and placed in the stage which facilitated blue luminescence until the sample holder thawed. Optimum working conditions for thin section petrography and double polished wafers were at ~17 keV and 450 mÅ (see section 2.7 for CL-SEM working conditions).

2.6 Scanning electron microscopy

Scanning electron microscopy was conducted using a JEOL JSM 840 SEM equipped with an EDS system in conjunction with an Oxford Instruments cathodoluminescence system at the Service Commun de Microanalyses de l'Université Henri Poincaré in Nancy, France. Optimum working conditions were at 20kV acceleration potential and 3 x 10^{-9} to 1 x 10^{-6} A. SEM analysis of selected sulphides were conducted as well as using SEM in conjunction with cathodoluminescence to determine zonation patterns in minerals (Figure 2.6).

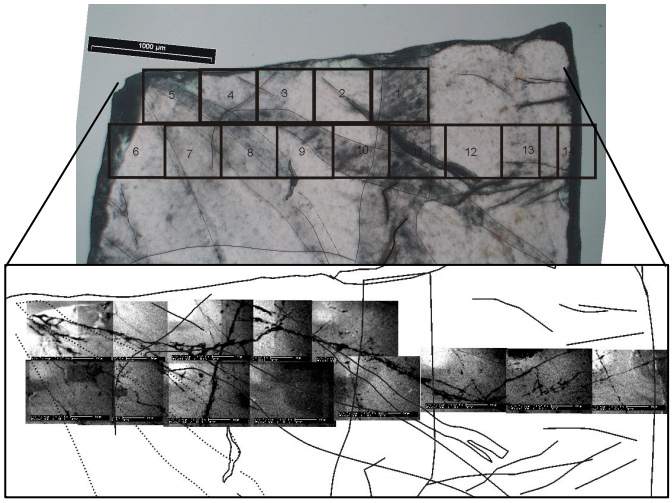

Figure 2.6. Double polished quartz wafers were considered in SEM-cathodoluminescence light, but did not reveal conclusive zonation patterns that could be attributed to mineral paragenesis or discernable fluid inclusion assemblages (sample CBSqz 3F). This image shows a double polished quartz wafer with noticeable fluid inclusion planes and trails. The overlay indicates composite CL scans across the width of the wafer. See Appendix III for selected spectra.

2.7 Stable isotope analyses

Oxygen isotope analyses of silicates and hydrogen isotope analyses of fluid inclusions in silicates were conducted at the Department of Geology at the University of Cape Town. The crushed samples of quartz (± minor feldspar) were hand picked and further crushed by agate mortar to a fine powder to yield ~10mg of powder for oxygen isotope analyses.

Oxygen isotope ratios are determined by conventional fluorination methods (Clayton and Mayeda, 1963). Samples containing carbonates were cleaned using dilute HCl. Oxygen isotope ratios were determined on 10 mg powder by conventional methods after drying samples in an oven at 500°C, and using ClF_3 (Borthwick and Harmon, 1982) as the oxidizing agent. The reaction time was 3 hours at 500-550°C. The O_2 was converted to CO_2 using a hot platinized carbon rod. Duplicates of a quartz standard (Murchison Line Quartz - MQ) were analysed with each run of eight samples as specified in Harris *et al.*, 2002. The $\delta^{18}O$ value of MQ was determined at 10.1 ‰ after calibration against the NBS-28 quartz standard, assuming a value of NBS-28 of 9.64‰ (Coplen *et al.*, 1983). The average value obtained for MQ was used to normalise the raw data to the SMOW scale. Data are reported in the δ notation where $\delta^{18}O = (R_{sample}/R_{standard} - 1)*1000‰$ and $R=^{18}O/^{16}O$. During the course of this work, the average difference between duplicates of MQ analysed were 0.11‰ (n = 8), which is equivalent to a 1σ value of 0.06.

Hydrogen isotope analyses were obtained according to the method by Vennemann and O'Neil (1993). Hydrogen was produced by thermal decrepitation from about 2g of quartz chips. Samples were degassed on the vacuum line at 200°C prior to decrepitation at ~500°C. The water was collected in Pyrex tubes containing Indiana Zn, and these tubes were heated to 450°C to reduce the water to Zn just prior to analysis on the mass spectrometer. Further detail on the above methods may be found in Vennemann and Smith (1990) and Harris and Erlank (1992).

The CO_2 and H_2 gases were introduced into a Finnegan MAT252 mass spectrometer via break-seal tubes, and samples were analysed in dual inlet mode. Data are reported in δ notation where δD is $(R_{sample}/R_{standard} - 1) * 1000‰$ and $R = {}^2H/{}^1H$. The typical precision of analyses is analogous to that of Harris *et al.*, (2005).

Chapter 3

CENTRAL AFRICAN COPPERBELT

REGIONAL GEOLOGY AND MINERALISATION

3.1 Geological setting of the Katanga Supergroup

The Neoproterozoic stratiform copper ores of the Central African Copperbelt are hosted by the metasediments of the Katanga Supergroup, located in the arcuate Lufilian fold belt, spanning the border of Zambia and the Democratic Republic of Congo (DRC) (Figure 3.1).

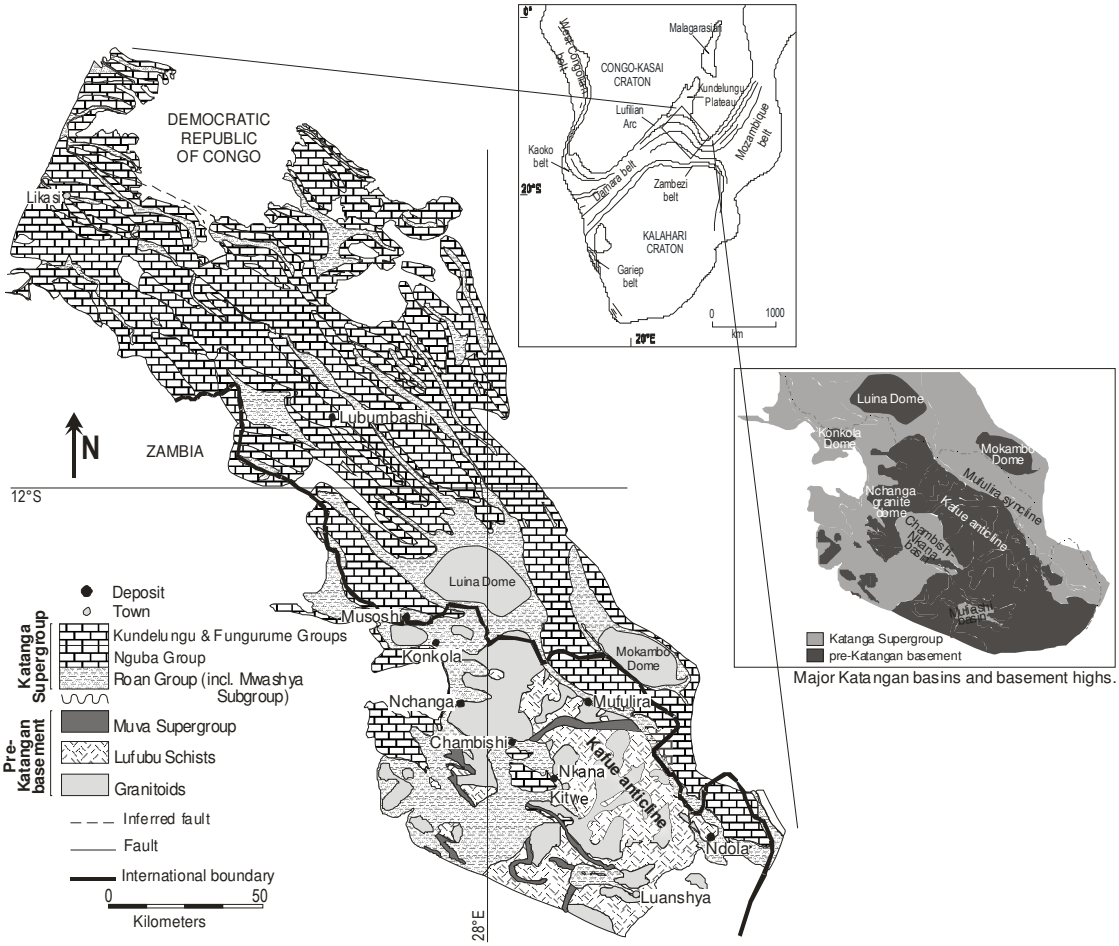

Major Katangan basins and basement highs.

Figure 3.1 Geological map of the Central African Copperbelt in the eastern and central section of the Lufilian Arc (modified from François, 1974, and Rainaud et al., 2003). Stratigraphic divisions are based on Wendorff, 2005 (see section 3.1.2 for explanation). The inset shows the major structural features of the central and southern Copperbelt which are referred to in the text.

3.1.1 The Basement to the Katanga Supergroup

The Katanga Supergroup unconformably overlies a complex basement which is comprised firstly of an exposed Palaeoproterozoic calc-alkaline volcanic arc terrain at *ca.*

2081 to 1836 Ma (Rainaud *et al.*, 1999; Master *et al.*, 2005). This terrain is composed of the Lufubu Schists and overlying quartzites of the Muva Supergroup. This magmatic arc is comprised of tonalitic-granodioritic gneisses (Mkushi) and granitoids (Mufulira, Samba, Chambishi; Rainaud *et al.*, 2002), and are interpreted as the intrusive equivalent of the intermediate-acid calc-alkaline metavolcanics of the Lufubu schists (Rainaud *et al.*, 2002).

A Mesoarchaean terrain underlies the Palaeoproterozoic magmatic arc (Rainaud *et al.*, 2002, 2003). The age of this Mesoarchaean terrain was determined by U-Pb SHRIMP analyses, at *ca.* 3.2 Ga, from detrital zircons from the Muva Supergroup, as well as from a xenocrystic Mwashya lapilli tuff from Likasi (Rainaud *et al.*, 2002, 2003). This terrain is interpreted to underlie the central part of the Lufilian arc (Rainaud *et al.*, 2002, 2003). The Palaeoproterozoic volcanic arc terrain is also intruded by granitoids, such as the Nchanga Red Granite, dated at *ca.* 880 Ma (U-Pb SHRIMP analyses; Armstrong *et al.*, 1999, 2005). The basement outcrops in the Zambia Copperbelt, and is mostly covered by younger Katanga Supergroup metasediments in the DRC (Figure 3.2).

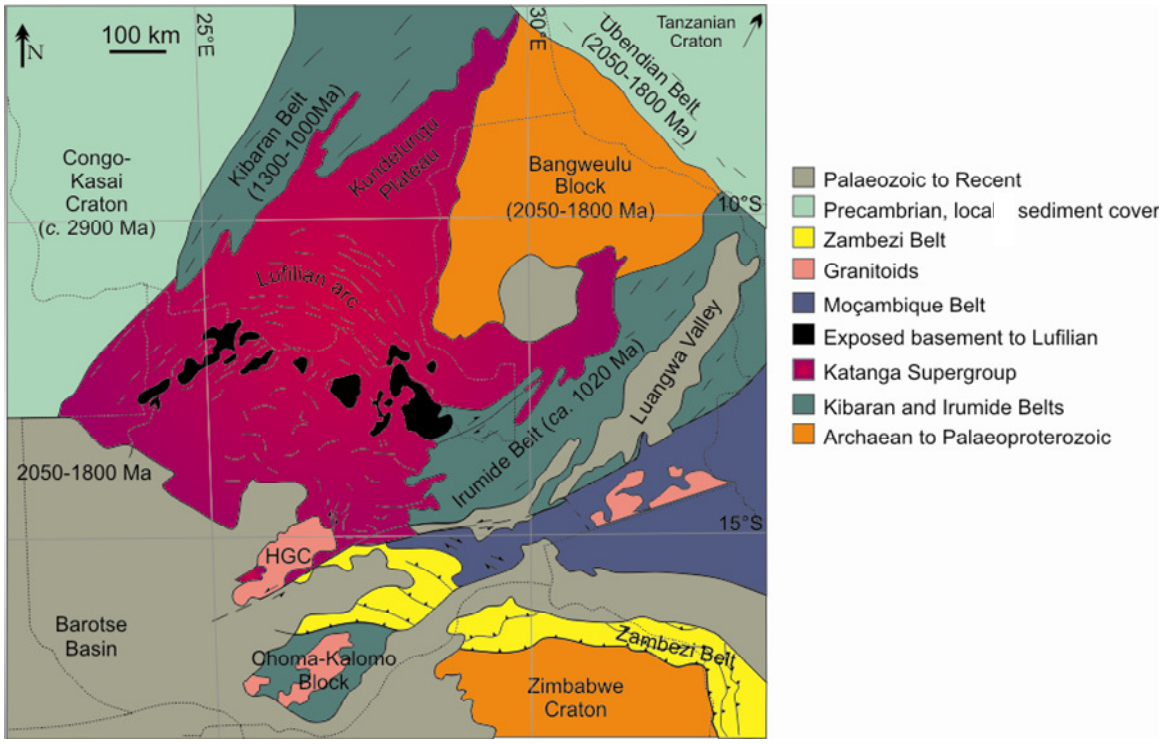

Figure 3.2 Regional geology of Zambia and neighbouring countries showing major crustal components (Walraven and Rumvegeri, 1983; Porada, 1989, Delhal, 1991; Binda and Porada, 1995; Rainaud et al., 1999).

3.1.2 Katanga stratigraphy

The Katanga Supergroup stretches across the border between Zambia and the DRC, and the initial stratigraphic correlation between the two sides was complicated by different nomenclature on either side (Gray, 1930; Robert, 1956). Several attempts were made over the years to rename the units and to correlate the lower Roan from north to south over the Congo-Zambia border (Binda and Mulgrew, 1974; Binda, 1994; Cailteux *et al*., 1994, 2005b, Cailteux, 2003).

In the Congo, the stratigraphy in the Katanga area was initially classified into the *Groupe du Katanga* which consisted of the Roan-, and overlying Kundelungu Supergroups (Bartholomé *et al*., 1973). The Roan Supergroup was divided into the *Roches Argilo-Talqueuses* (RAT) Group, the *Série des Mines* (Mines Group), and the uppermost Dipeta Group.

In Zambia, the Katanga Sequence was divided into the Mine Series (which contained the Lower Roan-, Upper Roan-, and Mwashia Groups), and the overlying Kundelungu Series (containing the Lower-, Middle-, and Upper Groups) as illustrated in Mendelsohn, (1961a). The Mine Series in Zambia was separated from the Kundelungu Series at the occurrence of a tillite, the so-called *Grand Conglomerát*. The strata of the lower Roan to lower Kundelungu were deposited in a rift environment (Annels, 1984), prior to northward thrusting and folding that occurred during upper Kundelungu times (Wendorff, 2003; Cailteux *et al*., 2005a).

Wendorff (2003) proposed the naming of a new lithostratigraphic unit, the Fungurume Group (Figure 3.3), and added this unit to the three major lithostratigraphic units of François (1974, 1995) namely the Roan, Nguba, and Kundelungu Groups (Cailteux *et al*., 2005b). Wendorff (2003) took the syn-orogenic sedimentary megabreccias and olistostromes (sub-aqueous sediment gravity flows) as the base of the Fungurume Group, and divides the Katanga Supergroup in Zambia into the Roan-, Guba-, and Kundelungu Groups (Wendorff, 2005), and into the Guba-, Fungurume-, and Plateau Groups in the DRC (Figure 3.3). The Guba Group of Wendorff (2003, 2005) is the Nguba Group of François (1974, 1995), and will be referred to from here on as the Nguba Group. In contrast to the stratigraphic framework by Wendorff (2000a, 2003, 2005), the R.A.T. is not viewed as having resulted from erosion of thrust fronts with subsequent deposition in a foreland basin by Cailteux *et al*., (2005b), and Kampunzu *et al*., (2005). The statement by Wendorff (2000a) that the R.A.T. and Mines Subgroups should be seen as two distinct tectono-sedimentary units is refuted by Kampunzu *et al*., (2005), indicating that the geochemical signatures of both the R.A.T. and Mines Subgroups show the same

provenance and depositional environment, and therefore, can not be viewed as two separate units.

The stratigraphic position of the transition between the lower and upper Roan has not always been clear, mainly due to the occurrence of lateral facies changes throughout the Copperbelt, hampering the correlation of various stratigraphic levels across the southwest to the northeast along the Kafue anticline (Mendelsohn, 1961a; Binda and Mulgrew, 1974). The Grand Conglomerat, previously signalling the start of the Lower Kundelungu Supergroup, is now interpreted as part of the Nguba Group, with overlying Petit Conglomerat as the base of the Kundelungu Group.

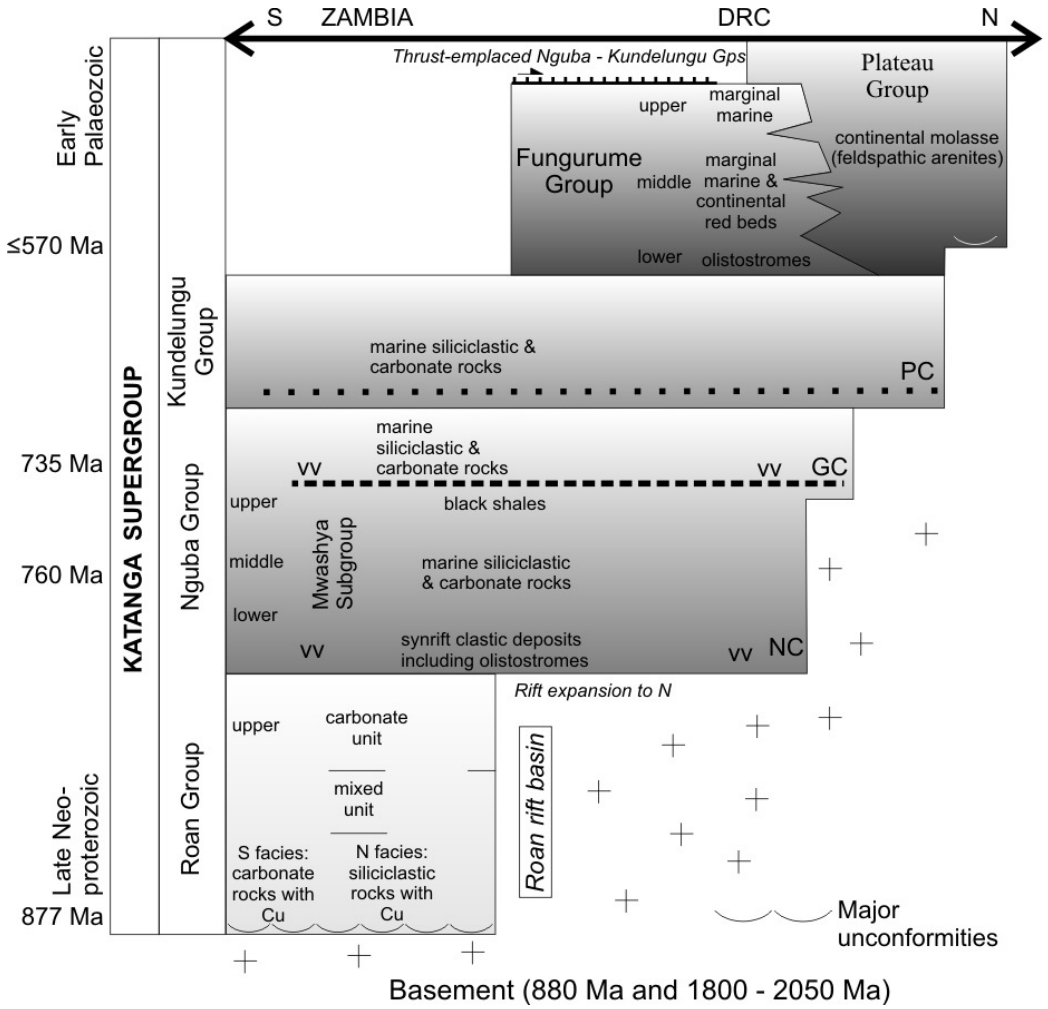

Figure 3.3 Stratigraphic correlation of the Katanga Supergroup between Zambia and the DRC according to Wendorff, 2005). GC: Grand Conglomerat; PC: Petit Conglomerat; NC: Nzilo Conglomerat; VV: rift volcanics.

3.1.3 Katanga deposition

The Palaeoproterozoic basement acted as provenance to the sediments at the base of the Roan Group (Master *et al.*, 2002). The valleys, formed by erosion of the basement, were initially filled with conglomeratic, arkosic, and arenaceous siliciclastics. Deposition of the Katanga Supergroup commenced in local basins during crustal extension as the sediments of the basal Roan Group, which is discussed below (Raybold, 1978; Annels, 1984; Wendorff, 2005). These basins, which include the Konkola, Chambishi, and Roan basins, were defined by the basement topography (Mendelsohn, 1961a). The onset of Katanga sedimentation is apparent in some areas in Zambia as a boulder conglomerate at the base of the lower Roan Group, non-conformably overlying the basement (Figure 3.4). In Zambia, the basal Roan Group is succeeded by the Nguba and Kundelungu Groups.

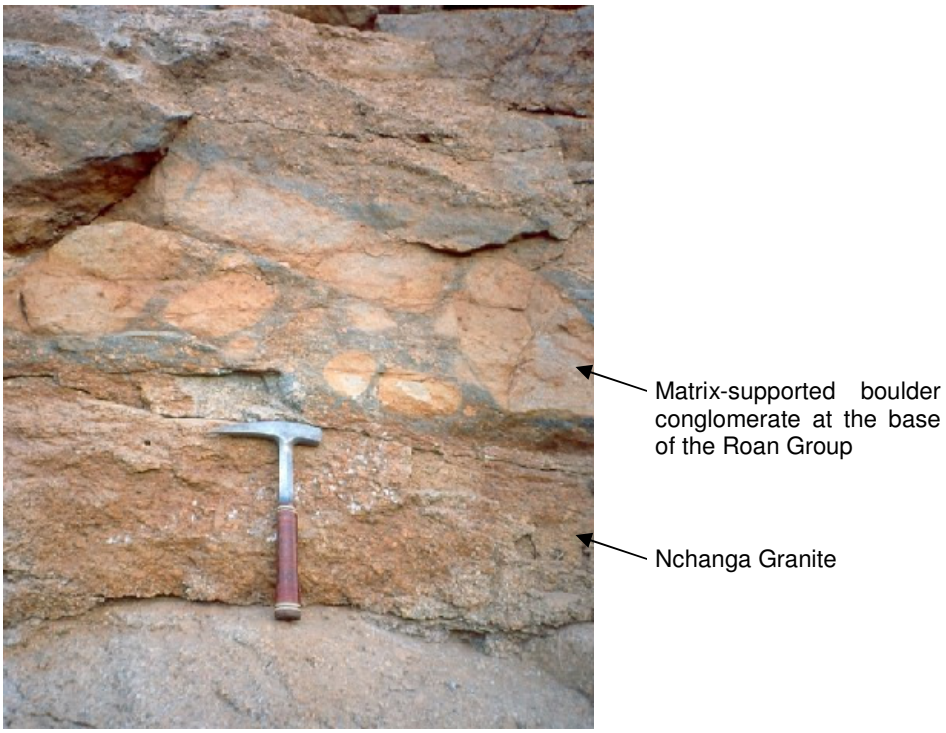

Figure 3.4. The base of the Katanga Supergroup marked by a non-conformity, exposed in the Nchanga Mine open pit.

The Roan Group

The age of Katanga sedimentation is constrained at between 880 Ma and 575 ±5 Ma ($^{40}Ar/^{39}Ar$ age on detrital muscovites of the Plateau Group – at the top of the previously called Upper Kundelungu Supergroup; Master *et al.*, 2002). The lower Roan is divided

into a boulder conglomerate at the base, followed by quartzites, a second conglomerate, and sandstones (Binda and Mulgrew, 1974). Hereafter, the first regional marine transgressive period of the Katanga is marked by the onset of shallow marine siliciclastics of the so-called Ore Shale. The Ore Shale is a silty- to carbonaceous argillite, varying in thickness of between 5 to >50 m, and can be followed throughout the Copperbelt for ~100 km from the Luanshya and Chambishi basins around the Kafue anticline to the Mufulira syncline (Figure 3.1). The colour of the Ore Shale varies laterally from grey-green to black in the south-western orebodies. The greywacke in the Mufulira syncline is taken as the Ore Shale equivalent, and is divided into three horizons, comprising wackes, arenites, argillites and dolomites. The ore-bearing greywackes at Mufulira are interpreted as the near-shore, coarser-grained facies of the Chambishi basin Ore Shale, deposited synchronously across the Kafue anticline during a major marine transgression (Binda and Mulgrew, 1974; Binda, 1994). However, Annels (1984) indicated the presence of a depositional hiatus at the top of the Ore Shale to the top of the lower Roan Group.

Overlying the Ore Shale horizon, are cross-bedded quartzites, argillites, and dolomites (Mendelsohn, 1961a), as well as a coarse arkosic (feldspathic) quartzite layer. A second transgression is present at the base of the upper Roan, which is dominantly comprised of argillaceous carbonates.

Coastal subkhas are indicated by the algal mats and dolostones of the Roan Supergroup in the DRC (Cailteux, 1983). The presence of evaporites in the Katanga Supergroup is further evidenced according to Jackson *et al.* (2003) by pseudomorphs of gypsum and anhydrite (De Magnée and François, 1988); anhydrite in the Roan clastics in Zambia (Garlick and Fleischer, 1972); by $MgCl_2$-$CaCl_2$-NaCl-KCl-bearing fluid inclusions from Shinkolobwe (Audéoud, 1982); by stratigraphic gaps representing dissolved horizons of evaporites in the DRC (De Magnée and François, 1988; Cailteux *et al.*, 1994).

The Nguba Group

Overlying the upper Roan Group is the Mwashya Subgroup of the Nguba Group. In the DRC, the Mwashya Subgroup non-conformably overlies the Kibaran basement with the Nzilo Conglomerate (François, 1995, Wendorff, 2000b, 2002, 2003). In the Kafue anticline region in Zambia, the Mwashya overlies the Roan with a paraconformity. Traditionally, the Mwashya was included within the Roan Group (Wendorff, 2003). The Mwashya Subgroup marks another transgression where sedimentation occurred in a marginal marine environment, under increasingly anoxic conditions, and consists of mainly black carbonaceous shales, algal dolomites, ironstones, with minor occurrences of quartzites (Mendelsohn, 1961a; Lefebvre, 1978; Wendorff, 2003). A U-Pb zircon age of

ca. 760 Ma was obtained from lower Mwashya volcaniclastics and lavas, deposited during rifting (Key *et al.*, 2001).

The first glacial diamictite, named the *Grand Conglomerat*, of the Katanga Supergroup is located within the Nguba Group (Wendorff, 2005), and is traceable throughout the southern and northern Copperbelt region (Bateman, 1930; Gray, 1930; Robert, 1956). It is stratigraphically correlated with extension-related volcanic rocks of the Katanga, yielding an age of *ca.* 735 Ma (Key *et al.*, 2001; Wendorff, 2005). This tillite is widely accepted as corresponding to the Sturtian glaciation (Robb *et al.*, 2003; Robb, 2005), and consists of unsorted angular fragments of granite, quartzite, and dolomite in an argillaceous-carbonaceous matix (Mendelsohn, 1961a). The *Grand Conglomerat* is succeeded by the cap carbonates of the Kakontwe limestones and dolomites, which is then overlain by shales.

The Kundelungu Group

The base of the Kundelungu Group is marked by the second glaciogenic horizon in the Copperbelt, the so-called *Petit Conglomerat* (Gray, 1930; Robert, 1956, Wendorff, 2005). This horizon may be correlated with the Marinoan glaciation (Bodiselitsch *et al.*, 2005). Marinoan glaciations are recognised in the diamictites of the Ghaub Formation of northern Namibia, the Elatina Formation in South Australia, and the Ice Brook Formation in northwest Canada (Rice *et al.*, 2003). The tillite horizon at the base of the Kundelungu is overlain by the *Calcaire Rose* cap carbonates in the DRC, and shales and feldspathic quartzites (Mendelsohn, 1961a).

3.2 Metamorphism and tectonics

The Katanga sediments were metamorphosed during the Pan-African Lufilian orogenic event at *ca*. 600-500 Ma (Mendelsohn, 1961b) to greenschist facies in the Copperbelt region in Zambia, and to amphibolite facies in the Solwezi area to the west of the Copperbelt. In the Copperbelt region, the Roan-Muliashi basin in the south exhibits the highest metamorphic grades at epidote-amphibolite facies. The metamorphic grade generally decreases to the northeast, towards the DRC (Mendelsohn, 1961b). The arcuate shape of the Lufilian arc is due to Pan African deformation with folding vergence to the northwest, where sediments were thrust in a north- to north-easterly direction against the basement of Kibaran massif in the northwest and the Bangweulu Block granite massif in the northeast (Figure 3.2). To the southeast, the Lufilian Arc is bounded by the Mesoproterozoic Irumide Belt. The basement to the Katanga also exhibits the

effects of greenschist-amphibolite grades of metamorphism, with distinct foliations developed in the schists of the Lufubu metavolcanics. There has been some evidence of long-lasting retrograde metamorphism of the basement during Lufilian orogenesis (Garlick, 1961b; Mendelsohn, 1961b).

Even though bedding, and cross-bedding, may still be observed, metamorphism of the Katanga Supergroup has resulted in the general resetting of original sedimentary features such as diagenetic overgrowths, and has led to the development of foliation in the less competent argillaceous rocks. Effects of regional metamorphism are observed in the presence of recrystallised textures and minerals such as clay minerals that were recrystallised to sericite or biotite, and the replacement or cementation of small quartz grains with interstitial silica (Garlick, 1961b). Common metamorphic minerals found in the Roan Group include scapolite, tourmaline, tremolite-actinolite, epidote, and apatite (Mendelsohn, 1961b). The presence of abundant quartz veins in the Katanga, not related to granite intrusives, was attributed to metamorphic processes by Garlick and Brummer (1951). These quartz veins were classified according to their orientations and occurrence (Mendelsohn, 1961b).

Biotite-kyanite-garnet gneisses and garnet amphibolites from within the Solwezi Dome, talc-kyanite (white) schists from within the Kabompo and Mwombezhi Domes and whiteschists from the rims of the Solwezi Dome in the Lufilian Arc studied by John *et al.*, (2004), yield peak metamorphic conditions of 750°C ± 25 °C at pressures of around 13 kbar ± 1 kbar. These whiteschists (talc-kyanite schists) are considered as the base of the Roan Group in the Dome region of the Lufilian Arc, where a sheared contact is interpreted between the basement and the lower Roan Group of the Katanga Supergroup. According to John *et al.*, (2004), the clockwise P-T paths indicated from these samples record the crustal thickening during Pan-African 529 ± 2 Ma and 531 - 532 ± 2 Ma of the Lufilian Arc - Zambezi belt. This crustal thickening is related to the collision between the Congo and Kalahari cratons during Gondwana assembly (John *et al.*, 2004), with cooling after peak orogenesis of *ca.* 6°-7 °/ Ma.

3.3 Mineralisation

The Central African Copperbelt (CAC) is comprised of polymetallic and polygenetic mineralisation types. This includes stratiform sediment-hosted Cu-Co mineralisation (e.g. Nchanga, Mufulira), Zn-Pb-(Cu-Cd-Ag-Ga-Ge-Mo-Co-W-Ni) deposits such as Kabwe and Kipushi (Kamona, 1993; Kampunzu *et al.*, 1998) formed after the SSC styles of mineralisation and are concentrated in discordant, but broadly stratiform pipe-like settings. Mineralisation at Kipushi is dated at 451.1 ± 6.0 and 450.5 ± 3.4 Ma (concordant

ages, from Rb-Sr and Re-Os dating, Schneider *et al*., 2007). This post-(Pan-African Lufilian) orogenic age reveals mineralising solutions in an extensional environment (Schneider et al., 2007). In addition to these mineralisation styles, a variety of ferruginous, discordant, vein and intrusion related Cu-U-(Au-Ag-Mo-Co) deposits occurs both within the confines of the Lufilian Arc, as well as in the proximity of Pan-African (500 Ma) aged granitoid-syenite-gabbro intrusions well outside the belt, e.g. Kansanshi, (Speiser *et al*., 1995), Cu-U Shinkwelobwe (Cahen and Snelling, 1984; Audeoud, 1982). A variety of ores are also found in the basement to the Katangan (Schneiderhöhn, 1932; Wakefield, 1978; Kamona 1993 and references therein). Stratiform, Cu-Co dominated mineralisation is still regarded as the economically most important style of mineralisation in the CAC.

Stratiform copper-cobalt mineralisation in Zambia and the DRC is mainly hosted in the lower Roan Group, but minor occurrences of mineralisation are also found in the overlying Nguba Group. Ore minerals are mostly sulphides (including chalcocite, bornite, chalcopyrite, carrollite, and pyrite), and secondary oxides and silicates (malachite, cuprite, azurite, chrysocolla). The chalcocite - bornite - chalcopyrite assemblage is often zoned away from basement highs and upwards in the mineralised succession.

Mineralisation is hosted throughout the Roan and Mwashya Groups. In the lower Roan Group in Zambia stratiform mineralisation is generally hosted in the Ore Shale, in bedding parallel units locally, but discordant at a regional scale (Unrug, 1988), traceable from Konkola in the northwest to Luanshya in the southwest along the western side of the Kafue anticline. The Ore Shale consists mostly of silty, micaceous (biotite or sericite ± muscovite), calcareous grains, with quartz, feldspar, carbonate, Cu-Fe sulphides, chlorite and organic carbon. The thickness varies from 5-20 m, and sulphides are generally disseminated through the Ore Shale, with concentrations along bedding planes (Mendelsohn, 1961a). Along the eastern side of the Kafue anticline in the Mufulira syncline, the ore-bearing horizons are greywackes, arenites, dolomites and argillites (Binda and Mulgrew, 1974). In addition to these host lithologies, stratiform mineralisation also occurs in conglomerates, calc-arenites, dolomitic siltstones, argillaceous dolomites, and at Shituru, in tuffaceous volcanic rock. Alteration includes silicification, feldspathization, sericitization, tourmalinization and dolomitization.

Early tectonic – structurally controlled, Pb-Zn-Cd dominated mineralisation is associated with carbonate host rocks at various stratigraphic levels in the Katangan succession. Mineralisation is discordant and ore bodies are often pipe-like or lode controlled. Fluid flow was episodic and yielded a complex, diverse paragenesis. Mineralisation nevertheless pre-dated the regional Pan-African compressive deformation and metamorphic climax at ca. 530 Ma (John *et al*., 2004, also see Hanson *et al*., 1993).

Also represented in this category of deposits is the shear-controlled Cu-vermiculite (décollement) mineralisation evident, for example, in the Nchanga open pit. There are no absolute age determinations for this style of mineralisation, but it is thought to post-date the stratiform mineralisation (possibly at ca. 650 Ma).

Late tectonic – structurally controlled Fe-Cu-Au-Ag-U±PGE dominated mineralisation is now known to be related to the metamorphic climax in the region and coincides with the intrusion of numerous alkali granite-syenite-gabbro intrusions at either 760 Ma or 510 Ma (Key *et al*., 2001). This style of mineralisation has similarities to the Fe oxide-copper-gold (or IOCG) type of ore deposit that is currently regarded world-wide as a very prospective target, but in Zambia are more likely to be skarnoid in nature. Mineralisation can often be demonstrably linked to Pan-African aged intrusions as well as large bodies of hydrothermal magnetite/hematite, milky quartz and breccia. In some cases (e.g. Kansanshi) a magmatic intrusion is not observed directly, and mineralisation is manifest as steeply dipping vein stockworks (possibly above an intrusion).

3.3.1 Ore genesis controversies

Theories on the genesis of mineralisation of the stratiform copper-cobalt ores have caused much debate throughout the history of the Copperbelt. Initially, the ores were thought of as epigenetic, and were attributed to hydrothermal fluids derived from granitic and pegmatitic intrusions (hydrothermal-magmatic, Gray, 1932; hydrothermal-metasomatic, Darnley, 1960). However, these intrusions were later shown to predate Katangan sedimentation, and were identified as the basement on which the Katanga Supergroup was unconformably deposited (Schneiderhöhn, 1932; Garlick and Brummer, 1951; Garlick and Fleischer, 1972).

A syngenetic model of stratiform mineralisation was advocated by Garlick (1953, 1961a, 1989 and references therein), and Garlick and Fleischer (1972), where hydrogen sulphide, available from anoxic marine environments facilitated the chemical precipitation of insoluble copper and cobalt sulphides, together with iron sulphides. The zoning of metals observed in the Copperbelt was explained as syngenetic with the interpretation that Cu-rich mineral species would precipitate closest to the palaeo-shoreline, grading into Fe-rich species offshore. This zoning of chalcocite-bornite-chalcopyrite-pyrite was distributed parallel to the palaeo-shoreline, and was influenced by marine transgressions and regressions. A syngenetic model of detrital transportation (Binda, 1975) and deposition of Cu sulphides was also invoked as explanation for mineralised arenitic ore horizons. Sweeney *et al.* (1991) and Sweeney and Binda (1994) proposed that ore formation was primarily due to bacterial reduction of seawater sulphate during early

diagenesis. They suggested that the pre-Katangan basement was the source of metal rich solutions. Annels *et al*., (1983), Annels (1984), and Annels and Simmonds (1984) indicated that metal sulphides were precipitated diagenetically, and that sulphate was available either from diagenetic anhydrite, or sulphate-rich interstitial connate waters.

Localised, epigenetic mineralisation due to thermochemical sulphate reduction was proposed by McGowan *et al.* (2003, 2006) for the Nchanga orebodies based on the varying sulphur isotopic signatures of diagenetic pyrite and copper-cobalt sulphides. The presence of methane in arenite horizons acted as the reducing agent for hydrothermal metal-rich brines, which migrated during deformation of the host rocks.

Generally, stratiform copper mineralisation is thought to be diagenetic, and pre-deformational in origin and related to rocks within which fluid mixing and strong redox fluctuations have played a role in metal precipitation. Variations on the exact stage of diagenesis remains, with some researchers favouring late-diagenesis specifically on the Zambian side (Selley *et al*., 2005), and some favouring early (to intermediate) diagenesis, specifically on the DRC side at Kamoto, Musonoi, Luiswishi (Muchez *et al*., 2008 and references therein). In the DRC stratiform mineralisation is located in highly deformed, allochthonous sedimentary mega-rafts and was in place prior to deformation and northward transport of the allochthons. Mineralisation will be associated with rocks that are stratigraphically below the Grand Conglomérat, and located in virtually any of the lithotypes that are characterized by a redox barrier. Rapitan banded iron-formations, bedded Mn deposits and metal-rich carbonaceous black shales should also be regarded as stratiform (and stratabound) styles of potential mineralisation in the CAC. Absolute age determinations of this style of mineralisation are not available.

3.4 Previous fluid inclusion studies in the Central African Copperbelt

Previous fluid inclusion studies in Zambia and the DRC include work by Pirmolin (1970), Audeoud (1982), Cunningham (1986), Sweeney (1987), Richards *et al.* (1988a), Speiser *et al.* (1995), Kamona (1993), Kampunzu *et al*., (1998), Dewaele *et al*., (2006a,b), McGowan *et al.* (2006), El Desouky *et al*., (2008a,b). A summary of the main results is presented in Table 3.1, with the section below outlining the main findings of each of these studies.

Pirmolin (1970)

Pirmolin (1970) described fluid inclusions from an unmineralised cherty dolomite layer of the Mines Group of the Roan Supergroup at Kamoto, in the DRC, and concluded that solutions reached temperatures of ~200°C with salinities of ~40 wt. % $NaCl_{equiv}$.

Audeoud (1982).

Epigenetic fluids from the Kamoto, Kambove and the Shinkolobwe deposits were studied by Audeoud (1982). Fluid inclusions were hosted in dolomite, and contained CO_2 and CH_4 in the gaseous phases. Aqueous phases were highly saline with >60 wt.% $NaCl_{equiv}$., and comprising Na, K, Ca, Mg-sulphates, with phosphates, carbonates, and chlorides.

Cunningham (1986)

Cunningham (1986) is quoted in Annels (1989) as reporting homogenisation temperatures of between 130 and 165 °C for veins associated with early pyrite and carrollite at the Chambishi deposit. Salinities for these fluids were calculated to between 9 and 16 wt.% $NaCl_{equiv}$. Later copper sulphides are linked to the fluids with homogenisation temperatures of 125 to 145 °C and salinities between 16 and 22 wt.% $NaCl_{equiv}$.

Sweeney (1987)

Crosscutting quartz veins at the Konkola and Chambishi Cu-Co deposits were studied by Sweeney (1987). These veins had undergone at least one post-formational tectono-thermal event. Scanning electron microscopy of decrepitated inclusion cavities showed the presence of Na, Al, Si, S, U, K, Ca, Fe, Cu, and Co, as well as KCl and NaCl daughter minerals. Gas analyses of decrepitated inclusions revealed the presence of CO_2, CH_4, and N_2. It was concluded that the veins formed by lateral migration of fluids during late diagenetic dewatering.

Richards et al. (1988a)

Richards *et al.* (1988a) indicated the presence of a sylvite and halite-saturated fluid in quartz-hematite-rutile veins hosted in the footwall sediments of the Musoshi copper deposit (DRC), where late hydrothermal veining caused extensive footwall- and ore shale- alteration. Fluid inclusions were found to consist of NaCl, KCl $\pm CO_2$. This hydrothermal event postdates stratiform copper mineralisation and is linked to compressional deformation and metamorphism during the Lufilian orogeny. They estimated the maximum homogenisation pressure at 1.2 kbar, which is the typical pressure for decrepitation of 12-13µm size fluid inclusions in quartz (Leroy, 1979).

Table 3.1 Comparative data from fluid inclusion studies conducted in the Central African Copperbelt

	Pirmolin (1970)	**Audeoud (1982)**	**Sweeney (1987)**	**Richards *et al.* (1988)**	**Kamona (1993)**	**Speiser *et al.* (1995)**	**Kampunzu *et al.* (1998)**	**McGowan *et al.* (2006)**	**Dewaele *et al.* (2006a)**	**Dewaele *et al.* (2006b)**	**El Desouky *et al.* (2008a)**	**El Desouky *et al.* (2008b)**
Area	Kamoto, DRC-Copperbelt	Kamoto Kambove Shinkolobwe, DRC	Konkola, Chambishi, Z-Copperbelt	Musoshi, DRC-Copperbelt	Kabwe, Central Zambia	Kansanshi, Solwezi, NW Zambia	Kipushi D.R.C.	Nchanga, Zambia	Musonoi, Kamoto DRC	Dikulushi, NE Kundelungu Foreland	Lufukwe Anticline, NE DRC	Dikulushi area NE DRC
Lithology	Mines Group, Roan (lower Roan Group)	R.A.T. (lower Roan Group)	lower Roan Group	lower Roan Group	Nguba Group (lower Kundelungu)	Nguba Group (lower Kundelungu)	?	lower Roan	R.A.T (lower Roan Group)	Lower Kundelungu	Nguba Group, DRC	Ngule Subgroup, Kundelungu Group
Host minerals	Cherty dolomite	dolomite	quartz veins	quartz-hematite-uraninite veins	dolomite	quartz veins	?	vein quartz	authigenic quartz	sphalerite, dolomite, quartz, barite and calcite	authigenic and detrital quartz	authigenic quartz overgrowths
Setting	Epigenetic stratiform Cu	Epigenetic Cu-U	Late diagenetic stratiform Cu	Epigenetic U-Pb hydrothermal	Epigenetic Pb-Zn	Epigenetic Fe-ox-Cu-Au	Epigenetic Pb-Zn	Epigenetic	Stratiform Cu-Co	Vein-type (1)Zn-Pb-Fe-Cu-As (2) Cu-Ag	hypogene Cu-Ag	hypogene, stratiform Cu
Fluid Composition	~40 wt.% NaClequiv.	>60 wt.% NaCl equiv. CO_2, CH_4 Na, K, Ca, Mg	H_2O, KCl, NaCl, CO_2, CH_4, N_2	H_2O, KCl-NaCl-$CaCl_2$-$FeCl_3$-CO_2, 39 wt.% NaCl, 15 wt.% KCl	11-31 wt.% NaClequiv.	H_2O, NaCl-$CaCl_2$-CO_2-(CH_4)	?	H_2O-$CaCl_2$-$MgCl_2$-NaCl	H_2O-NaCl 8.4-18.4 wt.NaClequiv.	(1)Ca-Na-Cl (2)Na-Cl-H_2O	(1)H_2O-NaCl-$CaCl_2$ (2)H_2O-NaCl	H_2O-NaCl-$CaCl_2$
Pressure (kbar)	?		?	<1.2	0.09	1.2 - 2.5	?	-	-	-	~1.7-3.3 km	-
Temperature (≥Th ℃)	?		120	~397 ~275	257-305	230 - 310	ca. 300	105-300	80-192℃	(1) 135-172 ℃ (2) 46-82 ℃	(1) 80-130 ℃ (2) 120-180 ℃	(1) 111-182 ℃ (2) 120-280 ℃

Speiser et al. (1995)

Epigenetic iron-oxide-Cu-Au type mineralisation at the Kansanshi Copper Mine (Solwezi area, north-western Zambia) was studied by Speiser *et al.* (1995). Hydrothermal veining at Kansanshi is connected with alteration of the host rocks, and mineralised (Cu-Mo-Fe) veins have been dated at ~503-511 Ma (Re-Os and U-Pb of molybdenite and monazite) by Torrealday *et al.* (2000). Fluid inclusions hosted in quartz veins, contemporaneous with hydrothermal veining and alteration, are composed of H_2O-NaCl-$CaCl_2$-CO_2-CH_4 at minimum trapping temperatures between 230-310 °C. Trapping pressures range between 1.2 and 2.5 kbar. Mineralisation at the Kansanshi Mine may also correspond to mineralisation at the Shinkwelobwe Mine (Cu-U), which is dated at 602 Ma (U/Pb, Cahen and Snelling, 1984).

Kamona (1993)

Kamona (1993) studied fluids from the epigenetic stratabound carbonate-hosted Pb-Zn Kabwe deposit, central Zambia. These epigenetic deposits are hosted by the Kabwe Dolomite Formation, where mineralising fluids were saline, ranging between 11-31 wt.% $NaCl_{equiv}$, and T_h ranged between 257 and 305°C, corresponding to ore deposition at 320°C.

Kampunzu et al. (1998)

Kampunzu *et al.* (1998) reported high homogenisation temperatures (300°C) from fluid inclusions representative of mineralising fluids from the epigenetic sediment-hosted Pb-Zn Kipushi deposit (~450 Ma, Schneider *et al.*, 2007). This style of mineralisation postdates stratiform copper mineralisation.

Dewaele *et al.*, (2006a)

Fluid inclusions hosted in authigenic quartz associated with stratiform mineralisation in the western part of the Copperbelt are described and show a H_2O-NaCl fluid with minimum trapping temperatures between 80 and 192 °C, with salinities between 8.4 – 18.4 wt.% NaClequiv. These samples were collected from the Roan Group lower orebody (“Roches Siliceuses Feuilletées”), the upper orebody “Black Ore Mineral Zone” from the Musonoi deposit, and from the intermediate orezone “Roches Siliceuses Cellulaires” of the Kamoto deposit in the Democratic Republic of the Congo. Multiphase Cu-Co mineralisation is indicated from this study.

Dewaele et al., (2006b)

Dikulushi Cu-Ag vein-type mineralisation was investigated by Dewaele *et al.*, (2006b) in the NE Kundelungu Foreland. They show that early Zn-Pb-Fe-Cu-As fluids were highly

saline, with Ca-Na-Cl at temperatures of 135-172 °C. Later-stage mineralisation associated with Cu-Ag was found to result from an intermediate saline fluid at lower temperatures (46-82 °C) composed of NaCl-H_2O. These fluids were found in sphalerite, dolomite, quartz, barite and calcite.

McGowan et al. (2006)

McGowan *et al.* (2006) documented fluid inclusions from quartz veins in the basement granite, Lower Arkose unit, Upper and Lower Orebodies, and thrust-related vein quartz from the Nchanga deposits. Homogenisation temperatures of aqueous inclusions were measured between 105 and 300 °C. Except for one inclusion which contained CO_2, all inclusions were aqueous and eutectic melting temperatures indicated $MgCl_2$-$CaCl_2$ and NaCl solutions, with possible Fe present in solution. They invoked the presence of NaCl-saturated (31-38 wt.% $NaCl_{equiv}$) mineralising brines with trapping temperatures ranging between 140-180 °C.

El Desouky et al., (2008a)

Mineralising solutions were investigated at the Lufukwe anticline in the eastern Lufilian Foreland, to the NE of the Copperbelt in the DRC. Authigenic quartz overgrowths and detrital quartz were found in the Monwezi Sandstone of the Bunkeya Subgroup (Nguba Group), where forming fluid temperatures were measured at 80-130 °C and contained a high salinity (18.8-23.4 wt.% $CaCl_2$ equiv) H_2O-NaCl-$CaCl_2$ fluid. Hypogene Cu-Ag fluids were found to have precipitated from a hot (120-180°C), low-moderate salinity (1.9-7.7 wt.% $NaCl_{equiv}$) H_2O-NaCl fluid.

El Desouky et al., (2008b)

Sandstone-hosted stratiform Cu is hosted in the Mwitapile sandstone in the Lufilian foreland to the NE of the Copperbelt, and microthermometry was completed on the authigenic overgrowths. Fluids are found to comprise H_2O-NaCl-$CaCl_2$ at minimum temperatures between 111-182 °C, with salinities between 22.0-25.5 $CaCl_{2equiv}$. Secondary trail inclusions in second authigenic quartz overgrowths reveal a higher temperature fluid minimum trapping temperatures of 120-280 °C and 2.4-19.8 wt.%$NaCl_{equiv}$. salinities.

3.5 Summary

The metallogenic history of the Katanga area is complex, and several mineralisation styles have been documented from stratiform copper-cobalt mineralisation to epigenetic iron-oxide copper-gold occurrences.

Detailed fluid inclusion data of the Copperbelt is scarce and most fluid inclusions in these studies have been hosted in quartz veins. The earliest documented inclusions are described in the work of Pirmolin (1970) and Sweeney (1987). These data indicate that fluids circulated early during the basin evolution, and were saline with moderate homogenisation temperatures. The present study, however, provides information on a vein set in a mineralised setting, where the tectonic and paragenetic relationships are better constrained. Accordingly this study will add to existing knowledge of fluids that circulated and evolved relatively early in the basin evolution by constraining the P-T-υ-X nature of fluids regionally over the basin. The present study also addresses this issue by comparing five deposits located in the Zambian Copperbelt, and is focussed on the implementation of new quantitative analytical techniques, notably Raman microscopy and laser ablation inductively coupled plasma mass spectrometry.

Chapter 4

GEOLOGICAL SETTING OF INDIVIDUAL DEPOSITS IN THE ZAMBIAN COPPERBELT

4.1 Introduction

Five ore deposits in Zambia were selected for the study in order to determine the conditions of fluid flow related to stratiform copper mineralisation and metamorphism in the Copperbelt region. These deposits are found at Chambishi, Nchanga, Mufulira, Nkana, and Konkola and were selected for study as deposits where stratiform Cu ± Co mineralisation is present and regional mineralising solutions circulated within the basin. These deposits are similar in terms of the host sediments, mineralisation styles and general metamorphic grades with localised changes in detailed mineralogy, alteration, and structural settings. Stratiform copper mineralisation is hosted in the metasediments of the lower Roan Group, with some variation in terms of host minerals, number of ore horizons, and metamorphic grade. Four of the five deposits occur along the south-western margin of the Kafue Anticline as illustrated in Figure 3.1, and one deposit (Mufulira) is located on the north-eastern edge of the anticline. Each deposit was studied in order to build a regional fluid character image. This chapter reviews the geological setting, ore mineralogy and general characteristics of each of the five deposits and sets the geological background to the following chapters that present the fluid inclusion results obtained from these deposits.

4.2 The Chambishi deposit

4.2.1 Geological setting of the Chambishi deposit

The Chambishi orebodies are situated along the south-western edge of the Kafue anticline, along the northern rim of the Chambishi-Nkana basin (Figure 3.1 inset). The Katangan metasediments strike east-west in this basin, and dip to the south at about 60° (Garlick, 1961d). They were folded against the basement during Pan African orogenesis, as is evidenced from the asymmetrical folding exposed in the open pit (Figure 4.1).

The basement to the Katanga Supergroup in the Chambishi area is comprised mainly of Muva quartzites and granites (Garlick, 1961d), together with Lufubu granitoids which sub-outcrops in the area (Fleischer *et al*., 1976; Rainaud *et al*., 2005a).

The lower Roan Group metasediments of the Katanga Supergroup overlie the basement and comprise a basal conglomerate, followed by crossbedded Footwall Quartzites, and the Cobble Conglomerate (Figure 4.2). These are succeeded by the Arkose and Argillite Formation, Footwall Conglomerate, the Ore Shale Formation, Hangingwall Quartzite-, Interbedded Quartzite and Argillite-, and Upper Quartzite Formations (Garlick, 1961d).

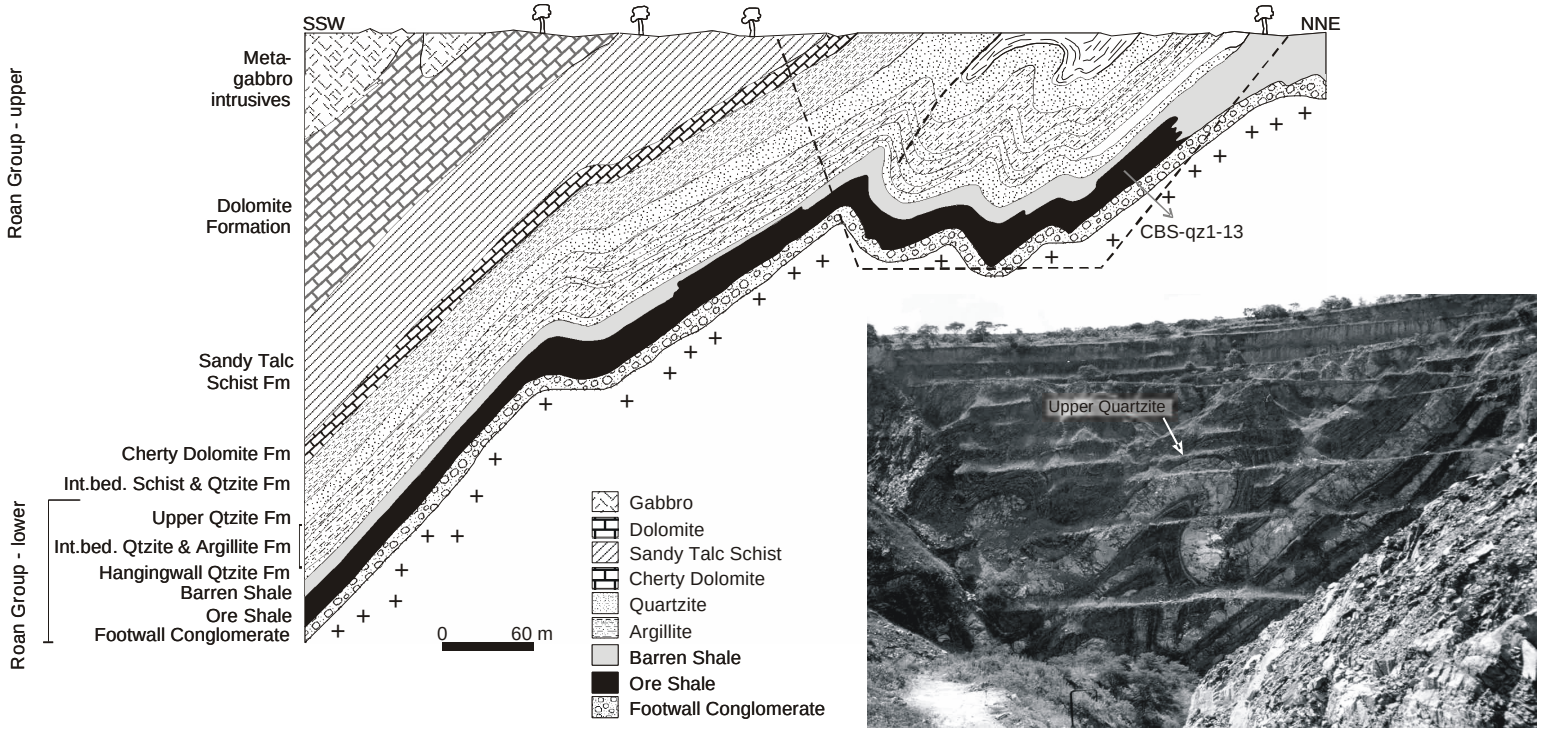

Figure 4.1. Cross section of the Chambishi Main orebody and open pit (from Garlick, 1961d), with visible overturned folding. Samples CBSqz1-13 were collected for the fluid inclusion study from this part of the open pit. The dashed line indicates the rough outline of the abandoned open pit.

The upper section of the Roan Group consists of the Interbedded Schist and Quartzite Formation, comprised of biotitic schists with interbedded crossbedded-ripple marked, feldspathic quartzites, followed by the Cherty Dolomite Formation, Sandy Talc Schist-, and Dolomite Formations. Anhydrite and carbonate muds are present in the topmost Dolomite Formation (Figure 4.2c-d). A meta-gabbroic sill intrudes the upper Roan dolomites in the Chambishi basin. This sill intrudes bedding-parallel to the dolomites, and was probably emplaced prior to, or during, folding (Garlick, 1961d). Overlying this sill are the Upper Dolomites, and the grey argillaceous sediments of the Mwashia. The Mwashia is followed by the tillite of the *Grand Conglomerat*, which is succeeded by the Kakontwe limestones and dolomites, with overlying Kundelungu Shales.

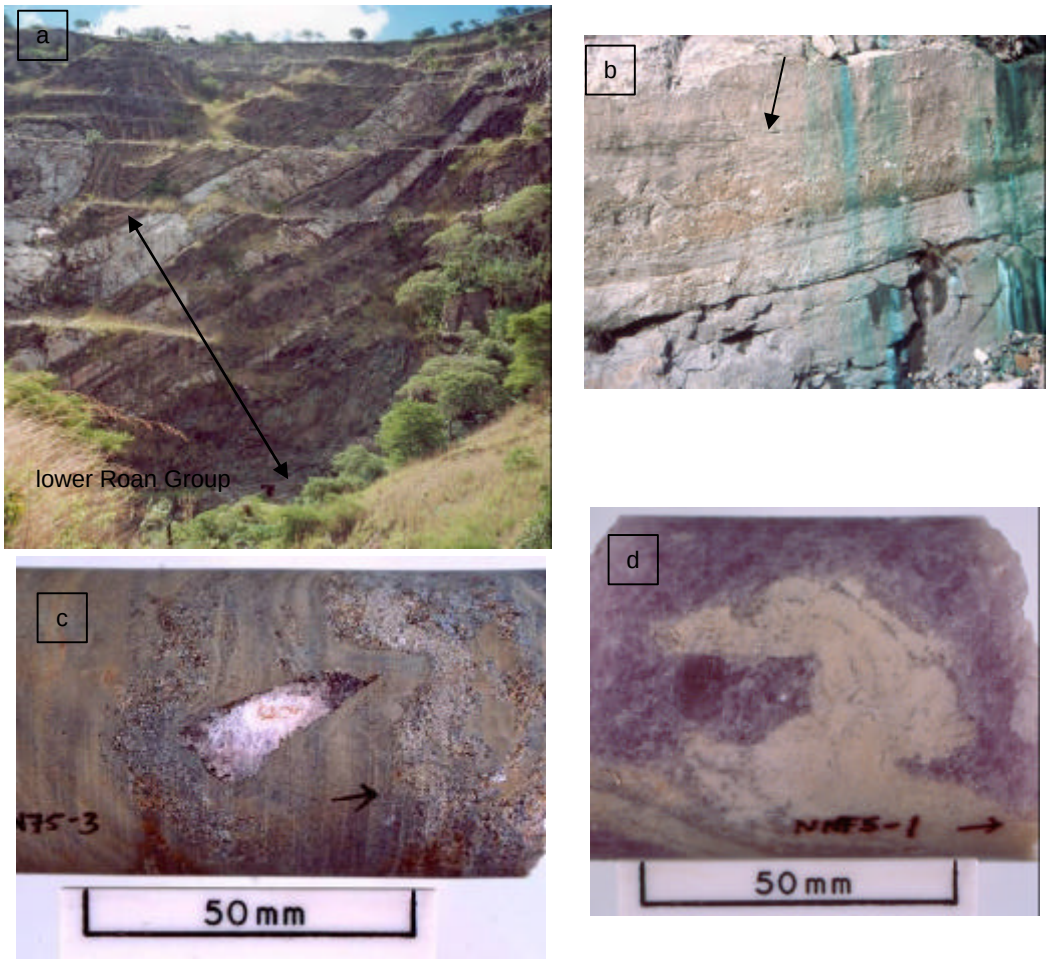

Figure 4.2. (a) The lower Roan Group metasediments, exposed in the Chambishi open pit are folded against the basement; (b) crossbedding in the Footwall Quartzites, with later copper oxidation staining the sediments; (c) rippled shale and grit with purple anhydrite in the upper Roan Group at 772.94m, NN75; (d) chicken-wire texture of anhydrite with thin stringers of carbonate mud in the upper Roan (borehole NN75, 570.45m).

The Katanga sediments have been regionally metamorphosed to low grade greenschist facies in the Chambishi area and the lower Roan rocks are now comprised of mainly fine-grained biotite ± sericite - quartz schists with disseminations of bornite and chalcopyrite (Figure 4.3). As is discussed in Chapter 3, the Katangan sediments were thrusted to the north during regional metamorphism, and asymmetric overturned folds are present in the Chambishi open pit (Figure 4.3). Despite metamorphism, original sedimentary features such as bedding may still be observed. Primary copper sulphide minerals are oxidised to malachite (± azurite, chrysocolla).

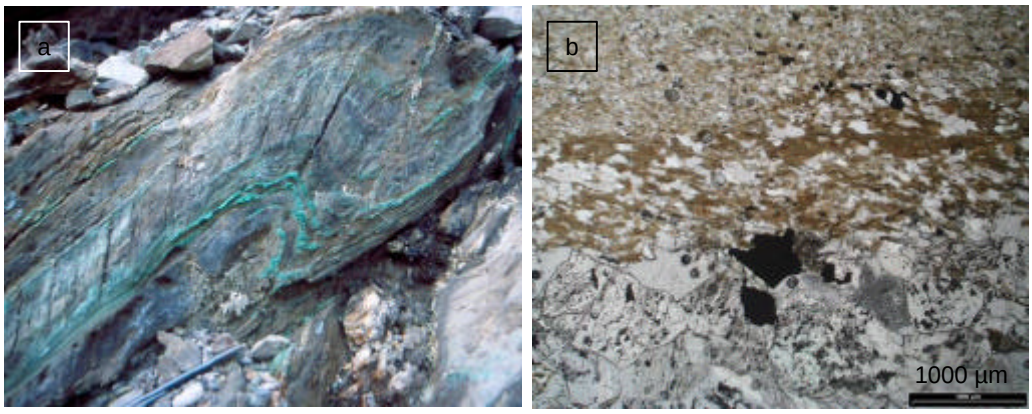

Figure 4.3. (a) The asymmetrically folded Ore Shale Formation, exposed in the Chambishi open pit (looking west), shows the redistribution of secondary malachite along the axial planar surface; (b) transmitted light micrograph of biotite-sericite-carbonate mineral grains (CHM1 TS) in the footwall sediments.

4.2.2 Mineralisation at the Chambishi deposit

Stratiform copper mineralisation

Two main ore bodies are identified in the Chambishi area, namely the Chambishi Main- and the Chambishi West orebodies (Garlick, 1961d, Fleischer *et al*., 1976), in addition to the smaller sulphide deposits in the Chambishi basin which includes the Mwambashi B, Pitanda, and Chambishi Southeast prospects (Annels, 1989). The Chambishi ore bodies are contained within the Ore Shale Formation of the lower Roan Group, and consists of carbonaceous shale, argillaceous siltstone, and interbedded dolomite layers (Figure 4.3 a, b). Stratiform copper mineralisation occurs mostly at the base of the Ore Shale horizon as disseminated and coarse accumulations of bornite and chalcopyrite, with some chalcocite ± digenite (Figure 4.4 a-d). The progressive oxidation

of copper sulphides is illustrated in Figure 4.4 b-d where bornite is replaced by digenite and covellite.

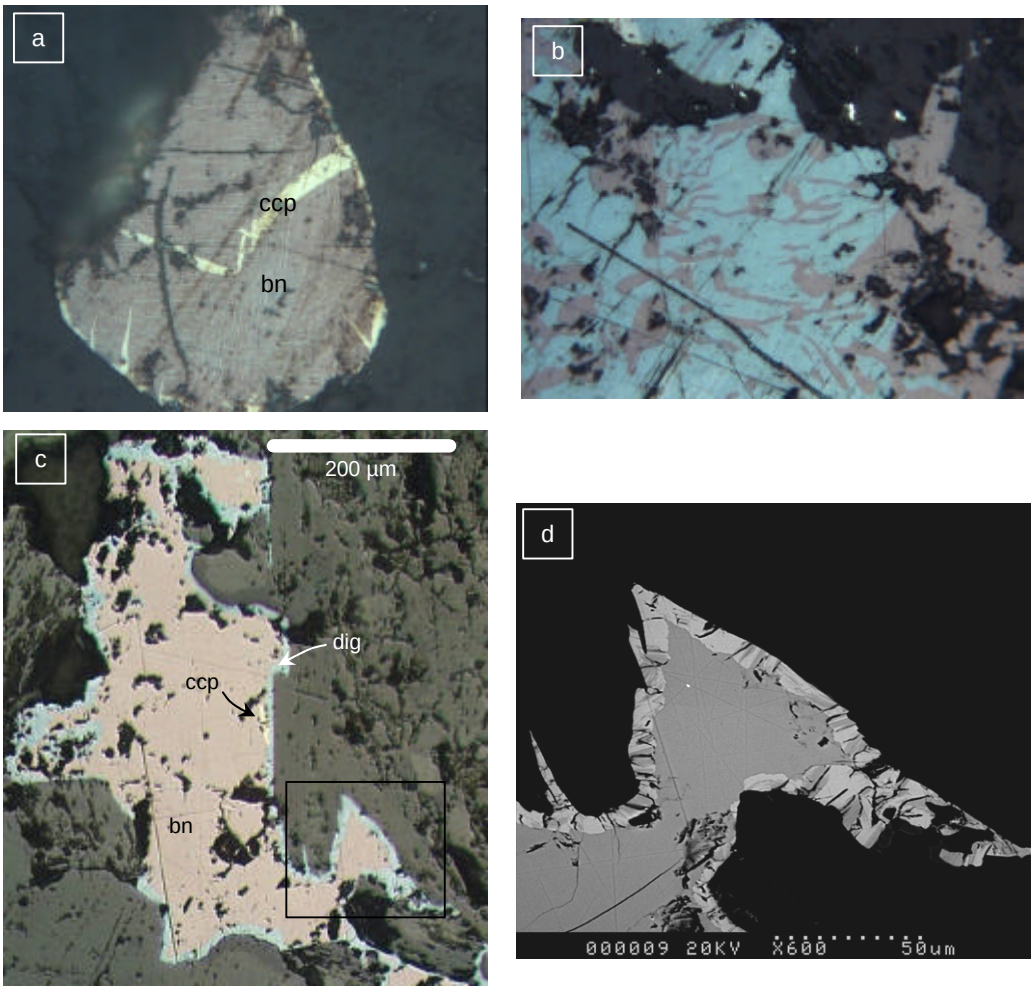

Figure 4.4. (a) Disseminated stratiform copper mineralisation of the Chambishi Ore Shale is present as bornite with chalcopyrite crosshatching and veins (FOV: 150 µm, sample CHM 5D); (b) Bornite replaced by digenite in the Ore Shale (FOV: 260 µm, sample CHM 5D); (c) Bornite rimmed by digenite and by dark blue covellite. The rectangle illustrates the area displayed in (d) under backscattered light during scanning electron microscopy showing alternating digenite and covellite bands rimming bornite (Sample CHM 8BTS). See Appendix III for SEM quantitative elemental analysis.

The primary paragenetic sequence of copper mineralisation is reflected in the assemblage of pyrite – chalcopyrite – bornite – covellite (Figure 4.5 a-c). Primary pyrite grains are rounded and are progressively replaced by chacopyite, and bornite. Covellite is

considered as a supergene product of the primary copper sulphide mineralisation along with malachite (Figures 4.2b and 4.3a).

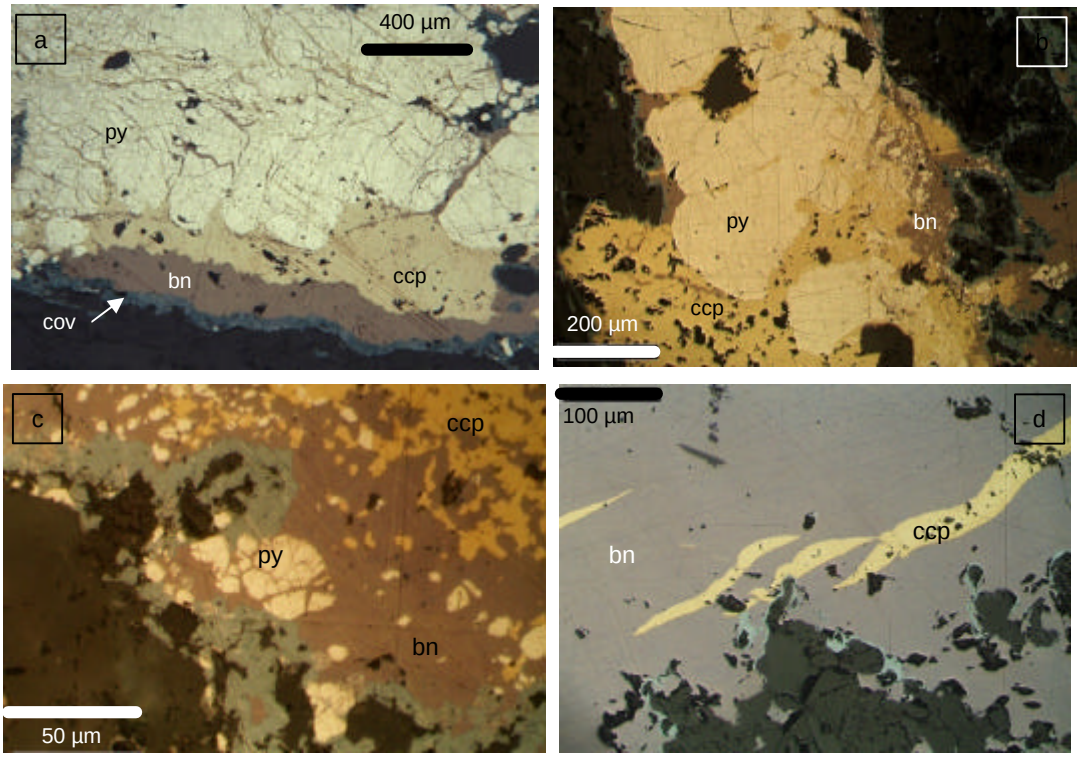

Figure 4.5. Pyrite frequently occurs as rounded grain aggregates with overgrowths of chalcopyrite and bornite. (a) This mineral sequence is illustrated by the presence of massive, fractured pyrite, replaced by chalcopyrite and bornite. Covellite rims are present on bornite mineralisation. (b) Pyrite grains with a rounded appearance replaced by chalcopyrite and bornite (sample CHM 8B). (c) Fractured well-rounded pyrite grains are filled by bornite, and rimmed by digenite. (d) Laths of chalcopyrite appear coeval with bornite. Digenite is present as a later rim on the bornite-chalcopyrite grain (sample CHM 8ATS).

Tellurobismuthinite, rutile and galena are accessory minerals identified with SEM analysis associated with stratiform copper mineralisation at Chambishi (Figures 4.6, 4.7, 4.8). Tellurobismuthinite is found as minor occurrence enclosed in disseminated bornite grains in the Ore Shale at the Chambishi deposit (Figure 4.6). Gangue minerals in the Ore Shale consist of fine grained biotite-quartz-scapolite, with disseminated bornite ± chalcopyrite mineralisation. Mica minerals are characteristically aligned to reflect the minimum stress direction during deformation and are elongated around more competent quartz grains.

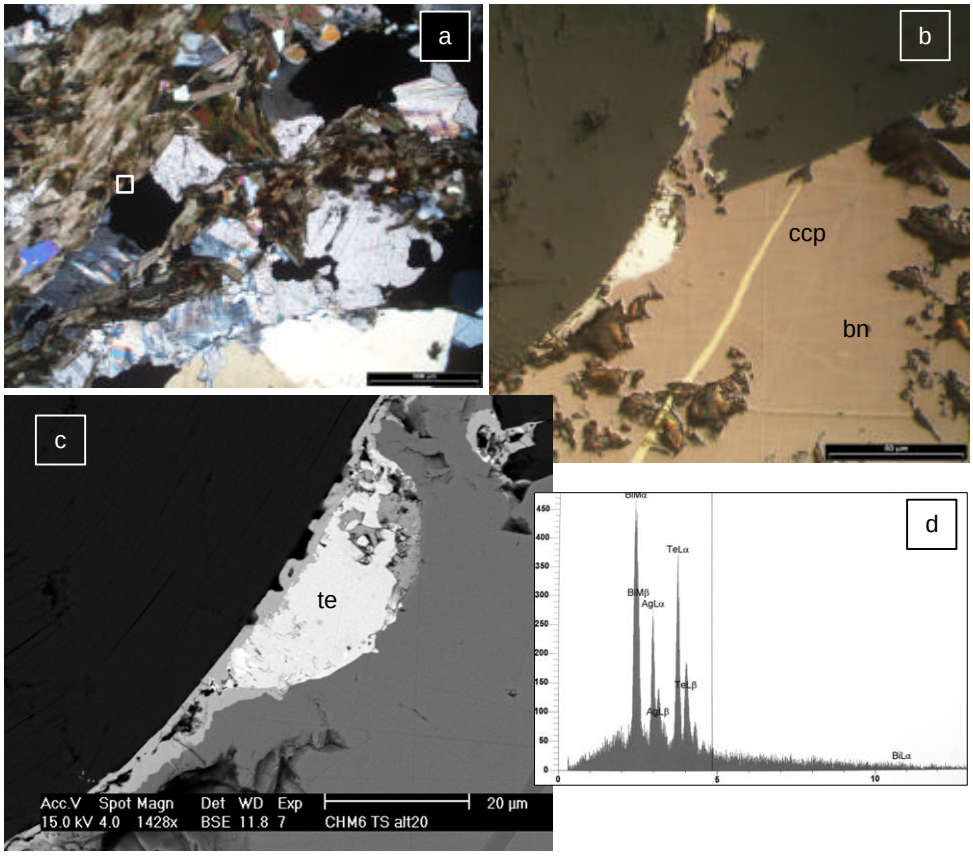

Figure 4.6. (a) Optical light micrograph taken under crossed polars of biotite with grains of quartz, calcite and disseminated opaque minerals. The scale represents 1000 µm, and the area highlighted by the white rectangle is shown in images (b) and (c). (b) Reflected light micrograph of bornite with chalcopyrite and a white, highly reflectant mineral present within the bornite. The scale bar represents 50 µm. (c) The presence of tellurobismuthinite is identified in this backscattered light image using scanning electron microscopy. (d) The spectrum generated in SEM. Acceleration voltage (keV) is plotted on the x-axis. Sample CHM 6TS of the Ore Shale of the Chambishi deposit.

Rutile is present in quartz veins hosted in the Chambishi Ore Shale (Figure 4.7). Rutile is often described occurring as hair-like needles in granite pegmatites and quartz and apatite veins, and may also be present as accessory mineral in metamorphic rocks (Deer *et al*., 1992). Elsewhere in the Copperbelt, the presence of rutile is also described in the basement and in the upper orebody horizons of the arenaceous Inter A/B beds at Mufulira (Brandt *et al*., 1961).

Argillites of the Roan Group contain abundant scapolite in the Roan-Muliashi basin probably resulting from regional metamorphism during Lufilian compression (Mendelsohn,

1961b). Evaporitic precursor sediments are also indicated by the presence of scapolites (e.g., in the Kola Peninsula gneisses and granulites according to Deer *et al*., 1992). Elsewhere in the Copperbelt, scapolite is recorded in upper Roan and Kundelungu dolomites in proximity to gabbroic intrusives in the Congo as alteration product of oligoclase (Mendelsohn, 1961a).

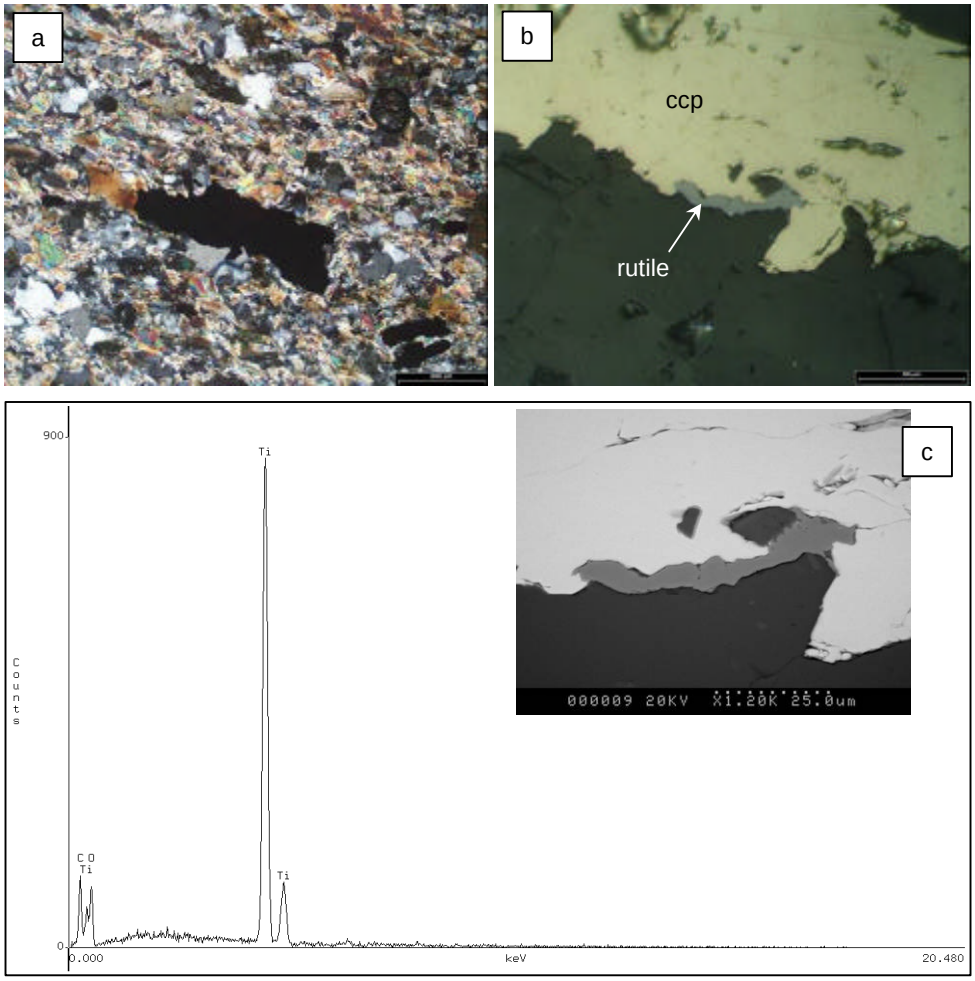

Figure 4.7. (a) Disseminated chalcopyrite with biotite-quartz-scapolite grains in the Chambishi Ore Shale in crossed polarised transmitted light. The scale bar represents 200 µm. (b) Reflected light microscopic image of chalcopyrite with light grey rutile, identified during (c) scanning electron microscopy. The scale bar in (b) represents 50 µm. Sample CHM 1TS. For details on the SEM quantitative elemental analysis, refer to Appendix III.

The presence of galena in the Ore Shale at Chambishi is not well-documented, and one isolated galena grain was found in one sample at Chambishi (Figure 4.8). Galena occurs as an isolated grain bordering bornite and chalcopyrite disseminations in the Chambishi Ore Shale where gangue minerals include biotite-scapolite-calcite. The

sulphides are concentrated at the interface between biotite-scapolite-calcite and rounded quartz grains.

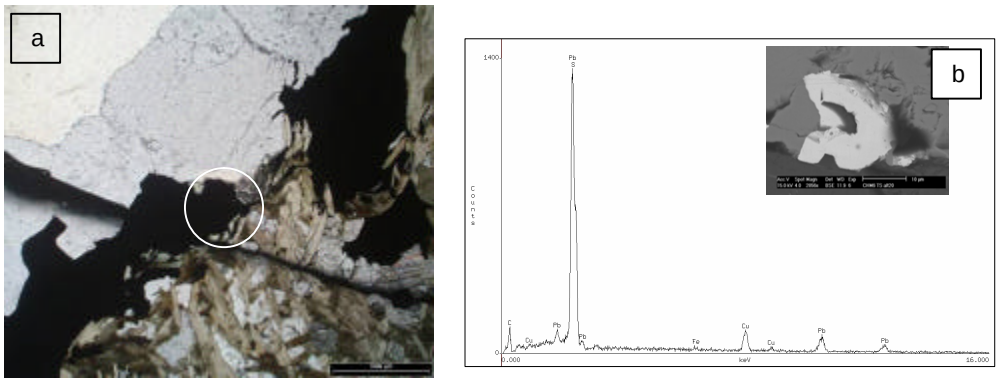

Figure 4.8. (a) Cross-polarised light micrograph of biotite-feldspar-calcite of the Chambishi Ore Shale with copper sulphide (bornite-chalcopyrite) mineralisation. The sulphides are found concentrated along the edge between the fine-grained micaceous-carbonate minerals (the bottom right half of the image) and the coarser quartz grains (dominating the upper left half of the image). Circle shows location of SEM image on right. (b) A small grain of galena was identified by SEM within the chalcopyrite-bornite disseminations in the Ore Shale. Sample CHM 6TS.

Zircons are contained within the Ore Shale horizon at Chambishi where alteration haloes in biotite surround the zircon grains (Figures 4.9, 4.10). Detrital, xenocrystic and magmatic zircons and the age dating thereof in the Copperbelt, are described in Rainaud *et al*., 2003), and zircons hosted in the Chambishi Ore Shale are probably detrital in nature. Rainaud *et al*., (2003) document the ages of xenocrystic zircons hosted in a lapilli tuff from the Mwashya Group in the upper Roan Group at 1018 ±27 to 1537 ±89 Ma. The maximum age of xenocrystic zircons in this particular tuff were dated at 3225 ± 11Ma (Rainaud *et al*., 2003), which infers the presence of a Mesoarchaean terrane (Likasi Terrane) under the central part of the Lufilian Arc. The provenance of the zircons in the Chambishi Ore Shale is uncertain, but they are probably detrital in origin.

Opaque cubic minerals with orange alteration haloes in close proximity to the zircons surrounded by biotite were petrographically identified as uraninite in the Chambishi Ore Shale. Minor uranium mineralisation occurs in some of the ore-bearing horizons in the Zambian Copperbelt, most notably at the Mindola-orebody at Nkana hosted in cherty dolomite mined in the 1950's (Jordaan, 1961; Mendelsohn, 1961c). The inverse relationship between uranium and stratiform copper mineralisation sees uranium grades decrease with increasing copper grades.

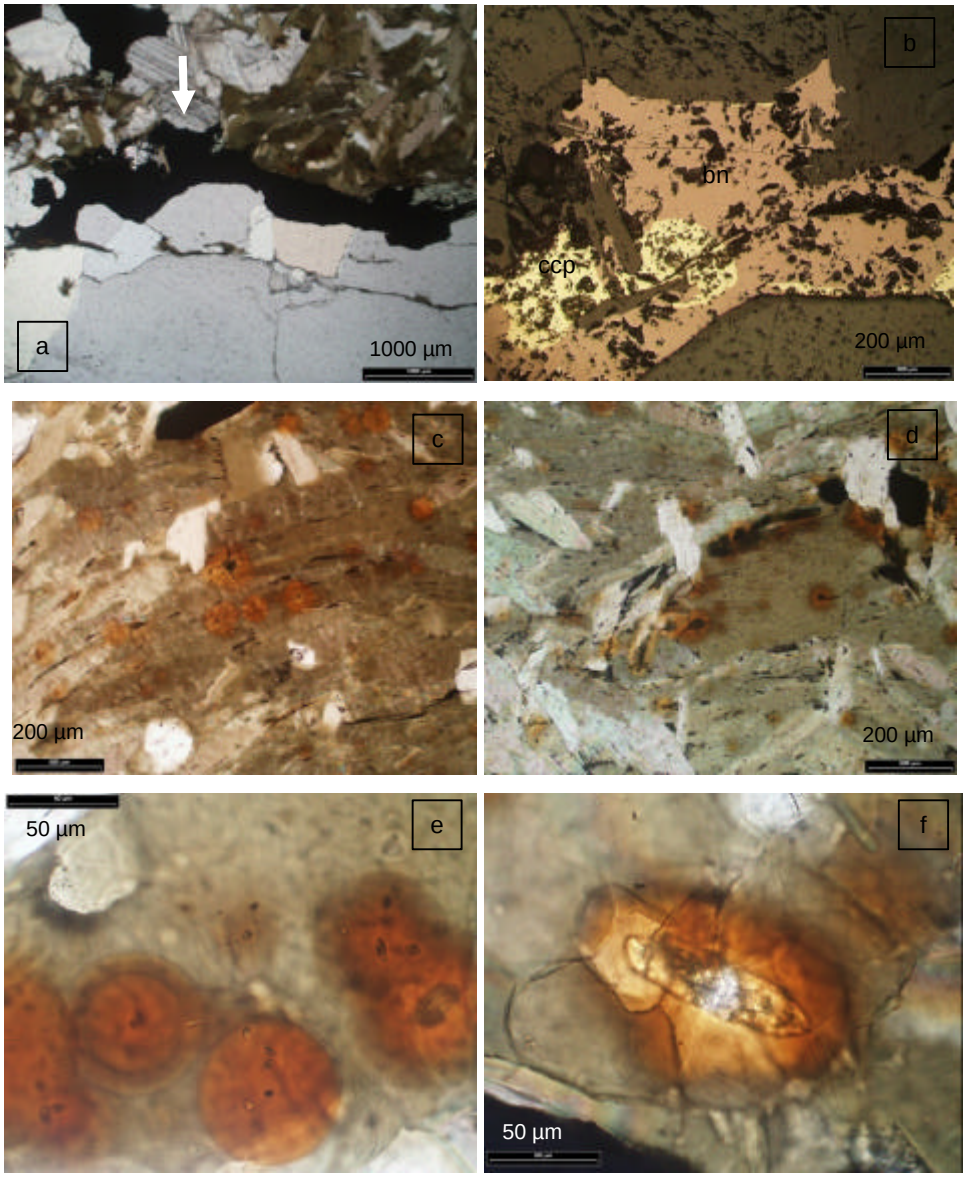

Figure 4.9. (a) Calcite, quartz, biotite, bornite-chalcopyrite assemblage in the Ore Shale horizon (crossed polars light micrograph). The arrow points to an alteration halo such as illustrated in images 'c-f'; (b) reflected light micrograph of 'a' at higher magnification showing bornite and chalcopyrite; (c-e) alteration haloes in biotite surrounding uraninite grains; (f) alteration halo surrounding a zircon crystal in biotite of the Ore Shale horizon. Micrographs from sample CHM6 TS. Images 'e' and 'f' were taken with convergent illumination.

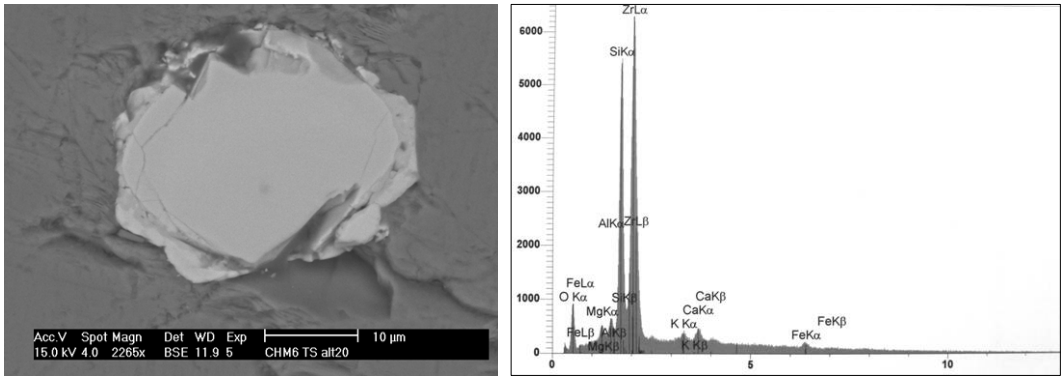

Figure 4.10. Zircons identified in samples from the Ore Shale of the Chambishi deposit were studied using SEM analysis (sample CHM6 TS).

4.2.3 Setting of samples for fluid inclusion study

Quartz veins from the Chambishi deposit were sampled and subjected to a fluid inclusion study. Two quartz vein types are identified from the Chambishi deposit: (1) a lateral secretion quartz-chalcopyrite vein, and (2) bedding parallel quartz-carbonate-bornite veins. The lateral secretion vein is hosted in the Ore Shale, and bedding parallel veins are hosted within the Footwall Formation overlying the Ore Shale. Fluid inclusion assemblages hosted in these two fluid types provide the identification of two distinct tectonic settings, namely a basinal setting, and early deformation setting.

Lateral secretion vein

A lateral secretion quartz vein is mineralised with chalcopyrite ± bornite, and its emplacement pre-dates the main stages of deformation of the basin. This lateral secretion vein reveals the relative chronological relationship between stratiform mineralisation, veining and subsequent deformation (Figure 4.11). This vein was extensively sampled for the fluid inclusion study, and several fluid inclusion populations were identified in terms of relative tectonic setting (see Appendix I for the sample list). Results of the fluid inclusion petrographic descriptions and microthermometry are discussed in subsequent chapters.

The envisaged paragenetic sequence related to the lateral secretion quartz vein recorded at Chambishi is as follows:

- Deposition of the Ore Shale was followed by (late-diagenetic?) stratiform mineralisation of disseminated Cu-sulphides (chalcopyrite and bornite).
- Emplacement of quartz veins parallel to bedding in the Ore Shale. Veins contain course-grained aggregates of chalcopyrite and bornite, which are partially oxidised to

malachite. The shale immediately adjacent to the vein is devoid of mineralisation (Figure 4.11 a-c). It is therefore, suggested that this vein emplacement resulted in the lateral secretion of disseminated Cu-sulphide mineralisation from the host rock into the quartz vein, leaving a halo depleted of mineralisation immediately surrounding the vein (Figure 4.11 a). The migration of sulphides into the vein from the host rock occurred during stress-induced transfer, similar to the process documented by Sawyer and Robin (1986) whereby the source of the migrated components is seen as pressure solution of the same minerals in the host rock. The needed stress to trigger the migration of sulphides is supplied by subsequent deformation of the vein together with the host sediments.

- Deformation of both the sedimentary succession and the quartz vein during regional metamorphism imprinted an axial planar cleavage on the host rock, which is refracted through the quartz vein (Figure 4.11 b-d), clearly illustrating the presence of the quartz vein prior to deformation.

Primary fluid inclusions hosted within the lateral secretion vein are indicative of fluids circulating within the basin during the early stages of basin evolution and maturation prior to the onset of peak metamorphic conditions. Unmodified primary inclusions preserve the *P-T-u-X* nature of fluids that predate regional deformation of the Katanga Supergroup. The *P-T-u-X* nature of basinal inclusions is described in detail in chapter 5.

Secondary fluid inclusions hosted within the lateral secretion vein are representative of fluids circulating during the early stages of deformation. These inclusions are older than basinal inclusions and correspond to early deformational fluids present during the ongoing maturation of the basin prior to the onset of peak metamorphism. These fluids may have been expelled during metamorphism of the basin and deformation lead to the imparting of the axial planar cleavage in the Ore Shale which is refracted through the quartz vein. The *P-T-u-V* nature of early deformation inclusions are described in chapter 6.

Bedding parallel veining

Bedding parallel quartz-carbonate-bornite veins are hosted in the Footwall Formation at the Chambishi deposit. These veins are locally seen to splay off the bedding and also form sub-vertical quartz veins in the Footwall. Fluid inclusions are mostly secondary in nature forming planes and trails which have formed subsequent to the quartz vein formation. In some instances, fluid inclusions also seem to group together in clusters which form part of a secondary inclusion assemblage together with nearby fluid inclusion planes. Primary isolated inclusions are nominal. These secondary inclusions are

considered to have trapped fluids circulating within the basin during the early stages of deformation prior to peak metamorphism and are grouped together with secondary inclusions of the lateral secretion vein discussed above.

Bedding-parallel quartz veining may have occurred later than that of lateral secretion quartz veining (evidenced by the presence of the refracted cleavage in the lateral secretion vein and absence thereof in the bedding-parallel quartz vein), and therefore, secondary inclusions hosted in the bedding-parallel quartz veins may be slightly older than their counterparts in the lateral secretion vein. However, on a regional scale, these inclusions reflect the nature of fluids circulating during the early stages of deformation prior to the onset of peak metamorphism and are grouped together and discussed in chapter 6.

The sequence of events is of great importance in unravelling the tectonic and fluid flow history of the basin. By identifying the host rock petrology, fluid inclusions of the Chambishi deposit contain answers as to the nature and *P-T-u-X* conditions prevailing prior to regional deformation of the basin, in an environment immediately postdating stratiform copper mineralisation.

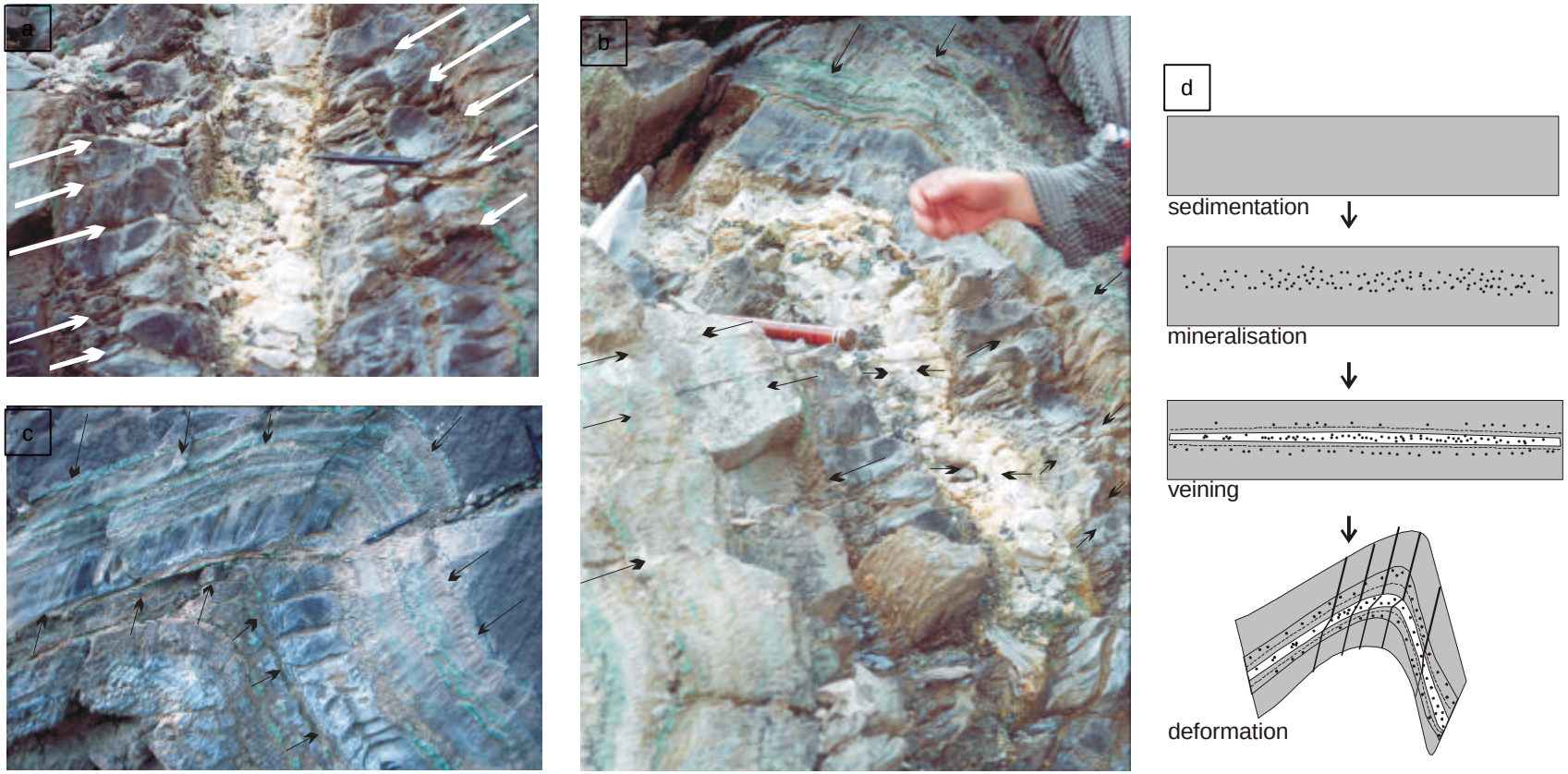

Figure 4.11. (a-b) Lateral secretion quartz vein in the Ore Shale Formation from the Chambishi open pit. The axial planar cleavage, indicated by arrows, is refracted when it passes from the silty shale into the quartz vein; (c) The axial planar cleavage is clearly visible in the nose of a nearby fold in the shale; (d) Schematic illustration of the development of the lateral secretion vein.

4.3 The Nchanga deposits

4.3.1 Geology of the Nchanga deposits

The stratiform copper-cobalt ores are hosted in the lower Roan Group of the Katanga Supergroup, which non-conformably overlies the basement (Figure 3.4). The basement comprises granites (Figure 4.12a-b), Lufubu schists and gneisses (McKinnon and Smit, 1961), as well as Muva quartzites in the southern Nchanga section, close to the Mimbula area (McKinnon and Smit, 1961).

The granites in the Nchanga mine area consist of the so-called Nchanga Red granite (Figures 4.12b and 4.13) – a coarse-grained porphyroblastic microcline-albite-oligoclase granite – and the Nchanga Dark Granite – a porphyroblastic biotite-rich microcline-albite granite (McKinnon and Smit, 1961). In addition to these granites, the Nchanga Grey granite is also known as a medium-grained microcline-oligoclase equivalent of the Red Granite (McKinnon and Smit, 1961). The Nchanga Red granite is dated at 883 ±10 Ma (Armstrong *et al*., 2005), which constrains the maximum age of Katangan deposition.

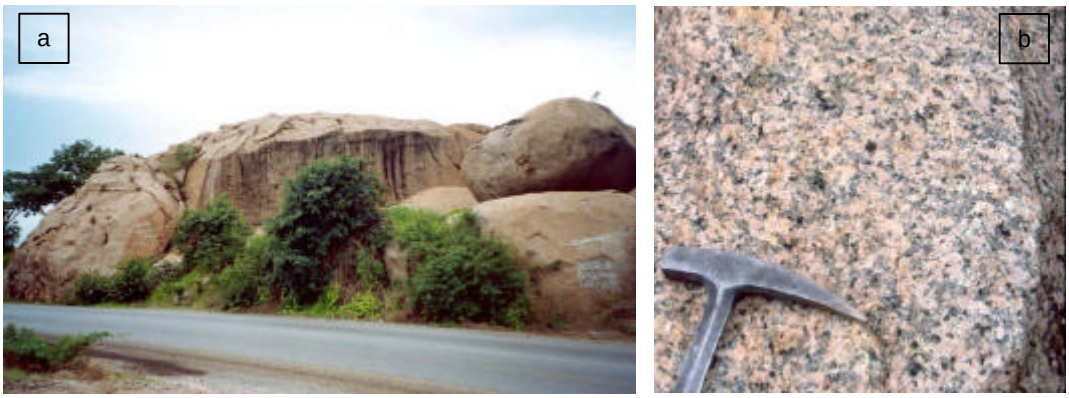

Figure 4.12. (a-b) The Nchanga Red Granite outcrops next to the road between Chingola and Chambishi, and also comprises the most part of the Nchanga Dome in Figure 4.13. The course-grained Red (pink) granite consists of microcline, albite-oligoclase, quartz, brown biotite, which may be altered to chlorite.

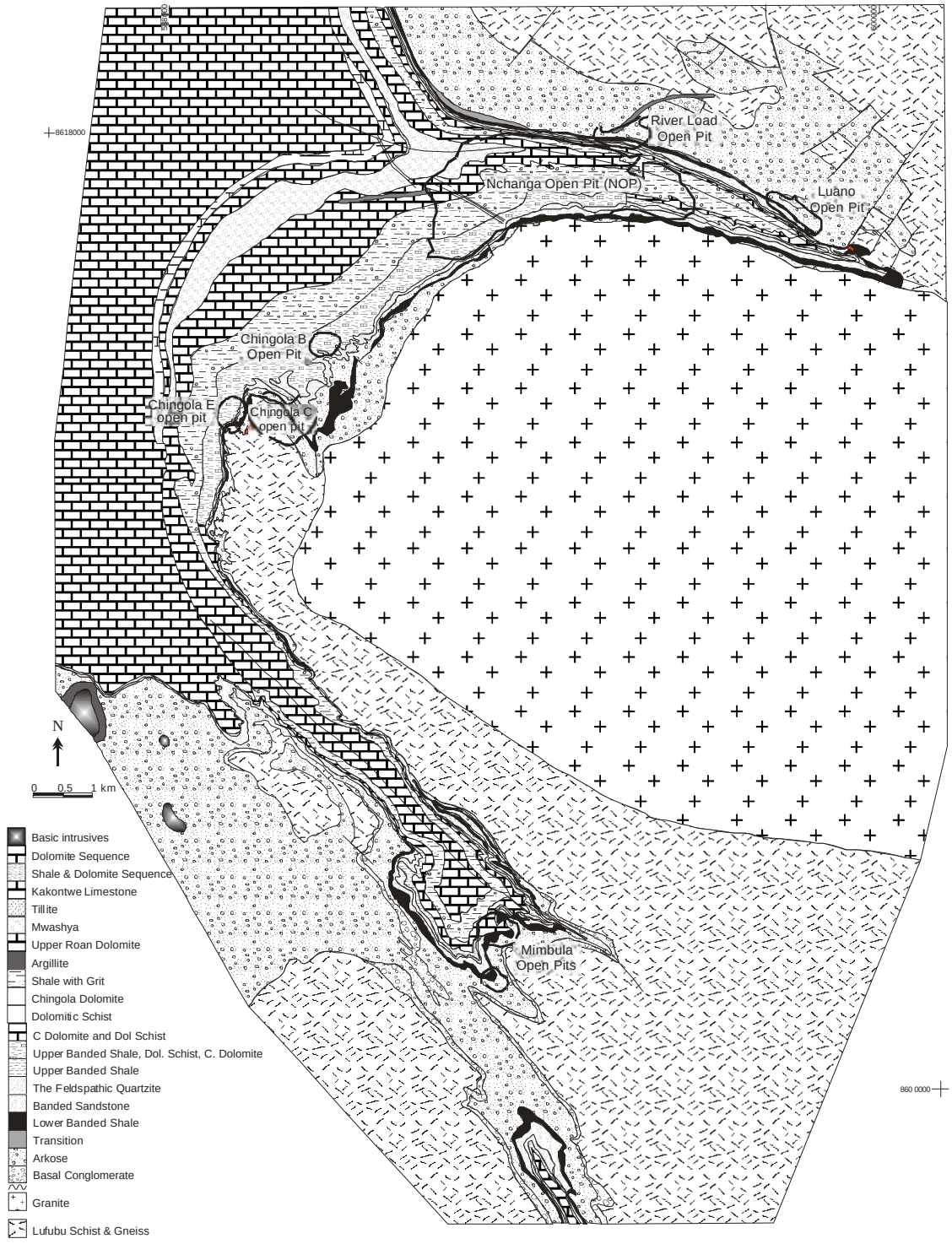

Figure 4.13. Geology of the Nchanga area consists of a central granite dome with onlapping metasediments of the lower Roan Group around the edges of the dome (modified from ZamAnglo Prospecting Limited, Konkola Copper Mines Plc.). The orebodies include the Nchanga, River Load, Luano, Chingola B-E, and Mimbula pits. Samples for this study were collected from the Nchanga open pit, C-shaft underground and Chingola B inclined shaft.

The stratigraphy of the Katanga Supergroup in the Nchanga area (Figure 4.14) consists of the Pebble-Boulder Conglomerate at the base, followed by the Arkose horizon which contains the Footwall Orebody. This is followed by the onset of the Lower Orebody (LOB) which consists of the so-called Transition Arkose and the Lower Banded Shale (LBS). The LBS is overlain by the Chert Marker, and Banded Sandstone Lower (BSSL), consisting of laminated- to bedded feldspathic sandstones and siltstones. The Shale Marker is the second marker horizon, and is comprised of a very fine grained quartzite layer. The Shale Marker is succeeded by the mineralised Pink Quartzite (PQ), which forms part of the Intermediate Orebody. This is overlain by the schistose Banded Sandstone Upper (BSSU), and following The Feldspathic Quartzite (TFQ), making up the Upper Orebody. Part of the Upper Orebody is also hosted in the Upper Banded Shale (UBS). Following this is the Dolomitic Schist, Chingola Dolomite, Shale with Grit, Upper Roan Dolomites, Mwashia, *Grand Conglomerat*, Kakontwe Limestone, schistose argillites, and talcose dolomite.

Deposition of the Katanga Supergroup commenced in rifted intra-cratonic marine basins evidenced by the clastic component to rocks of the lower Roan. The basal continental clastic sequence grades into a shallow marine evaporitic and then platform carbonate sequence (Fleischer *et al*., 1976).

Nchanga structural setting

The Katanga Supergroup has undergone regional metamorphism and the sediments of the Roan (and Kundelungu) Supergroups are metamorphosed to greenschist facies grades in the southern area of the Zambian Copperbelt, and folding and thrusting is evident at Nchanga (McGowan *et al*., 2006), with shearing and detachment folds around the syncline (Daly *et al*., 1984). A major structural feature at Nchanga is the presence of the WNW-plunging Nchanga Syncline (Figure 4.15), extending for ~12 km which indicates compression in a north-south direction (McKinnon and Smit, 1961). The River Lode- and Luano orebodies are situated on the northern limb of the Nchanga syncline, while the Nchanga open pit is present in the south of the syncline.

In addition to the Nchanga syncline, regional deformation is evident from parallel folding at Mimbula recumbent folds at Chingola B. McKinnon and Smit (1961) suggest compression in a north-west direction as well as the north-south direction indicated by the Nchanga syncline. McGowan *et al*. (2006) document north-east trending vergence (Figure 4.16a) of the lower Roan Group with detachment at the top of the Lower Arkose Unit during thrusting. Within the Nchanga syncline, internal folds may indicate SSW and SW trending vergence (McGowan *et al*., 2006).

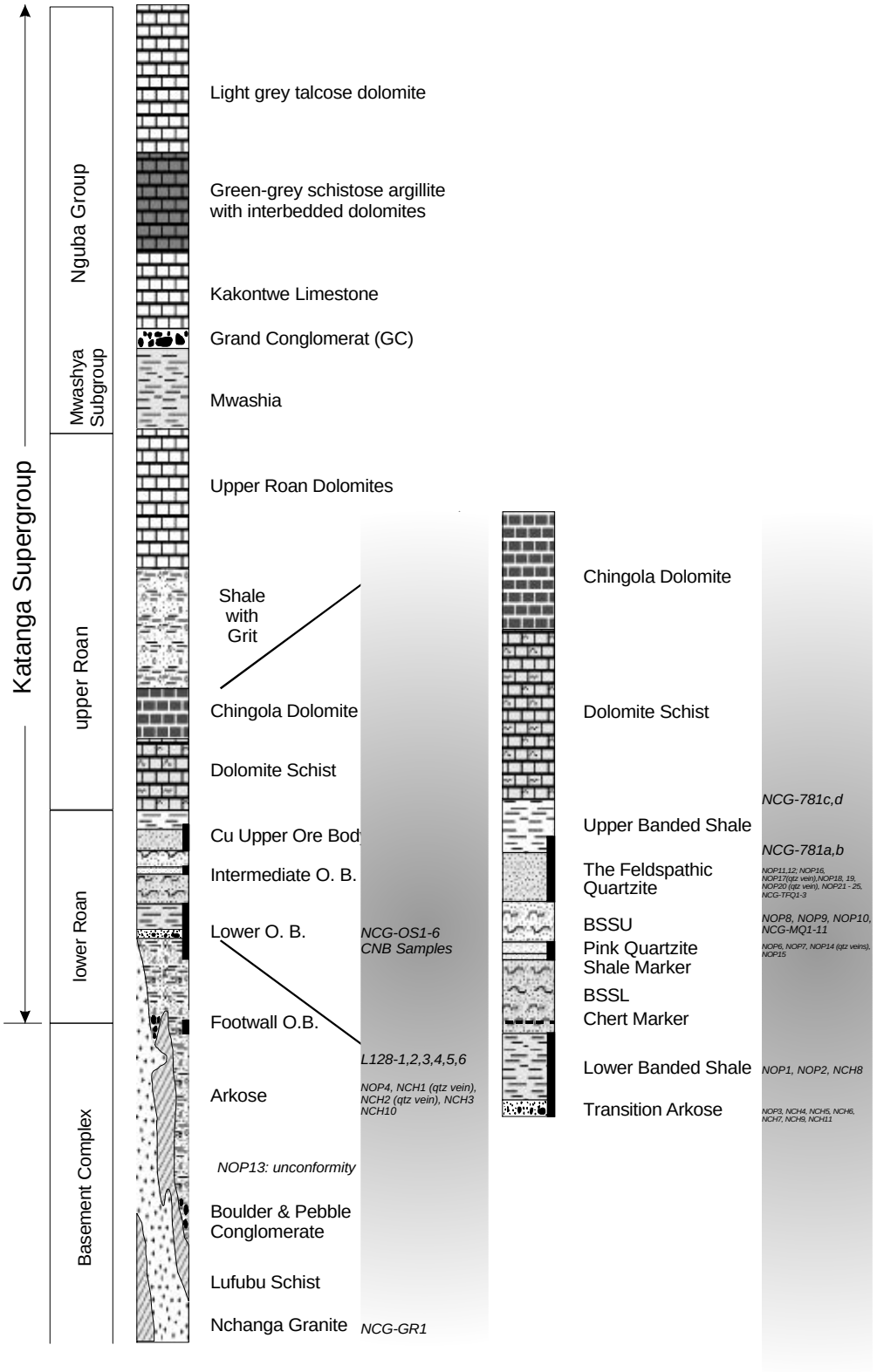

Figure 4.14. General stratigraphic profile of the Nchanga-Chingola area. Sample numbers are indicated in grey shading. Stratigraphic divisions are adapted from Wendorff, 2005 (modified from ZamAnglo Prospecting Limited, Konkola Copper Mines Plc.).

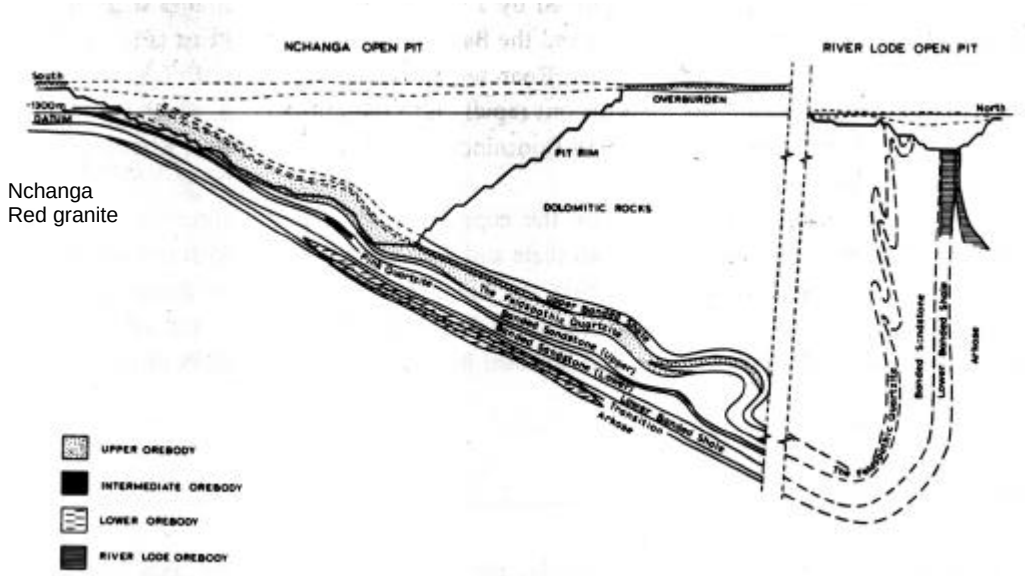

Figure 4.15. The asymmetric Nchanga syncline in cross section suggests a general north-south compressional direction and plunges to the west. The syncline extends for ~ 12 km (Fleischer et al*., 1976).*

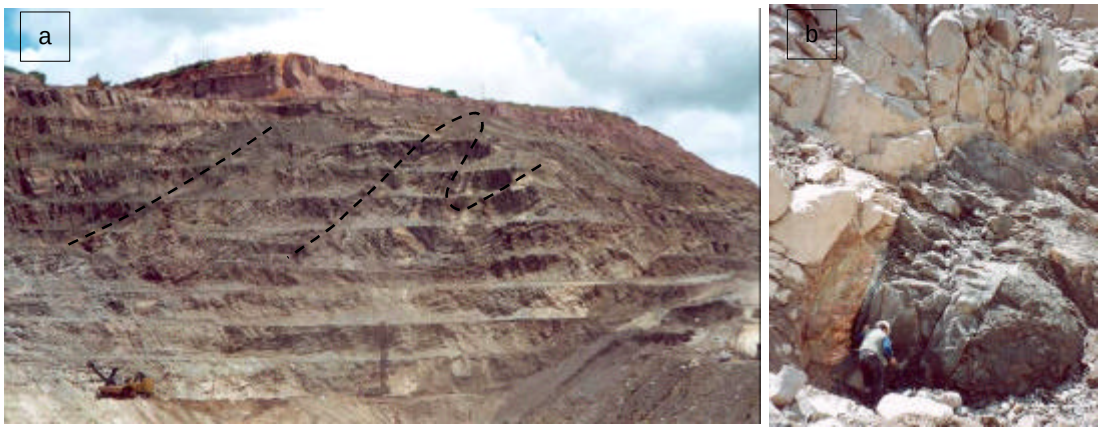

Figure 4.16. (a) The isoclinally folded Dolomite Schist in the hangingwall of the Upper Orebody in the Nchanga open pit is resultant of compressional deformation during Lufilian orogenesis. (b) A phlogopite-scapolite schistose unit in the Nchanga open pit has been described by various authors as a lamprophyre dyke (Diederix, 1977), a metamorphosed gabbro (Fleischer et al., 1976) and as fault gouge (McGowan, 2003).

Post-Katangan depositional rocks include minor mafic intrusives (Figure 4.16b). In particular one intrusive in the Nchanga open pit has been identified as a lamprophyre dyke (Diederix, 1977), and as a metamorphosed gabbro (Fleischer et al., 1976). The

intrusive origin is disputed by McGowan (2003), who interprets it as fault gouge. The sharp contact with the upper Roan metasediments suggests an intrusive nature of this lithology, which contains abundant ferromagnesian minerals such as biotite-phlogopite ± amphiboles. It is unclear whether this dyke intruded during the final stages of upper Katangan deposition or whether it is associated with the younger gabbroic sill-like bodies which intrude the upper Roan and Kundelungu metasediments, possibly associated with folding during the Lufilian orogeny.

4.3.2 Mineralisation of the Nchanga deposits

Several ore occurrences are found in the Nchanga area. These include the main Nchanga deposit, Chingola, Luano, and Mimbula orebodies (see Figure 4.13). The ore deposits at Nchanga consist of three orebody horizons in the lower Roan Group. Generally, two units are distinguished as copper-cobalt mineralised horizons, and copper-bearing mineralised horizons. The Lower Orebody contains copper only and consists of the Transition Arkose and the Lower Banded Shale, while the Upper Orebody contains copper and cobalt and consists of an arenaceous unit called The Feldspathic Quartzite.

The Lower Orebody

The Footwall Orebody is hosted in the Arkose horizon, which consists of medium-coarse to lithic greywacke and schist. This unit is overlain by the Lower Orebody (LOB), which consists of the so-called Transition Arkose (Figure 4.17a) and overlying Lower Banded Shale (LBS).

The Transition Arkose is a sedimentary calcareous and arenitic breccia. The LBS is comprised of black carbonaceous shale, grading to silty argillite (Figure 4.17b-c), and is the equivalent of the Ore Shale horizon found throughout the rest of the Copperbelt region.

The Lower Orebody is accessed via the Chingola B inclined shaft, where the top of the Arkose and the Transitional Arkose are economic (Figure 4.17d). The underlying Footwall Arkose at the Chingola B site is illustrated in Figure 4.17e. The LOB is also accessed from the C-shaft underground section where economic units include the Transitional Arkose and Lower Banded Shale (Figure 4.18). Grades of the LOB vary between 2-3 wt.% Cu at 6-10 m intersections.

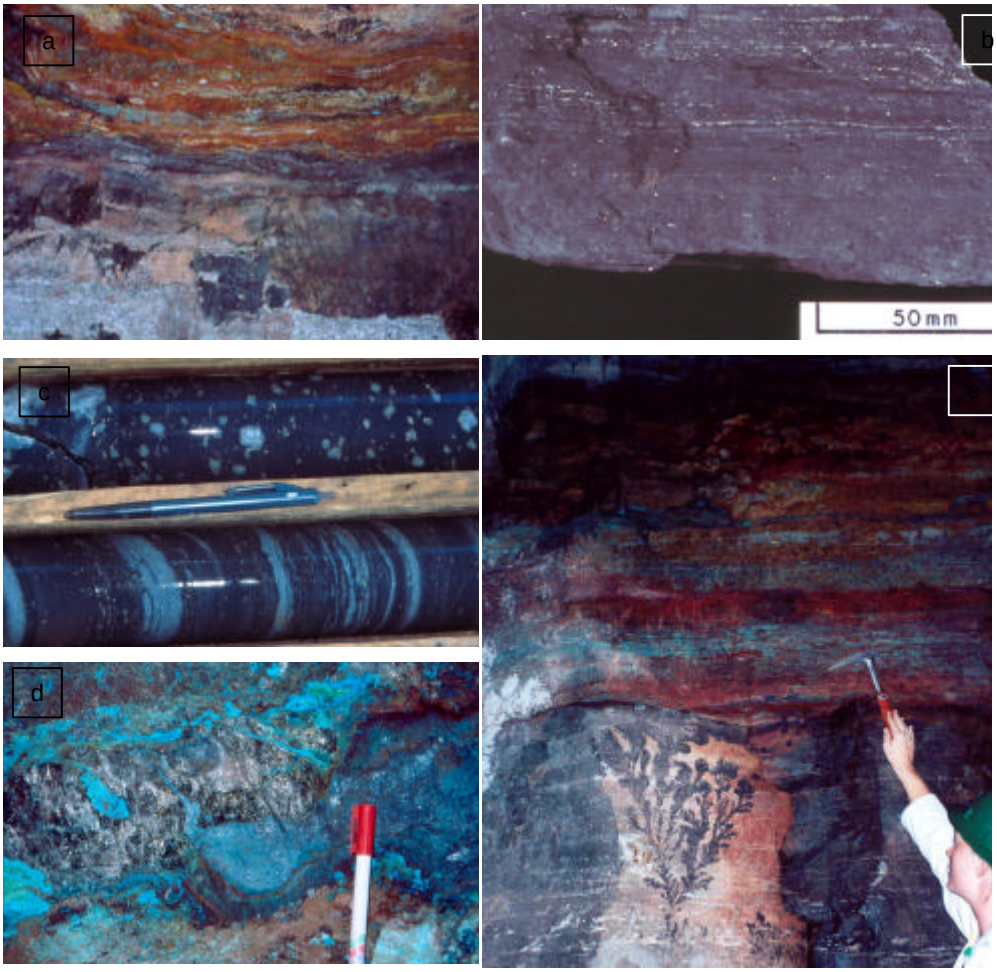

Figure 4.17. The Lower Orebody at Nchanga consists of: (a) Arkose ore in the Footwall at underground C-Shaft; (b) the carbonaceous Lower Banded Shale with fine laminations of diagenetic pyrite; (c) the LBS varies from black carbonaceous to silty argillaceous as can be seen from the lighter coloured laminations (diamond drill core NE-947), with diagenetic pyrite present as interlaminations and disseminated concretions; (d) chrysocolla and quartz veining of the LOB at the Chingola B inclined shaft; (e) bedding observed in the LOB with green-blue chrysocolla and black magnesium dendrites in a coarse banded underlying unit.

The Intermediate Orebody

The Intermediate Orebody is mined from the Nchanga open pit, and consists of the Shale Marker and the Pink Quartzite located between the Lower and Upper Orebodies (Figure 4.19b). Mineralisation is present as disseminations of bornite and, chalcopyrite with minor carrollite grains which are concentrated along bedding planes.

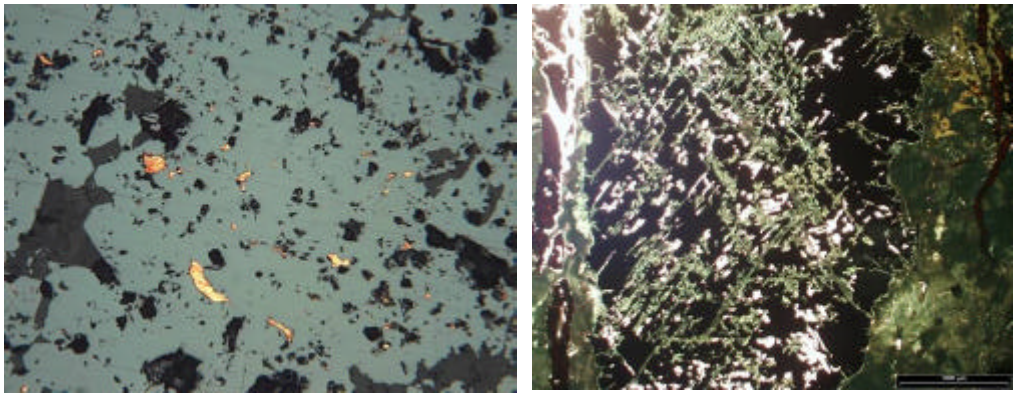

Figure 4.18. Ore micrographs of the Lower Orebody show (a) chalcopyrite specs among massive chalcocite (FOV: 300 µm , sample NCH 8A), and (b) transmitted light micrograph of chalcocite replaced by malachite along fractures (sample CHN12 TS).

The Upper Orebody

The Nchanga open pit is the largest of the Nchanga open pits with dimensions of ~ 5800m x 2000m (Figure 4.19a) and leads to access of the Upper Orebody which consists of The Feldspathic Quartzite and the lower section of the Upper Banded Shale. The UOB is mined for copper and cobalt and grades average 2.5-3 % Cu and 1 % Co in the Nchanga open pit. The Feldspathic Quartzite is an arenitic quartzite with a dolomitic composition in areas. Cu-Co mineralisation is found as bornite-chalcopyrite-digenite-carrollite (Figures 4.19 - 4.20). Mineralisation may occur as fine disseminations, concentrated along faint remnant bedding planes, but coarse accumulations of bornite-chalcopyrite-carrollite are also found where siliceous fluids have remobilised stratiform mineralisation. Malachite ± azurite mineralisation form as secondary ore minerals.

Nchanga Ore Genesis

McKinnon and Smit (1961) noted the palaeotopographic control on the distribution of the Nchanga orebodies. The transition between continental and marine sedimentary layers is also significant in grade distribution. Early workers suggested epigenetic ore genesis due to the proximity of granites in the area, but this theory was negated after the unconformable nature of the granites to the overlying metasediments came to light. Primary sulphide ore minerals are concentrated along bedding planes, and primary ore genesis has been attributed to hypogene solutions and bacterial action (McKinnon and Smit, 1961), and recently to fault-propagation folds and thrusts (McGowan *et al*., 2006).

Supergene mineralisation occurs as chalcocite, malachite, azurite, cuprite, and native copper.

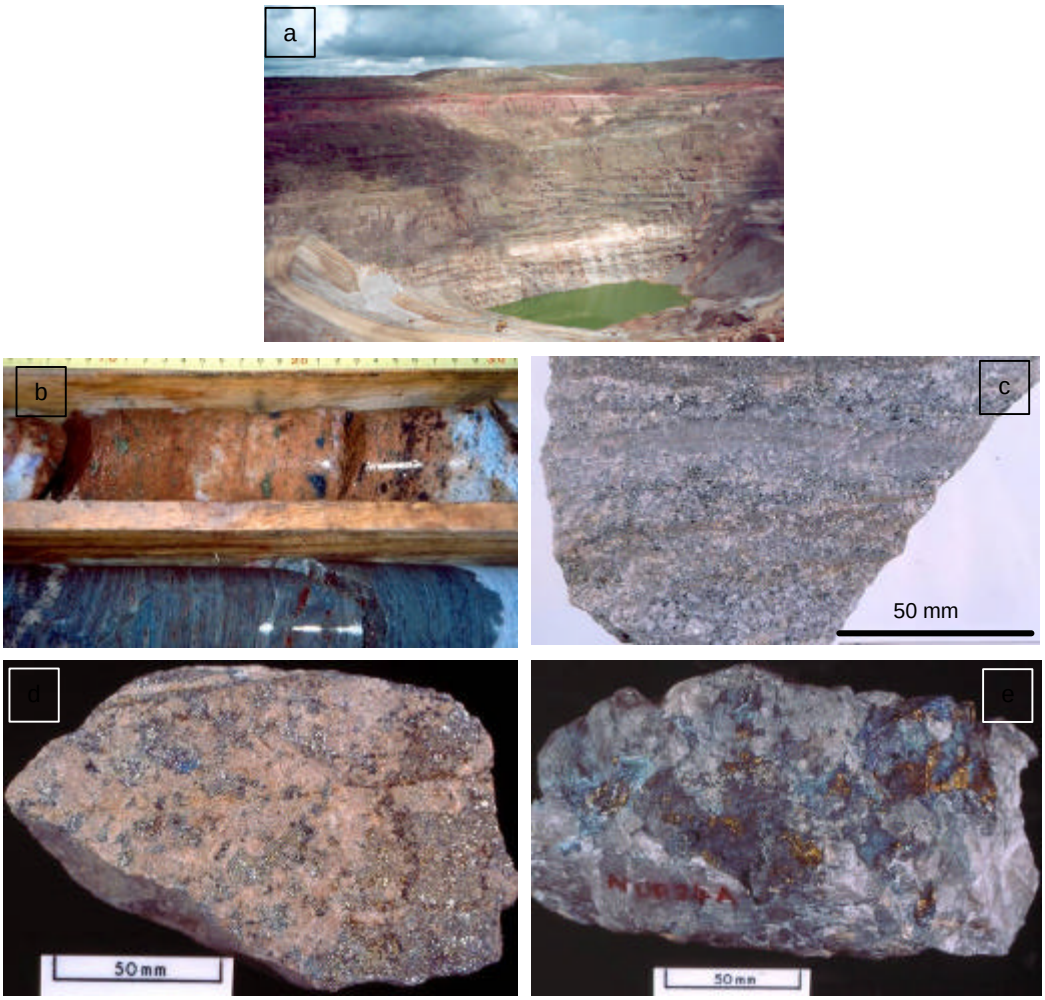

Figure 4.19. (a) View to the ENE of the Nchanga open pit. The Intermediate- and Upper orebodies at Nchanga consist of the: (b) the Pink Quartzite of the Intermediate Orebody, and (c-d) the Feldspathic Quartzite of the Upper Orebody (samples NOP22, NOP16); (e) recrystallised TFQ with bornite, chalcopyrite, and carrollite, and quartz (sample NOP24).

4.3.3 Sampling

Several samples were collected of the footwall, orebody, and hangingwall of the three Nchanga ore horizons. These were collected from the underground workings from the C-Shaft access, the underground workings at the inclined Chingola B Shaft, and from the Nchanga open pit. Selected diamond drill-core was also logged (refer to Figure 4.14 for stratigraphic section with sample numbers, and Appendix I for a detailed log of samples).

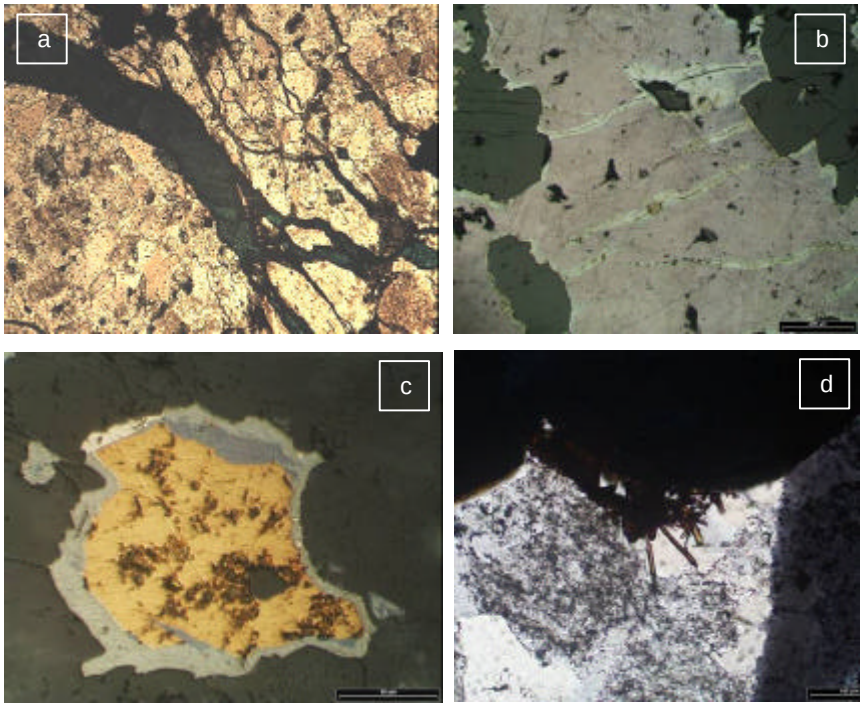

Figure 4.20. Micrographs of the Nchanga Upper Orebody show (a) replacement of primary sulphides by malachite along fractures and veins in transmitted light (FOV: 1.4mm, sample NOP 11). (b) Replacement of bornite by chalcopyrite along fractures is abundant viewed in reflected light (sample NOP25 TS) (c) Chalcopyrite is replaced by chalcocite and rimmed by digenite. Light yellow carrollite is present in the top left corner of the reflected light image (NOP 25TS), (d) rutile needles extending from bornite and carrollite grains into quartz-carbonate matrix observed in transmitted light (sample NOP16). Refer to Appendix III for SEM spectra.

4.4 The Mufulira deposit

4.4.1 Geology of the Mufulira deposit

The Mufulira deposit is located about 13 km from the Zambia-DRC border, on the western edge of the Kafue anticline (see Figure 3.1), in the south-western limb of the Mufulira syncline. The beds in the south-western limb dip at about 45° to the northeast. The basement to the Katangan in this area consists mainly of the Lufubu schists, which are intruded by granites (Brandt *et al*., 1961). The lower Roan Group of the Katanga Supergroup overlies the Lufubu schists with a basal conglomerate, and aeolian quartzites of the Footwall Formation (Figure 4.21). The basal conglomerate is found in the palaeo-valleys of the basement topography.

The Footwall Formation is overlain by the Ore Formation with the onset of the quartzites and greywackes of the C-horizon. The C-horizon is consistently overlain by a dolomitic fine-grained siltstone, called the Mudseam, which is then followed by the quartzites and greywackes of the B-horizon. This is overlain by dolomite, a marker grit horizon, shale, banded shale, and quartzites, which are then followed by the A-horizon. The A-horizon contains quartzite and black carbonaceous greywacke with anhydrite-filled cavities (Brandt *et al*., 1961), and marks the termination of the Ore Formation.

The Hangingwall Formation consists of argillaceous quartzites with shale and dolomite layers. Following the lower section of the argillaceous quartzite is another marker grit horizon. This marker grit is overlain by the argillaceous quartzite. Finally, this is overlain by dolomite, shale, and banded quartzites, and the Glassy Quartzite at the top of the lower Roan Group. The Glassy Quartzite is comprised of white-grey feldspathic quartzite and shales.

The upper Roan Group starts with the Intermediate Dolomite, which contains mostly dolomite with some siltstone layers, talc seams, quartzite and argillite beds. A consistent layer of grey-pink quartzite is found in the middle of the Intermediate Dolomite. This is succeeded by the Interbedded Shales and Quartzites, and finally Upper Dolomite, which contains argillite, talc, quartzites and conglomeratic breccia beds.

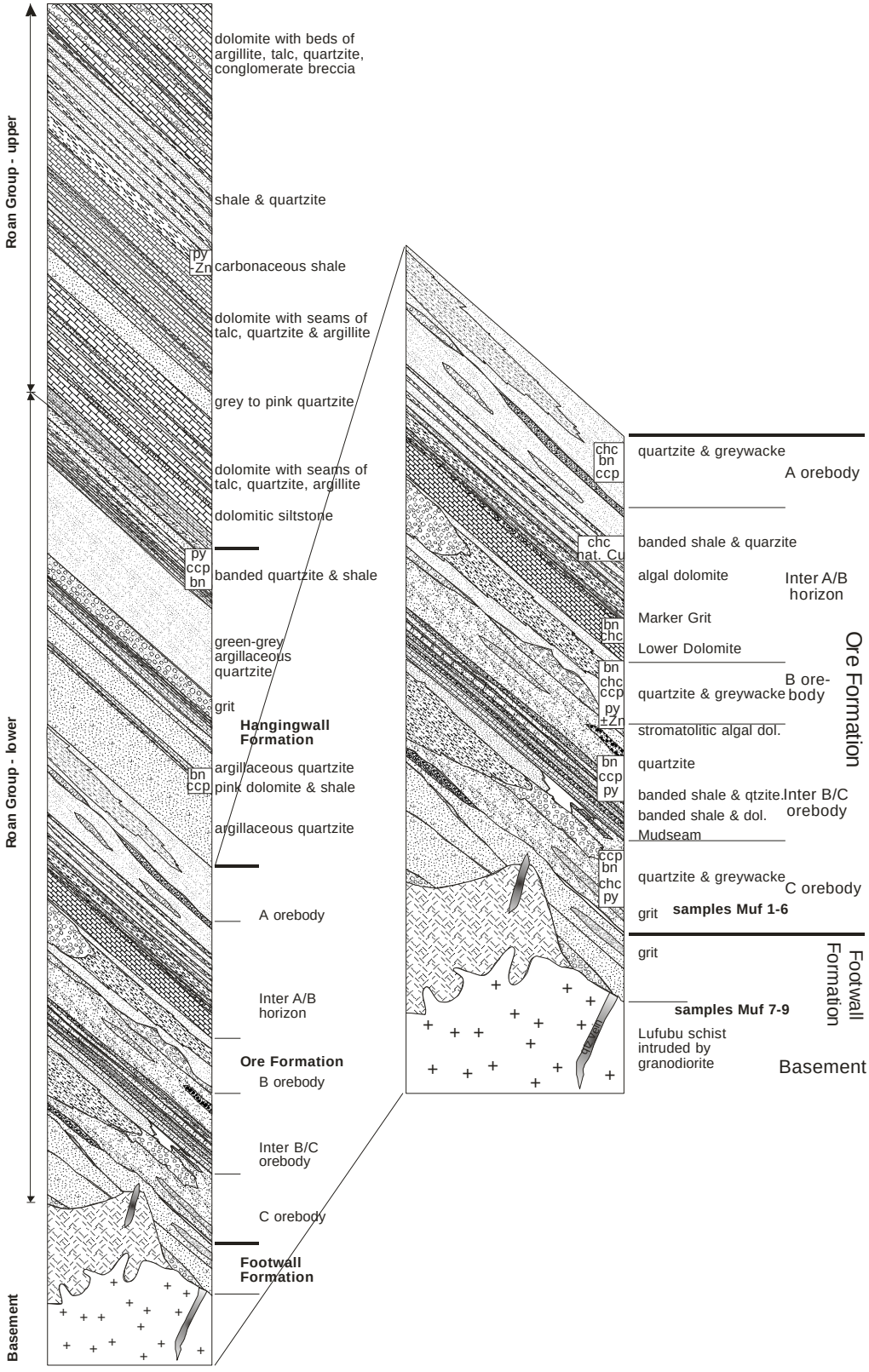

Figure 4.21. Generalised stratigraphic profile of the Mufulira deposit in the southwestern limb of the syncline (after V.D. Fleischer, Mopani Copper Mines Plc, Mufulira Division). The locations of samples Muf 1-9 are indicated on the right enlargement in the C-orebody and Footwall Formation to the C-orebody.

4.4.2 Mineralisation at Mufulira

Some occurrences of copper mineralisation are found in the basement as chalcopyrite-pyrite in fissures and cracks in the Lufubu schists and granite. This occurs generally near the C-horizon contact (Brandt *et al*., 1961). Chalcopyrite and pyrite also occur as disseminations in the Lufubu schists (Figure 4.22a), as well as in quartz-carbonate-anhydrite veins (Figure 4.22b-c) in both the granite and Lufubu schists.

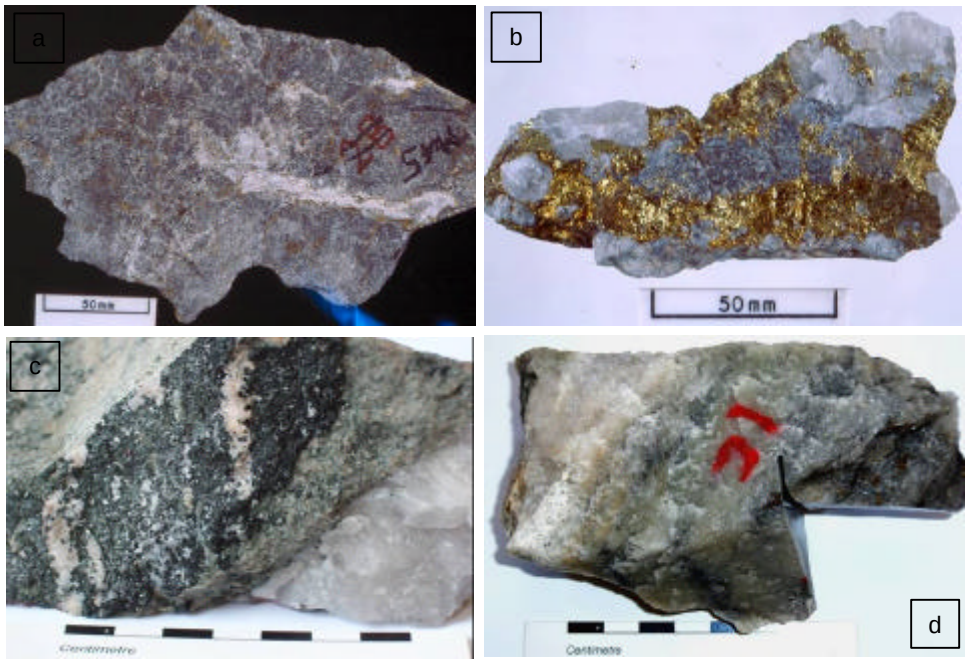

Figure 4.22. (a) Finely disseminated chalcopyrite mineralisation in the Lufubu schist basement (Muf 5); (b) massive quartz-chalcopyrite vein in Lufubu schist (Muf 8f); (c) Quartz ± anhydrite vein in Lufubu basement below contact between basement and Katangan (Muf 7h); (d) Bedding parallel quartz-anhydrite vein in the Footwall Quartzite of the C-orebody. Some disseminated chalcopyrite mineralisation is visible in the right section (Muf 3).

Stratiform copper mineralisation is found in the Ore Formation of the lower Roan Group. The Ore Formation is divided into the A-, B- and C-horizons, of which the C-horizon is at the base. The C-horizon is mineralised with chalcopyrite, bornite, minor chalcocite and pyrite, and is a fine- to medium-grained grey sericitic quartzite (Figure 4.22d). The C-horizon show lateral facies variation (Brandt *et al*., 1961). The dolomitic Mudseam overlies the C-horizon throughout the deposit at the base of the Inter B/C

horizon. This horizon is mineralised with occasional disseminated bornite, chalcopyrite and pyrite. Bornite with minor chalcocite, chalcopyrite, and pyrite is found in the sericitic quartzite-greywacke of the B-horizon. Some layers of dolomitic quartzite are also present in the B-horizon. The Lower Dolomite of the Inter A/B Orebody is mineralised with minor bornite and chalcocite, and above the dolomite the Inter A/B Orebody is mineralised with minor chalcocite and native copper in the banded shale and quartzite. The sericitic quartzite of the A-orebody is mineralised with chalcocite, bornite, and minor chalcopyrite. This overlies the mostly barren pink, feldspathic quartzite of the A-horizon. Lenses of greywacke are present in the upper section of the A-horizon. Brandt *et al*., (1961) noted that where the Cu/Fe ratio was low, pyrite and chalcopyrite coexist in the absence of bornite and chalcocite, and conversely, where the Cu/Fe ratio is higher, bornite and chalcocite or bornite and chalcopyrite coexist. Oxidation of primary sulphides occurred from supergene chalcocite, malachite, massive cuprite and native copper.

4.4.3 Sampling

Twenty-three samples were selected from the Lufubu schist basement and the overlying C- and A- horizons of the lower Roan from the 1140m Level and 1240m Level intersections from the 7 Shaft at the Mufulira mine (see Appendix I). In addition to the host rocks, chalcopyrite-anhydrite-quartz veins crosscutting the basement and overlying contact were also sampled (Figure 4.21). Inclusions contained within these veins were studied and are discussed in chapter 7.

Formation of these veins postdates the onset of Katangan deposition, and is believed to coincide with ongoing basin compaction after Katangan deposition and stratiform copper mineralisation. Solutions present during chalcopyrite-anhydrite-quartz vein formation this late in the basin history constrain the prevalent *P-T-u-X* conditions sufficient to transport copper in solution to precipitate chalcopyrite.

4.5 The Nkana deposit

4.5.1 The Geology of the Nkana deposit

The Nkana deposit occurs in the lower Roan Group on the southwestern side of the Kafue anticline in the Chambishi-Nkana basin (see Figure 3.1). The Katangan sediments are found in a northwesterly plunging syncline in this area (Jordaan, 1961; Figure 4.23a). The basement to the Katanga Supergroup consists of the Lufubu schists and quartzites, as well as intrusive granites and granitoid gneisses.

The Katanga Supergroup unconformably overlies the basement with lower Roan Group basal conglomerates and grit, deposited in the palaeo-valleys defined by the basement topography (Figure 4.21b). The conglomerate clasts consist of the pre-Katangan basement. This conglomeratic layer is overlain by the Footwall Quartzite, and in the absence of the basal conglomerate, these well-bedded, argillaceous- to feldspathic quartzites occur on the basement. The Footwall Quartzites are succeeded by the Footwall Transition Formation. This is a medium-grained sandstone bed. This bed is overlain by a conglomerate at the base of the Footwall Sandstone Formation, which grades into a coarse-grained quartzo-feldspathic sandstone. The Ore Formation overlies this horizon. The ore horizon consists of schistose argillaceous dolomite, argillite, micaceous- and black carbonaceous shales (Jordaan, 1961). The banded to massive Hangingwall Argillite overlies the Ore Formation. Lenses and veins of anhydrite and calcite are found in this argillite. The Hangingwall Sandstone Formation at the top of the lower Roan Group follows the argillite, and consists of medium-grained feldspathic sandstones and argillites. The base of the upper Roan Group consists of pyritic argillite and dolomite, overlain by the Mwashia Subgroup (Fleischer *et al*., 1976). Together with the rest of the Copperbelt, the Nkana area has been subjected to regional metamorphism to the lower greenschist facies with characteristic minerals such as tremolite, chlorite and biotite comprising much of the host sequence.

4.5.2 Mineralisation at the Nkana deposit

Some chalcopyrite-bornite mineralisation occurs in the Lufubu gneisses and schists at the contact between the basement and the Footwall Orebody (Jordaan, 1961). The main stratiform copper orebodies in the Nkana area are the North, South, and Mindola orebodies in the lower Roan Group in the northeastern limb of the Nkana syncline. Mineralisation occurs on both sides of the syncline. Local variation in the ore-bearing host rock lithology occurs among the orebodies, but stratiform mineralisation is correlated

through the section. The three orebodies are bounded by the underlying Footwall Conglomerate and overlaying Hangingwall Argillite.

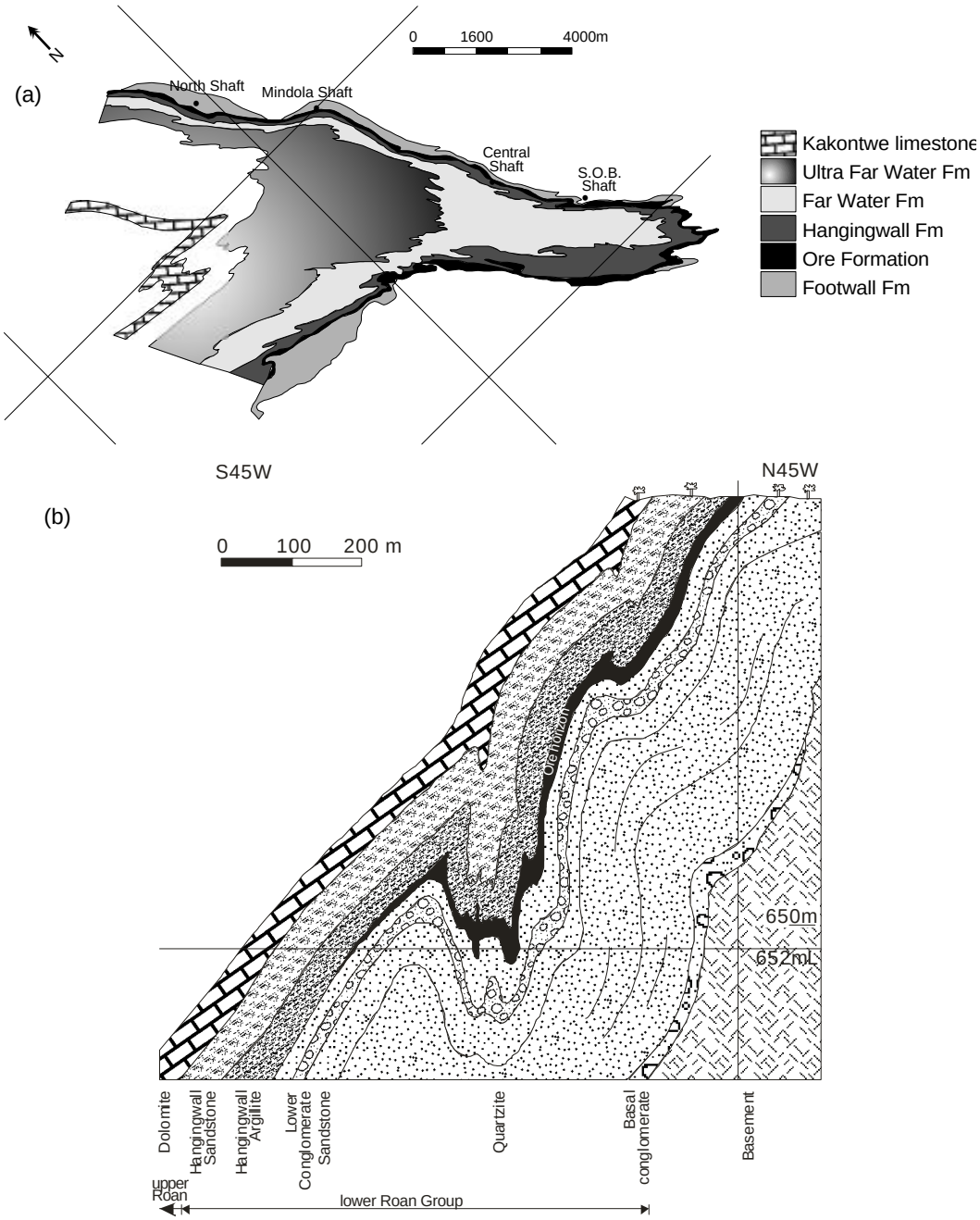

Figure 4.23. (a) Geology of the Nkana area, showing the North-, South-, and Mindola orebodies (map modified from First Quantum website); (b) Generalised cross-section from the Central Shaft section at the Nkana mine (Fleischer et al., 1976).

The South Orebody succession is divided into the Contact Shale, South Orebody shale, and Hangingwall (pyritic) Argillite (Jordaan, 1961). Copper mineralisation is hosted in chalcopyrite and carrollite mainly in the black graphitic South Orebody shale. Some occurrences of bornite and chalcopyrite appeared deformed against more competent minerals (Figure 4.24).

The Mindola orebody is divided into the Schistose Ore, Low-grade Argillite, Banded Ore, Cherty Ore, and Porous Sandstone. Disseminated bornite, chalcopyrite, chalcocite, and carrollite are found in the Schistose Ore at Mindola. Ore minerals include mainly chalcopyrite and bornite in the Low-grade Argillite, with disseminated bornite, chalcopyrite, and minor carrollite in the Banded Ore horizon where aggregates are found associated with quartz and calcite in courser-grained areas. Bornite, chalcopyrite, and carrollite disseminations are present in the Cherty Ore horizon, and additional chalcocite and pyrite in the overlying Porous Sandstone.

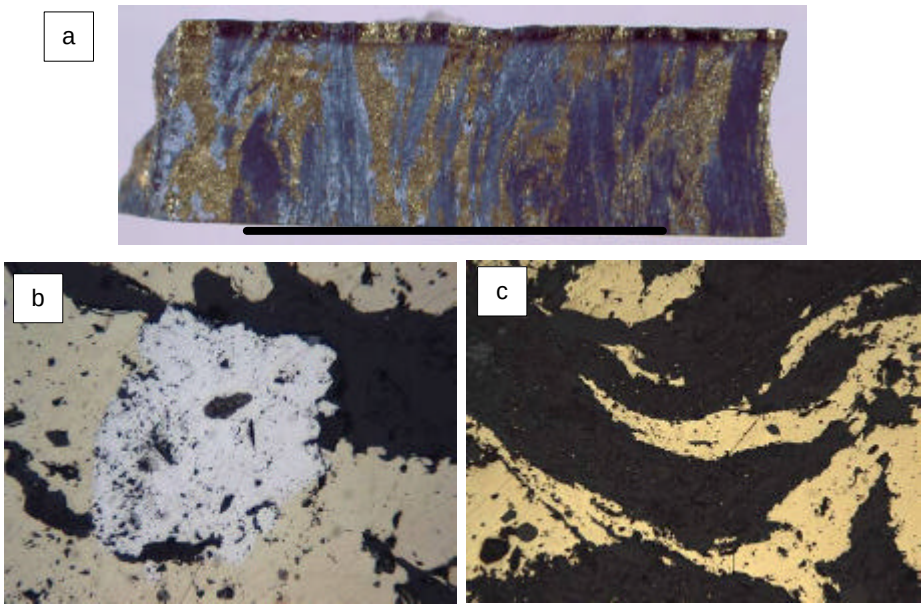

Figure 4.24. (a) Chalcopyrite-carbonate veins in the South Orebody Shale at Nkana. The black colour, due to graphitic carbon is typical of the fissile shale at this locality. (b) Reflected light micrograph of carrollite surrounded by chalcopyrite in the Ore Shale of the SOB. (c) Reflected light micrograph of chalcopyrite laths in the black shale. (a) Scale bar: 50 mm. (b) FOV: 0.6 mm .(c) FOV:1.6 mm.

The North Orebody is divided into the Tremolite Schist, which contains disseminated bornite, carrollite and chalcopyrite, and overlying Micaceous Shale, with chalcopyrite and carrollite.

Uranium mineralisation in the form of pitchblende, uraninite and brannerite was found, and briefly mined, in the southern Mindola metasediments during the late 1940's and 1950's, as well as in cross-cutting anhydrite-quartz-dolomite veins (Fleischer *et al*., 1976). Minor mineralisation comprising chalcopyrite, bornite, carrollite, and pyrite is found in the Hangingwall Argillite. Supergene alteration of the primary sulphides has resulted in the presence of malachite, chrysocolla, cuprite, tenorite, with minor azurite and libethenite.

Lateral variation in mineral composition is noted in Jordaan (1961), who illustrates the zonation of minerals between the orebodies. The zones are documented as bornite to bornite-chalcopyrite-carrollite to chalcopyrite-carrollite at Mindola, and bornite-chalcopyrite-carrollite to chalcopyrite-carrollite at the South and North orebodies. Stratigraphically, Jordaan (1961) also noted the zoning of chalcopyrite-carrollite at the base, to bornite-chalcopyrite-carrollite, to chalcopyrite and carrollite, to pyrite at the top. Early stratiform mineralisation was probably locally remobilised during metamorphism leading to occurrences of copper in quartz veins found within the South Orebody.

4.5.3 Sampling

Samples were obtained from diamond drill core which intersected the South Orebody. DDH hole NS-4 was drilled on a south-eastern azimuth through the synclinorium to a downhole depth of 420 m. This is the southernmost deposit sampled during this study, and rocks in this area have clearly been affected by regional metamorphism as is evident from the remobilised nature of chalcopyrite aggregates in Figure 4.24.

Samples isolated for the fluid inclusion part of the study yield evidence of the character of fluids present during metamorphism in this area.

4.6 The Konkola deposit

4.6.1 Geological setting of the Konkola deposit

The Konkola deposit is situated in the town of Chililabombwe in the north-western Copperbelt region. The basement to the Katanga Supergroup in this area is comprised of Lufubu biotitic gneisses and schists, which are intruded by later granites (Schwellnus, 1961). The Muva quartzites also form part of the basement as overlying the Lufubu gneisses with conglomeratic horizons (Schwellnus, 1961). The basement is also comprised of a granitic porphyry, called the Muliashi porphyry (Figure 4.25).

The Katanga overlies the basement and commences with a boulder- and pebble conglomerate, which is followed by the medium-grained Footwall Quartzite Formation of the lower Roan Group. This formation contains some layers of boulder conglomerates. The quartzites are overlain by the Footwall Aquifer which is divided into the Porous Conglomerate (Figure 4.26a), Footwall Sandstone (Figure 4.26b), and Footwall Conglomerate (Figure 4.26c-d). The Ore Shale follows paraconformably on top of the Footwall Conglomerate. The ore horizon is a sequence of siltstones and carbonate bands. The rest of the overlying lower Roan Group comprises the Hangingwall Quartzite, Hangingwall Aquifer, and Shale With Grit. The upper Roan Group is composed of dolomites with intercalated sandstones and shale layers. Another conglomeratic layer is located at the top of the upper Roan Group. The dolomitic siltstones and shales and massive dolomite of the Mwashya Subgroup overlies this conglomerate layer. The Mwashya is followed by the marker tillite horizon of the *Grand Conglomerat*, and the cap carbonate Kakontwe Limestone sequence.

4.6.2 Mineralisation at the Konkola deposit

Copper mineralisation is found in two orebodies in the Konkola area which are accessed through the southern No.1 and the northern No. 3 shafts. The ore horizon is divided into five lithological units: (a) Unit A at the base of the Ore Shale consists of a pink-white argillitic to dolomitic siltstone, ~0.5m thickness. Chalcocite is the main copper sulphide; (b) Unit B is bedded to massive fine-grained siltstone in the absence of dolomitic horizons, ~2.5m thickness; (c) Unit C consists of interbedded siltstone and dolomite, ~2.5m thickness; (d) Unit D is comprised of interbedded siltstone and dolomite layers where the beds are thicker than the underlying unit, ~2m thickness; (e) Unit E is a siltstone interbedded with lenses of dolomitic sandstone.

Thin laminations of secondary malachite (± bornite and chalcocite) are abundant in the Ore Shale and are commonly observed redistributed along sheared planes. Recently, Re-Os dating of disseminated chalcopyrite and bornite in pre-folding veinlets of the Konkola ore formation revealed an isochron age of 816± 62 Ma (Barra and Broughton, 2005, unpublished data in Selley *et al*., 2005).

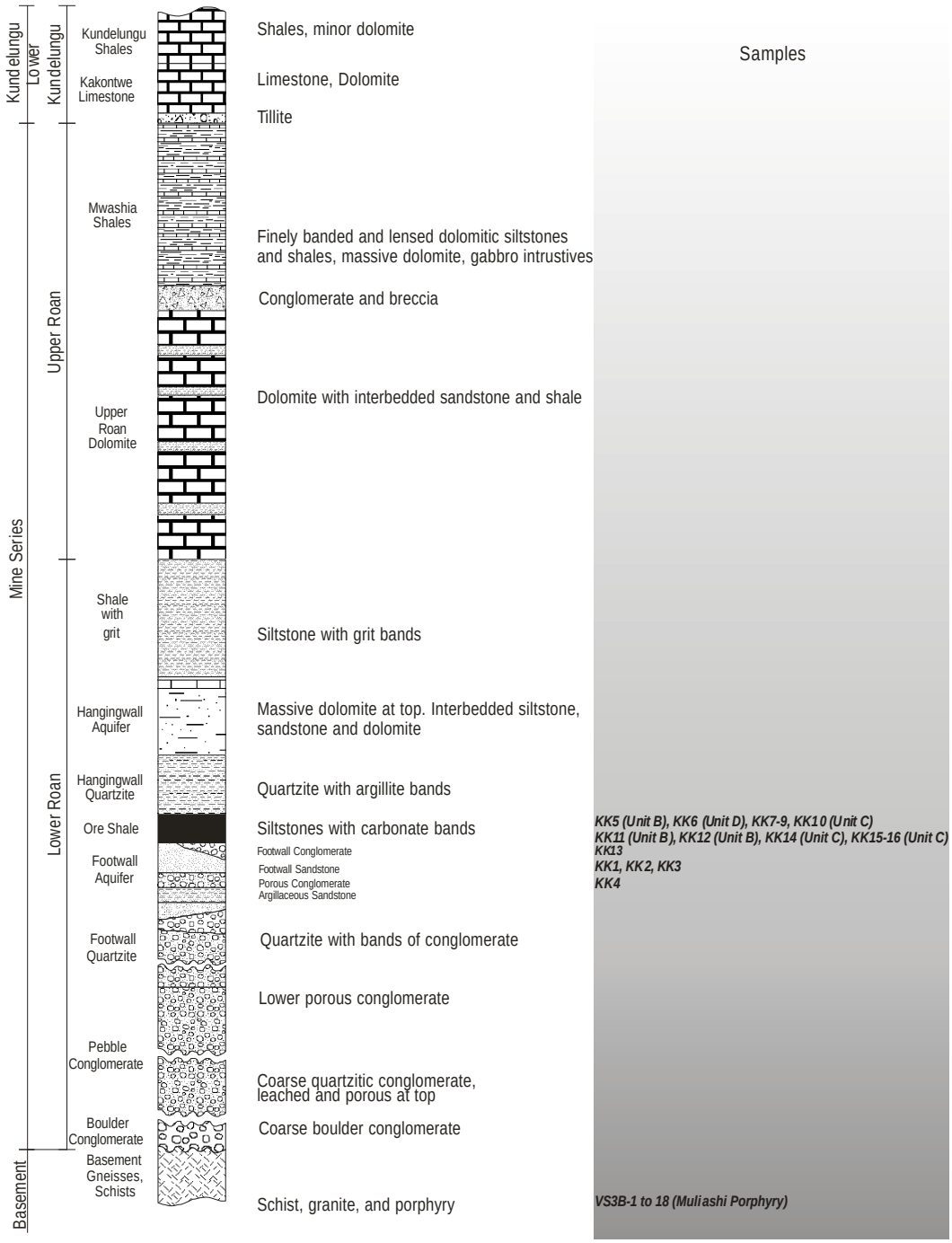

Figure 4.25. Generalised stratigraphic profile of the Konkola area, with list of samples (after Konkola Copper Mines plc, ZamAnglo Prospecting).

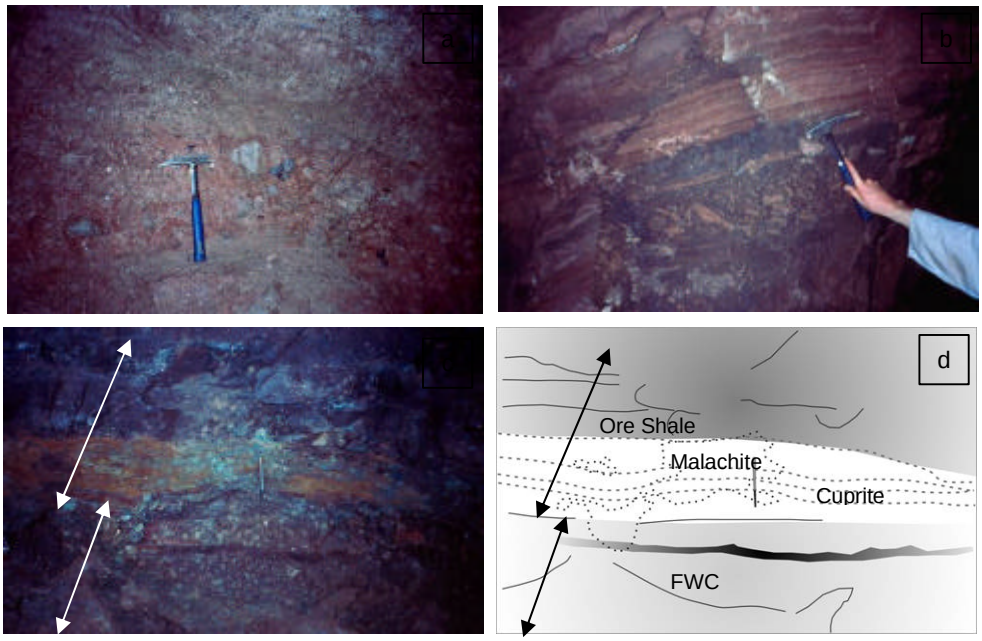

Figure 4.26. (a) the Porous Conglomerate with grey granite cobbles in the matrix-supported conglomerate, No.3 Shaft, 1750MW; (b) the Footwall Sandstone, and (c) Footwall Conglomerate with overlying Ore Shale horizon at No. 3 Shaft underground; (d) cartoon showing the Footwall Conglomerate and overlying Ore Shale horizon which is partly oxidized to malachite and cuprite. The underlying Footwall Conglomerate shows a reddish colour compared to the overlying black carbonaceous, silty shale.

4.6.3 Sampling at the Konkola deposit

Samples of the Footwall Sandstone, Porous Conglomerate, Unit B, C, and D of the Ore Shale, as well as bedding parallel- and crosscutting quartz-carbonate ± sulphide veins were taken at the No.3 Shaft underground section (see Figure 4.26). The Hangingwall Quartzite was sampled at the No.1 Shaft underground section. The earliest fluid inclusion assemblages trapped in the sandstones of the footwall to mineralisation would contain fluids that circulated within the basin during diagenetic stratiform copper mineralisation. In addition to these samples, the quartzite of the hangingwall formation was sampled in order to characterise fluids expelled during diagenesis. The reasoning for sampling crosscutting quartz veins was to constrain fluids present during basin compaction possibly during the onset of regional deformation.

Chapter 5

BASINAL FLUIDS OF THE ZAMBIAN COPPERBELT

- Chambishi
- Nchanga
- Konkola

5.1 Introduction

Samples from the Chambishi, Nchanga, and Konkola deposits yield evidence of the P-T-X conditions prevalent during the Katangan burial stage prior to the onset of regional deformation (Figure 5.1). This chapter documents the petrography, microthermometric and Raman spectroscopic results along with the P-T-υ-X nature of fluid inclusions trapped during the early stages of basin evolution subsequent to stratiform mineralisation but prior to regional deformation and metamorphism of the Copperbelt. Each section in this chapter describes the evidence for classification of inclusion assemblages of the Chambishi, Nchanga, and Konkola deposits. Metasediments and (quartz) veins containing fluid inclusions were sampled and described according to field relationships and relative timing in the regional tectonic framework (Figure 5.2). During the petrographic study, inclusions in these samples were classified based on fluid inclusion assemblages (FIA) which are in turn related to the tectonic framework.

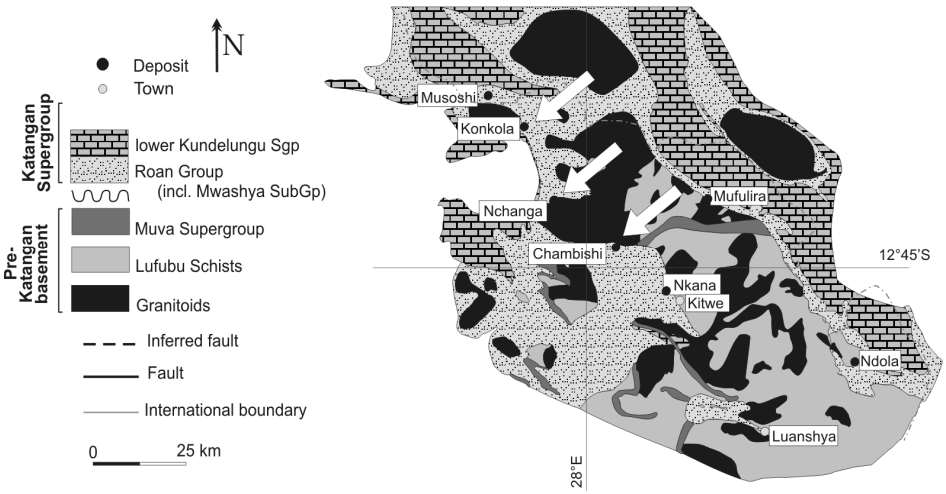

Figure 5.1. Geology map of the Zambian Copperbelt indicating the localities of the Chambishi, Nchanga, and Konkola deposits where early fluids are found.

The methodology used during sampling is of key importance in characterising fluids as either early or late in the regional tectonic framework (Figure 5.2). Samples were collected of lower Roan Group metasediments and of veins within the sequence. In samples of the metasediments, it was noted which features were identifiable such as authigenic overgrowths or growth-zone boundaries where fluids expelled during diagenesis may have been trapped. Samples of metasediments from the Nchanga and Konkola deposits were earmarked as possibly containing fluids that would have been expelled during diagenetic compaction prior to metamorphism. The nature of field associations with the host rock was described during vein sampling. A quartz vein in the

Ore Shale horizon formed by lateral secretion and shows a visible axial planar cleavage refracted through the shale into the quartz vein at the Chambishi deposit.

During the petrographic investigation of double polished wafers of these samples, fluid inclusion assemblages (FIA's) were identified, and individual inclusions were classified based on the surrounding assemblage. The initial stages of microthermometry revealed the composition of inclusions, and minimum trapping conditions of these assemblages.

Fluids circulating within the basin during the early stages of basin evolution were trapped in samples from Chambishi, Nchanga and Konkola. During the petrographic examination of several double polished wafers, fluid inclusions were classified based on their occurrence in relation to other inclusions as either isolated, clusters, or as fluid inclusion planes.

By identifying inclusions as part of fluid inclusion assemblages (Goldstein and Reynolds, 1994), inclusions were classified either as primary or secondary (see Chapter 2 for discussion on methodology). Data from fluid inclusions trapped during the early stages of basin evolution, after stratiform copper mineralisation, is presented in this chapter and include samples from the Chambishi, Nchanga and Konkola deposits.

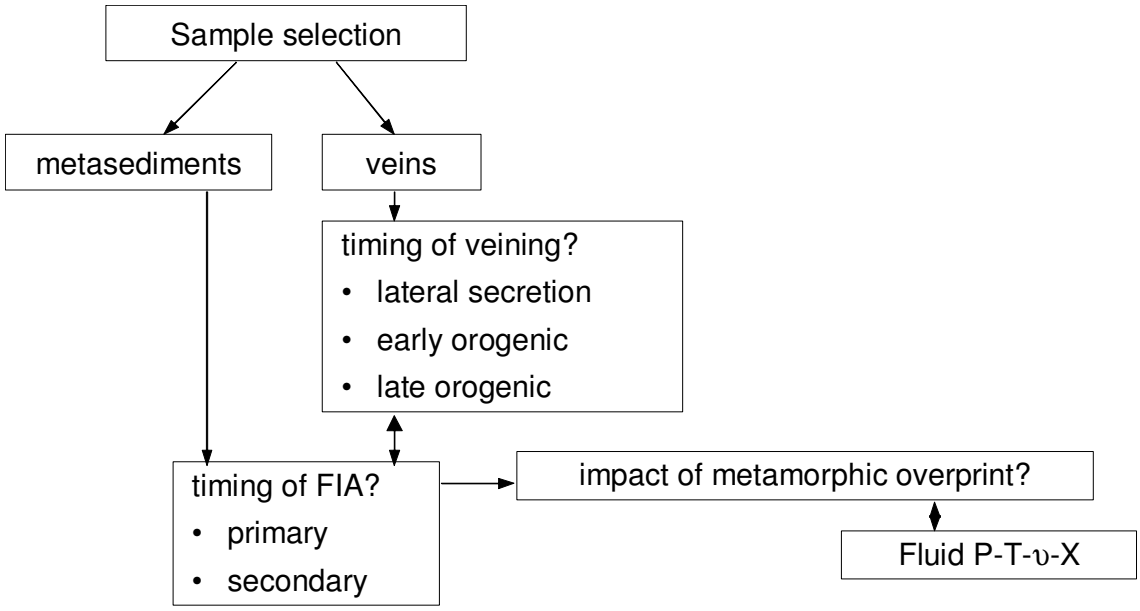

Figure 5.2. The sequence of actions used to determine the final P-T-υ-X conditions of fluids present during early basin history.

5.2 Chambishi

5.2.1 Chambishi sample selection

The lower Roan was sampled from the Chambishi open pit, which accesses the Chambishi Main Orebody (Garlick, 1961d; Fleischer *et al.*, 1976). Samples for the fluid inclusion study were selected from mainly two localities in the open pit, namely from a lateral secretion quartz vein, hosted in the Ore Shale (section 4.1.3; Figure 5.3), as well as from bedding-parallel quartz veins in the hangingwall metasediments in the east-south-eastern section of the open pit. In particular, the occurrence of a lateral secretion quartz vein enables the study of fluids circulating within the basin during the late stages of diagenesis, after stratiform copper mineralisation.

As discussed in Chapter 4, early fluids are hosted in inclusions of a lateral secretion quartz vein present in the Ore Shale horizon at the Chambishi deposit. Stratiform copper mineralisation in the Ore Shale is depleted around the quartz vein leaving a ~ 15cm depletion halo around the vein, which is mineralised with bornite and chalcopyrite. An axial planar cleavage, imprinted on the Ore Shale horizon during folding, is also present in the quartz vein and is refracted in the quartz vein due to different rheological characteristics of the quartz vein and silty shale. The introduction of the quartz vein therefore predates folding which is a result of basin deformation.

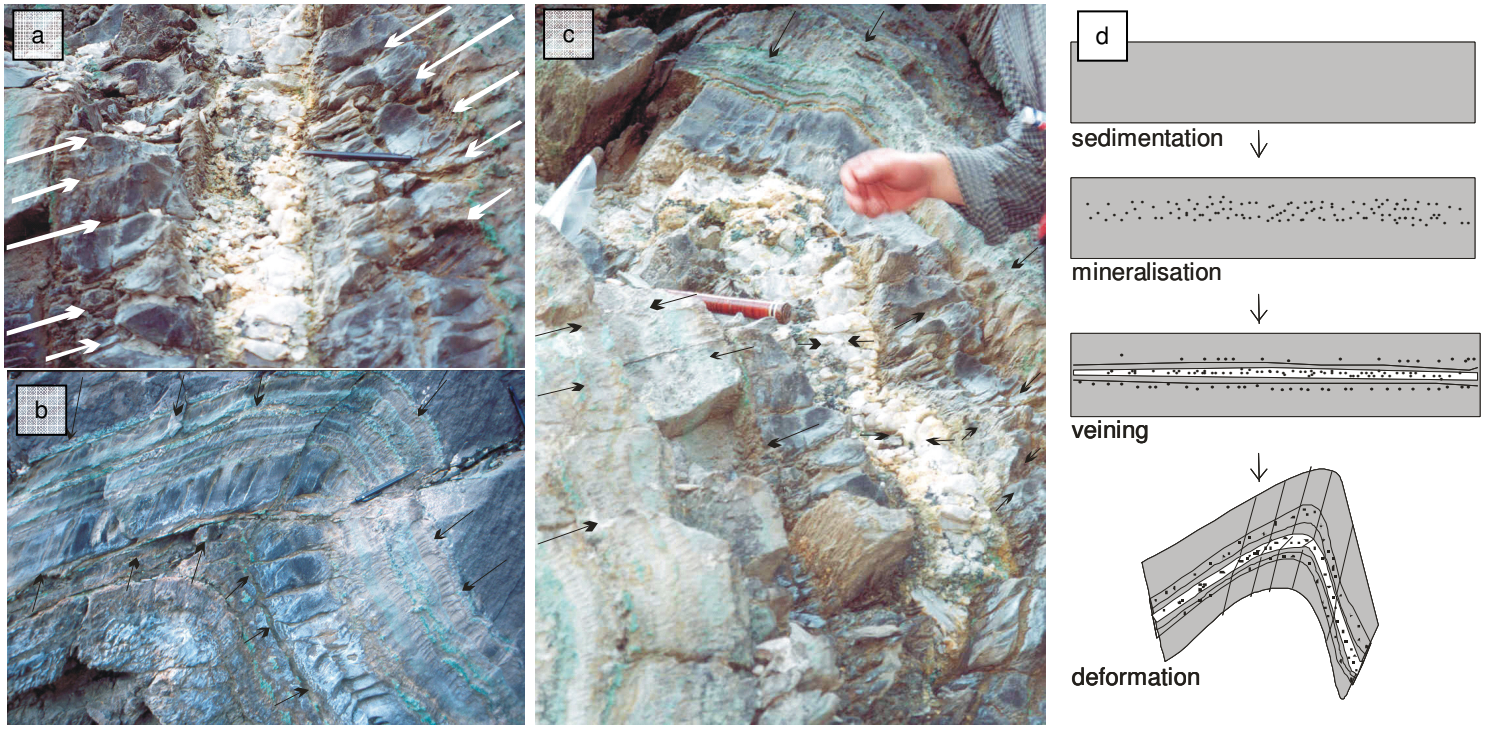

Figure 5.3. (a) Quartz veining in the mineralised and folded metasediments of the ore shale horizon in the lower Roan Group, at the Chambishi open pit. The quartz vein contains chalcopyrite and malachite. An axial planar cleavage, trending northeast-southwest in (b) is present within the ore shale, and becomes refracted through the quartz vein (c), which attests to the formation of the vein prior to deformation producing the cleavage. (d) Schematic illustration of the sequence of events, from sedimentation, followed by diagenetic stratiform mineralisation, veining, and subsequent deformation, resulting in the development of an axial planar cleavage in the host sediments. Also see Figure 4.2.

Isolated fluid inclusions hosted in the quartz vein are interpreted to be of primary origin and coincides with the quartz vein formation. Primary inclusions from these samples (Figure 5.3) are interpreted as representative of post-mineralising, pre-metamorphism fluids, and constrain P-T-υ-X conditions of fluids circulating within the basin during the final stages of diagenesis, after stratiform copper mineralisation prior to the onset of deformation.

The following fluid inclusion types are described based on their paragenetic setting in the tectonic framework and based on their composition determined from microthermometric investigation and Raman microspectroscopy.

5.2.2 Microthermometry

Primary aqueous inclusions

Aqueous fluid inclusions are found as both isolated inclusions and secondary planes (Figure 5.4). The secondary inclusions from the lateral secretion vein are considered to be early deformational in origin and are discussed in chapter 6. Isolated inclusions range in size between 7-18 µm diameter, and the amount of vapour is estimated at 8-20 vol.% of the total inclusion volume.

Initial melting of isolated inclusions at between -50 and -25 °C (n=10) is interpreted to be eutectic melting. Eutectic melting temperatures of isolated inclusions indicate the presence of H_2O - NaCl - $MgCl_2$ - $CaCl_2$ (Goldstein and Reynolds, 1994; Roedder, 1984). The melting of hydrohalite (T_mhh) is observed in some inclusions as a clearing of smaller crystals at low temperature, and this ranges between -22.4 and -19.0 °C (n=8). In all cases, melting of hydrohalite occurred prior to ice melting. These primary aqueous inclusions trapped during the early stages of basin evolution are moderately enriched in NaCl relative to $CaCl_2$ when plotted on a H_2O - $CaCl_2$ - NaCl ternary phase diagram as in Figure 5.5 (after Williams-Jones and Samson, 1990). Refer to Table 5.1 for a list of microthermometry results.

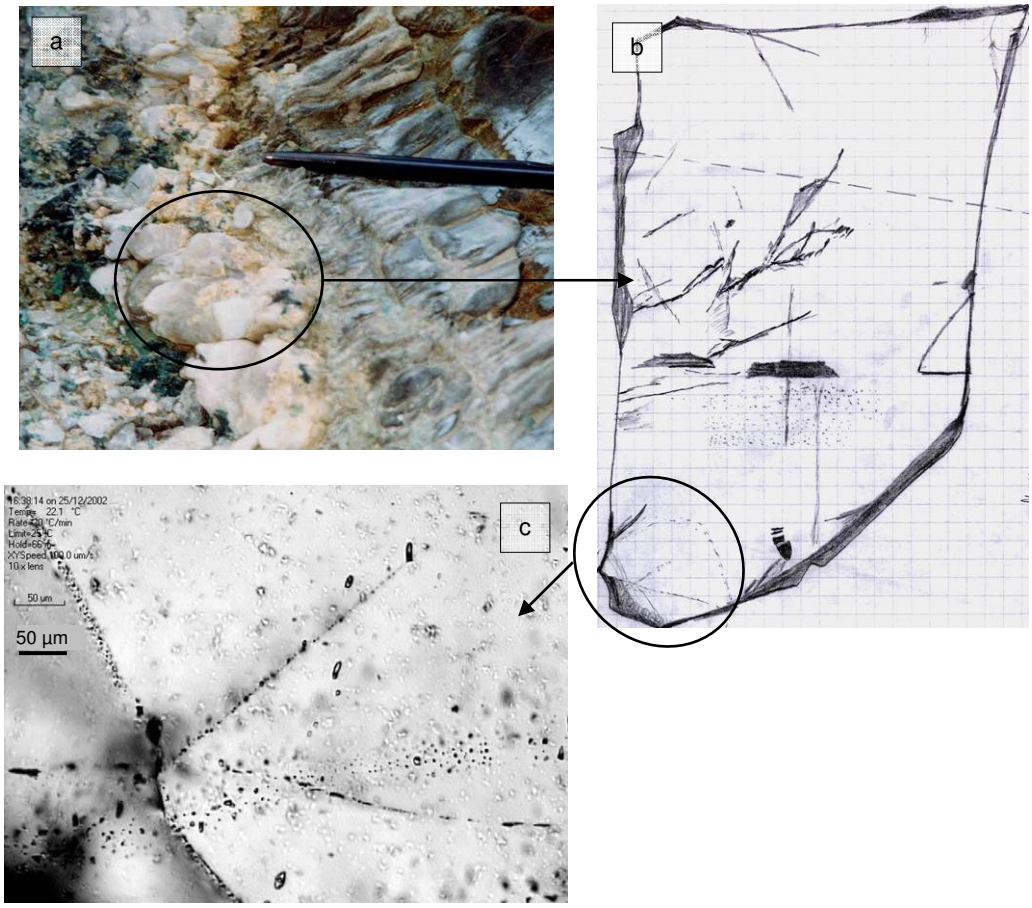

Figure 5.4. (a) A lateral secretion quartz vein in the Ore Shale from the Chambishi open pit contains primary chalcopyrite stratiform mineralisation which is oxidised to mainly malachite (see Figure 5.2). (b) During the petrographic investigation of this sample, a sketch of a double polished wafer was produced revealing the presence of isolated primary inclusions as well as secondary fluid inclusion planes. (c) Microthermometric study is applied to fluid inclusion assemblages identified during petrography. Isolated inclusions are less abundant than trails of various generations. Due to the tectonic setting of this vein and nature of inclusion trails, these trails are interpreted as secondary and their origin probably coincides with the onset of basin metamorphism (see following chapter). Flinc. no. CBSqz 3B.

Final ice melting temperatures (T_{mice}) for isolated inclusions range from -9.5°C to -21.1°C (Figure 5.6), corresponding to salinities of between 13.4 and 23.1 wt.% $NaCl_{equiv.}$ (Figure 5.7). Final homogenisation (T_{htotal}) was to the liquid phase ranging from 86 to 129°C (n=7, Figure 5.8).

Table 5.1. Data for isolated aqueous fluid inclusions from Chambishi (all from sample CBSqz8A). Salinity (expressed as eNaCl) is given in weight percent NaCl determined from microthermometry. Molality Cl^- is determined for specific inclusions from Raman microspectrometry. All inclusions are two-phase liquid and vapour at room temperature.

Flinc	Size µm	Vap Vol%	Te	Tmhh	Tmice	Th	Phase	Salinity eNaCl	Salinity after chlorinity	Cl^-	Bulk ρ g/cm^3	LA ICPMS
(1) 1	10	10	-35.0		-21.1	dec		23.1				-
(1) 2	9	10	-47.0		-21.1	129	L	23.1	11.39	2.2	1.11	-
(1) 5	18	20	<-25	-21.0	-12.3			16.2				-
(1) 6	9	10	-50.0	-21.0	-9.5	110	L	13.4			1.03	-
(1) 7	10	8	-50.0	-19.0	-9.5	109	L	13.4			1.03	-
(1) 8	9	10	-50.0	-19.0	-9.5	107	L	13.4			1.03	-
(1) 9	11	10	-45.0	-22.0	-13.6	126	L	17.4	16.98	3.5	1.05	-
(1) 10	10	10	-45.0	-22.0	-13.6	129	L	17.4			1.05	-
(1) 11	7	10	-45.0	-22.0		86	L					-
(2) 1	10	10	-40.0	-22.4	-12.3			16.2				-

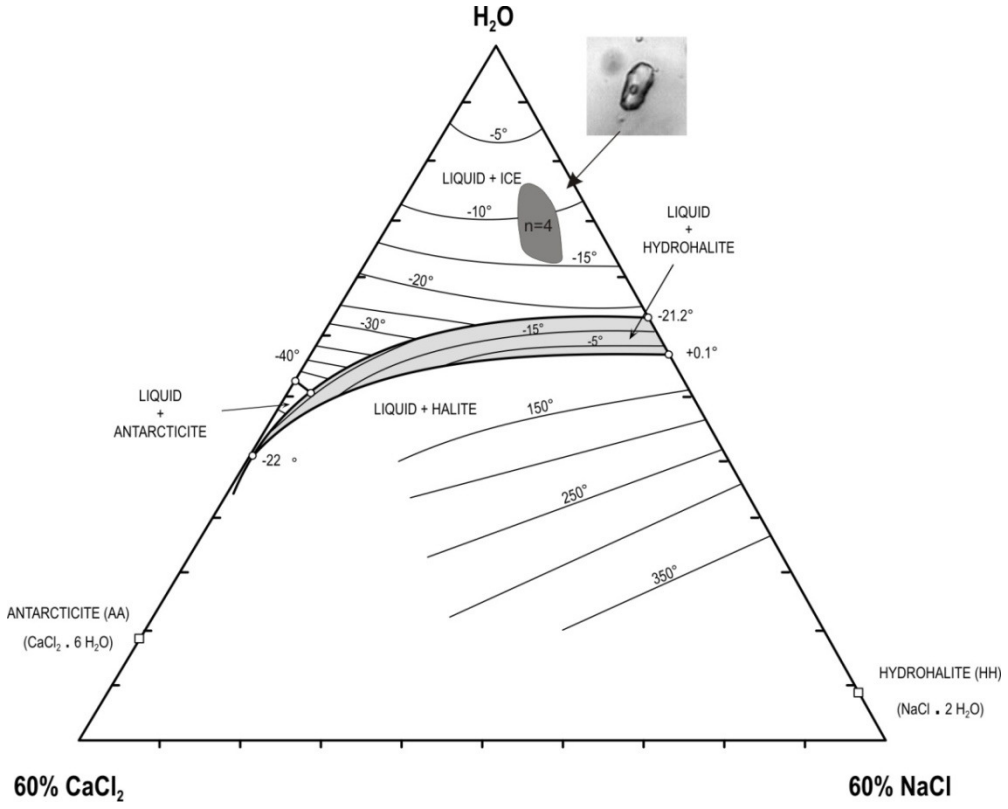

Figure 5.5. H_2O-$CaCl_2$-NaCl ternary phase diagram for primary aqueous inclusions of the Chambishi deposit representative of early fluids. No hydrohalite melting temperatures were measured for Nchanga and Konkola inclusions. Thick solid black lines correspond to cotectic curves separating the stability fields of halite, hydrohalite and ice. Thin solid lines represent isothermal fields in °C. Figure modified after Williams-Jones and Samson, 1990.

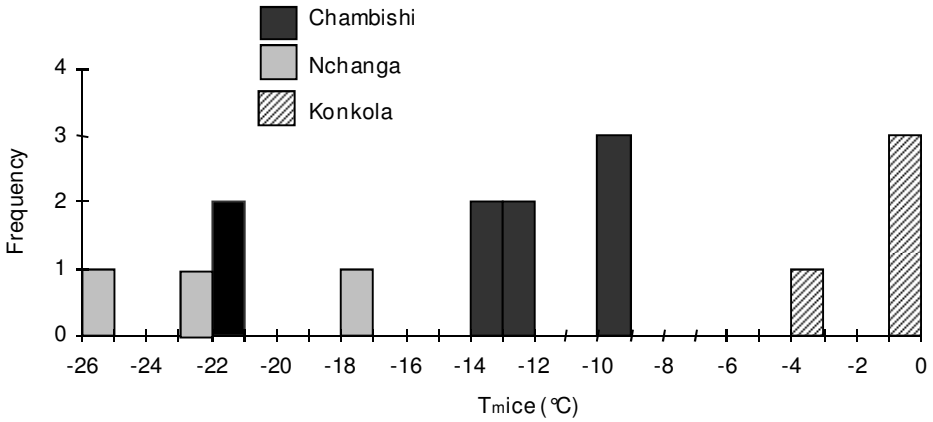

Figure 5.6. Histogram showing the distribution of final ice melting temperatures of aqueous inclusions in isolated early inclusions from the Chambishi, Nchanga and Konkola deposits.

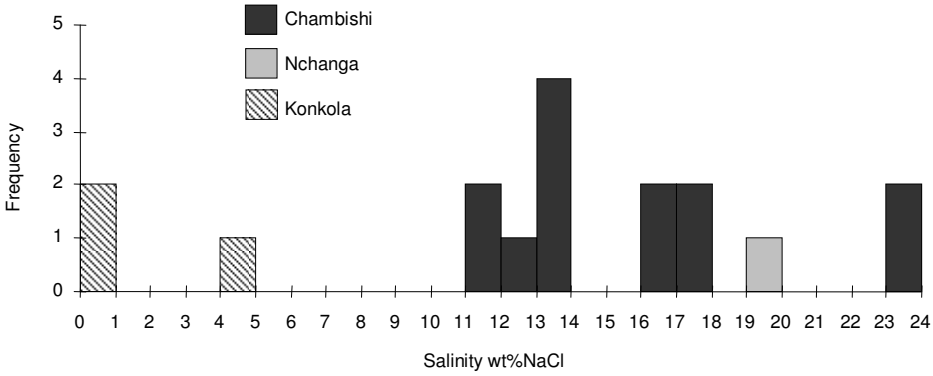

Figure 5.7. Salinities displayed for primary aqueous and aqueo-carbonic inclusions representative of early inclusions from the Chambishi, Nchanga, and Konkola deposits. Salinities are expressed in wt.% $NaCl_{equiv.}$ and are determined from microthermometric measurements for aqueous inclusions, and from chlorinity for aqueous-carbonic inclusions.

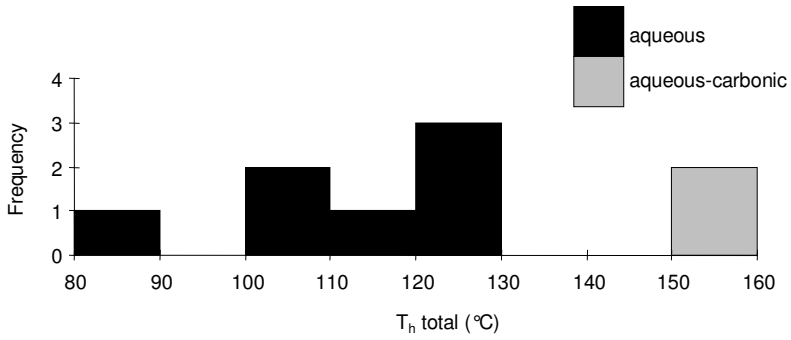

Figure 5.8. Histogram of final homogenisation temperatures ($T_h$total) for aqueous and aqueo-carbonic isolated inclusions of the Chambishi deposit representing early fluids.

Primary aqueo-carbonic inclusions

Several inclusions consist of mixed aqueous and non-aqueous phases (Figure 5.4). Isolated aqueo-carbonic inclusions range in size between 10-15 µm, containing between 10-60 vol.% vapour (Table 5.2). This inclusion type also occurs as secondary trails, and is discussed in the following chapter under *early orogenic fluids*. Melting of carbonic phases of isolated inclusions (T_mCO_2) occur between -56.8 and -57.9 °C (n=4). Homogenisation of the carbonic components (T_hCO_2) in isolated inclusions was to the liquid phase at between 11.8 and 26.9 °C (n=5). Salinities of the aqueous phases of inclusions were calculated from the chlorinity measurements (Table 5.3) between 11.9 – 13.2 wt.%$NaCl_{equiv}$ (Figure 5.7).

Table 5 2. Data for basinal primary aqueo-carbonic inclusions from Chambishi. Salinity if expressed in weight percent $NaCl_{equiv.}$ obtained from chlorinity measurements during Raman microspectroscopy.

Sample	Flinc	Type	Phase	Size µm	Vap Vol%	Te	Tmhh	Tmice	Th	Phase	$TmCO_2$	$ThCO_2$	Phase	Tmcla	Salinity eNaCl
CBSqz 3A	(6) 2	Lw-c	2ph	15	10	-37.0	-20.8	-	-	-	-	-	-	2.0	-
CBSqz 3A	(6) 10	Lc-w	3ph	11	60	-40.0	-	-22.1	-	-	-56.8	22.8	L	2	13.2
CBSqz 3A	(6) 11	Lw-c-s	4ph	12	20	-	-	-	-	-	-57.9	23.9	L	2	-
CBSqz 3A	(6) 12	Lw-c	3ph	12	20	-	-	-			-57.9	26.9	L	2.2	12.9
CBSqz 8A	(1) 3	Lw-c	3ph	12	25	-	-	-	150	L	-57.0	11.8	L	3.0	11.9
CBSqz 8A	(1) 4	Lw-c	3ph	10	25	-	-	-	150	L	-	15.0	L	3.0	-

Table 5.3. Raman data for basinal primary aqueo-carbonic inclusions from Chambishi. Salinity is calculated from chlorinity (expressed in molality Cl-) obtained from Raman microspectrometry and quoted in NaCl-equivalent in weight percent.

			%mol							Bulk composition (%)									LA-ICP-MS[1]
	Flinc	Salinity eNaCl	CO_2	N_2	H_2S	CH_4	C_2H_6	H_2	Cl^-	H_2O	CO_2	N_2	CH_4	H_2S	C_2H_6	H_2	NaCl	ρ g/cm^3	
CBSqz 3A	(6) 2	-	98.5	≤1	-	0.6	-	-	-	98.2	1.8		-	-	-	-	-	0.90	Available
CBSqz 3A	(6) 10	-	>98.5	1	≤0.2	-	-	-	-	62.1	33.9	0.5	-	-	-	-	3.5	0.86	Available
CBSqz 3A	(6) 11	-	99	≤1	-	-	-	-	-	85.4	9.7	0.1	-	-	-	-	4.8	0.99	-
CBSqz 3A	(6) 12	-	>99.5	≤0.2	≤0.2	-	-	-	-	85.7	9.6	0.0	-	-	-	-	4.7	0.98	Available
CBSqz 8A	(1) 3	10.93	98	≤0.5	-	2	-	-	2.1	82.4	13.0	0.2	-	-	-	-	4.4	0.99	-
CBSqz 8A	(1) 4	-	-	-	-	-	-	-	-	Bubble moved under Raman laser, no spectrum.									-

[1] In addition to these three inclusions, LA-ICP-MS was performed on another eight inclusions of the same type in sample CBSqz 3A in area 6 (see Chapter 8 for LA-ICP-MS results).

5.2.3 Raman microspectroscopy

Primary aqueous inclusions

Bulk fluid densities were calculated using the BULK computer programme as mentioned in Chapter 2, and the Zhang and Frantz (1987) equation of state for H_2O-NaCl-KCl-$CaCl_2$ solutions was used. Bulk inclusion densities for primary aqueous inclusions range between 1.03 and 1.11 g/cm^3 (see Table 5.1).

Raman analysis was performed on the aqueous phases of two inclusions where observational difficulties was experienced. For one inclusion, the correlation was poor between salinity determined from Tmice and that obtained using chlorinity. The other inclusion showed a good correlation (Table 5.1). For these two inclusions, chlorinity was measured at 2.2 and 3.5 mol/kg H_2O, which translates to a salinity of 11.39 and 16.98 wt.% $NaCl_{equiv}$. A higher confidence is placed in the salinity obtained using chlorinity concentration due to the size of the inclusion (9µm) and the difficulty in observing phase changes for this particular inclusion.

Primary aqueo-carbonic inclusions

Carbonic phases of isolated inclusions consist of CO_2 ranging between 98 and >99.5 mol%, with N_2 and CH_4 comprising the remainder of the vapour phases (Figure 5.9). Raman microspectroscopy revealed the presence of possible magnesite ($MgCO_3$) in one isolated inclusion (flinc no. CBSqz 3A(6)11) with T_hCO_2 = 23.9°C . The chlorinity of the aqueous phase of one inclusion was determined at 2.1 mol/kg H_2O, translating to a salinity of 10.9 wt.% $NaCl_{equiv}$ (Table 5.3).

Bulk densities range between 0.86 and 0.99 g/cm^3 (Table 5.3). Bulk inclusion compositions were determined ranging from 62.1 to 98.2 % H_2O, 1.8 to 33.9 % CO_2, 0.03 to 0.5 % N_2, and 3.5 to 4.8 % NaCl (Table 5.3).

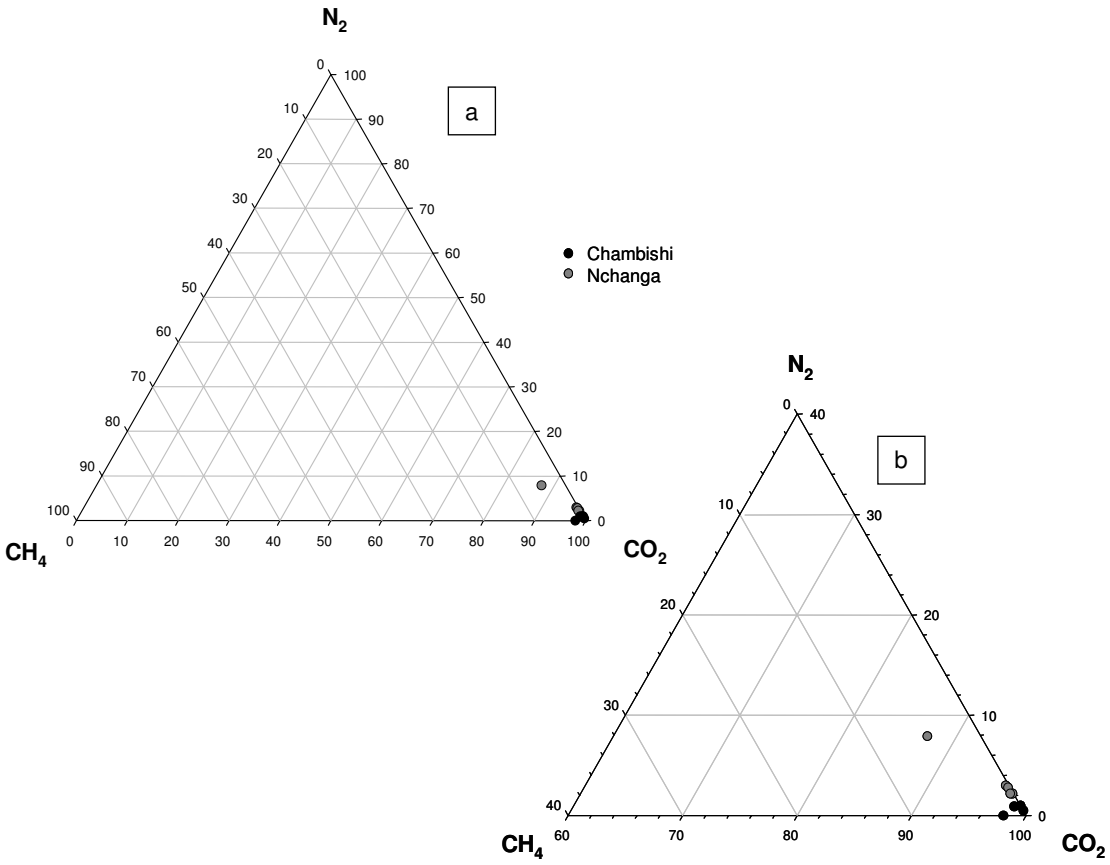

Figure 5.9. (a-b) Ternary CO_2 - N_2 - CH_4 plot of volatile compositions of primary aqueo-carbonic inclusions of early fluids of the Chambishi and Nchanga deposits. Compositions (in mol.%) are determined by Raman analysis. The area of interest around CO_2 in (a) is enlarged in diagram (b). See text for details.

5.3 Nchanga

5.3.1 Nchanga sample selection

Samples for the fluid inclusion study were collected from the footwall arkosic unit and Lower Banded Ore Shale (LBS), which were accessed from the underground C-Shaft section, and underground inclined shaft to the Chingola B area (Figure 4.14). The Pink Quartzite and Feldspathic Quartzite (TFQ) of the Intermediate- and Upper ore bodies were sampled from the open pit (Figures 5.10 and 5.11).

Several samples were investigated as possible fluid inclusion study specimens. Eleven (11) were selected for microthermometry (Table 5.4). These samples were selected based on the occurrence and fluid inclusion size, and are:

- non-mineralised arkose from the footwall below the lower orebody (LOB); samples NCH10A, NCH 10B.
- mineralised bornite-chalcopyrite-carrollite-quartzite from the Feldspathic Quartzite horizon of the upper orebody (IOB); samples NOP 16A and NOP 20A.

Table 5.4. Summary of primary fluid inclusions identified from the Nchanga deposits.

Area	Orebody and lithology	Sample	Host	Occurrence	Type
Nchanga open pit	Feldspathic Quartzite (TFQ)	NOP 16A	quartzite	isolated	Lw (±c, ±s)
		NOP 20A	quartz vein	isolated	Lw-s
C-Shaft	Lower Orebody, Arkose Footwall	NCH 10A	arkose	isolated	Lw (±s)
		NCH 10B	arkose	isolated	Lw-c-s

Primary inclusions found within the footwall arkose below the lower orebody, and the quartzite of the upper orebody, may represent fluids expelled during diagenesis and the early stages of maturation of the basin. The effects of preferential water leakage and other post-trapping modifications of early inclusions were considered during the microthermometric investigation. Irregular shaped inclusions and possibly modified liquid-vapour ratios were identified in inclusions from the Nchanga Lower Orebody in the arkosic footwall (NCH10B). Although these inclusions are hosted in the arkosic footwall sediments, and appear to be of primary origin in the quartz grains, these inclusions are considered to have been modified after trapping occurred. This hypothesis is further supported by elevated homogenisation temperatures (~240°C) which are not characteristic of diagenetic fluids, and these inclusions are further discussed in the chapter dealing with late orogenic fluid inclusions.

Inclusions in Nchanga quartzite samples were typically less than 10 µm in diameter which hindered the measurement of phase transitions during microthermometry. All inclusions were found in quartz grains and on grain boundary junctions (Figure 5.11). These textures may also be related to diagenesis or later recrystallisation during metamorphism.

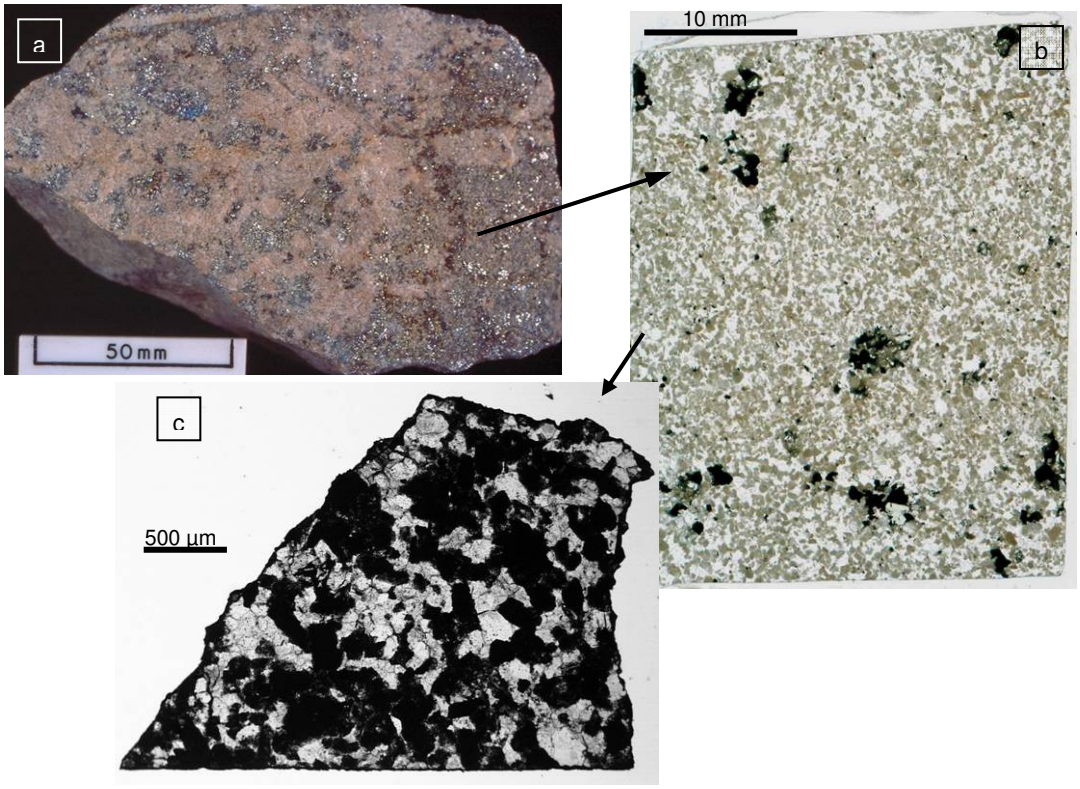

Figure 5.10. Feldspathic quartzite from the Upper Orebody with disseminated bornite, chalcopyrite and carrollite mineralisation (NOP 16) in hand-sample (a), as initial large double polished wafer (b), and as (c) broken double polished wafer ready for microthermometry. Fluid inclusions were identified in grains of quartz in the alkali-feldspar-quartz-bearing quartzite.

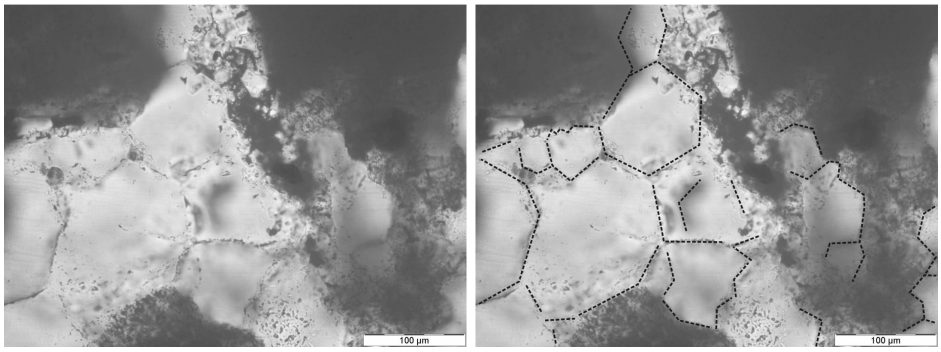

Figure 5.11. Prismatic recrystallisation textures in grains of quartz in a double polished wafer (quartzite sample NOP 16A-3). The image on the right outlines the prismatic textures which may be interpreted as authigenic overgrowths. Inclusions found in the centre of these textures are believed to be of primary origin, with inclusions in trails along the edges of the textures as secondary. Any inclusions along the edges of the prisms were too small for any reliable measurements to be taken and were mostly empty with large or total vapour phases. Opaque areas in the images are grains of alkali feldspar.

5.3.2 Microthermometry

Primary aqueo-carbonic inclusions

Isolated inclusions were identified in sample NCH 10B(1) of the arkosic footwall, and in mineralised feldspathic quartzite (sample NOP 16A). The majority of these inclusions contained a solid daughter crystal of halite, noted at room temperature. However, due to observation difficulties, it was not possible to obtain accurate salinity data from these inclusions (i.e., melting of halite was not accurately observed). Measurements of aqueous phase transitions were hampered due to observational difficulties related to the size and placement of inclusions. Inclusion sizes varied between 7 and 15 µm (Table 5.5). The percentages of vapour present are varied (Figure 5.12) and range from ~10% (sample NCH 10B), and between 10-80% (sample NOP 16A) using the volumetric estimation chart by Roedder (1972).

Initial melting of the aqueous phase was measured for two inclusions at -47 and -37 °C. Ice melting ($T_m$ice) was measured at -25 to -17 °C (Figure 5.6, Table 5.5). Three inclusions contained halite as daughter minerals (sample NOP 16A). T_mCO_2 for sample NCH 10B was measured at -97.6 and -97.4 °C, and between -57.5 and -57.3 °C for sample NOP 16A. T_hCO_2 was measured between -16.7 and -11.9 °C to the liquid phase. One inclusion showed T_hCO_2 at 0.3 °C, and another at 27.1 °C. $T_m$clathrate was measured between -10 °C and 14°C (Table 5.5). This is a high temperature for clathrate melting, however, the presence of CH_4-clathrates have been documented in inclusions at temperatures as high as +18 °C (Roedder, 1984, p. 241). Description of the Raman analysis results follows and data is displayed in Table 5.6.

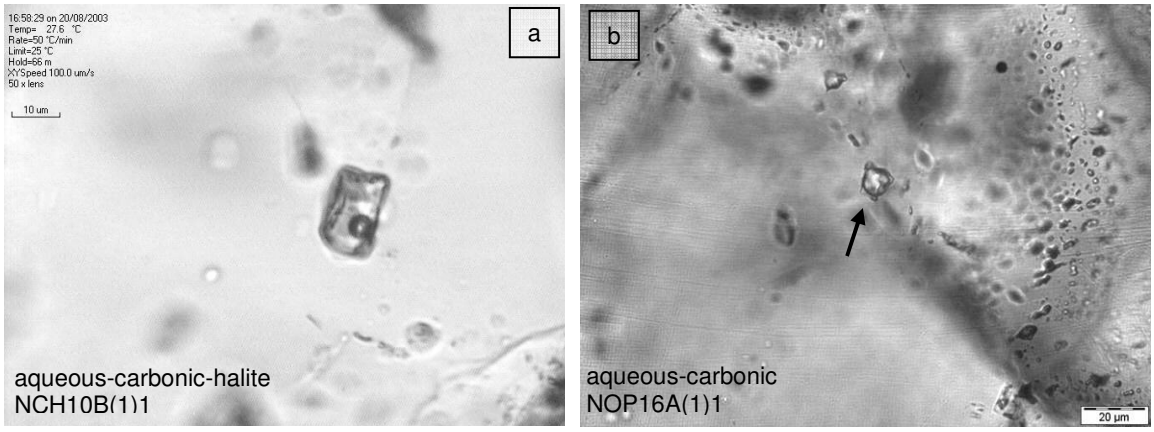

Figure 5.12. (a) Isolated aqueous-carbonic fluid inclusion with halite daughter crystal (top left corner) in arkosic footwall sediments underlying the lower orebody. (b) Isolated aqueous-carbonic inclusion from mineralised feldspathic quartzite of the upper orebody.

Table 5.5. Microthermometry data for primary aqueo-carbonic basinal inclusions of Nchanga.

Sample	Flinc	Type	Phase	Size µm	Vap. Vol%	Te	Tmice	$TmCO_2$	$ThCO_2$	Phase	Tmcla	LA-ICPMS
NCH 10B	(1) 1	Lw-c-s	3ph	15	10	-	-	-97.6	-	-	-	-
NCH 10B	(1) 2	Lw-c-s	3ph	9	10	-	-	-97.4	-	-	-	-
NOP 16A	(1) 1	Lc-w	2ph	11	70	-	-	-57.4	-16.7	L	-	Available
NOP 16A	(1) 2	Lc-w-(s)	3ph	9	80	-	-	-57.5	-11.9	L	-	Available
NOP 16A	(1) 3	Lc-w-(s)	3ph	8	70	-	-	-57.3	-15.0	L	-10	Available
NOP 16A	(1) 4	Lc-w	2ph	7	70	-	-	-	-	-	-	Available
NOP 16A	(2) 5	Lw-s-(c)	3ph	7	10	-	-25	-	-	-	12	Available
NOP 16A	(2) 6	Lw-s-(c)	3ph	8	10	-	-22	-	0.3	L	-	Available
NOP 16A	(3) 7	Lw-c-s	3ph	9	10	-37	-	-	27.1	L	14	Available
NOP 16A	(4) 8	Lw-s-(c?)	3ph	10	10	-47	-17	-	-	-	-	-
NOP 16A	(1)a	Lc-w	2ph	15	80	-	-	-	-	-	-	Available

Table 5.6. Raman data for primary aqueo-carbonic basinal inclusions of Nchanga.

						Mol%					
Sample	Flinc	Type	Phase	Size µm	Vap. Vol%	CO_2	N_2	H_2S	CH_4	C_2H_6	Comments
NCH 10B	(1) 1	Lw-c-s	3ph	15	10	-	-	-	-	-	
NCH 10B	(1) 2	Lw-c-s	3ph	9	10	87.4	7.9	-	4.7	-	
NOP 16A	(1) 1	Lc-w	2ph	11	70	97.7	2.2	-	<0.3	-	
NOP 16A	(1) 2	Lc-w-(s)	3ph	9	80	96.7	3	-	≤0.3	-	Solid carbon
NOP 16A	(1) 3	Lc-w-(s)	3ph	8	70	97	2.8	-	<0.3	-	Solid carbon
NOP 16A	(1) 4	Lc-w	2ph	7	70	-	-	-	-	-	
NOP 16A	(2) 5	Lw-s-(c)	3ph	7	10	-	-	-	-	-	
NOP 16A	(2) 6	Lw-s-(c)	3ph	8	10	-	-	-	-	-	
NOP 16A	(3) 7	Lw-c-s	3ph	9	10	97.5	2.2	-	≤0.3	-	
NOP 16A	(4) 8	Lw-s-(c?)	3ph	10	10	-	-	-	-	-	Bubble moves under laser
NOP 16A	(1)a	Lc-w	2ph	15	80	-	-	-	-	-	

5.3.3 Raman microspectroscopy

Primary aqueo-carbonic inclusions

Raman analyses indicate that CO_2 is the main component of the volatile phases of primary aqueo-carbonic inclusions (Figure 5.12, Table 5.6). Gaseous compositions range from 87.4 to 97.7 mol.% CO_2, 2.2 to 7.9 mol.% N_2, and from below ≤ 0.3 to 4.7 mol.% CH_4 (Table 5.6). The presence of solid carbon was revealed during Raman analysis in two inclusions with 70 to 80 vol.% vapour. Chlorinity determinations were not possible due to small inclusion sizes.

5.4. Konkola

5.4.1 Konkola sample selection and petrography

The Konkola deposit is situated along the north-western limb of the Kafue anticline in the town of Chillilabombwe in Zambia. The Ore Shale horizon consists of several siltstone horizons with intercalated carbonate bands, and these were sampled as well as the underlying Footwall Conglomerate, Footwall Sandstone and Porous Conglomerate. A detailed petrographic study of these samples revealed a paucity of sufficiently sized fluid inclusions in all abovementioned horizons except for the Porous Conglomerate (Figure 5.14). Therefore, microthermometry was conducted on fluid inclusions hosted in quartz grains of the Porous Conglomerate horizon (Figures 5.13 and 5.14). The Porous Conglomerate matrix feldspars did not yield inclusions suitable for reproducible measurements due to irreversible volume changes noted in alkali feldspars due to thermal expansion during homogenisation (Clarke, 1966; Roedder, 1984; Wilkins, 1979). Fluid inclusion planes of aqueous fluids were identified during the course of this study for the Konkola deposit. In addition to these inclusions, several monophase inclusions were observed at room temperature.

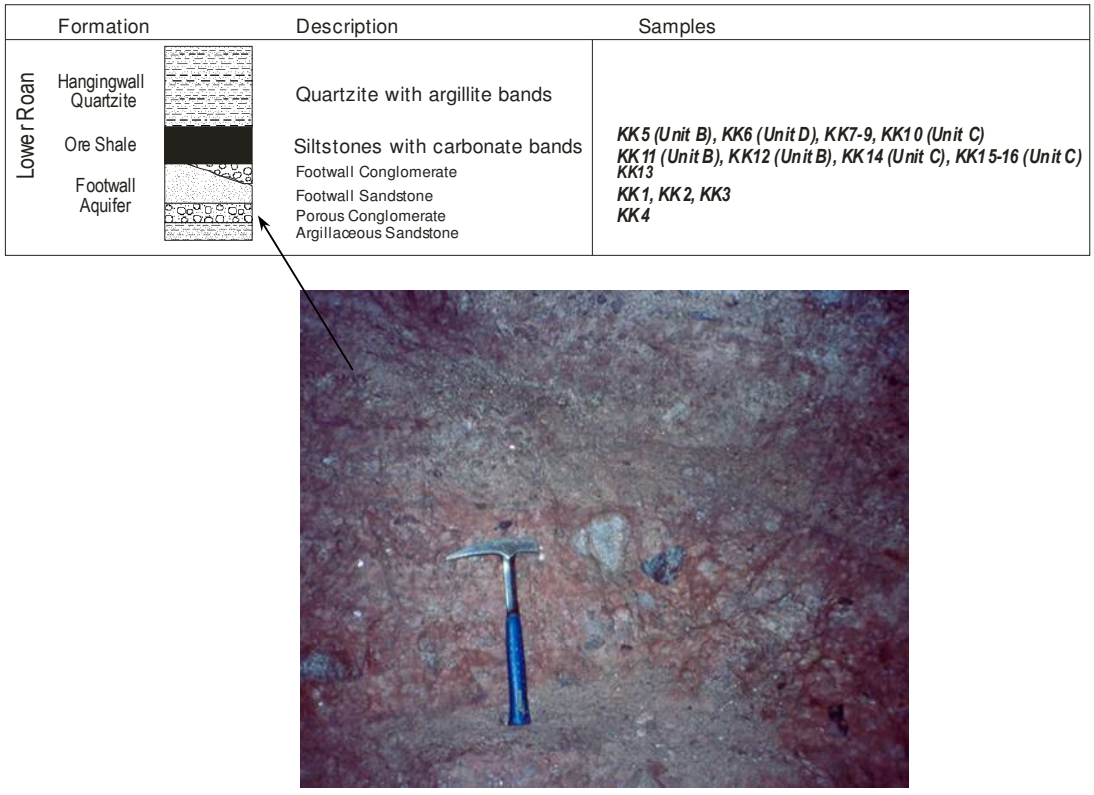

Figure 5.13. The Porous Conglomerate exposed in the No.3 Shaft area at the Konkola mine was sampled for the fluid inclusion study.

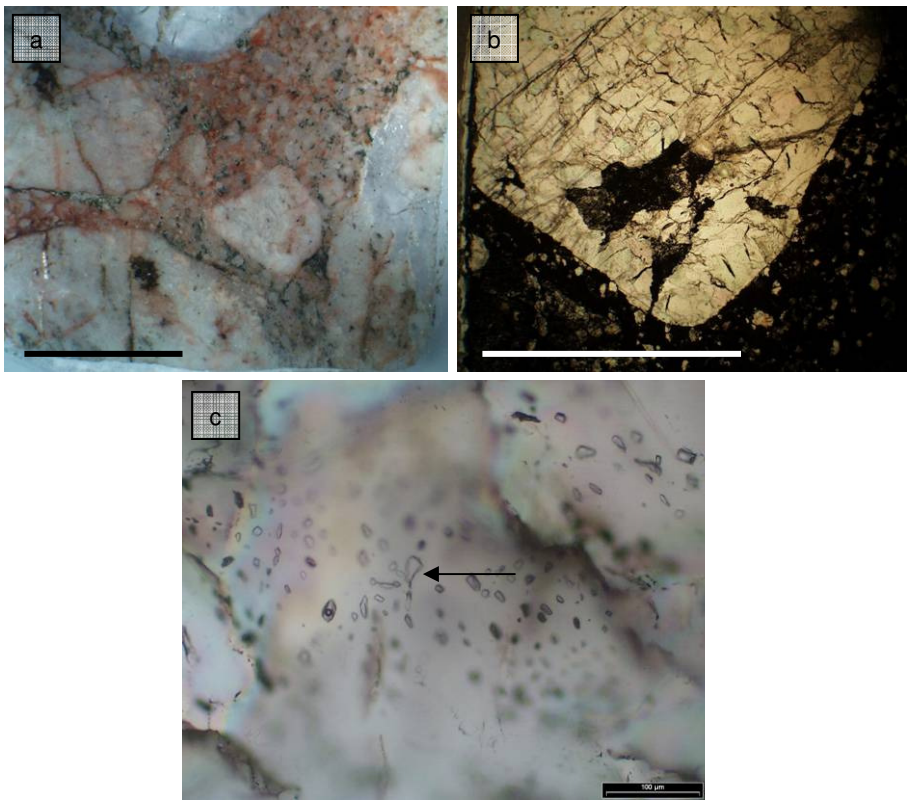

Figure 5.14. (a) Reflected light image of double polished wafers of the matrix-supported Porous Conglomerate in the footwall to the ore horizon at the Konkola deposit (scale bar = 0.5cm). (b) Transmitted light image showing a rounded quartz grain in a matrix of fine grained orthoclase and plagioclase feldspar. Several inclusion trails transect the quartz grain, as evidence of subsequent cracking and annealing. Many inclusions in these trails have leaked and show irregular shapes (scale bar = 0.5cm. (c) Conoscopic transmitted light image illustrates the presence of secondary aqueous fluid inclusion trails in the quartz grains of the conglomerate. Some necking-down textures is evident (arrow) in addition to monophase aqueous inclusions (see text for details).

5.4.2 Microthermometry

Secondary aqueous inclusions

Aqueous inclusions were identified in planes and trail assemblages in quartz grains of the Porous Conglomerate samples of the Konkola deposit (Figure 5.15). These inclusions range in size from 5 to 12 µm diameter (Table 5.7). Inclusions in these trails were generally necked and showed signs of other post-trapping modifications, such as irregular

inclusion shapes, and displayed a large variation in vapour volume fractions between inclusions of the same trail. Estimated vapour volumes range between 10 and 90 vol. % (Table 5.7).

Eutectic melting (T_e) was measured from -42 to -20 °C, which indicate possible solutions of $MgCl_2$ - KCl-H_2O ±NaCl (see Table 2.1 in Chapter 2). Melting of ice ($T_m$ice) was measured from -3.0 to -0.3 °C, which indicate bulk salinities in the range from 0.5 to 4.9 wt.% $NaCl_{equiv}$ for inclusions (Table 5.7). Homogenisation temperatures were measured between 132 and 160 °C to the liquid phase, but stretching of inclusion walls is not ruled out due to irregular inclusion shapes, which may result in volume changes of inclusions. Abundant trails of empty inclusions were also observed (Figure 5.15b).

In addition to empty inclusions, several monophase inclusions showed no nucleation of a vapour phase during repeated freezing runs to temperatures of -190°C and subsequent heating. Possible explanations for the existence of monophase inclusions are listed by Roedder (1984, p.222, 292) as the following:

- the inclusion may consist of a very low density gas,
- the inclusion might be composed of a solid phase,
- it may consist of a metastable or supercooled fluid,
- it may contain a low salinity aqueous fluid trapped at near surface temperatures. Due to the low birefringence of ice, it may be difficult to observe phase changes during cooling.

Aqueous trail inclusions in the same sample as monophase inclusions were found to contain low salinity fluids, and it is concluded that these monophase trails may have sampled fluids of the same low-salinity composition and the lack of a vapour phase nucleation may be a result of metastability or lack of observation due to the low birefringence of ice.

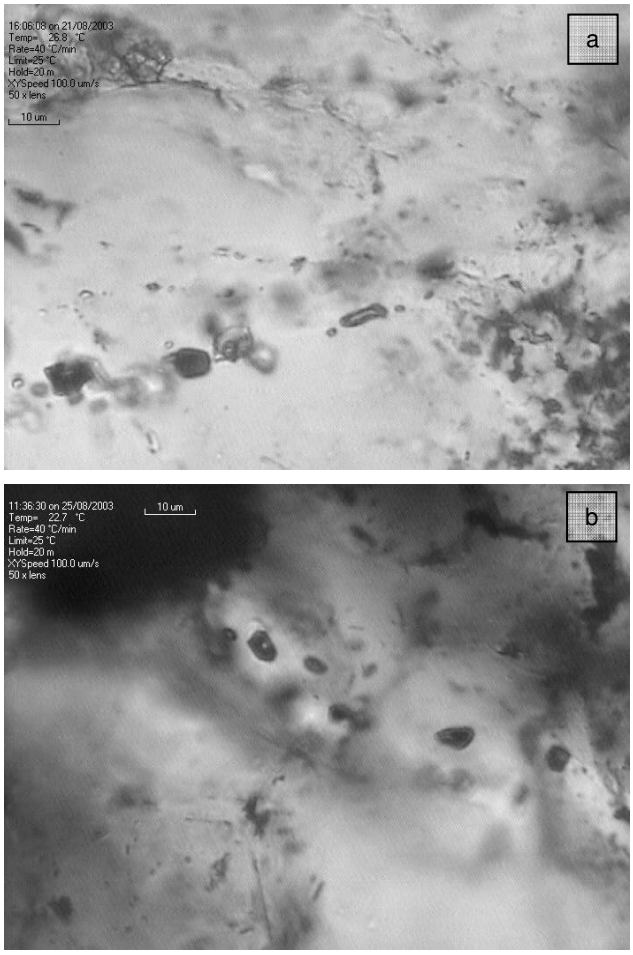

Figure 5.15. (a) Variation in vapour volumes of inclusions in the same trail was noticed in samples of the Konkola deposit. (b) Empty fluid inclusion trails indicate post-trapping modifications and decrepitation.

Table 5.7. Microthermometry results of basinal trail inclusions of the Konkola deposit.

Sample	Flinc	Type	FIA	RT	size	%vap	Te	Tmhh	Tmice	Thtot	Mode	Salinity wt%eNaCl
KK4A	(1)1	Lw	trail	2	7	30	-	-	-	-	-	-
KK4A	(1)2	Lw	trail	2	5	60	-	-	-	-	-	-
KK 4A	(2) 1	Lw	tr1	2ph	10	70	-33	?	-0.3	152	L	0.5
KK 4A	(2) 2	Lw	tr1	2ph	9	90	-	-	-	-	-	-
KK 4A	(2) 7	Lw	tr2	2ph	10	15	-31	?	-0.4	160	L	0.7
KK 4A	(2) 8	Vw	tr2	2ph	10	70	-20	?	0.0	132	L	-
KK 4A	(2) 9	Vw low dense?	tr2	2ph	10	90	-	-	-	-	-	-
KK 4A	(2)10	Lw	tr2	2ph	12	10	-42	?	-3.0	153	L	4.9

5.4.3 Raman microspectroscopy

Raman analysis confirmed the absence of carbonic phases in secondary aqueous inclusions.

5.5 Summary of basinal fluids of the Katanga Supergroup

5.5.1 Chambishi basinal fluids

Early fluids identified from the Chambishi deposit are mostly aqueous fluids of H_2O - NaCl - $MgCl_2$ - $CaCl_2$ composition. Non-aqueous phases comprise a minority compared to aqueous fluids and include CO_2, CH_4, and N_2. Aqueous fluids are of moderate salinities (~12-23 wt.% $NaCl_{equiv}$). The quartz vein in which these early fluids are trapped contains a chalcopyrite-bornite assemblage that was derived from the late diagenetic stratiform mineralisation in the adjacent host rock. These early fluids are not directly implicated in stratiform copper mineralisation, but were involved in the early remobilisation of stratiform mineralisation from the Ore Shale, and were present immediately after stratiform Cu-Co mineralisation in the basin prior to deformation.

5.5.2 Nchanga basinal fluids

Fluid inclusions studied in quartzites of the Upper Orebody horizon at the Nchanga deposits are composed of aqueo-carbonic compositions, and are notably small in size. These inclusions occur in quartz grains. Aqueous phases of these inclusions indicate the presence of $CaCl_2$ - H_2O and $MgCl_2$ - KCl - NaCl - H_2O solutions, with some NaCl-saturation. Carbonic phases are enriched in CO_2 with minor amounts of N_2 and CH_4, and the presence of solid carbon was confirmed in two inclusions. $Liquid_{aq}$-$vapour_{car}$ ratios are variable (between 10 and 80 vol. %) and indicate fluid trapping occurred while aqueous and carbonic fluids were unmixed.

5.5.3 Konkola basinal fluids

Fluids of the Konkola deposit consist of low salinity aqueous solutions that may have been trapped at temperatures below 100 °C. Eutectic melting temperatures indicate the presence of $MgCl_2$ - KCl - H_2O ± NaCl fluids, which are distinct from other $CaCl_2$ - NaCl - H_2O fluids dominant during the early stages of basinal evolution at the Chambishi and Nchanga deposits. Inclusions from the Konkola deposit show post-trapping modifications which may have resulted from changes in external confining pressures during the

evolution of the basin (Roedder, 1984). The variation in observed vapour-liquid ratios of aqueous inclusions may be due to selective leakage of the H_2O-liquid from the inclusion, resulting in increased vapour phases and higher measured homogenisation temperatures. Homogenisation temperatures are not considered as accurate due to post-trapping modifications to these inclusions.

5.6 The nature of basinal fluids in the Katanga Supergroup

Three main compositionally different fluids circulated the basin during the early stages of basin evolution, namely:

- H_2O - NaCl - $CaCl_2$ - $MgCl_2$ fluid
- H_2O - $MgCl_2$ - KCl ± NaCl fluid
- H_2O - $MgCl_2$ ± KCl - CO_2 -CH_4 - N_2 fluid

Low temperature - moderate-salinity aqueous fluids may result from dissolution of evaporites, or boiling of a lower salinity fluid. The effect of boiling, or effervescence, whereby the vapour of a high-density fluid is trapped as a low-density fluid (Roedder, 1984), was not observed at the Chambishi deposit. The Katanga sequence hosts abundant evaporites in the Roan Group at Mufulira and Konkola in Zambia, and within the Roan Group in the DRC (Garlick and Fleischer, 1972; De Magnée and François, 1988; Jackson *et al*., 2003). Therefore, the moderate salinities and low trapping temperatures of isolated aqueous fluid inclusions in this study are best explained by the dissolution of evaporites by circulating connate fluids. Low salinity – moderate temperature $MgCl_2$ - KCl - H_2O ± NaCl aqueous fluids are present in fluid inclusions from the Konkola deposit, which may indicate a meteoric water presence in these inclusions.

Fluid compositions in the diagenetic realms are well documented by Goldstein (2001), and he details the predominance of complex compositions in this environment. Major fluid types include freshwater environments yielding mostly H_2O-pure inclusions, or inclusions with minor salt concentrations. Methane may also be readily available from methanogenesis at the near surface environment due to the degradation of organic matter. Aqueous solutions may contain various amounts of NaCl and $CaCl_2$, depending on depth in sedimentary basins and fluid-rock interaction (Goldstein, 2001). In addition to freshwater and basinal fluids of mixed electrolytes with pure water, seawater may also be trapped in inclusions.

The presence of CO_2, and lesser amounts of N_2 and CH_4 in the early fluids of the Chambishi and Nchanga areas, may be explained by the decomposition of higher hydrocarbon organic matter (Roedder, 1984) present within the Katanga sedimentary

sequence and minor amounts of CH_4 may point to methanogenesis, which is active to temperatures of ~50 °C (Ohmoto and Goldhaber, 1997). No carbonic phases were identified at the Konkola deposit.

The presence of a low salinity, hotter fluid still may best be explained by devolatilization reactions during the onset of Lufilian regional metamorphism. With increasing metamorphism, the average hydrocarbon molecular weight decreases to that of methane (Roedder, 1984), and may explain the presence of methane, increasingly present in secondary aqueo-carbonic inclusions, and also in methane-dominated fluid inclusion trails, where methane is generally derived from the decomposition of hydrocarbon organic matter (Roedder, 1984; Killops and Killops, 1993). Later fluids exhibit a range of salinities (~6-23 wt.% $NaCl_{equiv}$), compositions, and trapping temperatures, and occur in prominent fluid inclusion planes that are tentatively correlated to the axial planar cleavage which is refracted in the quartz vein, linking fluids in these planes to metamorphism.

Raman analysis confirmed the presence of solid NaCl and $CaCO_3$. The presence of hematite in inclusions was also confirmed with Raman analysis (Figure 7.16).

Secondary aqueous-gaseous inclusions

Raman analysis was not successful in determining the vapour composition of these inclusions due to movement of the vapour bubbles under the laser.

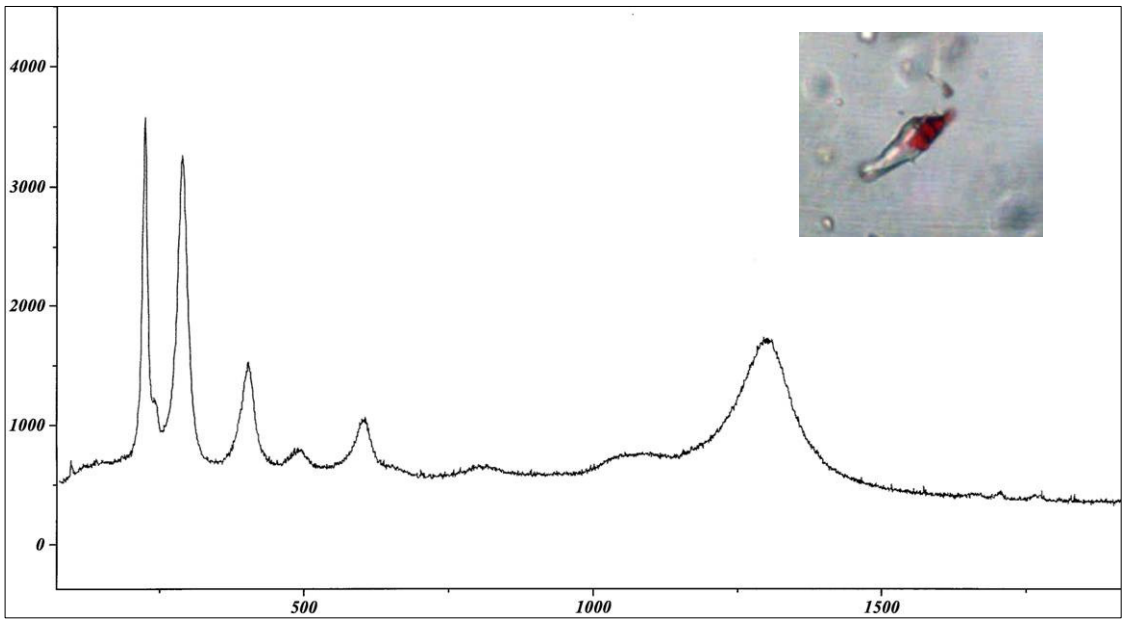

Figure 7.16. Raman spectra of solid hematite in an aqueous fluid inclusion hosted in quartz. Measurements were performed using a 514 nm Ar laser excitation source. The Raman shift ($\Delta\upsilon$) indicated on the x-axis is shown in cm^{-1}, with intensity (arbitrary units) indicated on the y-axis. Flinc. no. MUF7H-A(1)1.

7.5 Summary of late orogenic fluid characteristics

7.5.1 Summary of late orogenic fluids at Nchanga

Fluid inclusions in the arkosic metasediments below the lower orebody of the Nchanga deposit are composed of NaCl-saturated $CaCl_2$ - $MgCl_2$ ± KCl brines which were trapped at minimum temperatures of ~240 °C indicated by homogenisation temperatures.

7.5.2 Summary of late orogenic fluids at Nkana

Microthermometry of fluid inclusions of the Nkana deposit reveal the presence of aqueous fluids composed of possibly two end member fluids of NaCl - H_2O and $CaCl_2$ - H_2O ±$MgCl_2$ compositions respectively. The fluid inclusions measured here possibly represent the mixed end-product of a NaCl - H_2O fluid and a $CaCl_2$ - H_2O ± $MgCl_2$ fluid (Figure 7.17 a). Fluid mixing between these two miscible end-members occurred at constant densities (Figure 7.17b).

These fluids were trapped at minimum temperatures between 98 and 400 °C at fluid densities between 0.78 and 1.09 g/cm^3. Secondary inclusions may have sampled fluids present in the basin during the late stages of regional metamorphism, or later meteoric water infiltration, which is known to occur to depths up to 10km (Barker *et al.*, 2000; Roedder, 1984).

Distributions of T_{mice} versus T_h (Figure 7.7b), and T_e versus T_h data (Figure 7.17) further indicate that mixing may have occurred between a higher temperature $CaCl_2$ ± $MgCl_2$ -brine and a slightly lower temperature NaCl-brine. Fluid trapping occurred when mixing of these two brines was almost complete. A cooler NaCl-brine may have been present in the basin during the earlier stages of maturation leading up to regional metamorphism. Increasingly saline meteoric water reached salinities of > 8 wt. % $NaCl_{equiv.}$ (Figure 7.8). This NaCl-brine became modified as is evident by increasing homogenisation temperatures (Figure 7.17) and also by the distribution of T_{mice}-T_h data (Figure 7.7b) which is caused by partial heat exchange either between two fluids or between fluids and the host rock (Dubessy *et al.*, 2003). Trapping of the inclusions occurred when mixing was near completion at temperatures between ~120 and 280 °C.

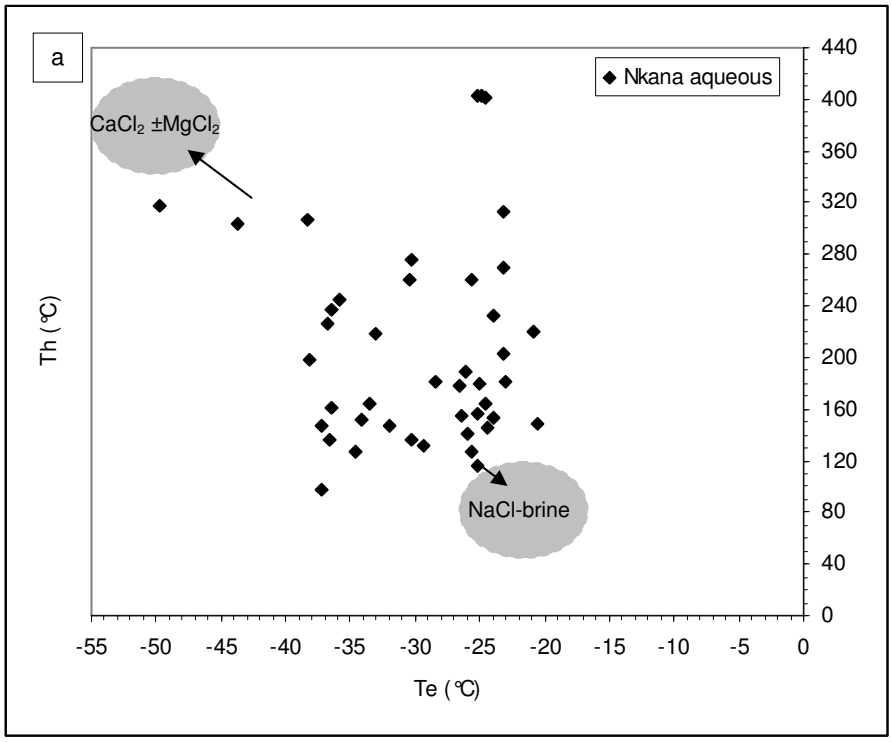

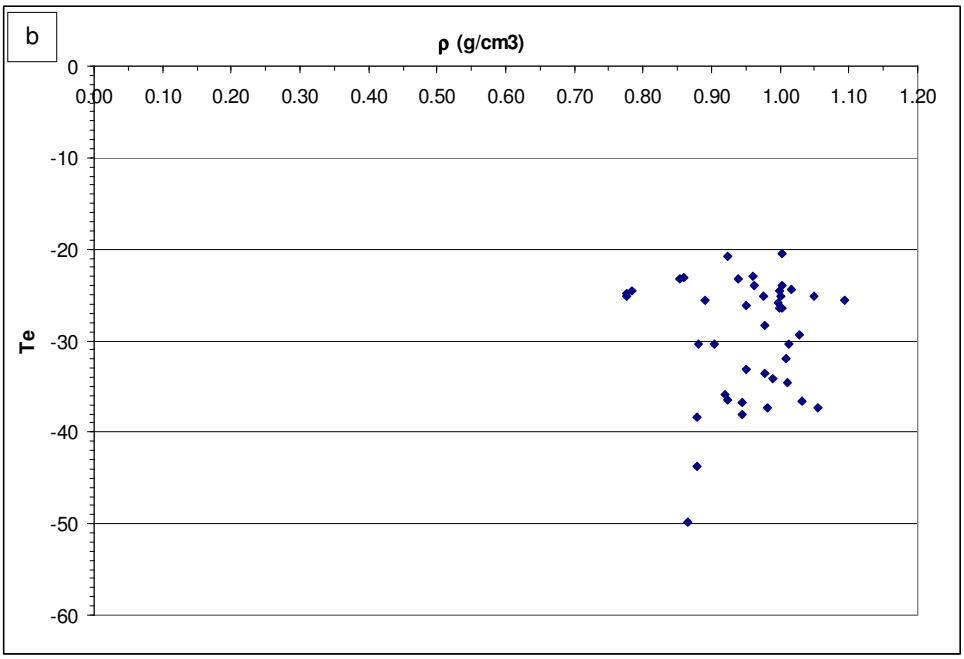

Figure 7.17. (a) Distribution of eutectic melting temperatures (T_e) and homogenisation temperatures (T_h) of aqueous inclusions of the Nkana deposit may indicate the mixing of a higher temperature $CaCl_2 \pm MgCl_2$ -brine and a lower temperature NaCl-brine during partial heat exchange either with each other, or between the fluids and host rocks. (b) Density vs eutectic melting temperatures for aqueous Nkana fluid inclusions.

7.5.3 Summary of late orogenic fluids at Mufulira

Inclusions from a quartz vein from the Mufulira deposit occur in planes and are considered to postdate vein quartz formation. These trails were found to contain NaCl-saturated aqueous fluids with accidentally trapped solid $CaCO_3$. In addition to NaCl-saturation, these solutions may contain a number of possible complexes such as LiCl and $CaBr_2$, as is evidenced from very low eutectic melting temperatures determined during microthermometry. However, metastability in the NaCl-$CaCl_2$-H_2O system may also not be ruled out. These saturated solutions were trapped in the presence of solid Fe_2O_3 which lead to the heterogeneous trapping of hematite solids in several inclusions. Fluids that circulated within the basin in the Mufulira area were at temperatures greater than 290 °C, contained ~40 wt.% $NaCl_{equiv.}$, and were buffered by rocks bearing Fe_2O_3. Moreover, solutions were trapped in the presence of $CaCO_3$. The presence of solid hematite trapped heterogeneously in inclusions from the Mufulira deposit indicates that fluids must have been buffered with the host rock at sufficiently neutral and alkaline conditions to enable the precipitation of Fe_2O_3. The occurrence of solid $CaCO_3$ present in the same fluid inclusions further constrains the acidity of solutions to increasingly alkaline conditions at pH levels greater than 5 (Figure 7.18).

Volatile phases of inclusions are exclusively composed of N_2, and are notably devoid of CO_2 or CH_4. Along with minimum trapping temperatures, deduced from inclusion homogenisation temperatures, up to 379 °C, these fluids are hot, complex brines, and contain significant amounts of Sr, Pb and Cu (see Chapter 8).

Aqueous-nitrogen fluid inclusions have been documented by Andersen *et al.*, (1989) from eclogites in Norway, and attributed the provenance of nitrogen in aqueous inclusions either from degassing from an external source such as from metasedimentary units, sourcing nitrogen from biological material within the metasedimentary rocks or from melting of continental crust. Andersen *et al.*, (1989) also mentions the possibility that nitrogen may be sourced from NH_4^+ ions substituting for K^+ in pre-metamorphic minerals such as feldspars, sheet silicates or amphiboles.

In the case of late orogenic inclusions from Mufulira, the presence of nitrogen in the hot aqueous phase along with NaCl, $CaCO_3$, and hematite illustrates the complexity of this late fluid type, and supports the notion that these fluids have evolved along complex P-T-υ-X paths prior to trapping. Nitrogen found in these inclusions was possibly sourced from early biological nitrogen present within the sedimentary rocks and evolved to become hot, hypersaline inclusions.

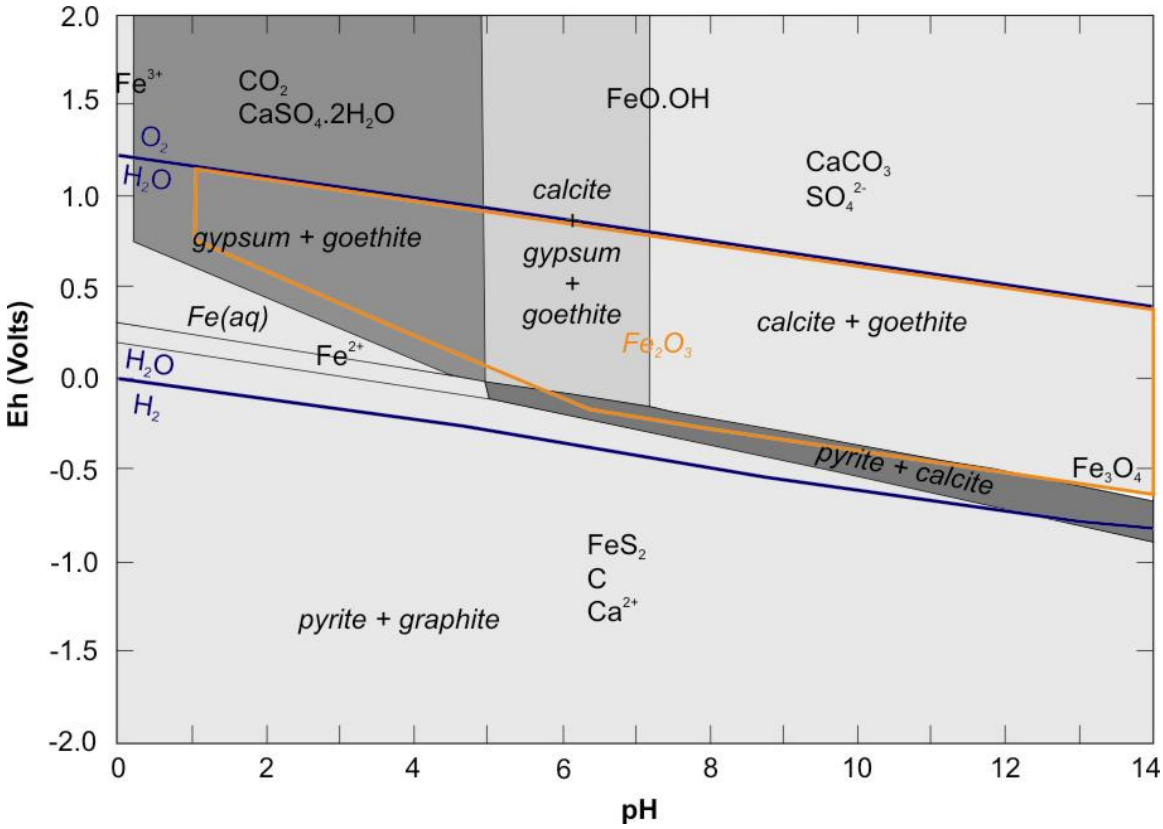

Figure 7.18. Reduction potential - pH diagram showing the stability fields of the C-Ca-Fe-S-H_2O system, and stability field for hematite in orange at 25°C, and 1atm (modified after Geological Survey of Japan, 2005; Vink, 1996).

7.6 The nature of late orogenic fluids

Late orogenic fluids are compositionally complex consisting of at least four different fluid types and exhibit a range of cations present as chloride complexes:

- NaCl - saturated, Ca - Mg - K brine
- NaCl - $CaCO_3$ - saturated brines with N_2
- Mg - Na ± Ca brine
- Aqueous-gaseous fluid

These fluids were sampled from the Nkana, Nchanga, and Mufulira areas of the Zambian Copperbelt, and present an image of the state of metamorphic fluids from the southwest of the Kafue anticline to the north-eastern area of Mufulira. Fluids that were circulating within the basin during metamorphism in the north-eastern part of the anticline at Mufulira were hot, and saturated in NaCl in the presence of oxidised $CaCO_3$. The

salinity of these fluids are higher than normal metamorphic fluids, and these fluids were probably modified metamorphic fluids that originated as a result of having been present in the basin over a prolonged period of time in order to sufficiently equilibrate with high temperatures achieved during metamorphism and thereby also dissolving the salts present in an evaporite-rich saline basin.

Lower salinity fluids towards the southwest of the Kafue anticline at Nkana account for late meteoric fluids that infiltrated the basin causing lower salinities with relatively high trapping temperatures.

Chapter 8

LA-ICP-MS ANALYSIS OF FLUID INCLUSIONS FROM THE ZAMBIAN COPPERBELT

8.1 Introduction

Laser ablation inductively coupled plasma mass spectrometry (LA-ICP-MS) is a relatively new analytical method in determining major, minor, and trace compositions of individual fluid inclusions (Allan *et al*., 2005). Inclusions from the Chambishi, Nchanga, Nkana and Mufulira deposits were analysed using laser ablation inductively coupled plasma mass spectrometry (LA-ICP-MS). LA-ICP mass spectrometry was applied to the same inclusions already studied by microthermometry and Raman microspectroscopy (Figure 8.1). LA-ICP-MS analyses were conducted at the School of Earth and Environment at the University of Leeds in England. A total of 191 inclusions were measured including 92 inclusions from Chambishi, 58 from Nchanga, 6 from Nkana, and 35 from Mufulira.

Analytical procedures are described in chapter 2, and the reader is referred to the work of Shepherd and Chenery 1995; Audétat *et al*., 1998; Günther *et al*., 1998; Ulrich *et al*., 2001; Allan *et al*., 2005 for a review of LA-ICP-MS methodology as applicable to the analysis of fluid inclusions. Fluid inclusions were analysed using a Ar-F laser beam that penetrates the quartz host mineral and breaches individual inclusions (Figure 8.2a-b and c-d); the fluid is vapourized and introduced into the plasma stream, whereafter a spectrum is generated for particular elements analysed (Figure 8.2e).

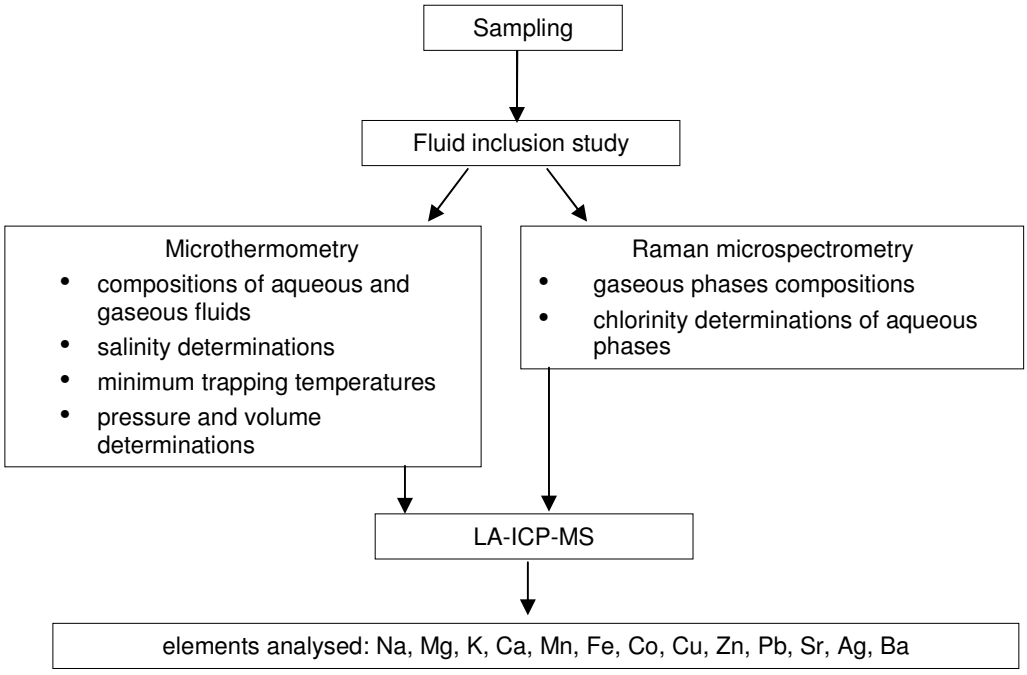

Figure 8.1. Flow sheet of methodology employed during the investigation of the nature of fluids of the Zambian Copperbelt and methods used prior to LA-ICP-MS.

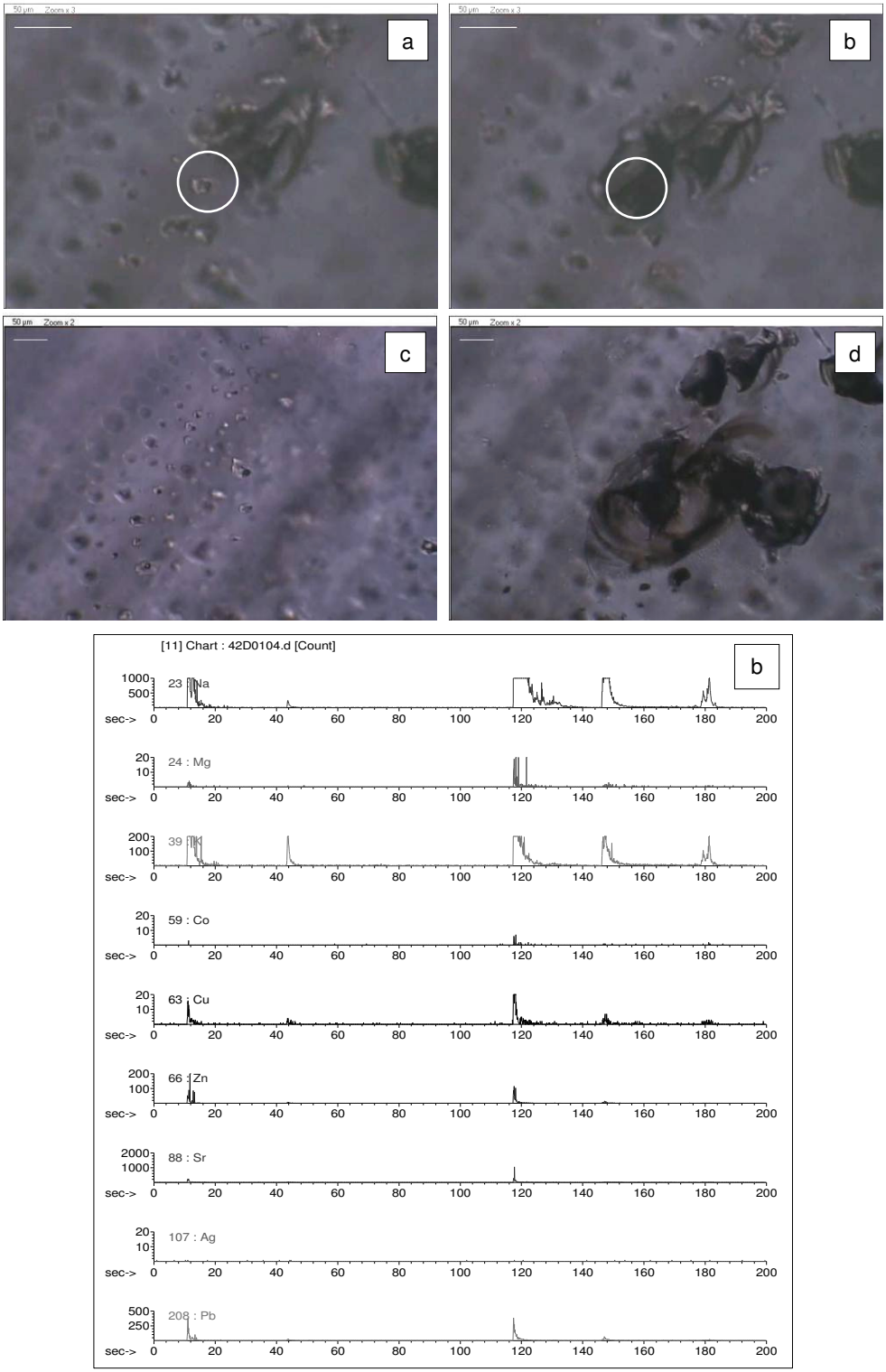

Figure 8.2. Secondary planes of NaCl-saturated aqueous fluid inclusions in reflected light shown prior to ablation in (a) and (c) and after laser ablation in images (b) and (d). (e) Spectra generated by ablation of two inclusions. Ablation is achieved first using a 5µm laser beam diameter until the inclusion is reached; thereafter the beam diameter is increased to excavate the inclusion cavity to ensure the measurement of less volatile phases. Time is presented along the X-axis, with counts as the Y-axis. The first spike in the spectrum represents the opening of the inclusion, with beam diameter increase resulting in an additional, weaker signal at ~44 seconds into ablation. The spike for all elements at ~120 seconds signifies the opening of the second inclusion. Flinc. No. Muf7D(1)5.

LA-ICP-MS analysis was conducted on inclusions representative of the three tectonic stages, namely basinal, early orogenic, and peak orogenic as discussed in the preceding chapters. Inclusions representative of these tectonic settings are found at the Chambishi, Nchanga, Nkana, and Mufulira deposits. Ablation was also carried out only on inclusions where the P-T-υ-X conditions were known from prior microthermometric and Raman study (Table 8.1). Basinal fluids were sourced from inclusions of the Chambishi and Nchanga deposits, while inclusions representative of early orogenic fluids were sampled at the Chambishi, Nchanga, and Nkana deposits. These early orogenic fluid inclusions are numerous, and constitute the majority of microthermometric measurements. Thus, the majority of LA-ICP-MS measurements were also performed on these inclusions due to abundance and size suitability for laser ablation. Inclusions representative of peak metamorphic fluids are hosted in samples of the Mufulira deposit and were not found at any of the other deposits. LA-ICP-MS analysis yielded the concentrations of the following element suite - Na, Mg, K, Ca, Co, Cu, Zn, Pb, Sr, Ag, Mn, Fe, and Ba.

Table 8.1. Sample distribution and fluid types for LA-ICP-MS analysis

Deposit	Basinal fluids	Early orogenic fluids	Peak orogenic fluids
Chambishi	**x**	**x**	
Nchanga	**x**	**x**	
Nkana		**x**	
Mufulira			**x**

Weight ratios relative to Na^+ were determined for certain elements during laser ablation ICP-MS analysis and were converted to ppm concentration using the known Na^+ concentration derived from microthermometric measurements (Appendix IV). Microthermometric measurements enable the calculation of the NaCl-equivalent concentration of fluids whereby all salts dissolved in the aqueous solution are normalised to the NaCl concentration. Salinities were determined from final ice melting temperatures of aqueous inclusions during microthermometry, and from clathrate melting and CO_2 homogenisation temperatures of aqueo-carbonic inclusions. Salinities of aqueo-carbonic inclusions with large vapour-liquid ratios were calculated from chlorinity values which were determined from Raman microspectroscopy. For certain inclusions, the observation of final ice melting or clathrate melting was hampered due to the size or shape of the inclusion, depth of the inclusion within the host mineral etc. Chlorinity values were used to determine salinities for such inclusions.

8.1.1 Methodology of contour plots using LA-ICP-MS data

In an attempt to visualize the spatial variations in fluid compositional data, contour plots were generated from elemental concentrations (in weight percent) of the four deposits where LA-ICP-MS analysis was derived. Although there are only four sample sites, the weight ratio data was gridded and contoured in an attempt to visualise compositional trends over the width of the Copperbelt from the Nkana deposit in the southeast to the Nchanga deposit in the northwest. Elemental concentrations were used from 19 inclusions representative of basinal fluids, 151 inclusions of an early orogenic setting, and 35 peak metamorphic inclusions. Easting and northing coordinates were assigned to individual samples and inclusions therein based on the longitude and latitude of the Chambishi, Nchanga, Nkana, and Mufulira deposits, and individual inclusions were spread out in close radius to the actual mine sites. It has to be stressed that these do not reflect actual sample coordinates, but rather should be viewed as an area around each deposit.

Cation concentrations were regionally interpolated using the regression technique of Kriging to generate contour plots of the area. Oridinary Kriging (OK) determines the weighting of data values (concentration of cations in this case) by considering the spatial correlation structure of the data using the assumption of homogeneity of spatial variation. The gridding methods using Minimum Curvature and Radial Basis Functions were considered and tested in addition to the Kriging method, but the latter technique was found to be best suited to small data sets (< 250 observations). No nugget effects were applied during the Kriging process in order to honour the data as best as possible and the data points coincide with the interpolated grid node. Information on Kriging methods are provided in Journel and Huijbrechts, 1978; Heine, 1986; Royle, 1986; Cressie, 1990; Oliver, 1990, and references therein.

It is emphasized that fluid compositional trends presented in the contour diagrams are based on essentially four spatial points, and these trends should be read in conjunction with the histograms provided. Kriged plots are employed for the sole use of estimating spatial variation in trends across a section of the Zambian Copperbelt.

8.2 Basinal fluids

The P-T-υ-X characteristics of basinal fluids from the Chambishi and Nchanga deposits are described in chapter 5. The cationic compositions of these fluids, obtained from LA-ICP mass spectrometry, are documented below.

Aqueous and aqueo-carbonic inclusions were ablated in sample CBSqz3A of a lateral

secretion quartz vein found at the Chambishi deposit. Aqueous inclusions were analysed in sample NOP20A of the Feldspathic Quartzite of the upper orebody of the Nchanga deposit. These inclusions are representative of fluids circulating during the early stages of basin evolution.

8.2.1 LA-ICP-MS results

The majority of inclusions identified as basinal are aqueo-carbonic in composition, with only two inclusions from the Nchanga deposit identified as pure aqueous inclusions. Aqueous inclusions representative of basinal fluids at the Nchanga deposit are saturated with NaCl at room temperature and show elevated concentrations of Na, K, Zn, Ag and Pb when compared to basinal aqueous-carbonic inclusions (Figure 8.3). Unfortunately, salinity could not be determined due to the size of the inclusions and observation difficulties, but it was noted that these inclusions have NaCl cubes at room temperature. Therefore an assumed minimum salinity of 26.3 wt.% eNaCl as assigned to these inclusions in order to calculate ppm concentrations. Na concentrations of Nchanga basinal aqueous fluid inclusions are between ~80430 ppm and ~97400 ppm (Table 8.2). Comparatively, Na-concentration in aqueo-carbonic inclusions of the Chambishi and Nchanga deposits range between ~32800 – 101100 ppm. Mg concentrations of aqueo-carbonic inclusions of basinal fluids range between ~1150 – 34800 ppm, and the K-concentration in aqueo-carbonic inclusions range between ~730 ppm and 33280 ppm.

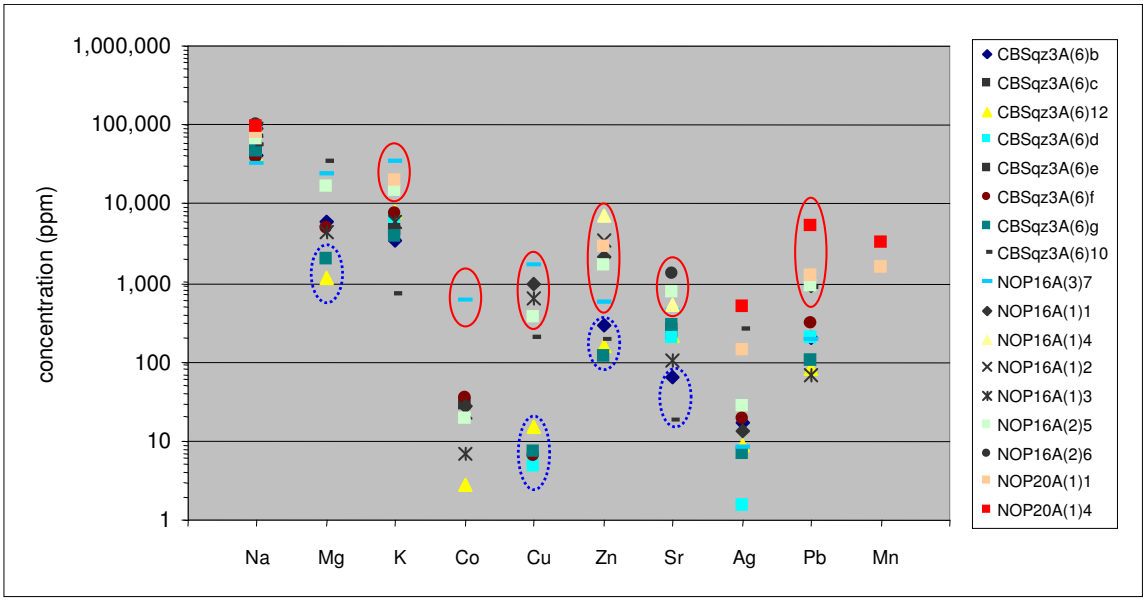

Figure 8.3. Selected cation concentrations (in ppm) of inclusions representative of early basinal fluids of the Chambishi and Nchanga deposits. Individual symbols indicate individual inclusions. Nchanga inclusions are outlined in red circles, with Chambishi inclusions outlined in blue dashed circles.

Table 8.2. Summary of elemental compositions of early basinal fluids measured from fluid inclusions from the Chambishi (sample CBSqz3A) and Nchanga (samples NOP16A, NOP20A) deposits.

			weight ratios											ppm									
Type	Sample		Na	Mg	K	Co	Cu	Zn	Sr	Ag	Pb	Mn	Salinity (wt%eNaCl)	Na	Mg	K	Co	Cu	Zn	Sr	Ag	Pb	Mn
aq-car	CBSqz3A	Mean	1	0.085	0.135	0.001	0.000	0.004	0.005	0.000	0.004	-	13	43949	3474	5681	22	8	189	216	11	180	-
		Stdev	0	0.057	0.053	0.000	0.000	0.002	0.002	0.000	0.002	-	-	4196	2245	1990	17	5	87	83	7	92	-
		%RSD	-	67.062	39.558	81.802	54.667	49.186	40.461	72.991	56.564	-	-	-	-	-	-	-	-	-	-	-	-
aq-car±s	NOP16A	Mean	1	0.053	0.070	0.000	0.009	0.048	0.004	0.000	0.005	-	24	87953	4461	5857	19	815	4266	324	13	482	-
		Stdev	0	-	-	0.000	0.002	0.030	0.004	-	0.006	-	-	3546	-	-	11	228	2588	313	-	588	-
		%RSD	-	-	-	54.577	22.395	63.260	95.082	-	120.417	-	-	-	-	-	-	-	-	-	-	-	-
aq-car-s	NOP16A	Mean	1	0.241	0.224	0.000	0.006	0.025	0.012	0.000	0.014	-	26	84208	16204	15090	19	377	1713	1059	28	916	-
		Stdev	0	-	-	-	-	-	0.001	-	-	-	0	23888	-	-	-	-	-	399	-	-	-
		%RSD	0	-	-	-	-	-	9.840	-	-	-	0	28	-	-	-	-	-	38	-	-	-
aq-s	NOP20A	Mean	1	-	0.251	-	-	0.036	-	0.003	0.034	0.027	27	88909	-	20171	-	-	2869	-	315	3213	2423
		Stdev	0	-	-	-	-	-	-	0.002	0.027	0.011	0	11986	-	-	-	-	-	-	251	2786	1268
		%RSD	0	-	-	-	-	-	-	69.943	77.787	40.287	0	13	-	-	-	-	-	-	80	87	52

			weight ratios						ppm				
Type	Sample		Na	Ca	Mn	Fe	Ba	Salinity (wt.%eNaCl)	Na	Ca	Mn	Fe	Ba
aq	CBSqz3A	Mean	1	0.792	1.414	2.753	0.020	5.26	4631	3007	3342	9683	62
		Stdev	0	0.403	1.952	1.868	0.018	-	3284	737	4395	393	19
		%RSD	0	50.817	138.049	67.842	92.115	-	71	25	132	4	31

Co concentrations in basinal fluids range between 3 - 600 ppm in aqueo-carbonic inclusions of the Chambishi and Nchanga deposits, and Cu concentrations range between 5 - 1680 ppm. Zn concentrations of aqueo-carbonic inclusions range between 120 - 7140 ppm. One aqueous inclusion contained 2869 ppm Zn. Sr concentrations for aqueo-carbonic inclusions range between 18 – 1340 ppm, and Ag concentrations range between 2 - 260 ppm. Ag concentrations in aqueo-carbonic inclusions range between 138 – 490 ppm. Pb concentrations in basinal aqueo-carbonic range between 82 and 900 ppm, and were measured at 1240 and 5180 ppm Ag in aqueous inclusions.

Cu, Co, Zn and Pb concentrations are notably enriched in Nchanga inclusions compared to those found at Chambishi. This also holds true for Sr concentrations. The concentrations of Co, Cu, Zn, Ag and Pb are displayed in Figure 8.4 and show the absolute abundances of these elements in basinal fluids.

Selected elements were contoured and are displayed showing distribution plots for **basinal aqueous and aqueo-carbonic inclusions** of the Nchanga and Chambishi deposits. These plots were generated to detect a general spatial trend in data and show a general pattern of enrichment in Co (Figure 8.4a), Cu (Figure 8.4b), Zn (Figure 8.4c) and Pb (Figure 8.4d) in the Nchanga area relative to the Chambishi area of fluids circulating within the basin after stratiform copper mineralisation prior to the onset of regional deformation.

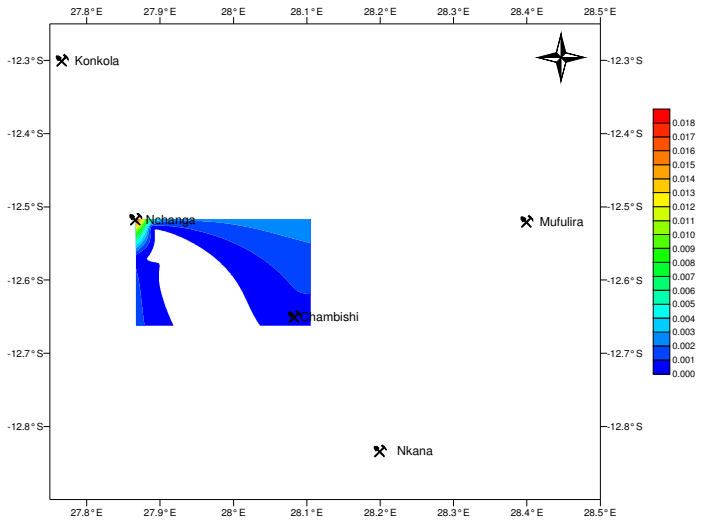

*Figure 8.4. (a) **Co** distribution in fluid inclusions representative of an early basinal setting for the Chambishi and Nchanga deposits. The scale bar is indicated in weight ratios and shows kriged interpolated values of cation concentrations. The coordinate system is in longitude-latitude. See text for details.*

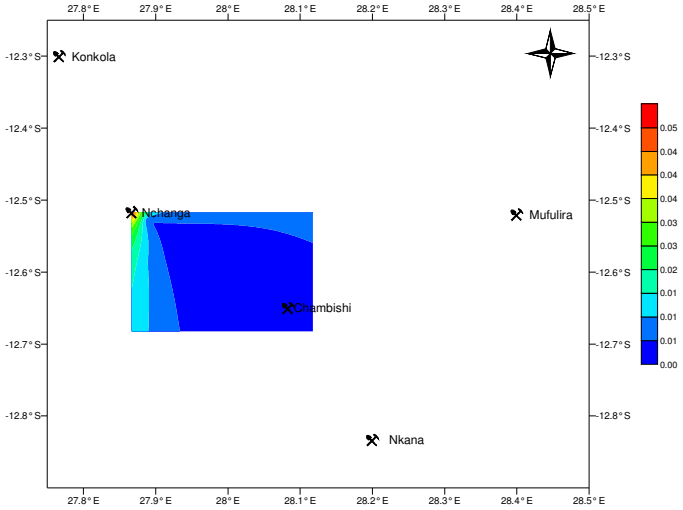

*Figure 8.4. (b) Contour plot showing the kriged interpolated **Cu** distribution over the Copperbelt in the Nchanga and Chambishi areas during the early stages of basin evolution. Units are in weight ratios, with exaggerated longitude-latitude as the coordinate system. See text for details.*

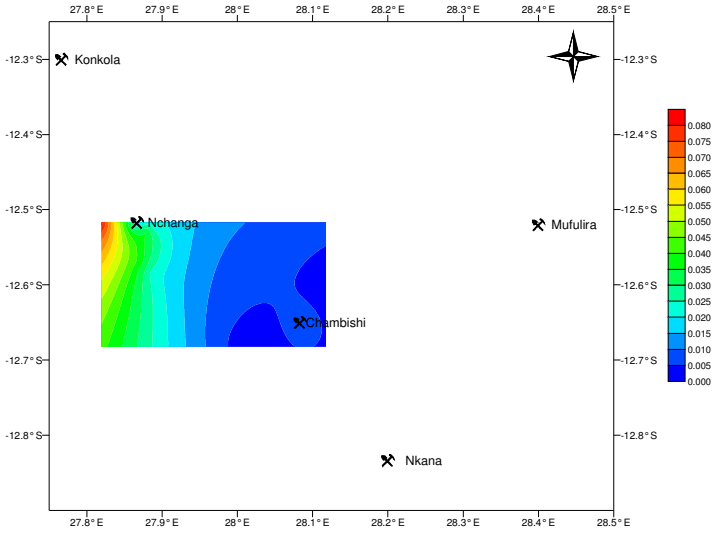

*Figure 8.4. (c) Contour plot of the distribution of **Zn** in the Zambian Copperbelt from the Nchanga and Chambishi deposits during the early stages of basin burial. Scale bar units are in weight ratios and coordinate system shows exaggerated longitude-latitude. See text for details.*

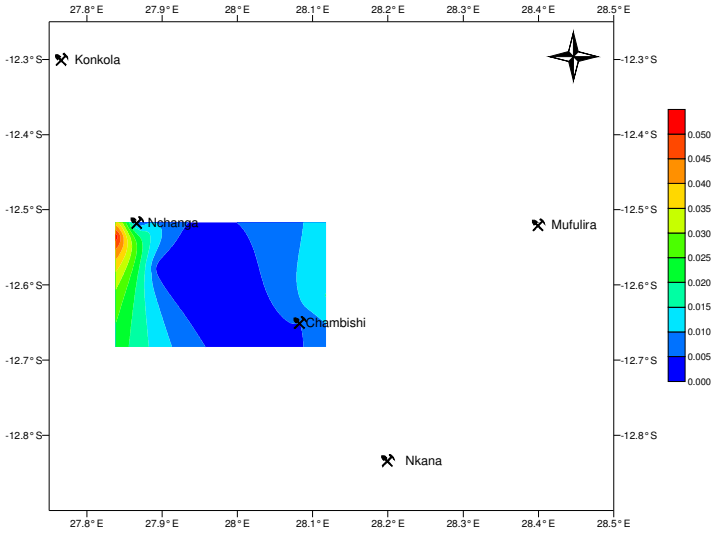

*Figure 8.4. (d) Contour plot of the distribution of **Pb** in weight ratios in the Zambian Copperbelt from the Nchanga and Chambishi deposits during the early stages of basin burial. Scale bar units are in weight ratios and coordinate system shows longitude-latitude. See text for details.*

8.3 Early orogenic fluids

Early orogenic fluids were analysed from inclusions hosted in quartz veins and metasediments of the ore deposits at Chambishi (samples CBSqz3A, n = 54; CBSqz3By, n = 13, see Figure 8.5; CHM7B-A, n = 10; CBSqz7B-A, n = 25), Nchanga (NOP8B-A, n = 24; NCG-mq9d, n = 22; NCG-mq9e, n = 7), and Nkana (NS4-7bA, n = 6).

8.3.1 LA-ICP-MS results

Aqueous, aqueo-carbonic and methane rich inclusions from the Chambishi deposit are representative of palaeofluids circulating during the early stages of deformation in the present day Copperbelt region, and were analysed for major, minor, and trace element compositions during laser ablation ICP-MS. Aqueous inclusions of the Nkana and Nchanga deposits were analysed during laser ablation in addition to carbonic and methane rich inclusions of the Nchanga deposit. Aqueo-carbonic inclusions of the Nchanga deposit contained halite as daughter minerals and were also ablated.

Early orogenic aqueous inclusions

Early orogenic aqueous inclusions of the Chambishi deposit are enriched in Na relative to inclusions from the Nchanga and Nkana deposits (Figures 8.6 and 8.7) as is shown by an average of ~80000 ppm Na of the Chambishi inclusions (Table 8.3). In comparison, the average concentration of Na at the Nchanga deposit is ~ 28500 ppm and ~28100 ppm Na at the Nkana deposit (Figure 8.7). The strong linear correlation depicted in Figure 8.7 between Na abundance and salinity determined from microthermometry shows that salinity may be largely a function of NaCl concentration in early orogenic fluids with a contribution from other cations such as Ca, Mg and K.

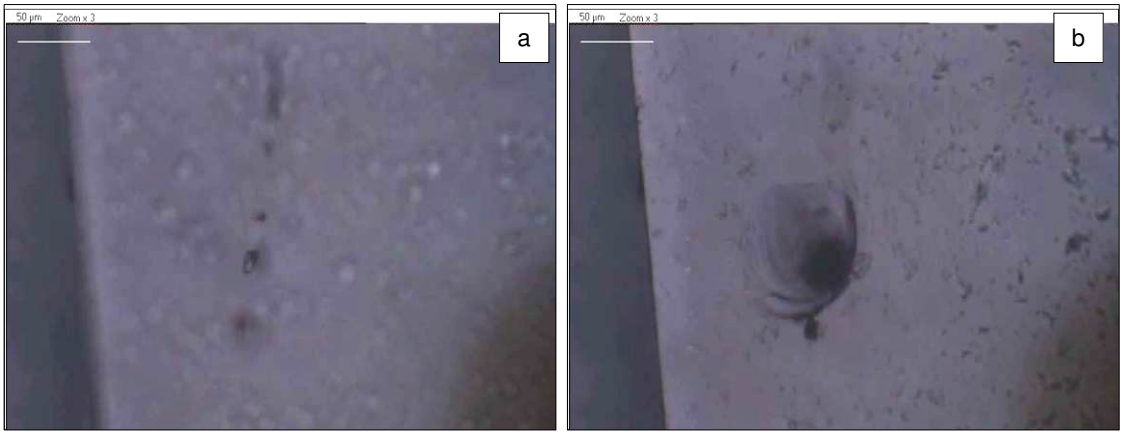

Figure 8.5. (a) Reflected light image of secondary aqueo-carbonic trail inclusions hosted in quartz of the Chambishi samples prior to laser ablation, and (b) post laser ablation. Flinc. no. CBSqz3By(4)11.

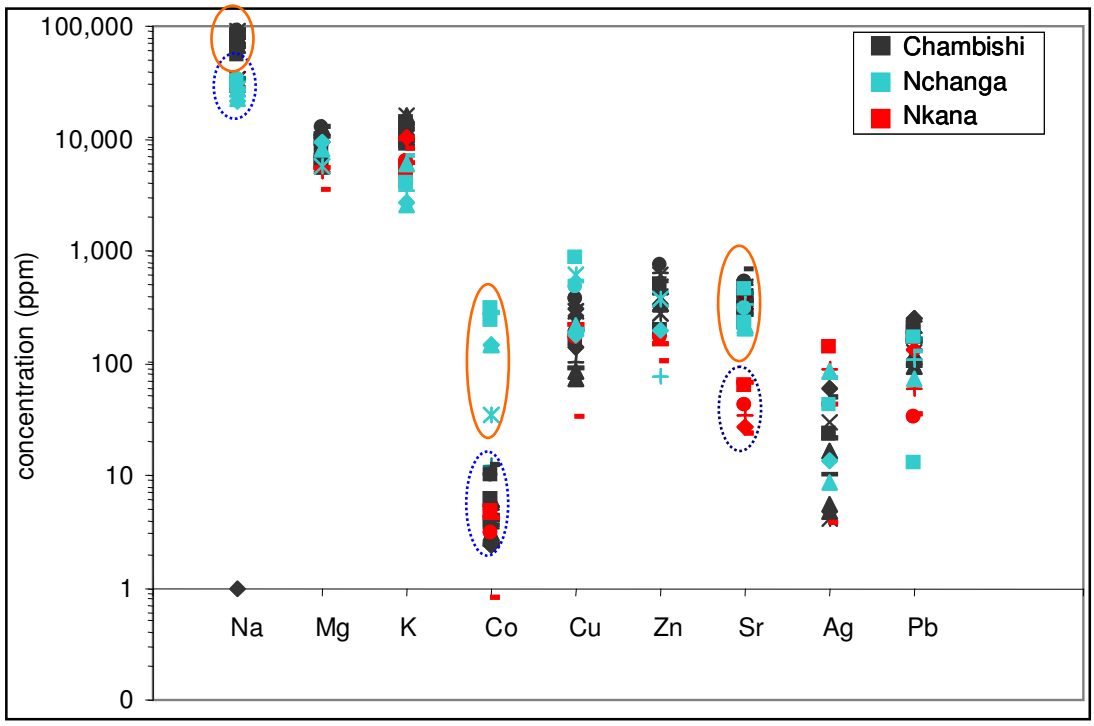

Figure 8.6. Cation concentrations of aqueous inclusions of an early deformational setting of the Chambishi, Nchanga, and Nkana deposits, indicated in grey, blue, and red respectively. Note enrichment in Na of Chambishi inclusions relative to Nchanga, and higher Co concentrations at Nchanga relative to those at Chambishi and Nkana. Sr levels are elevated at Nchanga and Chambishi relative to those at Nkana.

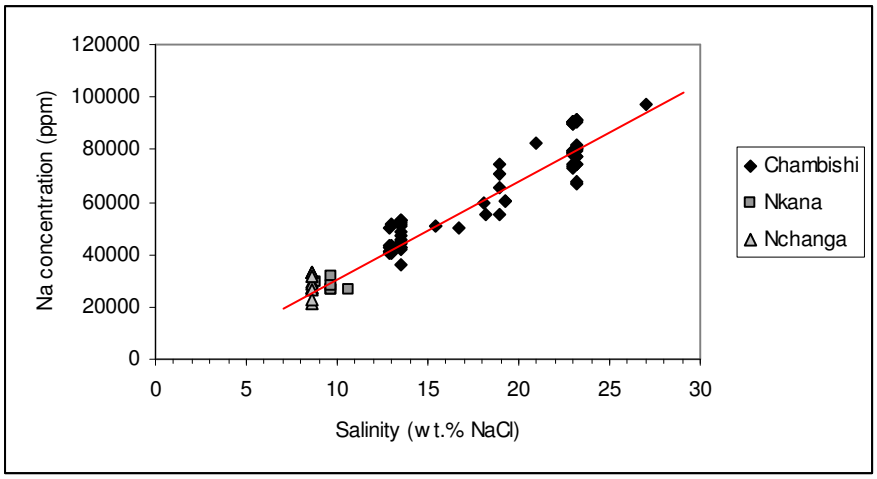

Figure 8.7. Salinity vs. Na-concentration of aqueous early orogenic inclusions of the Chambishi, Nkana, and Nchanga deposits.

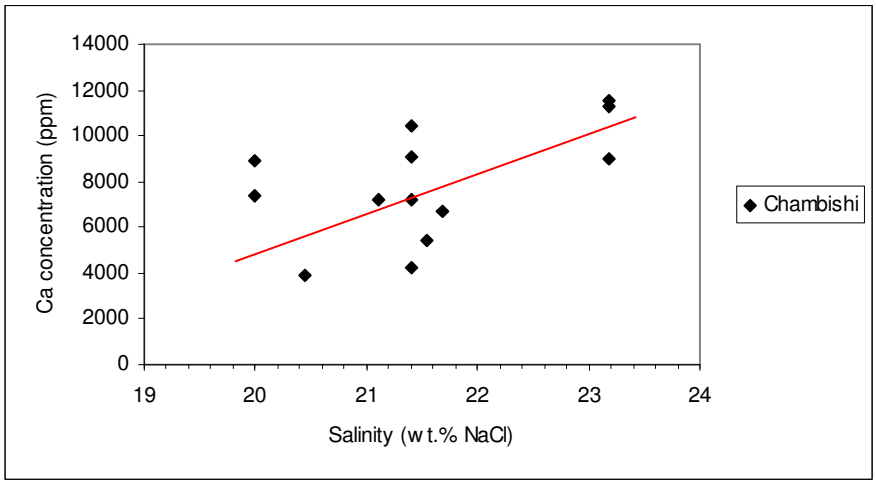

Figure 8.8. Salinity vs. Ca-concentration of aqueous early orogenic inclusions of the Chambishi, deposit. No available data for the Nchanga and Nkana deposits.

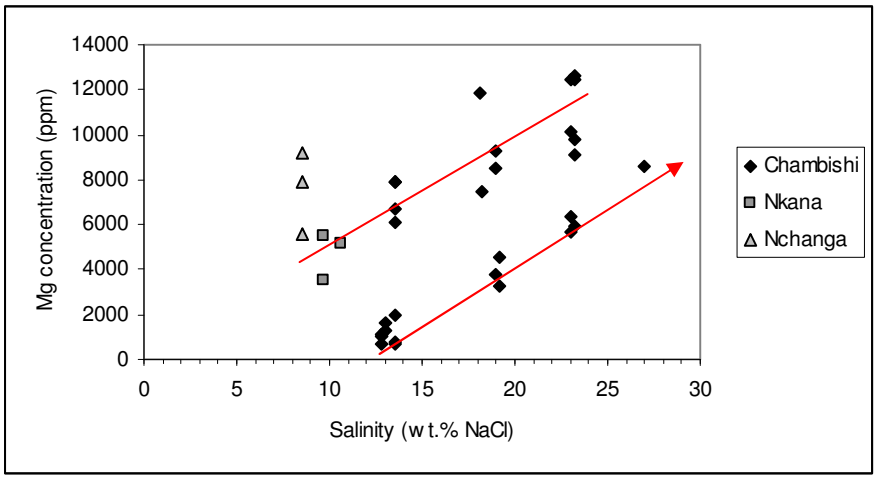

Figure 8.9. Salinity vs. Mg-concentration of aqueous early orogenic inclusions of the Chambishi, Nkana, and Nchanga deposits.

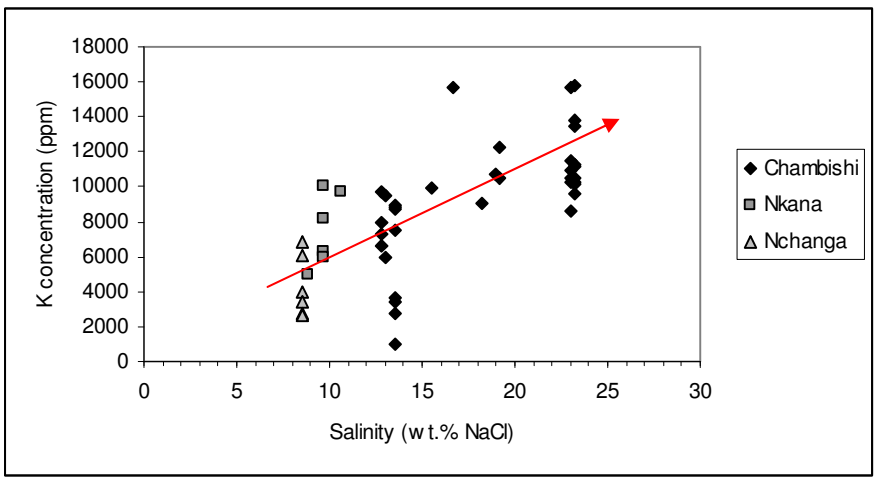

Figure 8.10. Salinity vs. K-concentration of aqueous early orogenic inclusions of the Chambishi, Nkana, and Nchanga deposits.

Ca concentrations of Chambishi aqueous inclusions were measured at ~7800 ppm, and increasing Ca concentration is observed at constant salinities at ~ 20 wt.% NaCl, 22.1 wt.% NaCl, and 23.2 wt.% NaCl (Figure 8.8).

A weakly positive correlation is present in Mg concentration when comparing the Chambishi, Nchanga and Nkana early orogenic fluid inclusions (Figure 8.9), with Chambishi inclusions exhibiting the higher range of values at ~700 - 12620 ppm Mg. Two linear trends are observed which show a positive correlation between Mg and salinity and may be indicative of two fluid populations present during early orogenesis.

Early orogenic fluids contain moderate potassium and a positive correlation exists between salinity and potassium contents. Potassium contents increase at constant lower salinities between ~ 8-10 wt.% NaCl of fluids present at Nkana and Nchanga (Figure 8.10). The largely positive correlation between salinity and major cations is to be expected with increasing chloride availability in fluids, which become complexed with cations.

Early orogenic fluids are markedly enriched in cobalt at Nchanga compared to depleted values at the Chambishi and Nkana deposits (Figure 8.6, Table 8.3). Conversely, early orogenic fluids are depleted in sodium at Nchanga and Nkana, and enriched at Chambishi. Along with cobalt abundances, copper levels are slightly elevated at the Nchanga deposit at ~440 ppm Cu compared to ~200 ppm Cu at Chambishi and ~140 ppm Cu at Nkana. A weak inverse relationship is noted between copper and cobalt at Nchanga, and depleted levels of zinc and lead at Nchanga and Nkana. Early orogenic fluids are enriched in zinc and lead at Chambishi.

Inclusions of the Nkana deposit show depleted values in Sr at less than 50 ppm compared to higher values at the Nchanga (~300 ppm) and Chambishi (~370 ppm) deposits.

Early orogenic aqueo-carbonic inclusions

Aqueo-carbonic inclusions hosted in samples of the Chambishi deposit were analysed for elemental compositions (Figure 8.11, Table 8.3). Aqueo-carbonic inclusions contain ~ 45000 ppm Na. Halite-saturated inclusions contain ~97000 ppm Na. Aqueo-carbonic inclusion of the Nchanga deposit contain ~50000 ppm Na and ~18000 ppm Ca.

Table 8.3. Summary of LA-ICP-MS data for early orogenic inclusions.

			weight ratios										Salinity	ppm								
Type	Sample		Na	Mg	K	Co	Cu	Zn	Sr	Ag	Pb	Mn	(wt%eNaCl)	Na	Mg	K	Co	Cu	Zn	Sr	Ag	Pb	Mn
aqueous	CBSqz3A	Mean	1	0.127	0.154	0.000	0.002	0.006	0.005	0.000	0.002	-	22.9	80,292	9,189	11,425	6	194	452	373	23	162	-
		Stdev	0	0.038	0.031	0.000	0.001	0.002	0.001	0.000	0.001	-	1.0	8,590	2,769	2,168	3	95	168	123	19	55	-
		%RSD	0	29.744	20.401	63.067	48.819	35.845	21.812	82.107	34.260	-	4.2	11	30	19	57	49	37	33	86	34	-
aqueous	NS47b-A (2)1	Mean	1	0.179	0.271	0.000	0.005	0.005	0.001	0.002	0.002	-	9.7	28,117	4,736	7,534	3	140	137	42	69	64	-
		Stdev	0	0.032	0.076	0.000	0.003	0.001	0.001	0.002	0.001	-	0.5	1,927	865	1,898	2	78	27	16	52	40	-
		%RSD	0	18.141	28.013	47.749	58.014	15.382	38.072	71.575	62.344	-	5.3	7	18	25	47	56	20	37	75	62	-
aqueous	NOP8B-A (3)n	Mean	1	0.328	0.163	0.007	0.015	0.008	0.010	0.002	0.004	-	8.6	28,597	7,580	4,265	202	441	213	315	44	107	-
		Stdev	0	0.093	0.057	0.003	0.007	0.004	0.002	0.001	0.002	-	0.0	3,937	1,496	1,611	90	237	121	88	30	53	-
		%RSD	0	28.441	34.787	41.367	46.895	53.257	20.957	67.173	43.733	-	0.0	14	20	38	44	54	57	28	68	49	-
aq-car-n	CBSqz7B-A	Mean	1	0.024	0.198	0.000	0.001	0.002	0.000	0.000	0.001	-	13.3	45,792	1,043	8,561	5	63	83	15	9	23	-
		Stdev	0	0.007	0.029	0.000	0.001	0.001	0.000	0.000	0.000	-	0.8	4,647	217	1,201	2	30	36	5	6	19	-
		%RSD	0	26.878	14.734	46.520	52.237	33.314	31.176	62.206	74.574	-	5.8	10	21	14	41	48	43	33	72	83	-
aq-car	CBSqz3By	Mean	1	0.108	0.123	0.002	0.017	0.015	0.002	0.000	0.005	-	13.5	46,952	4,562	5,135	90	781	668	71	19	222	-
		Stdev	0	0.084	0.082	0.002	0.021	0.012	0.001	0.000	0.003	-	0.0	5,198	3,299	3,166	66	962	507	73	14	107	-
		%RSD	0	77.645	67.246	75.672	119.849	78.200	91.057	71.217	51.491	-	0.0	11	72	62	74	123	76	103	73	48	-
aq-car	CBSqz3A	Mean	1	0.102	0.205	0.000	0.001	0.003	0.003	0.000	0.001	-	18.0	59,811	6,119	11,032	8	52	161	176	14	33	-
		Stdev	0	0.062	0.066	0.000	0.001	0.001	0.002	0.000	0.000	-	2.0	9,725	3,752	3,520	10	38	53	86	8	13	-
		%RSD	0	60.699	32.226	116.411	65.300	38.003	67.306	56.388	57.270	-	11.3	16	61	32	125	73	33	49	58	40	-
aq-car	CHM7B-A +s	(1)2	1	0.088			0.001	0.002	0.003			-	27.0	97,337	8,584			53	148	258			
methane	CBSqz7B-A	Mean	1	0.161	0.211	0.002	0.010	0.036	0.001	0.000	0.006	-	12.0	40,193	5,599	7,446	106	326	1,427	25	13	231	-
		Stdev	0	0.089	0.047	0.003	0.009	0.023	0.000	0.000	0.005	-	0.0	5,780	2,978	1,805	127	268	1,010	17	10	201	-
		%RSD	0	55.340	22.445	113.432	89.845	61.942	58.890	77.072	86.336	-	0.0	14	53	24	120	82	71	68	74	87	-
methane	NOP8B-A	Mean	1	-	0.446	-	0.018	0.091	-	0.038	0.021	0.566	8.3	21,498	-	8,996	-	353	2,086	-	1,095	375	9,805
		Stdev	0	-	-	-	-	0.007	-	-	0.012	0.531	0.0	5,278	-	-	-	-	443	-	-	209	6,388
		%RSD	0	-	-	-	-	8.222	-	-	58.703	93.941	0.0	25	-	-	-	-	21	-	-	56	65
carbonic	NCGmq9d	Mean	1	0.581	0.424	0.002	0.011	0.039	0.007	0.002	0.016	-	24.0	67,588	29,899	20,838	126	737	2,105	443	175	1,127	-
		Stdev	0	0.203	0.194	0.001	0.008	0.026	0.003	0.002	0.007	-	0.0	19,312	6,498	8,310	127	587	1,067	214	147	715	-
		%RSD	0	34.994	45.691	76.740	68.952	65.636	37.577	89.948	42.124	-	0.0	29	22	40	101	80	51	48	84	63	-

			weight ratios					Salinity	ppm				
Type	Sample		Na	Ca	Mn	Fe	Ba	(wt.%eNaCl)	Na	Ca	Mn	Fe	Ba
aqueous	CBSqz3A	Mean	1	0.104	0.003	0.018	0.001	21.5	78,063	7,874	214	1,420	89
		Stdev	0	0.032	0.001	0.004	0.000	1.1	4,991	2,460	90	309	36
		%RSD	0	31.270	41.974	23.799	37.998	5.1	6	31	42	22	40
aq-car+s	NCGmq9d	Mean	1	0.510	0.008	0.499	0.011	22.0	50,119	18,006	391	17,681	483
		Stdev	0	0.623	0.002	0.606	0.006	3.3	24,239	18,865	109	18,284	15
		%RSD	0	122.180	22.048	121.411	51.074	14.8	48	105	28	103	3
carbonic	NCGmq9d	Mean	1	0.345	0.016	0.193	0.023	24.0	61,074	20,611	958	11,336	1,412
		Stdev	0	0.096	0.008	0.089	0.004	0.0	6,949	3,392	456	4,171	193
		%RSD	0	27.841	50.249	45.917	17.027	0.0	11	16	48	37	14
carbonic	NCGmq9e	Mean	1	0.575	0.049	0.271	0.003	24.0	72,029	30,415	3,339	18,486	290
		Stdev	0	0.371	0.011	-	0.001	0.0	19,413	16,464	1,147	-	103
		%RSD	0	64.614	22.778	-	34.824	0.0	27	54	34	-	35

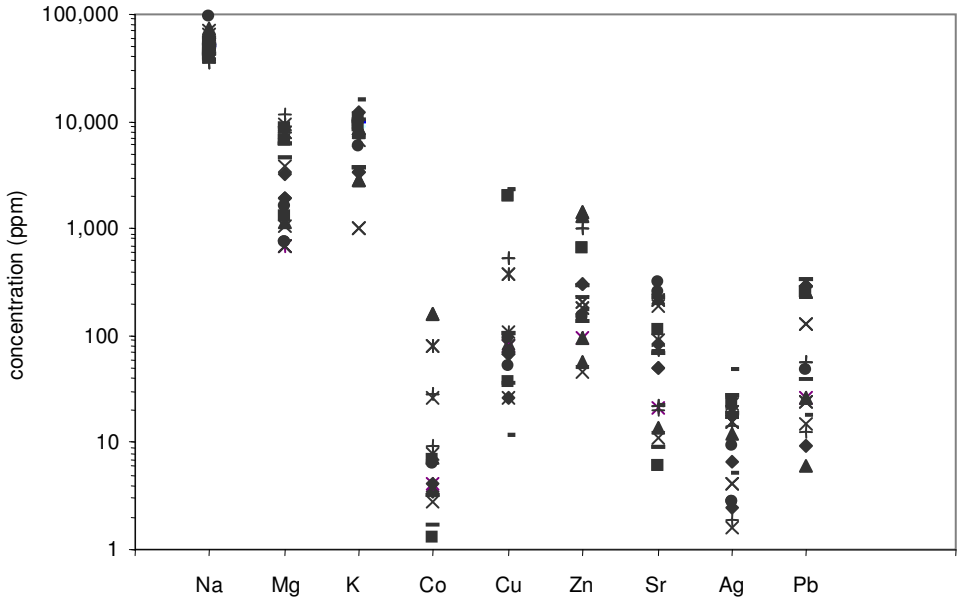

Figure 8.11. Aqueo-carbonic fluid inclusions from early orogenic fluids at the Chambishi deposit.

Early orogenic carbonic inclusions

CO_2-rich inclusions from the Nchanga deposit are enriched in Mg compared to methane-rich inclusions at the Chambishi deposit (Figure 8.12). Sr and Ag abundances are both greater in Nchanga CO_2 - rich inclusions relative to methane-rich inclusions from the Chambishi deposit. A wide range in Ag counts are present.

Copper and cobalt concentrations show a large range of values with no clear distinction between the two localities. Notably, Sr content is elevated in the Nchanga inclusions and correspondingly lower in similar inclusions from Chambishi. Ag concentrations are also elevated in Nchanga inclusions with lower concentrations in Chambishi inclusions. Mn was measured in inclusions from the Nchanga deposit, but data is absent from the Chambishi deposit. Pb values are also slightly elevated in samples from Nchanga, and lower in Chambishi carbonic inclusions.

The comparative plot of concentrations in carbonic fluid inclusions displayed in Figure 8.12 shows contents of selected elements in weight ratio abundances. Salinity determinations were not possible during microthermometry or Raman microspectroscopy due to the absence of aqueous phases in these inclusions. Therefore, the obtaining of absolute cation contents in ppm is not possible. Where possible, the chlorinity of three aqueo-carbonic inclusions at Nchanga was determined at 0.9, 4.5 and 5.5 molal respectively using Raman microspectrometry. This was done where a thin film of water

was detected during microspectrometry and was used during calculations to determine ppm for aqueo-carbonic inclusions.

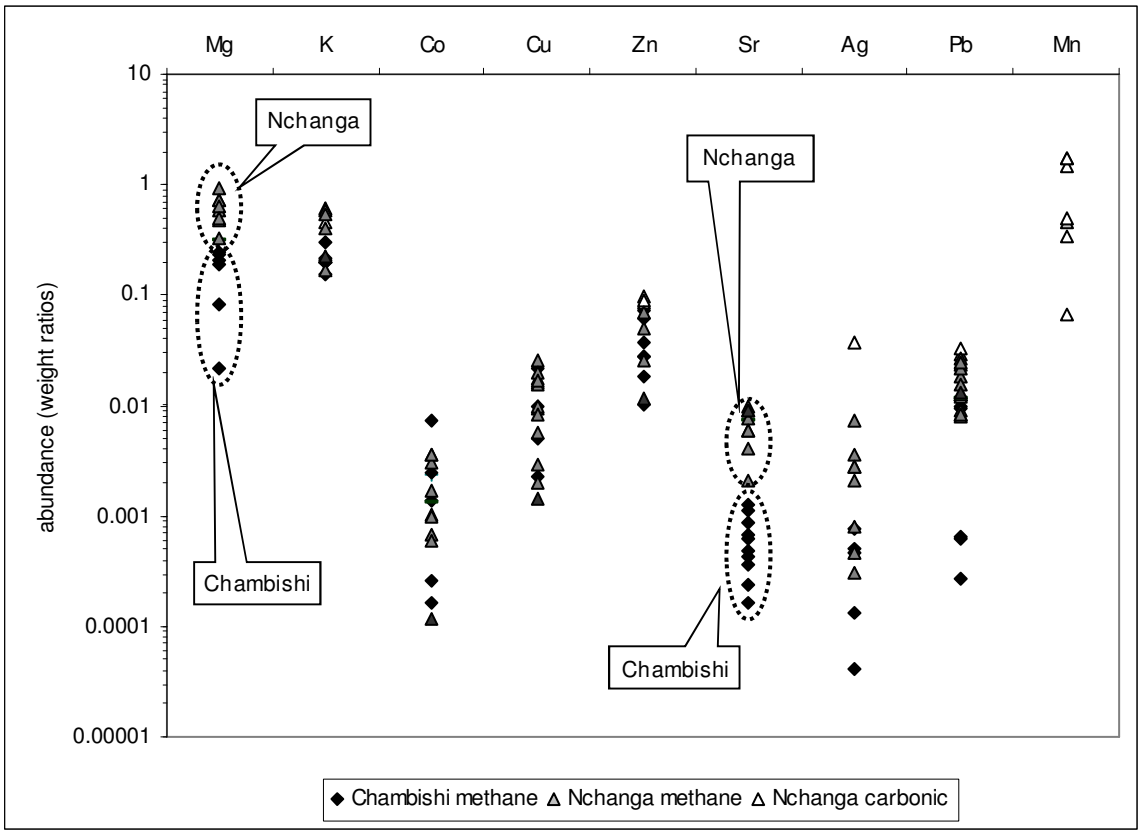

Figure 8.12. Abundances of selected cations in carbonic (CO_2 - dominated) and methane inclusions representative of early orogenic fluids in the Chambishi and Nchanga deposits.

Early orogenic bulk distributions

The following figures (Figures 8.13a-j) illustrate the distribution of selected elemental concentrations over the Chambishi-Nchanga ± Nkana areas for combined fluid inclusion types (i.e., aqueous, aqueo-carbonic ± solid, carbonic). Where possible, selected elements were gridded and plotted accordingly, however, for Co and Ag, the number of analyses was insufficient to generate reliable contoured plots. For these two elements, concentrations for the Nchanga, Chambishi and Nkana deposits are displayed as column charts.

Na concentration is generally higher at the Chambishi deposit compared to the Nchanga and Nkana areas as is evidenced primarily by elevated Na concentrations in aqueous inclusions (Figure 8.13a). These elevated values at Chambishi are also reflected

in salinity values calculated from microthermometry measurements which show salinities at Chambishi between 12 – 27 wt.% $NaCl_{equiv}$. Salinities at Nkana range between 8.8 – 10.6 wt.% $NaCl_{equiv.}$, and were calculated at ~ 8.6 wt.% $NaCl_{equiv.}$ at Nchanga.

In contrast to Na values, elevated levels of the following elements are present at the Nchanga deposit, namely Ca, Mn, Fe, Ba, Co, Ag, and Pb (Figures 8.13b-e, g, i, j). Copper concentration is essentially equally distributed among the Nchanga and Chambishi deposits, but is comparatively depleted at the Nkana deposit (Figure 8.13f). Zn concentration is elevated in samples of Nchanga and Chambishi, but relatively depleted at Nkana (Figure 8.13h).

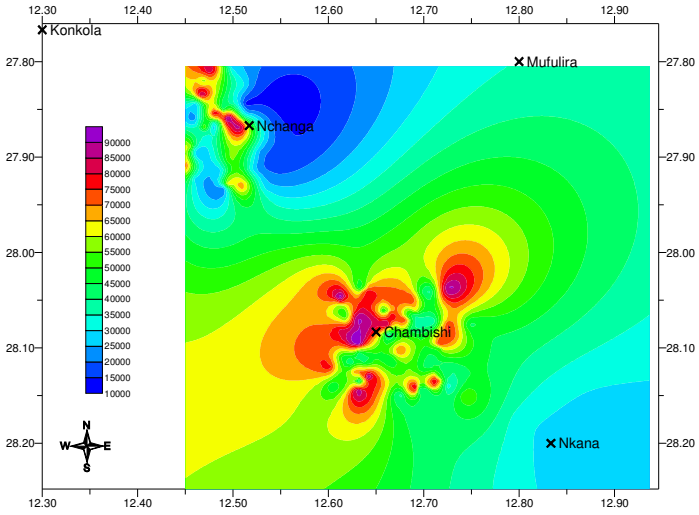

*Figure 8.13. (a) Distribution of **Na** of inclusions representative of early orogenic fluids of the Nchanga, Chambishi, and Nkana deposits. Scale bar units are in ppm.*

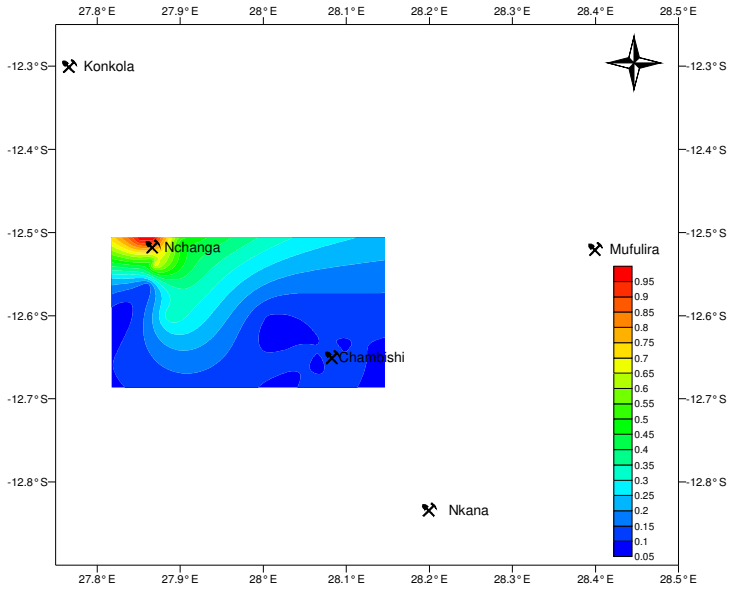

*Figure 8.13. (b) Distribution of **Ca** of inclusions representative of early orogenic fluids of the Nchanga and Chambishi deposits. Nchanga inclusions show enrichment in Ca compared to inclusions of the Chambishi deposit. Scale bar units are in weight ratios.*

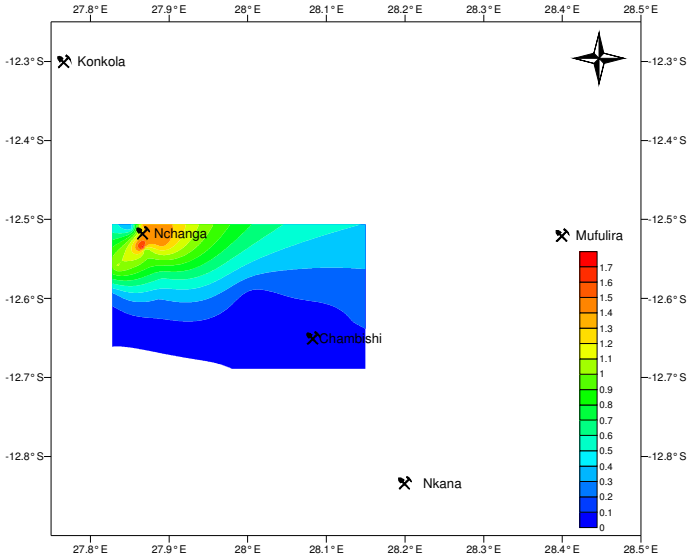

*Figure 8.13. (c) Distribution of **Mn** of inclusions representative of early orogenic fluids of the Nchanga and Chambishi deposits. Nchanga inclusions are enriched in Mn relative to those at Chambishi. Scale bar units are in weight ratios.*

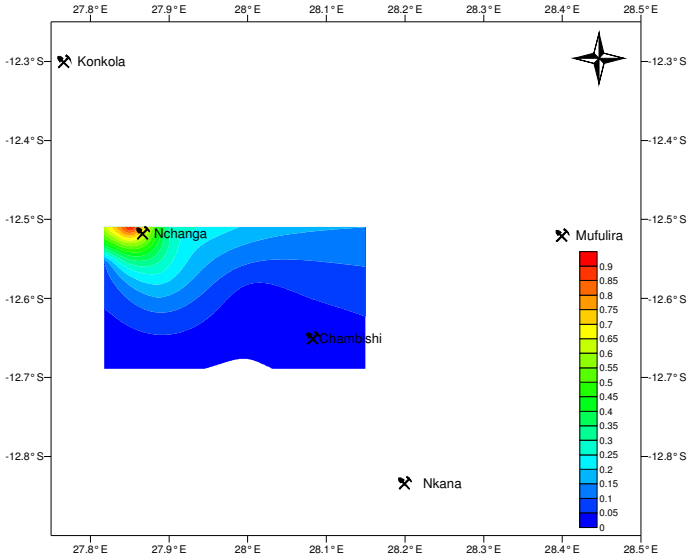

*Figure 8.13. (d) Distribution of **Fe** of inclusions representative of early orogenic fluids of the Nchanga and Chambishi deposits. Inclusions at Nchanga are enriched in Fe compared to inclusions of the Chambishi deposit. Scale bar units are in weight ratios.*

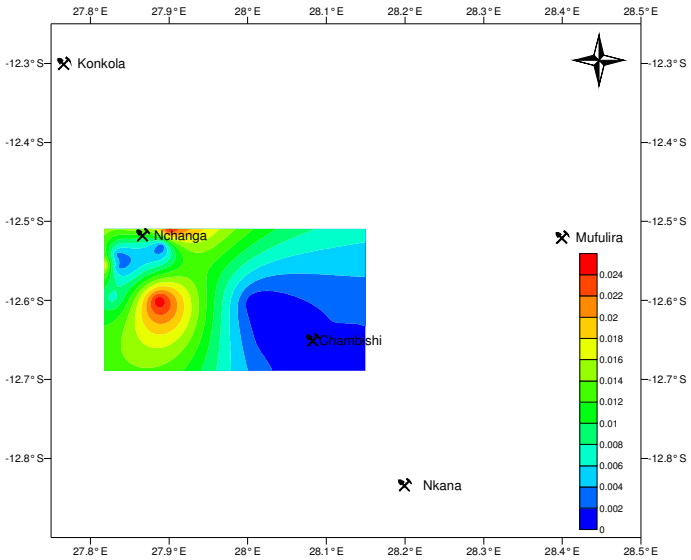

*Figure 8.13. (e) Distribution of **Ba** of inclusions representative of early orogenic fluids of the Nchanga and Chambishi deposits. Inclusions at Nchanga are enriched in Ba compared to inclusions of the Chambishi deposit. Scale bar units are in weight ratios.*

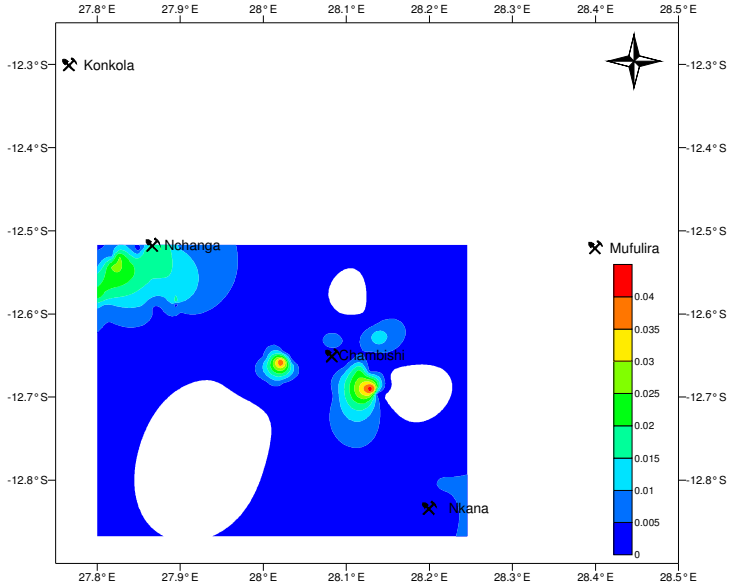

*Figure 8.13. (f) Distribution of **Cu** concentrations of inclusions representative of early orogenic fluids of the Nchanga, Chambishi and Nkana deposits. Higher values of Cu are present at Nchanga and Chambishi. Scale bar units are in weight ratios.*

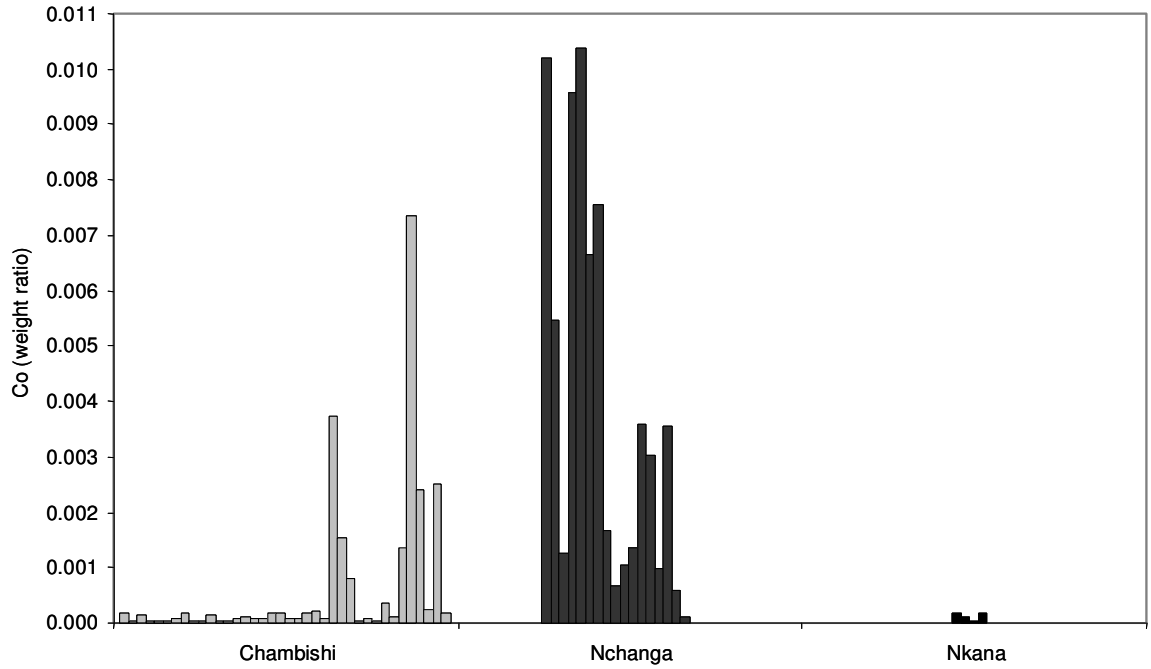

Figure 8.13 (g). Co in early orogenic fluids from the Nchanga, Chambishi, and Nkana deposits. Units are in weight ratio concentrations. Co is plotted as a distribution bar graph due to insufficient points for Kriging.

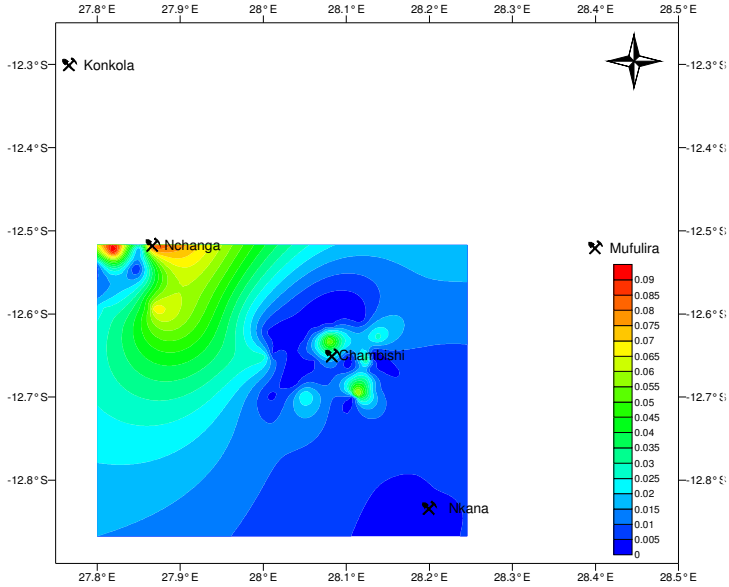

*Figure 8.13. (h) Distribution of **Zn** concentrations of inclusions representative of early orogenic fluids of the Nchanga, Chambishi and Nkana deposits. Compared to Nkana, inclusions are enriched in Zn at the Nchanga and Chambishi deposits. Scale bar units are in weight ratios.*

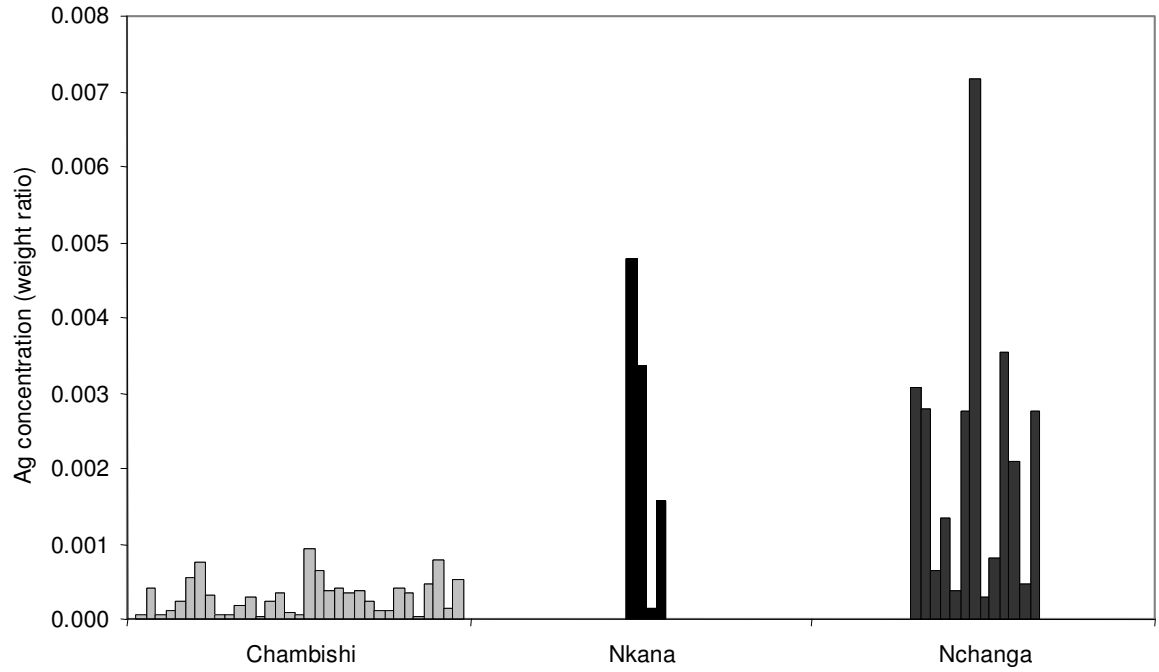

*Figure 8.13. (i) Distribution of **Ag** concentration in inclusions representative of early orogenic fluids of the Nchanga, Chambishi, and Nkana deposits. Nchanga inclusions contain the highest Ag values. Units are displayed in weight ratios. Ag is plotted as a distribution bar graph due to insufficient points for Kriging.*

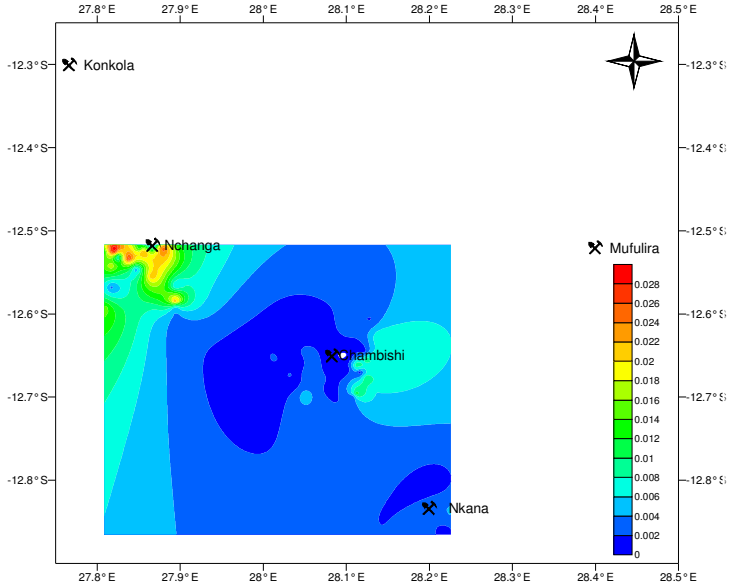

*Figure 8.13 (j) Distribution of **Pb** concentrations of inclusions representative of early orogenic fluids of the Nchanga, Chambishi and Nkana deposits. Nchanga inclusions exhibit the highest Pb values followed by Chambishi, and Nkana. Scale bar units are in weight ratios.*

8.4 Late orogenic fluids

Fluids circulating during the late stages of basin evolution and metamorphism in the Copperbelt were sampled from inclusions at the Mufulira and Nkana deposits. Here, LA-ICP-MS data is only available from fluid inclusions of the Mufulira deposit which is also the deposit located the furthest to the east of the five deposits studied on the north-eastern side of the Kafue anticline. Inclusions at Mufulira were sampled from the lower C-orebody horizon at the contact with the basement gneisses (sample MUF7D, n = 13; MUF7H-A, n = 21). Quartz veins abound along this contact and project into the basement with coarse crystals of chalcopyrite in anhydrite-quartz assemblage veins.

Microthermometry of aqueous fluid inclusions of the Mufulira deposit indicated NaCl-$CaCl_2$ - saturated inclusions. In addition to these complexes, Fe-chlorides are suspected in the solution due to low eutectic temperatures and the presence of colourless solids at room temperatures and above. Crystals of hematite are present in several inclusions as heterogeneously trapped solids (Figure 8.14), and Raman microspectroscopy revealed the presence of N_2 as the major constituent in the vapour phases of the majority of inclusions. LA-ICP-MS was conducted to determine the cation concentration of these inclusions. Results are displayed in Table 8.4.

8.4.1 LA-ICP-MS

Cobalt and copper concentrations in late orogenic NaCl-$CaCl_2$ saturated aqueous ± N2 ± hematite fluid inclusions are widely constrained between ~ 1 - 1000 ppm Co and ~

30 - 16000 ppm Cu (Figure 8.14). NaCl-$CaCl_2$ -saturated aqueous-N_2 fluid inclusions contain less than 10 ppm Co, less than 200 ppm Cu, and between 6000 and 8100 ppm Pb (Figure 8.14). These inclusions, in addition to inclusions containing hematite solids are enriched in high Fe counts between ~18000 to 53800 ppm Fe. Inclusions containing hematite solids contain up to 16000 ppm Cu (average 4600 ppm), < 6600 ppm Zn (average 2100 ppm), and a maximum of 19000 ppm Pb (average 5800 ppm). By comparison, NaCl-$CaCl_2$-saturated aqueous inclusions without hematite contain up to 440 ppm Cu (average 350 ppm), 3,500 ppm Zn (average 2,400 ppm), and 9,600 ppm Pb (average 4,100 ppm).

The explanation of the large spread in copper and cobalt contents of this fluid type may be related to the tectonic setting of these particular fluids:- These fluids were trapped during peak metamorphic conditions, as is evidenced by high trapping temperatures from microthermometry. During this stage of basin evolution, fluids were at sufficient temperatures to dissolve and carry metals which were concentrated in the host sediments during earlier diagenetic processes.

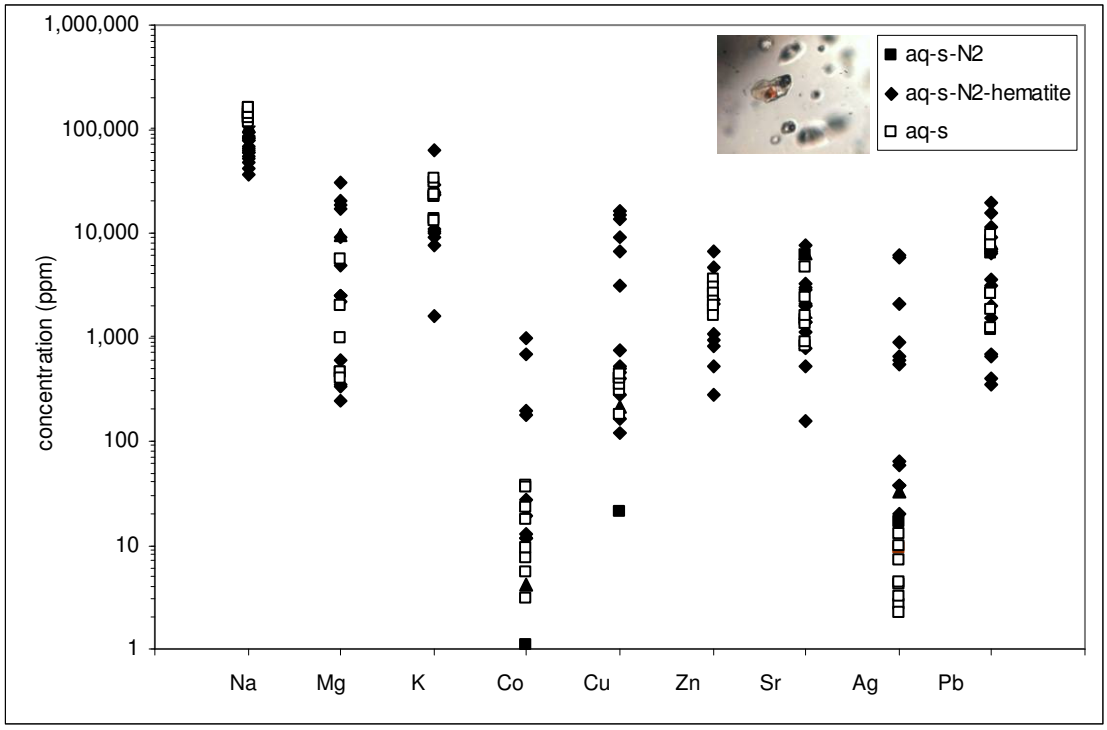

Figure 8.14. Cation contents in ppm of inclusions representative of late orogenic fluids sampled from Mufulira.

Table 8.4. Summary of LA-ICP-MS data of late orogenic fluids.

			weight ratios										ppm								
Type	**Sample**		**Na**	**Mg**	**K**	**Co**	**Cu**	**Zn**	**Sr**	**Ag**	**Pb**	**Salinity (wt‰eNaCl)**	**Na**	**Mg**	**K**	**Co**	**Cu**	**Zn**	**Sr**	**Ag**	**Pb**
aq-s-n	Muf 7H-A	Mean	1	0.093	0.189	0.000	0.001	0.020	0.042	0.000	0.063	34.7	108,763	9,757	21,064	3	118	2,611	4,737	25	7,236
		Stdev	0	-	0.117	0.000	0.001	-	0.021	0.000	0.020	9.2	18,287	-	10,462	2	137	-	2,578	12	1,214
		%RSD	0	-	61.935	91.187	120.652	-	49.688	59.848	30.905	26.6	17	-	50	82	116	-	54	47	17
he	Muf 7H-A	Mean	1	0.177	0.321	0.005	0.095	0.033	0.035	0.025	0.108	25.1	64,312	8,389	18,839	235	4,761	2,139	2,177	1,415	5,879
		Stdev	0	0.240	0.317	0.008	0.129	0.036	0.031	0.039	0.108	4.1	16,254	9,940	17,296	350	6,128	2,148	1,972	2,222	5,940
		%RSD	0	135.223	98.776	152.720	135.768	108.666	88.198	157.364	100.065	16.5	25	118	92	149	129	100	91	157	101
aq-s	Muf 7D	Mean	1	0.012	0.193	0.000	0.003	0.019	0.014	0.000	0.030	40.0	138,869	1,644	24,103	17	357	2,405	1,890	6	4,170
		Stdev	0	0.014	0.066	0.000	0.001	0.005	0.009	0.000	0.022	0.0	14,422	2,018	7,106	14	88	724	1,353	4	3,330
		%RSD	0	116.267	34.411	79.225	26.598	26.598	64.106	51.820	73.848	0.0	10	123	29	78	25	30	72	60	80

			weight ratios					ppm			
Type	**Sample**		**Na**	**Ca**	**Mn**	**Fe**	**Ba**	**Salinity (wt.‰eNaCl)**	**Na**	**Ca**	**Mn**	**Fe**
Lw±s±he-(n)	Muf 7H-A	Mean	1	0.501	0.216	0.366	-	35	81,663	32,919	15,076	36,360
		Stdev	0	0.197	0.013	0.216	-	8.660254038	26,155	1,279	4,511	24,708
		%RSD	0	39.305	6.099	58.930	-	24.74358297	32	4	30	68

8.5 Comparative fluid compositions of the Copperbelt: regional distributions

8.5.1 Basinal fluids

Basinal fluids of the Nchanga deposits are enriched in Cu and Co content relative to similar fluids of the Chambishi deposit. Pb and Zn concentrations are generally consistent for both the Nchanga and Chambishi deposits during basinal circulation.

8.5.2 Early orogenic fluids

Early orogenic fluids at the Chambishi deposit are enriched in Na. Conversely, Ca is present at the Nchanga deposits, but mainly absent from the Chambishi and Nkana samples. Fluid inclusions of the Nchanga deposit trapped early orogenic fluids comparatively enriched in Co, Zn, Ag, and Pb. Cu concentrations are more or less evenly distributed between the Chambishi and Nchanga deposits in the early orogenic environment.

8.5.3. Late orogenic fluids

Aqueous-N_2 inclusions at the Mufulira deposit are saturated in NaCl-$CaCl_2$ and are enriched in Fe and Mn relative to early orogenic aqueous, aqueo-carbonic fluids from the Chambishi and Nchanga deposits (Figure 8.15). Pb values are elevated and average 5400 ppm with a maximum value of 19800 ppm. Sr values average ~2400 ppm (maximum 7600 ppm). Copper and cobalt concentrations are the highest compared to early orogenic and basinal fluids.

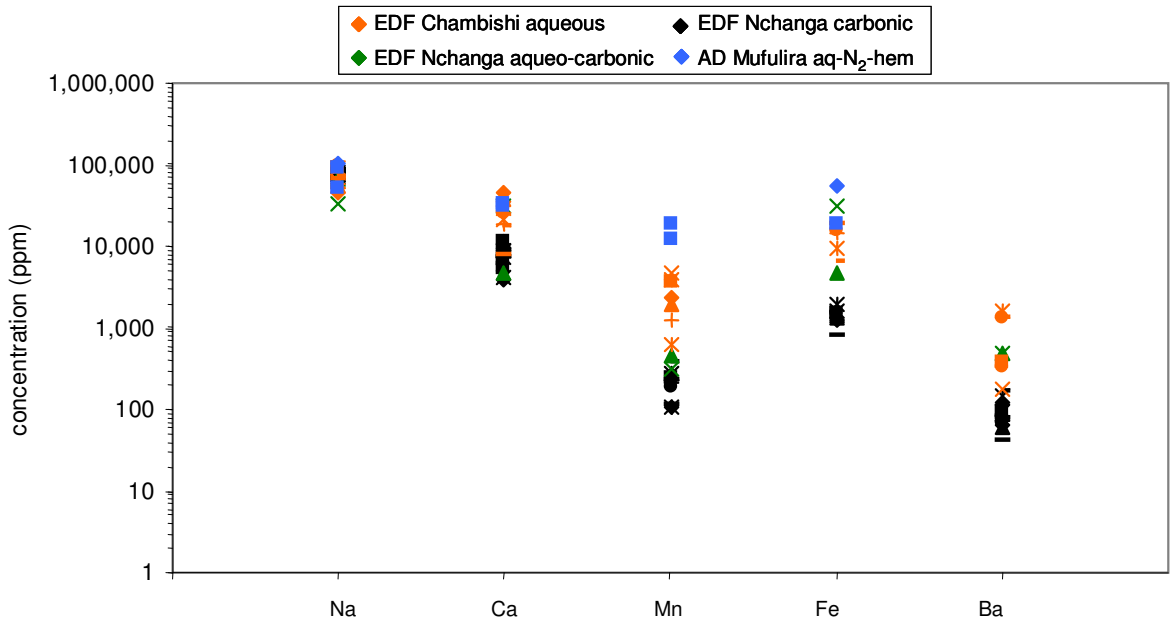

Figure 8.15. Concentrations of selected elements of fluid inclusions representative of early orogenic fluids (EDF) of the Chambishi and Nchanga deposits compared to elemental concentrations of inclusions of late orogenic (AD) fluids of the Mufulira deposit.

8.6 Comparison of the fluid compositions of the Copperbelt: timing constraints

The complex, polymetallic nature of the Lufilian arc mineral deposits is well documented, and early stratiform Cu-Co mineralisation is succeeded by epigenetic Pb-Zn-Ge-Ga-Ag deposits and Cu-Au-Ag-Fe-U deposition along the Lufilian arc. This regional picture of prolonged polymetallic fluid flow is supported during this study by microscale evidence from fluid inclusions trapped during the early stages of basin maturation until regional metamorphism.

8.6.1 Base metals

Fluids circulating the sedimentary pile during the early stages of basin maturation are relatively depleted in Co in comparison with later fluids present during the early stages of orogenesis and peak metamorphism (Figure 8.16). Seward and Barnes (1997) indicate a minimum concentration of 10 ppm Cu and Co is required for ore deposit formation when considering known base metals from MVT, skarn, porphyry, vein Cu-Pb-Zn and massive sulphide type deposits. Cobalt concentrations in basinal fluids range between 0 and 34 ppm, with an average value of 18 ppm. One anomalous value of 608 ppm is present in an

H_2O - KCl - $MgCl_2$ - CO_2 - N_2 inclusion saturated with NaCl of the Nchanga Feldspathic quartzite. Except for this one anomalous value, Co concentrations are lower in basinal fluids than in early orogenic fluids where values range between 1 and 345 ppm, with an average value of 64 ppm. This is significantly enriched when compared to the Co concentration in normal modern day seawater of 0.00039 ppm at 3.5 % salinity (Turekian, 1968). Co concentrations in late orogenic fluids range between 1 and 958 ppm with an average value of 119 ppm (Table 8.5). A general increase in Co concentration is observed with basin maturation.

A similar pattern is exhibited for Cu concentration (Figure 8.17) with basinal and early orogenic fluids generally depleted in Cu which increases during late orogenesis. Basinal fluid Cu concentrations range between 5 and 1683 ppm, with an average of 436 ppm (Table 8.5). Early orogenic fluids contain between 11 and 2303 ppm Cu with an average value of 390 ppm Cu. Late orogenic fluids contain between 21 and 16,309 ppm Cu with an average of 3,017 ppm Cu.

Table 8.5. Selected average and maximum element concentrations (ppm) of early basinal, early deformational, and advanced deformational fluids.

	Basinal		Early orogenic		Late orogenic	
	Avg. (ppm)	Max. (ppm)	Avg. (ppm)	Max. (ppm)	Avg. (ppm)	Max. (ppm)
Cu	436	1,683	390	2,303	3,000	16,100
Co	18	608	64	345	120	960
Pb	855	5,183	450	2,383	5,400	19,800
Zn	1,870	7,100	774	3,000	2,270	6,650
Ag	91	493	70	1,100	740	6,100

Pb concentrations increase during basin maturation and increasing metamorphism as is seen by the concentrations of 66 – 5183 ppm Pb (average: 855 ppm) in basinal fluids, 6 – 2,383 ppm (average: 450 ppm) in early orogenic fluids, and 352 – 19,836 ppm Pb (average: 5,400 ppm) in late orogenic fluids (Figure 8.18, Table 8.5).

Zn concentrations remain fairly consistent during basin evolution with a slight depletion in early orogenic fluids (Figure 8.19). Basinal fluids contain between 120 – 7,143 ppm Zn (average: 1,870 ppm). Early orogenic fluids contain between 45 – 3,016 ppm Zn (average: 774 ppm). Late fluids contain between 281 – 6,655 ppm Zn (average: 2,276 ppm).

Ag concentrations in basinal fluids range between 2 – 493 ppm (average: 91 ppm), 2 – 1,095 ppm (average: 70 ppm) in early orogenic fluids, and 2 – 6119 ppm Ag (average: 743 ppm) in late orogenic fluids (Figure 8.20, Table 8.5). Late orogenic fluids are enriched in Ag compared to early fluids.

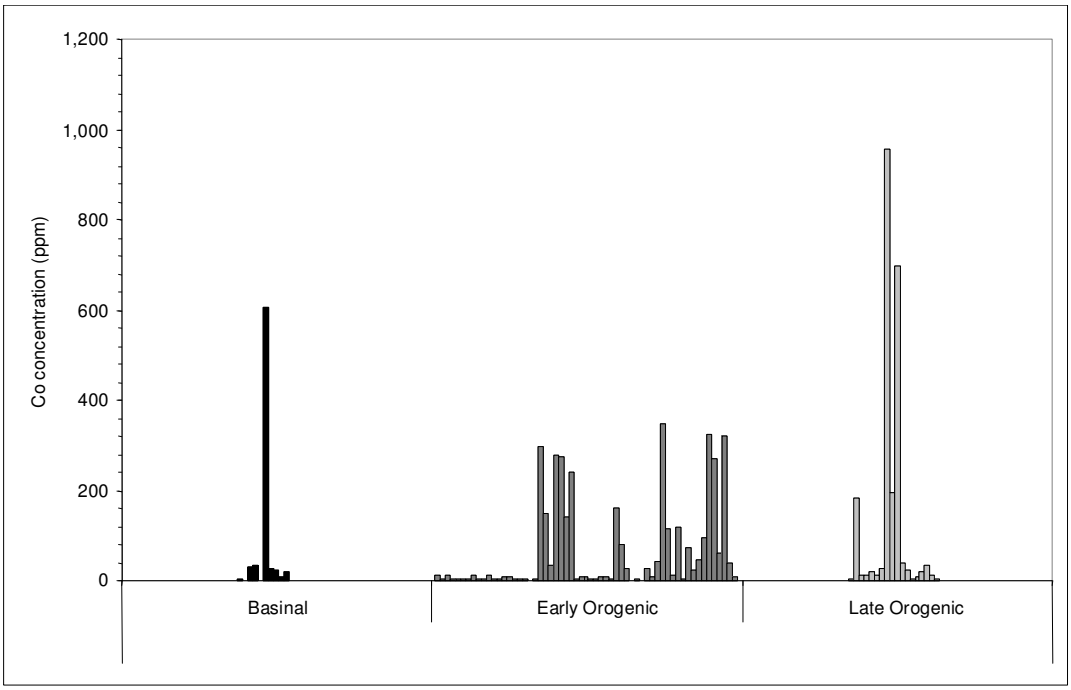

Figure 8.16. The Co concentration (ppm) in basinal, early orogenic, and late orogenic fluids shows a general increase with ongoing basin maturation.

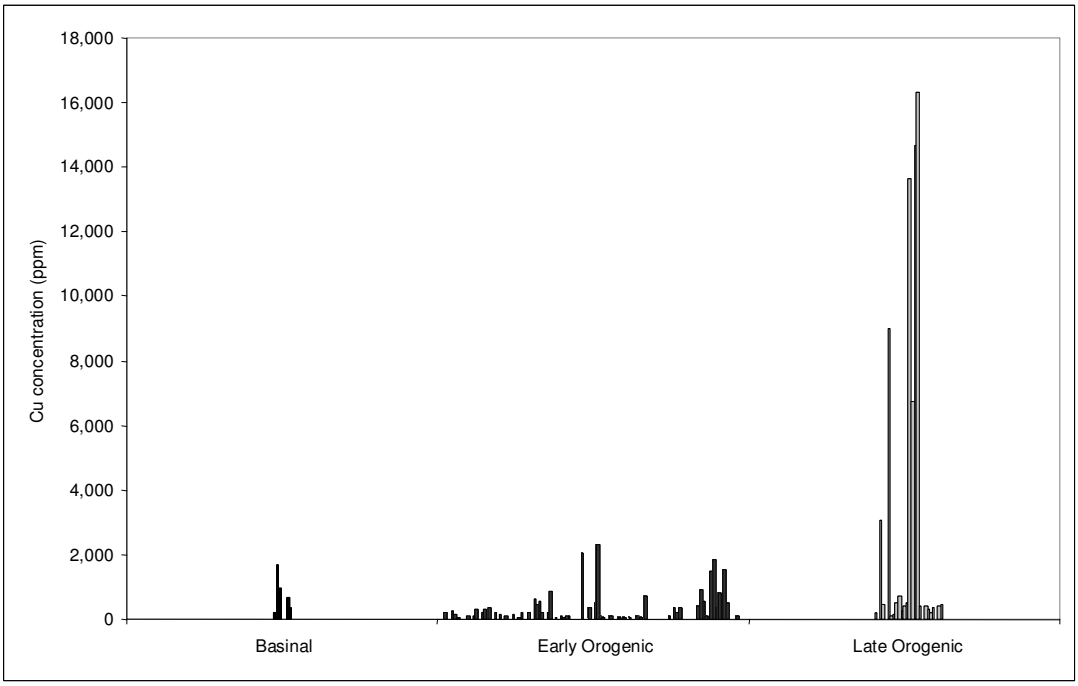

Figure 8.17. Cu concentration (ppm) in basinal, early orogenic, and late orogenic fluids as determined by LA-ICP-MS for inclusions from the Chambishi, Nchanga, Nkana, and Mufulira deposits.

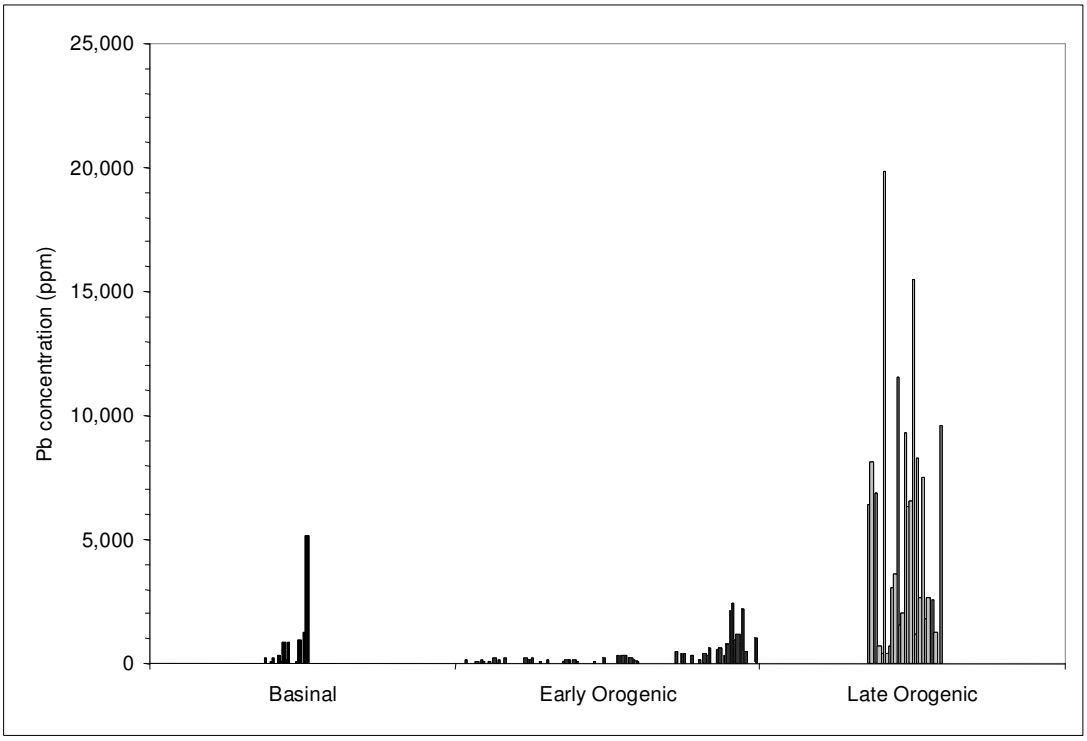

Figure 8.18. Pb concentration (ppm) of basinal, early orogenic and late orogenic fluids from the Chambishi, Nchanga, Nkana and Mufulira deposits show an increase in concentration in late fluids sampled from Mufulira.

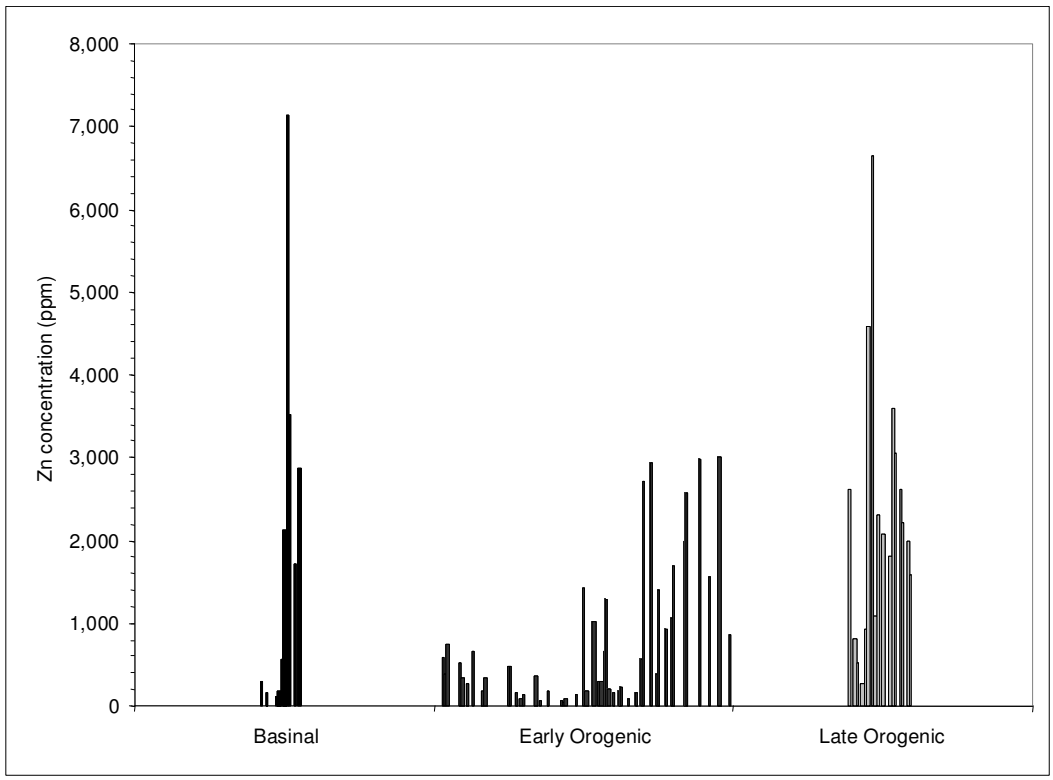

Figure 8.19. Zn concentrations (in ppm) are consistent in basinal, early orogenic and late orogenic fluids with isolated high concentration spikes in basinal and late orogenic fluids.

In order to further decipher the nature of fluids and fluid evolution during basin maturation, the average concentrations of selected elements are plotted for basinal, early orogenic and late orogenic fluids (Figures 8.21 - 8.24, Table 8.5). It follows that the average Cu, Co, Pb and Ag concentrations in basinal fluids increased during basin maturation and metamorphism (Figure 8.25).

Zn concentrations are slightly lower in early orogenic fluids than in basinal fluids, but show an increase during the final stages of orogenesis. A time plot is presented in Figure 8.25 considering Cu and Co. Although there is a clear overlap between early and late orogenic fluids, more Cu and Co are found in mature solutions when compared to earlier fluids.

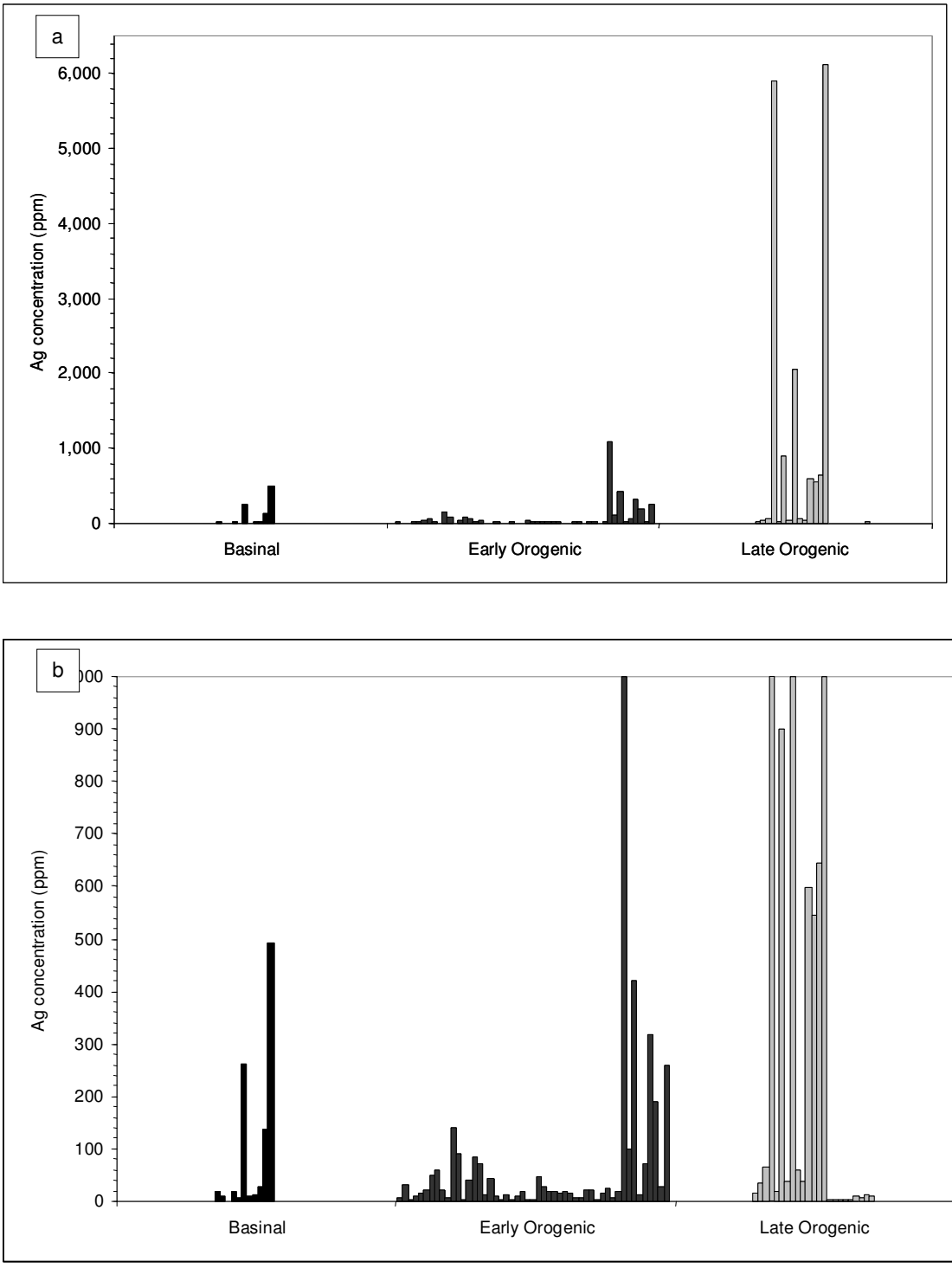

Figure 8.20. Ag concentrations (ppm) are elevated in late orogenic fluids compared to basinal and early orogenic fluids. Ranges from 0 – 1000 ppm Ag is enlarged in diagram (b).

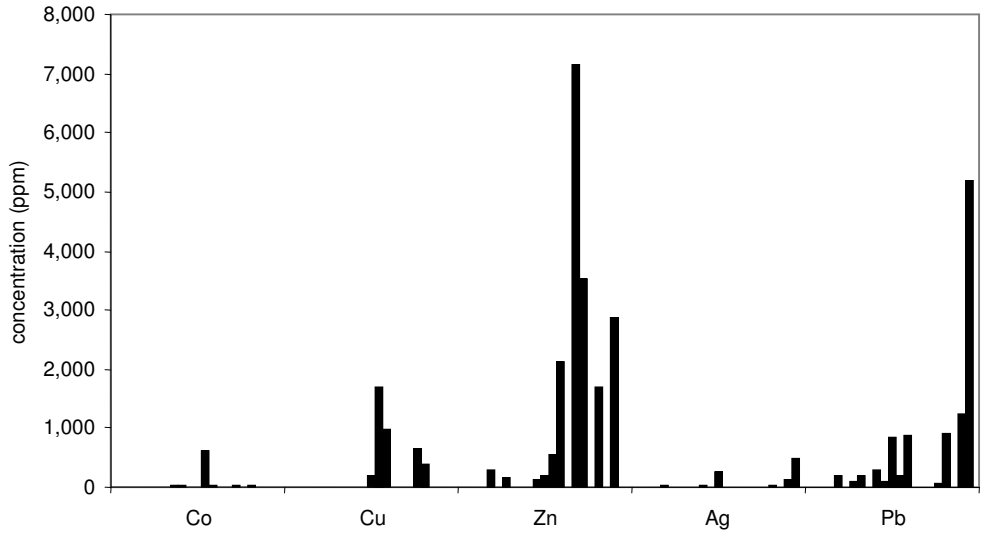

Figure 8.21. Contents of selected base metals and silver of basinal fluids from the Chambishi and Nchanga deposits.

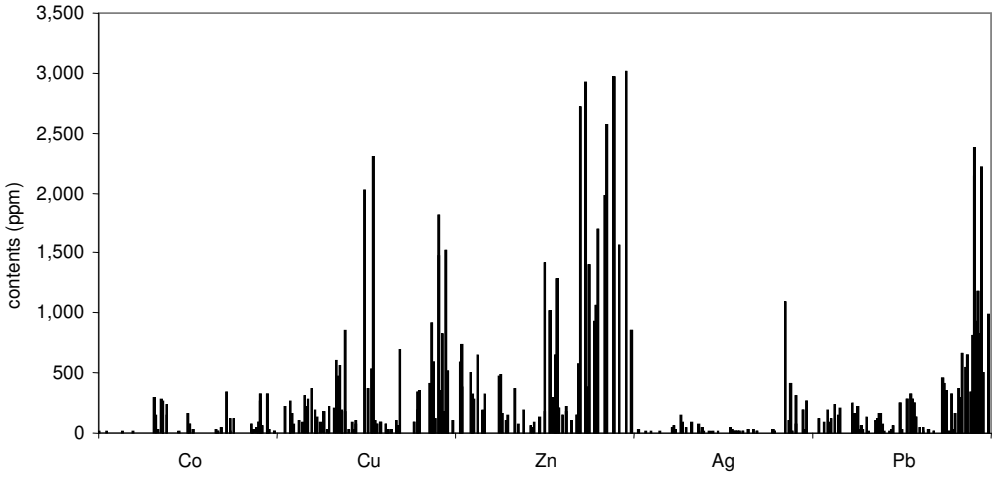

Figure 8.22. Base metal (and silver) contents of early orogenic fluids in the Copperbelt.

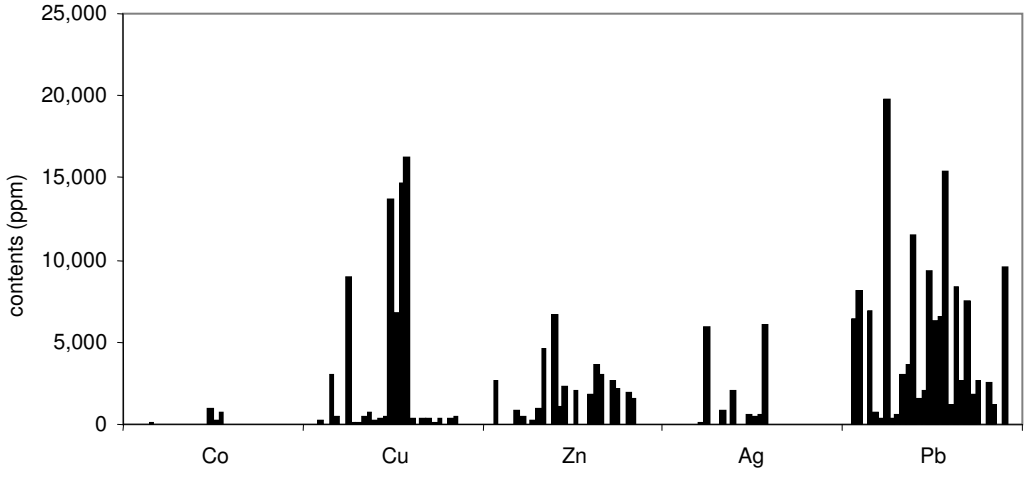

Figure 8.23. Base metal (and silver) contents of late orogenic fluids of the Copperbelt.

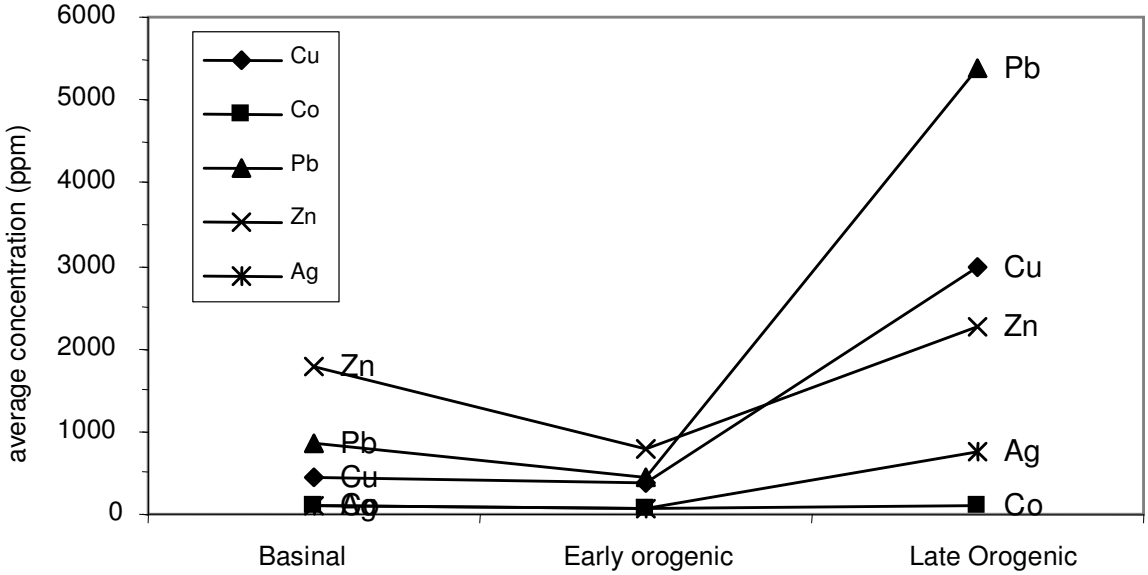

Figure 8.24. Average concentrations of Cu, Co, Pb, Zn and Pb of all fluid types of basinal, early orogenic and late orogenic timing.

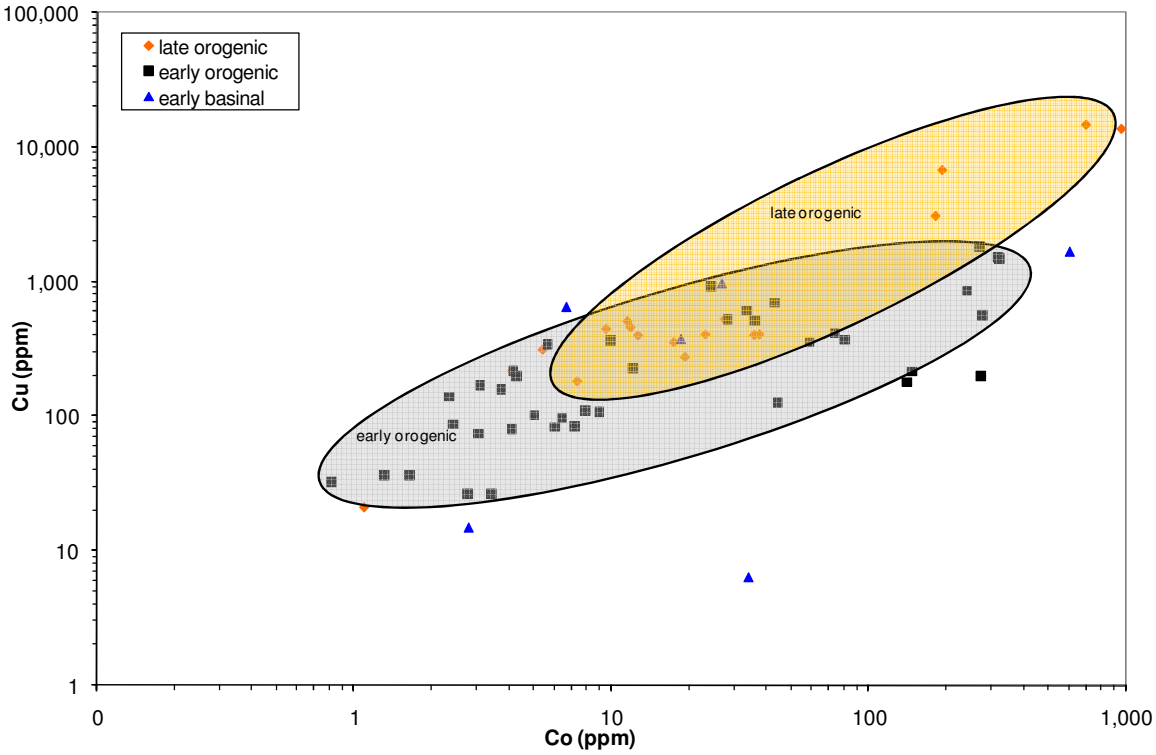

Figure 8.25. Comparative plot of copper and cobalt for all fluid types of the Zambian Copperbelt during early basinal, early orogenic, and late orogenic time periods.

The correlation between salinity and Cu (Figure 8.26), and salinity vs. Co (Figure 8.27) show a random pattern, where higher Cu and Co concentrations are found in the

moderate salinity fluids and not in the high-salinity late orogenic fluids of Mufulira. The highest Cu and Co concentrations are present in moderate-salinity fluids of late orogenic origin. Basinal and early orogenic fluids show a weak positive correlation between salinity and Pb concentration (Figure 8.28), whereas late orogenic fluids of moderate salinities contain slightly higher Pb values.

Zn concentrations are elevated in basinal fluids of moderate salinities, and early orogenic fluids are slightly depleted in Zn (Figure 8.29). High salinity late orogenic fluids are relatively enriched in Zn.

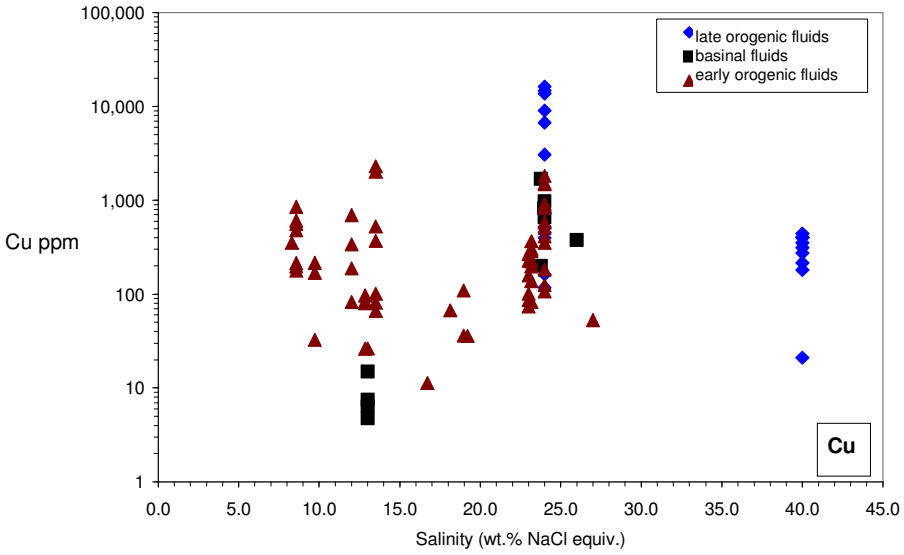

Figure 8.26. Salinity vs. Cu concentration (ppm) in basinal, early orogenic, and late orogenic fluids in the Zambian Copperbelt.

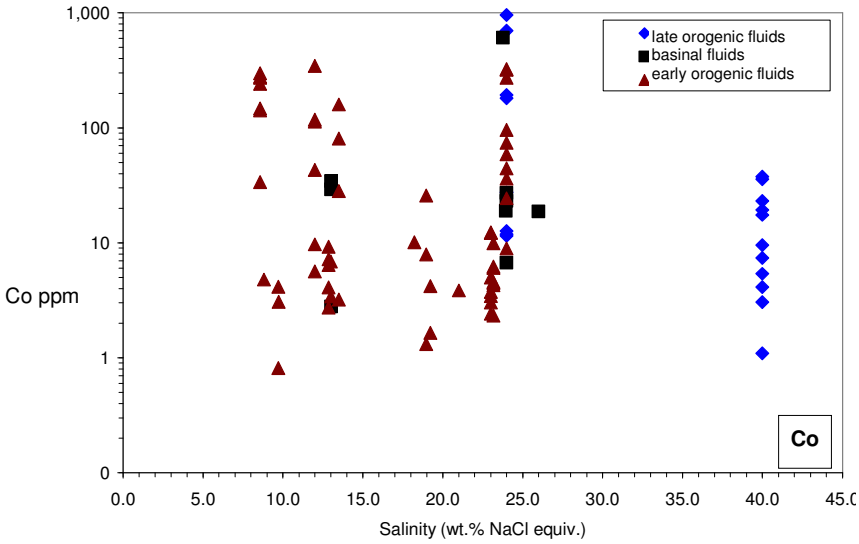

Figure 8.27. Salinity vs. Co concentration (ppm) in basinal, early orogenic, and late orogenic fluids in the Zambian Copperbelt.

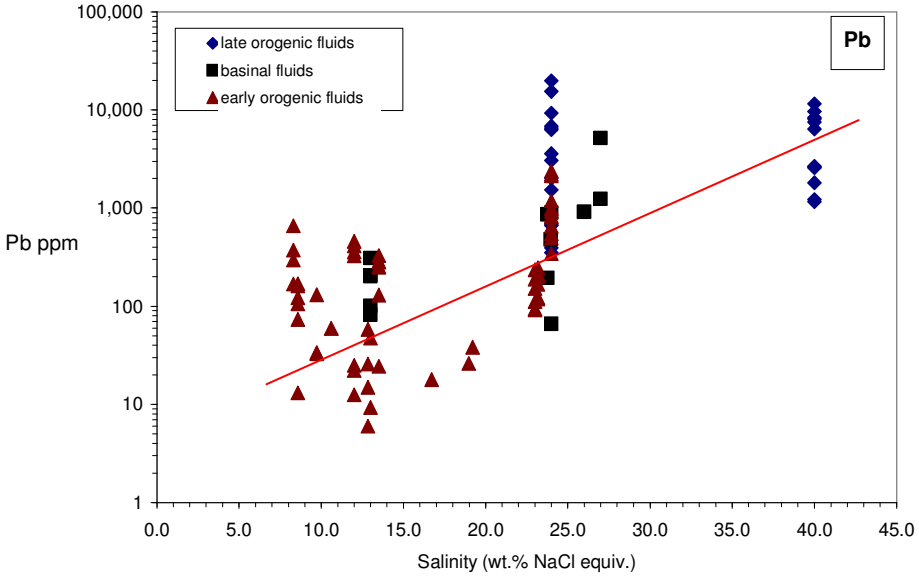

Figure 8.28. Salinity vs. Pb concentration (ppm) in basinal, early orogenic, and late orogenic fluids in the Zambian Copperbelt.

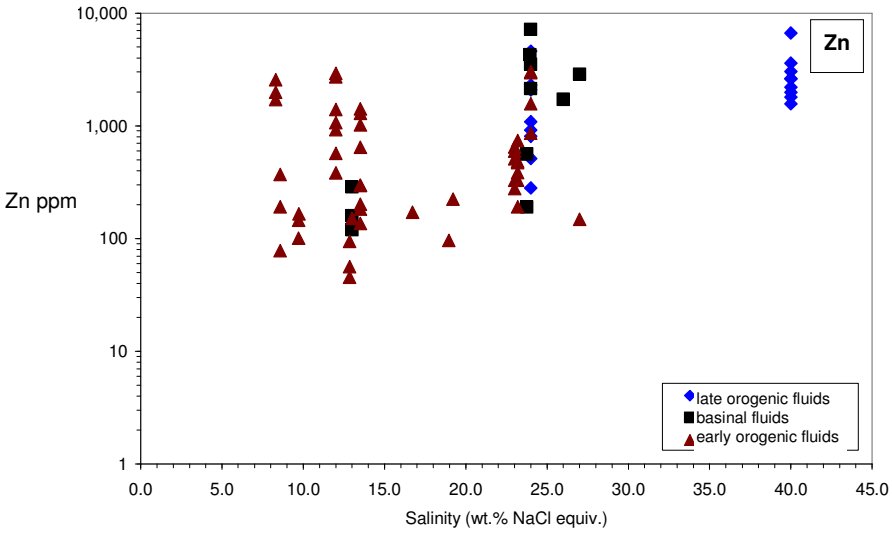

Figure 8.29. Salinity vs. Zn concentration (ppm) in basinal, early orogenic, and late orogenic fluids in the Zambian Copperbelt.

The abundance of Mn and Fe is largely unaffected by salinity while early orogenic fluids of moderate salinities (approaching NaCl-saturation) contain a range of Zn concentrations and a slight positive correlation may be inferred from high salinity, late orogenic fluids. Sr and K contents show a positive correlation with increasing salinities for basinal, early orogenic, and late orogenic fluids. Basinal fluids of moderately high salinities contain high Sr and K concentrations, and high salinity late orogenic fluids exhibit the highest Sr and K concentrations (see Appendix IV for plots).

From the data presented here, it becomes clear that mineralisation was long-lived and involves several events of remobilisation and concentration.

8.6.2 Major cations

In addition to base metal concentrations, late orogenic fluids also contain higher concentrations of Na, Ca, Mn, and Fe compared to basinal and orogenic fluids (Figure 8.30). Basinal and late orogenic fluids contain roughly the same ratios of Na, Ca, Mn and Fe with the absence of Ba. Notably, Fe concentrations are high in basinal fluids, even when compared to late orogenic fluids. Early orogenic fluid compositions are dominated by Na with lesser amounts of Ca and traces of Fe.

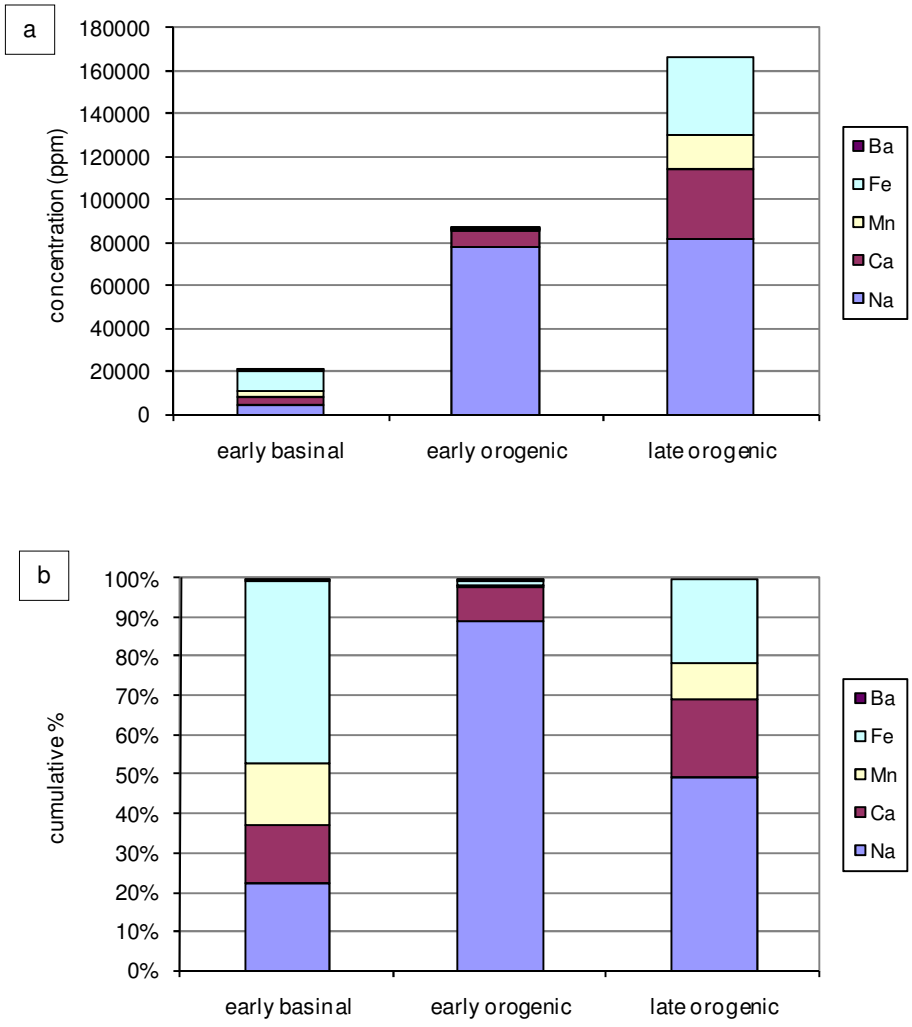

Figure 8.30. Average compositions of selected elements of aqueous inclusions trapped during basinal, early orogenic, and late orogenic environments. (a) Absolute average concentrations (ppm) of Na, Ca, Mn, Fe and Ba show an increase in concentrations from early to late fluids. (b) Relative cumulative percentages of early and later fluids are calculated from average concentrations.

8.7 Discussion and Conclusions

Fluids at the Nchanga deposit were enriched in Co and Cu during the early stages of basin evolution and, conversely, the basinal fluids of the Chambishi deposit were relatively depleted in Cu and Co compared to Nchanga. Early circulating brines were composed of Na, Mg and K, with minor Ca. With increasing salinities, Cu concentrations became elevated in basinal fluids, possibly due to the progressive dissolution of evaporites with increasing basin temperatures due to burial. The presence of evaporites have been well documented at Nchanga (Annels, 1989; McGowan *et al*., 2006 and references therein), and the increasing Sr concentration in early Nchanga basinal fluids with increasing salinity may also suggest that the increase in salinity is largely due to progressive evaporite dissolution (West, 1973). Sr contents increase with one order of magnitude between early basinal fluids and late orogenic fluids.

Cu contents in fluids increased from basinal fluids during the onset of deformation, in the presence of a dominating Na-brine, particular in the Chambishi basin. Interestingly, early fluids were originally moderately enriched in Pb and Zn, and the abundance of these metals decreased slightly during the onset of orogenesis, but levels increased to elevated concentrations again in late orogenic fluids. Basinal Na-Ca-K brines contained Mn, and were modified during the onset of orogenesis during which Fe and Mn are absent from inclusions and these fluids became enriched in Na and minor Ca. Late fluids see the return of Mn and Fe while Na and Ca concentrations are slightly negatively maintained.

Late orogenic fluids at Mufulira are distinctly different from early fluids in terms of temperature, salinity and composition, and contain the highest Cu and Co concentrations. High Cu and Co concentrations in late orogenic fluids are associated with moderately saline (approaching NaCl-saturation) fluids and not with NaCl-saturated high temperature fluids. High Cu and Co values in late fluids may be attributed to remobilisation of early stratiform Cu-Co mineralisation, but the relative depletion in Cu and Co concentration at NaCl saturation suggests that fluids were buffered at high salinities. High Pb and Zn contents of late orogenic fluids may be correlated to the later epigenetic Pb-Zn-Ge-Ga-Ag deposits which are present to the north and south of the Copperbelt.

8.7.1 Implications for ore genesis

Fluid inclusions give evidence of increasing copper and cobalt contents over time in the Copperbelt region. Stratiform Cu-Co mineralisation, which was deposited during late diagenesis, is remobilised and precipitated during the maturation of the basin, effectively

upgrading the metal concentration in the host sediments.

The fluid evolution of the Copperbelt is complex and the region hosts polymetallic deposits including stratiform Cu-Co deposits, epigenetic Pb-Zn-Ge-Ga-Ag deposits and Cu-Au-Ag-Fe-U deposits. This polymetallic nature on a regional scale is also represented in fluid inclusions from selected deposits in the Copperbelt, where late orogenic fluids contain not only high values of Cu and Co, but also the highest abundances of Pb, Zn, and Ag, which is probably a footprint of Pb-Zn-rich solutions that gave rise to epigenetic Pb-Zn-Ga-Ge-Ag deposits located off the Copperbelt.

Chapter 9

HYDROGEN AND OXYGEN ISOTOPIC CHARACTERISTICS OF FLUIDS OF THE COPPERBELT

9.1 Introduction

Oxygen and hydrogen are major components of the Earth's crust, and analysis of their isotopic signatures may be used to determine fluid origin, physicochemical nature of ore forming fluids, and temperatures of mineralisation (Hoefs, 1997). Ore forming fluids may be dereived from seawater, meteoric water, juvenile, or magmatic water (Hoefs, 1997), and the contribution of these fluids are important when considering ore forming processes such as mixing of two or more fluids, or redox state fluctuations. Oxygen and hydrogen isotopes of palaeo-fluids may be measured from hydroxyl-bearing minerals with subsequent fluid isotopic composition calculated from temperature-dependant mineral-water fractionation factors; or by extraction of palaeo-fluids preserved in inclusions in various host minerals (Hoefs, 1997). During this study, $\delta^{18}O$ of silicates and δD of fluids were analysed at the Department of Geology, University of Cape Town (see Chapter 2).

The three stable isotopes of oxygen are ^{16}O, ^{17}O, and ^{18}O, with abundances at 99.763%, 0.0375%, and 0.1995% respectively (Hoefs, 1997). The ratio determined during isotopic analysis is that of $^{18}O/^{16}O$, and is given relative to either the Cretaceous Pee Dee belemnite (PDB) or Standard Mean Ocean Water (SMOW) scales (Hoefs, 1997) and reported in δ-notation (refer to chapter 2 for the analytical methodology).

Fractionation of oxygen isotopes may occur between water in the liquid and vapour phases due to the presence of electrolytes and CO_2. Oxygen isotopes may also reveal the nature and extent of fluid-rock interactions due to isotopic exchange mechanisms such as (i) solution-precipitation, (ii) chemical reaction, (iii) diffusion (Hoefs, 1997).

Hydrogen consists of two stable isotopes (hydrogen, deuterium), and one radioactive isotope (tritium). Average abundances of the two stable isotopes are 99.9844% ^{1}H, and 0.0156% ^{2}D (Way *et al.*, 1950 in Hoefs, 1997). The measured D/H ratio is determined from H_2 gas and is referenced to the SMOW scale, in δ notation (see Chapter 2 for detailed methodology). Hydrogen isotopes are fractionated mainly during phase transitions by means of water evaporation-precipitation and boiling-condensation at shallow crustal levels, as well as during surficial and atmospheric processes (Hoefs, 1997). Notably, fractionation of hydrogen isotopes decreases with increasing temperatures. Hence, at ~220 °C, deuterium is the dominant isotope in water vapour relative to liquid water (Hoefs, 1997). At increasing temperatures thereafter, fractionation approaches zero again. Hydrogen isotope fractionation is also influenced by the presence of electrolytes such as $CaCl_2$, $MgCl_2$, $MgSO_4$, KCl, NaCl, $NaSO_4$ (Horita *et al.*, 1993). Another factor influencing hydrogen isotope fractionation may be that of clay membrane filtration (Coplan and Hanshaw, 1973).

Due to the proportional fractionation of the hydrogen and oxygen isotopes during water evaporation and condensation, Craig (1961) defined the relationship for meteoric waters as stated in Hoefs (1997) as:

$$\delta D = 8\delta^{18}O + 10$$

This relationship defines the present-day meteoric water line (MWL). The mutual consideration of the stable isotopes of oxygen and hydrogen may reveal the nature of the original fluid reservoir (Hoefs, 1997).

Oxygen isotopes were measured in silicates of sediments and veins of the Chambishi, Nchanga, Konkola, and Mufulira deposits. Hydrogen isotopes were measured from selected quartz veins and sediments in the Chambishi, Nchanga, Konkola, Mufulira, and Nkana deposits.

9.2 $\delta^{18}O$ isotope results

Oxygen was extracted and the isotopic ratios were measured from footwall arkosic horizons, Ore Shale siltstones and quartzites, as well as for quartz veins in which fluid inclusions were studied and described earlier. Table 9.1 lists the sample descriptions referenced. Also refer to previous chapters for local deposit-specific fluid characterisations.

9.2.1 Chambishi

Oxygen isotopic signatures were measured from (i) mineralised quartz veins within the Ore Shale, (ii) from barren quartz-calcite veins from the hangingwall to the Ore Shale, and (iii) the mineralised fine-grained, silty Ore Shale (Figure 9.1, Table 9.2). $\delta^{18}O$ signatures of the mineralised pre-tectonic quartz vein described in Chapter 6, range between 10.9 and 12.1 ‰ (samples CBSqz 3, CBSqz 6, CBSqz 10, CBSqz 11, CBSqz 12). The $\delta^{18}O$ signature of a quartz vein in the hangingwall to the Ore Shale was measured at 12.2 ‰ (sample CHM 7B). The mineralised Ore Shale yielded $\delta^{18}O$ signatures of 8.9 and 9.5 ‰ (samples CHM 3 and CBSos 3 respectively). The $\delta^{18}O$ signature of a mineralised bedding parallel quartz vein was measured at 11.3 ‰ (sample CHM 5).

9.2.2 Konkola

Oxygen isotopic signatures of the Footwall Sandstone from the Konkola deposit were obtained from quartz veins and the Footwall Quartzite horizon (Figure 9.1, Table 9.2). The $\delta^{18}O$ signature of a bedding-parallel quartz vein in the Footwall Quartzite horizon was 13.1 and 15.2 ‰ (samples KK 1A-h, KK 2). The $\delta^{18}O$ signature of a mineralised bedding-parallel quartz-feldspar vein in the Ore Shale horizon was 16.8 ‰ (sample KK 8A), and a crosscutting quartz vein in the Ore Shale was measured at 15.2 ‰ $\delta^{18}O$ (sample KK 16A). The Footwall Quartzite yielded $\delta^{18}O$ signatures of 10.1 and 11.2 ‰ (samples SS 12, SS 18).

Table 9.1. Description of samples analysed for $\delta^{18}O$ and δD signatures (see Appendix I for detailed description of all sample localities). Unless otherwise indicated, measurements were carried out on hand-samples from underground or open pit exposures.

Sample No.	Description	δ18O silicates	δD flincs
CBSqz 3	Quartz vein with disseminated sulphides (ccp, bn) in ore shale.	✓	✓
CBSqz 6	Quartz vein with disseminated sulphides (ccp, bn) in ore shale.	✓	✓
CBSqz 10	Quartz vein with disseminated sulphides (ccp, bn) in ore shale.	✓	✓
CBSqz 11	Quartz vein with disseminated sulphides (ccp, bn) in ore shale.	✓	✓
CBSqz 12	Quartz vein with disseminated sulphides (ccp, bn) in ore shale.	✓	
CBSos 3	Grey/green ore shale with disseminated sulphides (ccp, bn, py) along micro-scale layers.	✓	
CHM 3	Host around quartz vein immediately to right of vein. Strike of vein: 270° in open pit. Fold.	✓	
CHM 5	Ore shale with bedding parallel quartz, bornite, and malachite. Strike: 261°. Dip 21°. Dip direction:157°.	✓	✓
CHM 7B	Barren quartz-calcite vein bedding parallel in hangingwall metasediments.	✓	✓
CHM 7C	Barren quartz-calcite vein bedding parallel in hangingwall metasediments.		✓
KON 1	Mineralised quartz vein in quartzite. Reduction spots visible in qtzite.	✓	
KK 1A-h	1850ft level, 1750mW, bedding parallel quartz vein in Footwall sandstone. Strike: 350°. Dip: 25°. Dip direction: 30°.	✓	
KK 2	1850ft level, 1750mW, bedding parallel quartz vein in Footwall sandstone. Strike: 350°. Dip: 25°. Dip direction: 30°.	✓	
KK 4	Porous Conglomerate immediately above unconformity with granite. Strike: 340°. Dip: 10°. Dip direction: 270°.	✓	✓
KK 8A	In nose, Strike of samples: 30°. Direction: 300°. Ore shale with bedding parallel quartz-bn-ccp-chalcocite-feldspar vein.	✓	
KK 16A	Samples strike: 350°. Dip direction: 260°. Crosscutting qtz vein in Unit C of Ore Shale. Vein terminates in above and below beds to silty Ore Shale.	✓	✓
SS 12	Super Shaft, borehole sample, Footwall Quartzite.	✓	
SS 18	Super Shaft, borehole, Footwall Quartzite.	✓	
Muf 7H	1240mL, 56-57 Crosscut North. Crosscutting qtz-anhydrite veins in Lufubu Basement just below contact betw. basement and seds.	✓	✓
NS4-7	Drill-core. Ccp-qtz-carbonate vein crosscutting Ore Shale. Ccp is disseminated through qtz. 33.53-33.61m.		✓
NCGmq 2	Smokey-white quartz vein in micaceous shear zone in open pit.	✓	✓
NCGmq 5	Smokey-white quartz vein in micaceous shear zone in open pit.	✓	✓
NCGmq 9	Smokey-white quartz vein in micaceous shear zone in open pit.	✓	✓
NCGmq 11	Smokey-white quartz vein in micaceous shear zone in open pit. Euhedral qtz.	✓	✓
NCGTFQ 2	Quartzite containing disseminated sulphides (+ azurite, malachite) in upper ore bed.	✓	
NCGTFQ 3	Quartzite containing disseminated sulphides (+ azurite, malachite) in upper ore bed.	✓	
NCH 1	Quartz vein in Footwall Arkose. Underground C-Shaft.	✓	
NOP 8	Banded Sandstone Upper (BSSU). Cupriferous vermiculite. Syn-tectonic quartz vein in schist. Foliation deformed around qtz.	✓	
NOP 13	Matrix and pebbles above Nchanga Granite unconformity.	✓	
NOP 14	Quartz vein subvertical to Pink Quartzite. Terminated by overlaying BSSU and underlying SM.	✓	✓
NOP 15	Pink Quartzite, unmineralised (minor disseminated chalcocite).	✓	
NOP 16	Mineralised TFQ, disseminated carrollite, bn, ccp. Bedding planes visible.	✓	
NOP 20	Quartz vein in TFQ. Bn mineralisation in vein and TFQ.	✓	
NOP 21	Bn and carrollite disseminations in TFQ.	✓	
NOP 24	Course-grained bornite in quartz infilling in TFQ. Silica-rich fluid seemed to have percolated through	✓	✓
NOP 25	Disseminated accumulations of bornite in TFQ.	✓	
CNB 1	Footwall Arkose just below mineralised Arkose (Lower Orebody)	✓	
CNB 4	Lower Orebody, Chingola B orebody. Chalcocite & quartz, Panel 5.	✓	✓
CNB 12A	Quartz vein mostly parallel to bedding, also disseminated, sediments strike: 351°. Dip: 10°. Direction: 272°.	✓	✓

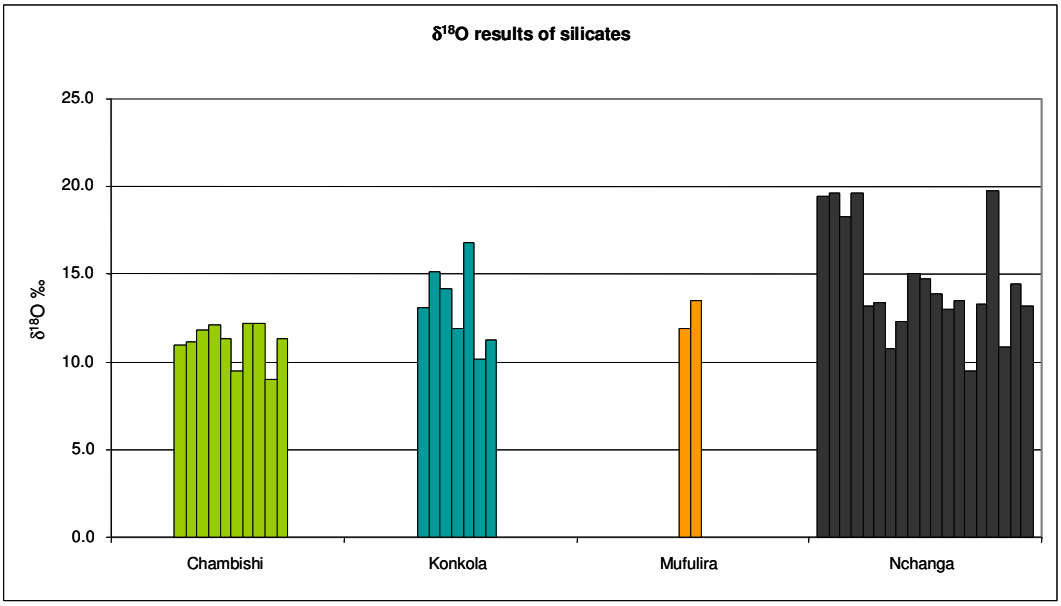

Figure 9.1. Comparative plot of $\delta^{18}O$ isotopic signatures of silicates for individual deposits (see Table 9.1 for raw data).

Table 9.2. Results of silicate $\delta^{18}O$ analysis.

	$\delta^{18}O$		$\delta^{18}O$		$\delta^{18}O$		$\delta^{18}O$
Chambishi		***Konkola***		***Mufulira***		***Nchanga***	
CBS qz 10	10.9	KK 1A-h	13.1	MUF 7 H h	12.0	NCG-MQ 11	19.5
CBS qz 11	11.2	KK16A	15.2	MUF 7 H v	13.4	NCG-MQ 9	19.6
CBS qz 12	11.8	KK2	14.2			NCG-MQ2	18.2
CBS qz 3	12.1	KK4	12.0			NCG-MQ5	19.6
CBS qz 6	11.4	KK8A	16.8			NCG-TFQ 3	13.1
CBS-OS 3	9.5	SS12	10.1			NCG-TFQ2	13.4
CHM 7B 1	12.2	SS18	11.2			NCH1	10.7
CHM 7B 2	12.2					NOP13	12.3
CHM3	8.9					NOP14	15.0
CHM5	11.3					NOP15	14.8
						NOP16	13.8
						NOP20	13.0
						NOP21	13.5
						NOP24	9.4
						NOP25	13.3
						NOP8	19.7
						CNB1	10.8
						CNB12A	14.5
						CNB4	13.1

9.2.3 Mufulira

Quartz-anhydrite veins were found to crosscut the basement, and in some instances, the basement-Katangan contact. Two samples from the same vein gave $\delta^{18}O$ isotopic signatures of 12.0 and 13.4 ‰ (see Figure 9.1 and Table 9.2).

9.2.4 Nchanga

Several $\delta^{18}O$ isotopic signatures were obtained from silicates of the Nchanga deposit (Figure 9.1, Table 9.2). The arkose immediately overlying the Nchanga Granite unconformity gave a $\delta^{18}O$ signature of 12.3 ‰ (sample NOP 13). The Lower Orebody (accessed from the Chingola B inclined shaft, sample CNB 1) yielded a $\delta^{18}O$ isotopic signature of 10.8 ‰. The $\delta^{18}O$ signatures of quartz veins in the footwall arkose were measured between 10.7 and 14.5 ‰ (samples NCH 1, CNB 4, CNB 12A).

Barren, crosscutting quartz veins in the Pink Quartzite of the Intermediate Orebody were measured at 15.0 ‰ $\delta^{18}O$ (sample NOP 14), and the Pink Quartzite was 14.8 ‰ $\delta^{18}O$ (sample NOP 15). Syn-tectonic quartz veins in the Intermediate Orebody and fluids are described in Chapter 7, and these veins yielded $\delta^{18}O$ signatures between 18.2 and 19.7 ‰ (samples NCGmq 2, NCGmq 5, NCGmq 9, NCGmq 11, NOP 8).

Quartzites of the Upper Orebody, the so-called Feldspathic Quartzite (TFQ), yielded $\delta^{18}O$ signatures ranging between 13.1 and 13.8 ‰ (samples NCGTFQ 2, NCGTFQ 3, NOP 16, NOP 21, NOP 25). This feldspathic quartzite is mineralised with disseminations of bornite, carrollite and minor chalcopyrite. Massive accumulations of crystalline quartz are also hosted by the quartzite. $\delta^{18}O$ signatures of quartz veins within the Feldspathic Quartzite were measured at 13.0 and 9.4 ‰ (samples NOP 20, NOP 24).

9.3 δD isotopic analysis of fluid inclusions

The δD ratio of fluids was measured directly by decrepitating fluid inclusions hosted in quartz veins and arenitic host rocks (see Chapter 2 for a detailed description of the methodology employed, and Table 9.1 for description of samples analysed for δD in fluid inclusions). The comparative results are depicted in Figure 9.2, with raw data in Table 9.3, and are discussed for the individual deposits below.

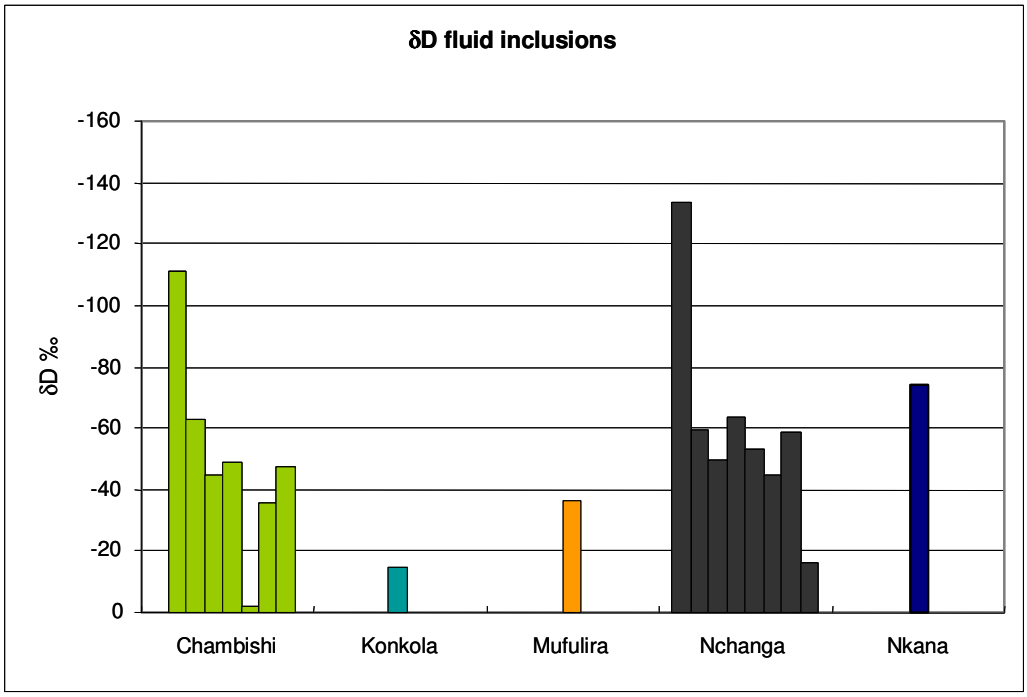

Figure 9.2. δD signatures of fluids in inclusions for individual deposits. Refer to Table 9.3 for raw data.

Table 9.3. Results of δD isotope analysis of fluid inclusions.

Samples	δ D	wt mg	P inlet	mg H_2O	wt% H_2O
Chambishi					
CBS qz 10	-111		11.6	0.41	
CBS qz 11 fi	-63	617.00	10.9	0.39	0.064
CBS QZ 6 fi	-45	2047.00	50	1.81	0.088
CBS-92 3	-49		115.8	4.06	
CHM 7B fi	-2	2128.00	50	1.81	0.085
CHM 7C	-36		23.5	0.82	
CHM5 fi	-48	2000.00	20	0.72	0.036
Konkola					
KK16A	-15		37.7	1.32	
KK4	120		20	0.70	
Mufulira					
MUF 7 HV	-37	2081.00	35.5	1.28	0.062
Nchanga					
NCB-MQ 11	-134		18.6	0.65	
NCQ MQ 2 fi	-60	1374.00	5	0.18	0.013
NCQ MQ 5 fi	-50	1939.00	12.3	0.44	0.023
NCQ MQ 9 fi	-64	2019.00	6	0.22	0.011
NOP14 fi	-53	2173.00	25.7	0.93	0.043
NOP24 B fi	-45	2108.00	45	1.63	0.077
CNB 12A fi	-59	2279.00	8.1	0.29	0.013
CNB4	-16		14.4	0.50	
Nkana					
NS4-7 fi	-74	2158.00	7.4	0.27	0.012

9.3.1 Chambishi

δD signatures of fluids hosted in a pre-tectonic mineralised quartz vein within the Ore Shale with developed axial planar cleavage (see Chapter 5) of the Chambishi deposit range between -111 and -45 ‰ (samples CBSqz 3, CBSqz 6, CBSqz 10, CBSqz 11). Two analyses were obtained from a barren quartz-calcite vein in the hangingwall to the Ore Shale. These two measurements plot at -2 and -36 ‰ δD (samples CHM 7B and CHM 7C). Fluids within the Ore Shale (sample CHM 5) were measured at -48‰ δD.

9.3.2 Konkola

δD measurements were obtained from two samples from the Konkola deposit. A crosscutting quartz vein in Unit C of the Ore Shale (sample KK 16A) yielded a δD signature of -15 ‰. Analysis of fluids within the Porous Conglomerate horizon of the Footwall Aquifer below the Ore Shale horizon did not yield a reliable measurement at 120‰ δD, and was disregarded.

9.3.3 Mufulira

Crosscutting quartz-anhydrite veins in the Lufubu basement below the basement-Katangan contact yielded a δD signature of -37‰. Some of these veins also crosscut into the Katangan sediments.

9.3.4 Nchanga

Bedding parallel quartz veins in the Lower Orebody, exposed at the Chingola B inclined shaft were -59 ‰ δD (sample CNB 12A). Fluids hosted in the Lower Orebody at the Chingola B inclined shaft area were measured at -16 ‰ δD (sample CNB 4). Fluids in crosscutting quartz veins hosted in the Pink Quartzite below the Intermediate Orebody were measured at -53 ‰ δD (sample NOP14). Syntectonic quartz veins identified along the décollement plane in the Intermediate Orebody of the Nchanga deposit yielded δD signatures between -50 and -134 ‰ (samples NCGmq 2, NCGmq 5, NCGmq 9, NCGmq 11). Fluids hosted within The Feldspathic Quartzite (TFQ) of the Upper Orebody were measured at -45 ‰ δD.

9.3.5 Nkana

A quartz-carbonate-chalcopyrite vein crosscutting the Ore Shale was sampled from drill core at the Nkana deposit. After isolation of quartz, this vein yielded a δD signature of -74 ‰ (sample NS4-7).

9.4 Interpretation and discussion of δD and $\delta^{18}O$ ratios

$\delta^{18}O$ signatures of quartz veins from the Chambishi deposit coincide with values obtained from sedimentary-, and metamorphic rocks (Figure 9.3). The samples analysed from the Chambishi Ore Shale have similar $\delta^{18}O$ signatures to that of sedimentary and metamorphic rocks (Figure 9.3).

The Konkola Footwall Sandstone is enriched in the lighter oxygen isotope compared to quartz veins that are found within the sandstone and within the Ore Shale (Figure 9.3), while $\delta^{18}O$ signatures of quartz-anhydrite veins present in the Lufubu meta-volcanic basement at the Mufulira deposit coincide with sedimentary-, and metamorphic rock signatures. Quartz veins present below the Nchanga Lower Orebody (in the footwall arkose), and within the Intermediate Orebody are progressively depleted in ^{16}O with increasing stratigraphic distance from the footwall arkose (Figure 9.3). The $\delta^{18}O$ signatures of The Feldspathic Quartzite of the Nchanga Upper Orebody plot within the range of sedimentary and metamorphic rock isotopic compositions. One sample of a quartz vein in the feldspathic quartzite is enriched in ^{16}O relative to the quartzite and corresponds with sedimentary rock isotopic signatures.

δD values of samples analysed from selected deposits are displayed in Figure 9.4 relative to known geological reservoirs. Pre-tectonic quartz veins of the Chambishi deposit described in chapter 6 correspond to the δD isotopic signatures of meteoric waters, sedimentary and metamorphic rocks (Figure 9.4). A quartz vein in the hangingwall to the ore horizon of the Chambishi deposit is depleted in hydrogen relative to the pre-tectonic veins. The Chambishi Ore Shale δD isotopic signature corresponds to that of meteoric water and sedimentary rocks. Preferential movement of hydrogen relative to deuterium (Mavrogenes and Bodnar, 1994) may be recorded in the δD isotopic signatures of fluid inclusions during annealing. This could explain relatively low δD values (Simon, 2001). The δD signature of a single quartz vein in the Ore Shale of the Konkola deposit approaches SMOW values (Figure 9.4).

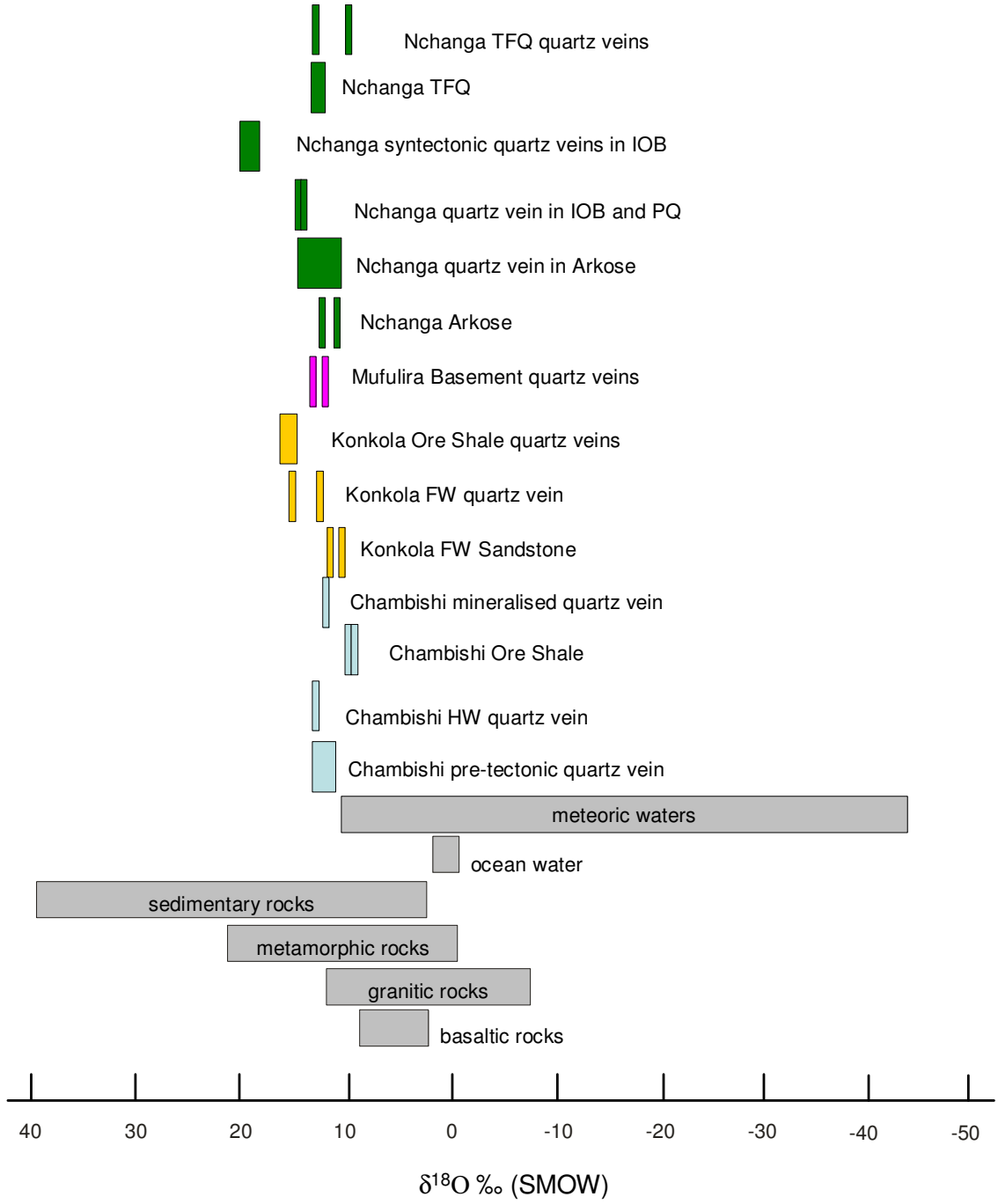

Figure 9.3. $\delta^{18}O$ (in ‰) of silicates analysed of areas within the Chambishi, Konkola, Mufulira, and Nchanga deposits. The known $\delta^{18}O$ signatures of meteoric, and ocean water, sedimentary, metamorphic, granitic, and basaltic rocks are indicated according to Hoefs, 1997.

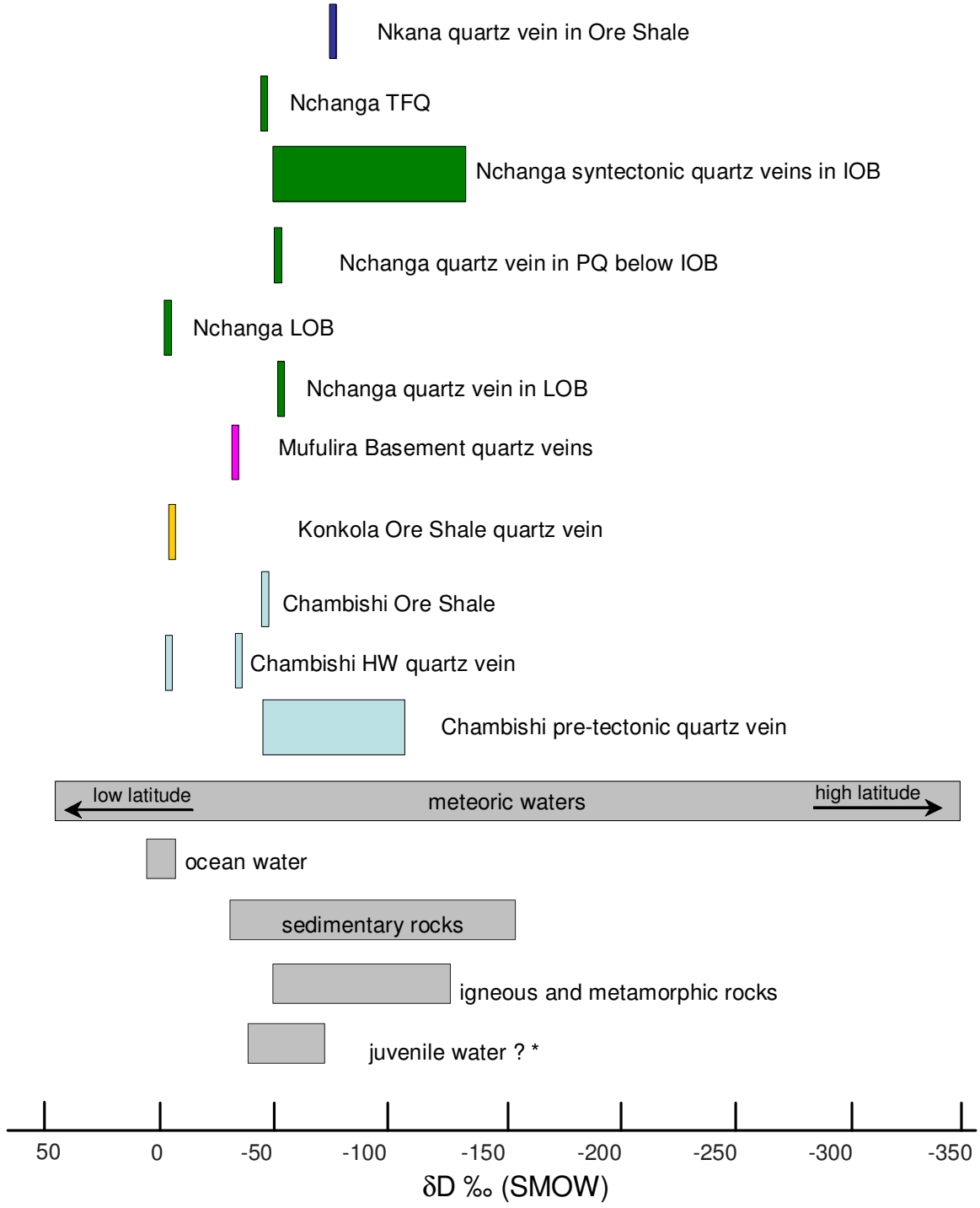

Figure 9.4. δD (in ‰) of fluids hosted within veins and meta-sediments of the Chambishi, Konkola, Mufulira, Nchanga, and Nkana deposits. Known δD signatures are indicated for meteoric, ocean, and juvenile water, sedimentary, igneous and metamorphic rocks (Hoefs, 1997).

* Juvenile water is considered to have formed due to degassing of the mantle, and remnants may be present as hydroxyl-bearing minerals derived from the mantle. This type of water has not interacted with surficial or atmospheric processes (Hoefs, 1997).

Quartz veins present within the meta-volcanic basement to the Katangan at the Mufulira deposit exhibit the same δD signature as that of meteoric water and sedimentary rocks (Figure 9.4). A quartz vein hosted in the Lower Orebody of the Nchanga deposit is depleted in deuterium compared to the host ore horizon (Figure 9.4). δD signatures of syntectonic quartz veins present in the Nchanga Intermediate Orebody correspond to meteoric water, sedimentary, igneous, and metamorphic rocks.

The δD signature of the feldspathic quartzite of the Nchanga Upper Orebody is similar to that of known sedimentary rocks. The δD signature of a mineralised quartz vein present in the Nkana Ore Shale is in accordance with the signature for meteoric waters, sedimentary, igneous and metamorphic rocks (Figure 9.4).

The $\delta^{18}O$ of inclusion water may be plotted together with δD of inclusion water to compare the signatures with known (e.g., meteoric, metamorphic) reservoirs. Rye and O'Neil (1968) showed the necessity of a fractionation conversion factor when converting the d18O of the host mineral to $\delta^{18}O$ of the fluid (Ohba *et al.*, 1995, Matsuhisa *et al.*, (1979). Conversely, Vityk *et al.*, (1993) showed the preservation of $\delta^{18}O$ in water from an epithermal environment.

It is further showed by Ohba *et al.*, (1995) that with a rapid cooling rate, and sufficiently large inclusions, the diffusional $\delta^{18}O$ loss from inclusion water may be minimized. Moreover, the exchange rate between oxygen-bearing phases is affected by fluid salinity, temperature, and the difference in oxygen isotopic composition between initial reagents (Ligang *et al.*, 1989). Since inclusions in this study were generally small and constraints on cooling rates are not implicated, a fraction factor is used according to Ligang *et al.*, (1989) of $1000\ln_{\alpha Q\text{-}H2O} = 3.306 \times 10^6 \times T^{-2} - 2.71$.

A temperature of 260 °C is assigned to the samples which correspond to the upper trapping temperatures obtained from microthermometry during early orogenic times (Table 9.4, Figure 9.5). A limitation to this method is due to multi-generation fluid inclusions hosted in the same sample. The fractionation factor decreases with increasing temperature.

Table 9.4. Fractionation factors and $\delta^{18}O_{fluid}$ derived from the conversion of $\delta^{18}O_{silicate}$.

Samples	$\delta^{18}O$ silicates	δ D fluid	T (°C)	T (K)	fractionation factor	$\delta^{18}O$ fluid
Chambishi						
CBS qz 10	10.9	-111	260	533	8.9	2.0
CBS qz 11 fi	11.2	-63	260	533	8.9	2.3
CBS QZ 6 fi	11.4	-45	260	533	8.9	2.5
CBS-92 3	12.1	-49	260	533	8.9	3.2
CHM 7B fi	12.2	-2	260	533	8.9	3.3
CHM 7C	12.2	-36	260	533	8.9	3.3
CHM5 fi	11.3	-48	260	533	8.9	2.4
Konkola						
KK16A	15.2	-15	260	533	8.9	6.3
KK4	12.0	120	260	533	8.9	3.1
Mufulira						
MUF 7 HV	13.4	-37	260	533	8.9	4.5
Nchanga						
NCB-MQ 11		-134	260	533	8.9	-8.9
NCQ MQ 2 fi	18.2	-60	260	533	8.9	9.3
NCQ MQ 5 fi	19.6	-50	260	533	8.9	10.7
NCQ MQ 9 fi	19.6	-64	260	533	8.9	10.7
NOP14 fi	15.0	-53	260	533	8.9	6.1
NOP24 B fi	9.4	-45	260	533	8.9	0.5
CNB 12A fi	14.5	-59	260	533	8.9	5.6
CNB4	13.1	-16	260	533	8.9	4.2
Nkana						
NS4-7 fi	-	-74	260	533	8.9	-8.9

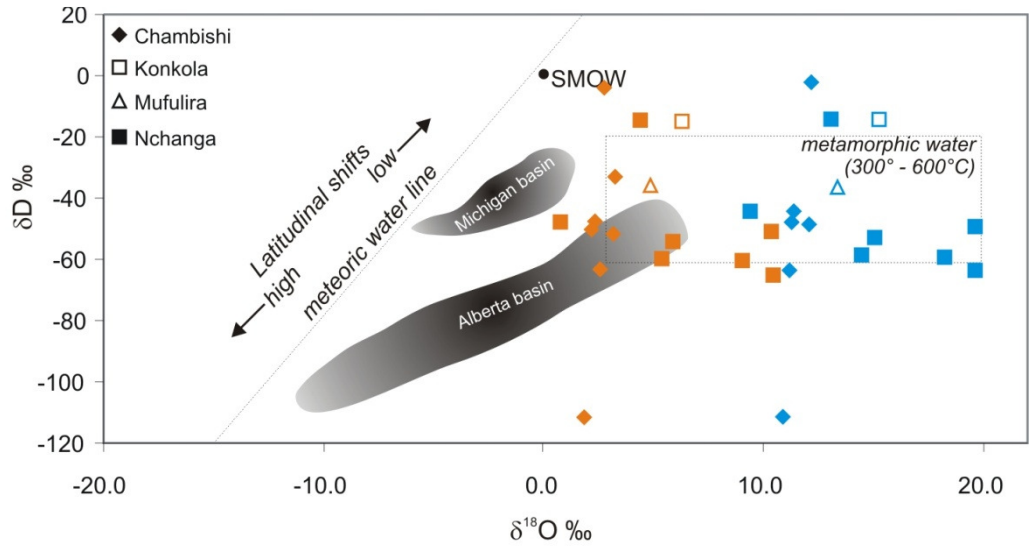

Figure 9.5. δD vs $\delta^{18}O$ comparative plot for fluids of selected samples with known reservoirs of metamorphic water and sedimentary basins plotted together with SMOW and the meteoric water line. Orange symbols show fluid δD-$\delta^{18}O$ with corrected $\delta^{18}O$ for the fluid using the fractionation factor mentioned in the text. Light blue symbols show $\delta^{18}O$ measured from the silicate without application of the fractionation factor. Data is plotted as permil and shows known reservoirs after Taylor, (1997).

According to Hoefs (1997), the factors controlling the isotopic composition of metamorphic rocks are: (i) the pre-metamorphic protolith composition, (ii) volatilization effects associated with increasing temperatures and (iii) exchange occurring with infiltrating fluids or melts. In addition to these factors, the temperature of exchange determines the metamorphic rock isotopic signature.

Lower $\delta^{18}O$ values for metasediments compared to quartz veins (Chambishi, Konkola, Nchanga) may result from devolatilization reactions during metamorphism which reduce the $\delta^{18}O$ values of a rock because of CO_2 (and H_2O) loss, which are the constituents enriched in $\delta^{18}O$ (Hoefs, 1997). Stable δO^{18} signatures of silicates correspond largely to signatures of fluids trapped during metamorphic processes (8.9 - 19.7 ‰ $\delta^{18}O$), and δD signatures of fluid inclusions also indicate a substantial metamorphic component (Figure 9.5). Connate waters' δD signatures decrease with increasing distance from the equator, and higher $\delta^{18}O$ signatures are according to Taylor (1997) associated with higher temperatures and salinities. This may hold true when comparing Nchanga fluids to Chambishi (Figure 9.5), but one would expect higher $\delta^{18}O$ values from samples at Mufulira, although only one sample was successfully analysed. Chambishi samples show

a spread in δD values which may be attributed to varying salinities, where a general increase in δD is contributed to increasing salinity and $\delta^{18}O$ content (Taylor, 1997).

By bulk-crushing the inclusions and analysing the decrepitated matter for their O and H isotopic ratios, it is clear that orogenic fluids trapped as inclusions have overprinted any significant earlier (basinal) fluid signature. This may be due to the abundance of orogenic fluid inclusions in comparison to earlier basinal inclusions.

Chapter 10

DISCUSSION AND CONCLUSIONS

10.1 Introduction

The status of the Central African Copperbelt as one of the world's largest ore deposit districts is undisputed. On a regional scale, mineralisation is viewed as a long-lived process characterized by a suite of polymetallic ores comprising early stratiform Cu-Co mineralisation and later epigenetic Pb-Zn-Ge-Ga and Fe-Cu-Au-U mineralisation. Several episodes of fluid flow have left their imprint on the metallogenic history of the basin, as evident in fluid inclusions of various generations. This study documents the nature of fluids present from relatively early in basin evolution up until peak metamorphism, and is the first study to document fluid characteristics on a regional scale encompassing the Chambishi, Nkana, Nchanga, Mufulira and Konkola deposits. Regional fluids are classified and described in three relative time intervals, namely basinal, early orogenic, and late orogenic. The use of microthermometry and Raman microspectrometry is combined with stable isotope geochemistry and laser ablation inductively coupled plasma mass spectrometry (LA-ICP-MS) to obtain the compositional and P-T-υ nature of fluids circulating after stratiform copper deposition, during the onset of metamorphism, and during peak metamorphic conditions.

This chapter summarizes the findings of the study by discussing the nature of basinal, early orogenic and orogenic fluids and conclusions are made as to the origin of these fluids. The documented changes in fluid composition, pressure and temperature from early to late builds a picture of the fluid history in the basin - this chapter summarizes the secular evolution from early basinal brines to later metamorphic fluids.

10.2 Basinal fluids

The earliest fluids documented in this study were found at the Chambishi, Nchanga and Konkola deposits. Inclusions preserving these fluids are generally small and scarce and have trapped fluids that circulated through the basin immediately after the formation of late diagenetic stratiform copper mineralisation. These fluids are hosted in the arkosic sediments of the Nchanga deposit which comprise the footwall beds underlying the basal orebody. The footwall conglomeratic beds are also the hosts to basinal fluid inclusions at the Konkola deposit. At the Chambishi deposit, early fluids were hosted in a quartz vein which was introduced into the sediments immediately after stratiform copper mineralisation, thereby trapping early basinal fluids in addition to later circulating fluids.

Basinal brines are characterised by three compositionally different fluids. These fluids are aqueous solutions dominated by the combinations of several cations including Na,

Ca, Mg, and K as chloride complexes. The gaseous phases are composed of CO_2 -CH_4 - N_2.

10.2.1 Na - Ca - Mg brines

This fluid type is found at the Chambishi and Nchanga deposits, and records fluid compositions in the basin immediately after stratiform copper mineralisation but prior to the onset of regional deformation. These moderately saline fluids (11.9 - 23.1 wt.% $NaCl_{equiv}$) were trapped at (minimum) temperatures of between 86 and 129 ° C, and contain chloride ligands as their main anionic species. In addition to Na-Ca-Mg brines, a few NaCl saturated inclusions were also found at the Nchanga deposits and it is suggested that these high salinity fluids may have been implicated in the original metal transportation and precipitation of stratiform copper and cobalt.

10.2.2 Mg - K brine

A low salinity basinal Mg-K rich fluid, with minor NaCl, is found at the Konkola deposit. Minimum trapping temperature for this fluid was between 132 and 160 °C. As suggested by the temperature, this fluid is believed to have been derived from meteoric waters circulating through the basin during the onset of late diagenesis.

10.2.3 Mg - K brine with CO_2 -CH_4 - N_2

A third type of basinal fluids at Chambishi and Nchanga is composed of H_2O - $MgCl_2$ - ± KCl - CO_2 - CH_4-N_2 with up to 600 ppm Co and 1680 ppm Cu. This fluid is believed to have formed as a result of mixing between the end member Mg-K-rich fluid seen at Konkola with volatiles such as CO_2 and CH_4 that were probably derived from the decomposition of hydrocarbons in the host sediments. Early fluids may have captured biogenic methane generated during methanogenesis, at temperatures lower than 50°C (Ohmoto and Goldhaber, 1997, Figure 10.1). The presence of methane in later inclusions is best explained by the higher temperature fragmentation of kerogen at temperatures between ~100 and 230°C (Ohmoto and Goldhaber, 1997). The CO_2 present in these fluid inclusions may have been generated early during the basin maturation at temperatures between 50 and 150°C (catagenesis), depending on the organic compound source (Figure 10.1). Distinction is made between sapropelic (Kerogen Type I/II) and humic (Kerogen Type III) sources. At temperatures higher than 100 °C, CH_4 is increasingly produced during metagenesis, rather than CO_2, from the breakdown of organic compounds. Abundant CO_2 and solid carbon at Nchanga may be attributed to slightly elevated temperatures at Nchanga, compared to those at Chambishi and Konkola during

the early stages of basin evolution.

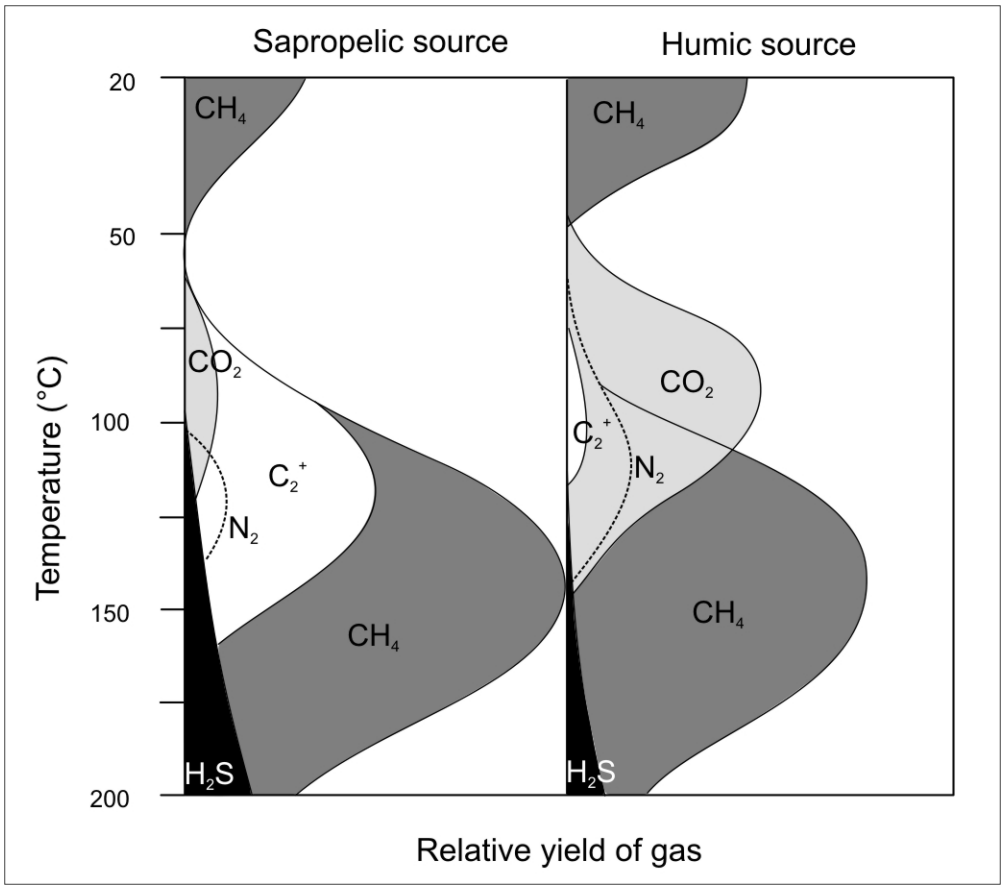

Figure 10.1. The stability fields of various organic compounds at varying temperatures. Gas is produced from organic maturation at temperatures up to 230 °C. Note the two periods of methane production, one at lower temperatures (methanogenesis) and the other above 100 °C. Modified after Ohmoto and Goldhaber (1997).

10.2.4 Basinal fluid summary and trapping conditions

Basinal fluids of the Chambishi deposit comprised NaCl-$MgCl_2$ ± $CaCl_2$ solutions, while at the Nchanga deposit they are represented by NaCl-saturated - $CaCl_2$ - H_2O and $MgCl_2$ - KCl - NaCl - H_2O systems. Inclusions measured at the Konkola deposit are composed of $MgCl_2$ - KCl-H_2O ± NaCl. Gas phases in fluids are dominated by CO_2, with subordinate amounts of CH_4 and N_2 evident in the Chambishi and Nchanga areas.

Fluid inclusions are considered to have evolved along isochoric (constant volume) and isoplethic (constant composition) paths after trapping (Diamond, 1996). Isochores (lines

of constant density) were constructed for aqueous and aqueo-carbonic inclusions for early fluids for the Chambishi deposit and of aqueous fluids of the Konkola deposit (Figure 10.2) using the bulk fluid properties (density and composition), with due consideration given to the compressibility and expansion of the fluid inclusion host mineral (Bakker, 2003).

Evidence of post-trapping modifications are observed in inclusions from the Nchanga and Konkola deposits and indicate a variation in the confining pressures of the fluid inclusion hosts after fluid trapping (Roedder, 1984). The effect of post-trapping modifications of inclusions was considered during pressure and temperature estimates. The observation that fluid inclusions were subjected to post-trapping pressures, illustrates that the host mineral must have been subjected to varying pressures after fluid trapping. Depending on whether inclusions imploded or exploded, a relative increase or decrease in pressure may be evident. It is assumed that surrounding pressures must have increased after basinal fluid trapping; however the fluid inclusion shapes do not yield absolute measurements. Isochores were not calculated for inclusions which are thought to have been modified after trapping.

Even though the local pressure present in a particular fluid inclusion is naturally hydrostatic (Roedder and Bodnar, 1980), the effect of the overburden during the time of trapping has to be considered as well. Lithostatic conditions would increasingly prevail as pore spaces are decreased and trapping continued after diagenesis, sediment burial, compaction and during metamorphism (see later fluid descriptions). Gradually, lithostatic conditions are reached, and lithostatic conditions prevail during fluid inclusion trapping. There are several ways in which to obtain an estimate of fluid trapping pressures using microthermometric data (Roedder and Bodnar, 1980; Shepherd *et al*., 1985). Evidence for fluid immiscibility during the early stages of basin evolution which may in some cases enable the inclusionist to ascertain the maximum pressure and temperature conditions along an isochoric path was not obtained. A geothermal gradient may aid in the determination of temperatures of entrapment and may be used to determine the range of pressures of entrapment (Touret, 1994).

A present day lithostatic gradient of 28°C / 226 bar and a hydrostatic gradient of 28°C / 100 bar (as used in Goldstein, 2001) is plotted in Figure 10.2 to indicate a possible range in trapping temperatures and pressures for aqueous inclusions. Intersection of a *hydrostatic gradient* of 28°C/100 bar and basinal isochores produces fluid trapping pressures between 350 and 600 bar at temperatures between 120 and 190°C. Pure *lithostatic conditions* using a present-day lithostatic gradient of 28°/226 bar yield a range of 950 - 1900 bar at temperatures between 145 and 260 °C. Even though the measured

pressure is actually hydrostatic because fluid pressure is measured, the source of the pressure is implied by either hydrostatic or lithostatic, which indicates a closed/partially open rock column above the fluid trapping (Roedder and Bodnar, 1980).

Fluid pressures were likely closer to hydrostatic pressure conditions than lithostatic during the trapping of basinal fluids in the late diagenetic realm. These fluids were probably expelled during the final stages of diagenesis prior to the onset of metamorphism. Basinal fluid trapping is considered to have taken place between hydrostatic and lithostatic conditions. This equates to temperatures between 120 and 190 ℃, and trapping pressures between 350 and 600 bar (Figure 10.2). These temperature and pressure values serve as minimum estimations of trapping conditions.

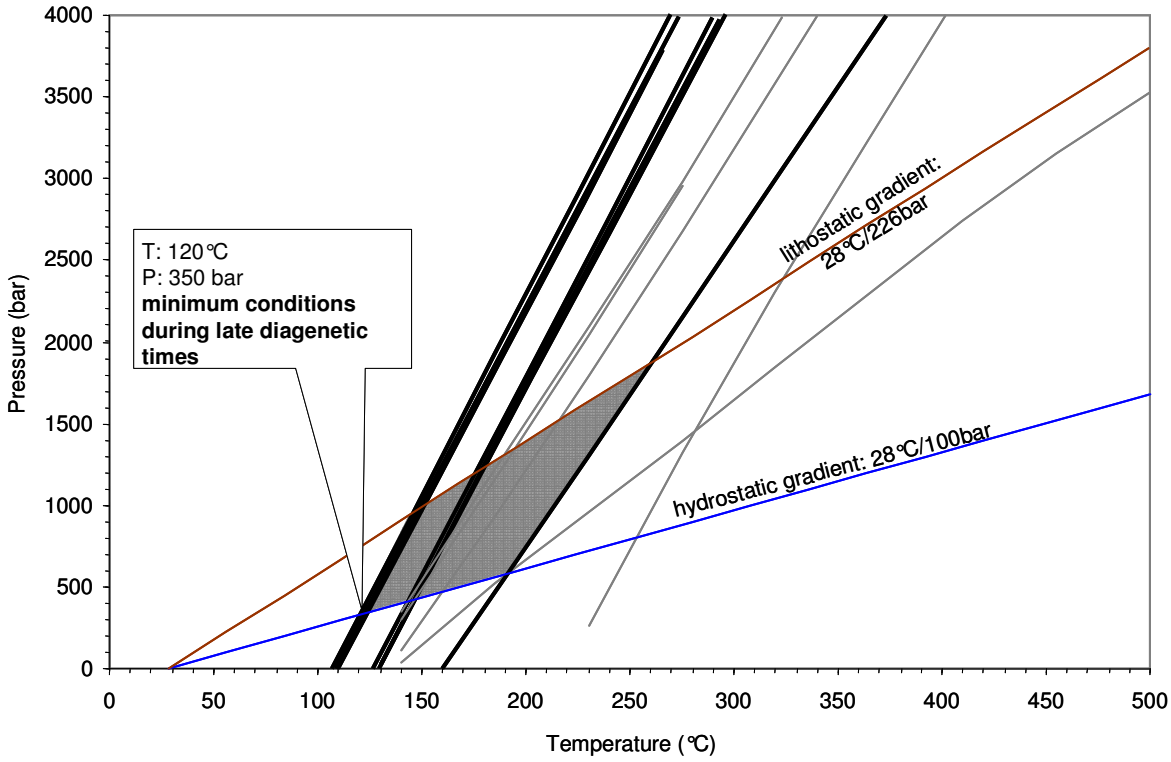

Figure 10.2. Isochors showing a range of possible trapping conditions for basinal fluids at Chambishi and Konkola. Isochors of basinal aqueous inclusions are indicated in solid black lines, with basinal aqueo-carbonic inclusions indicated in solid grey lines. See text for details.

The source of basinal fluids may be considered as fluids similar in composition and salinity to oceanic water becoming increasingly modified during basin maturation and ongoing dissolution of salts (e.g., in the presence of evaporites). During this time, basinal

fluids were relatively enriched in copper, cobalt and CO_2 contents in the Nchanga area compared to the Chambishi region, with Na, Mg, K, and Ca additionally present in the fluids. Fluids also contained dissolved CO_2 and CH_4, which was conceivably derived from host sediments. The absolute value of the redox state of this early fluid is unknown, but this fluid is considered to be more reduced relative to later orogenic fluids.

10.3 Early orogenic fluids

The early orogenic fluids in the Katangan basin are considered to be modified basinal fluids that circulated some time after stratiform copper-cobalt mineralisation had formed. Metamorphism during at least one compressional deformation phase of the Katanga Supergroup resulted in a greenschist to lower amphibolite facies overprint. Fluids trapped during the early orogenic environment were detected in the Chambishi, Nchanga, and Nkana deposits and are the most numerous inclusion type found during the course of this investigation. These fluid inclusions are hosted in veins which crosscut and occur along bedding planes, and inclusions are typically located along secondary fracture planes that formed during the onset of metamorphism. In addition to these secondary planes, primary inclusions in bedding parallel quartz veins from the Chambishi deposit are also early orogenic in nature. Early orogenic fluids consist of a variety of fluid compositions, with abundant electrolytes in the aqueous phase and a compositionally variable gaseous component. Stable δD and $\delta^{18}O$ isotope signatures of early orogenic fluids show an overlap with metamorphic and sedimentary rock signatures. Four fluid types are characteristic of early orogenic fluids:-

10.3.1 Na - Ca - Mg - K brine

This fluid group is present at the Chambishi deposit and is characterised by two distinct salinity populations, namely a low-salinity (~6 wt.% $NaCl_{equiv}$) higher temperature (~140-210 °C) group, and a moderate-salinity (~18-23 wt.% $NaCl_{equiv}$) lower temperature (~130-160°C) group (Figure 10.3). The moderate-salinity group is considered to have formed from circulating basinal fluids that became increasingly saline and warmer with progressive burial and dissolution of evaporites. The presence of the hotter, low-salinity fluid is considered to be the result of fluid production during devolatilization reactions linked to the onset of Lufilian regional metamorphism.

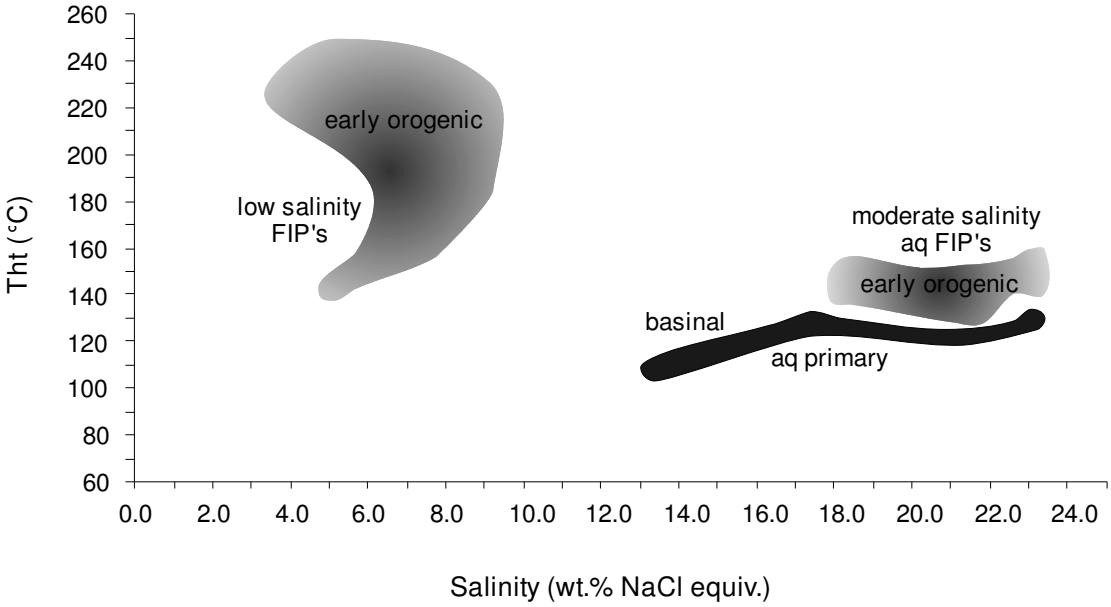

Figure 10.3. Salinities of secondary inclusions of early orogenic derivation from the Chambishi deposit, showing the grouping into low- and moderate salinity populations.

10.3.2 Ca - K brine

Aqueous - $CaCl_2$ - KCl fluids are identified in inclusions of early orogenic origin at the Nkana and Nchanga deposits. In addition, at Nkana, this brine contains methane, and a methane hydrate ($CH_4 \bullet 5.75\ H_2O$) in the presence of solid graphite. At Nchanga, $CaCl_2$ is dominant over minor KCl in the aqueous phase, and fluids contain low salinities of between 5.1 and 9.2 wt.% $NaCl_{equiv}$, and minimum trapping temperatures of around 130 °C.

10.3.3 Na- brine with CO_2, CH_4, N_2

A mixed aqueo-carbonic fluid of early orogenic derivation was identified at the Chambishi deposit. Salinities of the aqueous phase range between 3.4 and 15.8 wt.% $NaCl_{equiv}$, with minimum trapping temperatures between 116 and 245 °C. At Nchanga, the aqueous phase in mixed H_2O-CO_2 fluid inclusions are saline and the non-aqueous phase consists of CO_2 - rich fluids. In isolated occurrences, halite saturation was achieved and a small group of Nchanga inclusions contain NaCl daughter crystals. This is in good agreement with the chlorinity determination of the aqueous film in gaseous CO_2-inclusions where salinities were calculated at 19.7 -24.3 wt.% $NaCl_{equiv}$.

10.3.4 Carbonic fluids

A pure CO_2 fluid containing minor N_2 is present at the Nchanga deposit. In addition to pure CO_2 inclusions, several aqueo-carbonic inclusions also contain high CO_2 contents. Methane is abundant at Nchanga and was trapped as relatively pure monophase CH_4 inclusions. At Chambishi, methane-rich inclusions contain N_2 and C_2H_6. With increasing grade of metamorphism, the average hydrocarbon molecular weight decreases to that of methane (Roedder, 1984), and may explain the presence of methane, commonly present in secondary aqueo-carbonic inclusions, as well as in methane-dominated fluid inclusion planes where the gas is considered to have been derived from the decomposition of hydrocarbon organic matter (Roedder, 1984; Killops and Killops, 1993; Figure 10.1).

10.3.5 Early orogenic fluid summary

The constituents of early orogenic fluids are both aqueous and aqueo-carbonic and are compositionally more complex than earlier basinal fluids. Moreover, fluids present during this stage of basin evolution contain abundant volatile constituents such as methane, nitrogen, and CO_2 which result from the breakdown of higher hydrocarbons with increasing temperatures, and by decarbonization reactions (Van den Kerkhof and Thiéry, 1994).

Isochors plotted on a pressure-temperature diagram give an estimation of P-T conditions during fluid trapping (Roedder, 1984; Goldstein & Reynolds, 1994) and the intersection of aqueous and carbonic isochors of homogeneously trapped inclusions helps to constrain the range of P-T conditions applicable to this stage of basin evolution. Although abundant aqueo-carbonic inclusions are present together with pure CO_2 and aqueous inclusions, the majority of pure-CO_2 inclusions are believed to have been trapped as homogeneous fluids on a local scale. Regionally, this fluid formed part of a mixing system and a small population of aqueo-carbonic inclusions, with varying volatile volume percentages, was probably trapped heterogeneously.

Isochores were constructed for aqueous, aqueo-carbonic and methane inclusions of the Chambishi and Nchanga deposits, and are plotted with current-day lithostatic and hydrostatic gradients of 28°C/226 bar and 28°C/100 bar (Figure 10.4). Trapping temperatures are constrained by the difference in slopes of aqueous and methane inclusion isochores. If these fluids were trapped as separate phases from the same parent fluid, the isochores may be intersected in order to obtain the trapping conditions. Using this method, the lower pressure-temperature limit is obtained at 153-260°C at pressures between 550-800 bar. C_2H_6 found in very small quantities in Chambishi early

orogenic aqueo-carbonic inclusions (<0.5 mol%) with Raman microspectrometry supports the argument that these inclusions are representative of an early orogenic environment and that these inclusions were not affected by temperatures higher than 250-300°C. This temperature range is reported as the limit of breakdown of higher hydrocarbons (HHC) to CO_2, CH_4, and N_2 generally at higher temperatures (Roedder, 1984, pg. 347). These data point to the pressure- and temperature conditions of the environment at some stage after stratiform copper-cobalt mineralisation had formed, but prior to peak metamorphism. The presence of abundant CO_2, albeit with some CH_4, may indicate that early orogenic fluids were probably more oxidised, having interacted with red-bed sediments at the base of the stratigraphic column. Copper and cobalt concentrations in early orogenic fluids remain similar to earlier basinal fluids, but zinc and lead are slightly depleted in early orogenic fluids.

Trapping temperatures of these early orogenic fluids are hotter than earlier basinal fluids, which is consistent with the premise that these fluids were trapped during increased temperatures in the basin where metamorphism has started to impact on the host rocks.

Pressures during trapping conditions may either be hydrostatic, lithostatic, or probably somewhere in between. In this environment where fluids are believed to have been trapped during the onset of compressional tectonics, the fluid pressures may even be more than lithostatic if they were trapped during regional compression in ductile host rocks (Roedder and Bodnar, 1980). The relationship between pure hydrostatic fluid and lithostatic pressures may be expressed as:

$$P_{hydrostatic} = \lambda \times P_{lithostatic}$$

and λ = pore-pressure gradient where $\lambda \equiv \frac{\rho fluid}{\rho rock}$ (Ridley, 1993)

A fluid density of 1 g/cm^3, and rock density of 2.7 g/cm^3 is assumed;

The depth of trapping is expressed as:

$$P = H\rho g$$

where: H = depth
P = pressure
ρ = density of overlying material
(1.00 g/cm^3 for hydrostatic head, 2.70 g/cm^3 for lithostatic head)
g = gravitational acceleration 9.80665 m/s^2

Early orogenic fluids were most likely trapped at close to hydrostatic conditions corresponding to depths of 5.6 – 8.2 km, where the methane-rich fluid isochores are intersected with aqueous fluids isochors (Figure 10.4). Intersection of these isochores may be done if trapping of the methane-rich and aqueous fluids occurred simultaneously, which envisaged for early orogenic fluids.

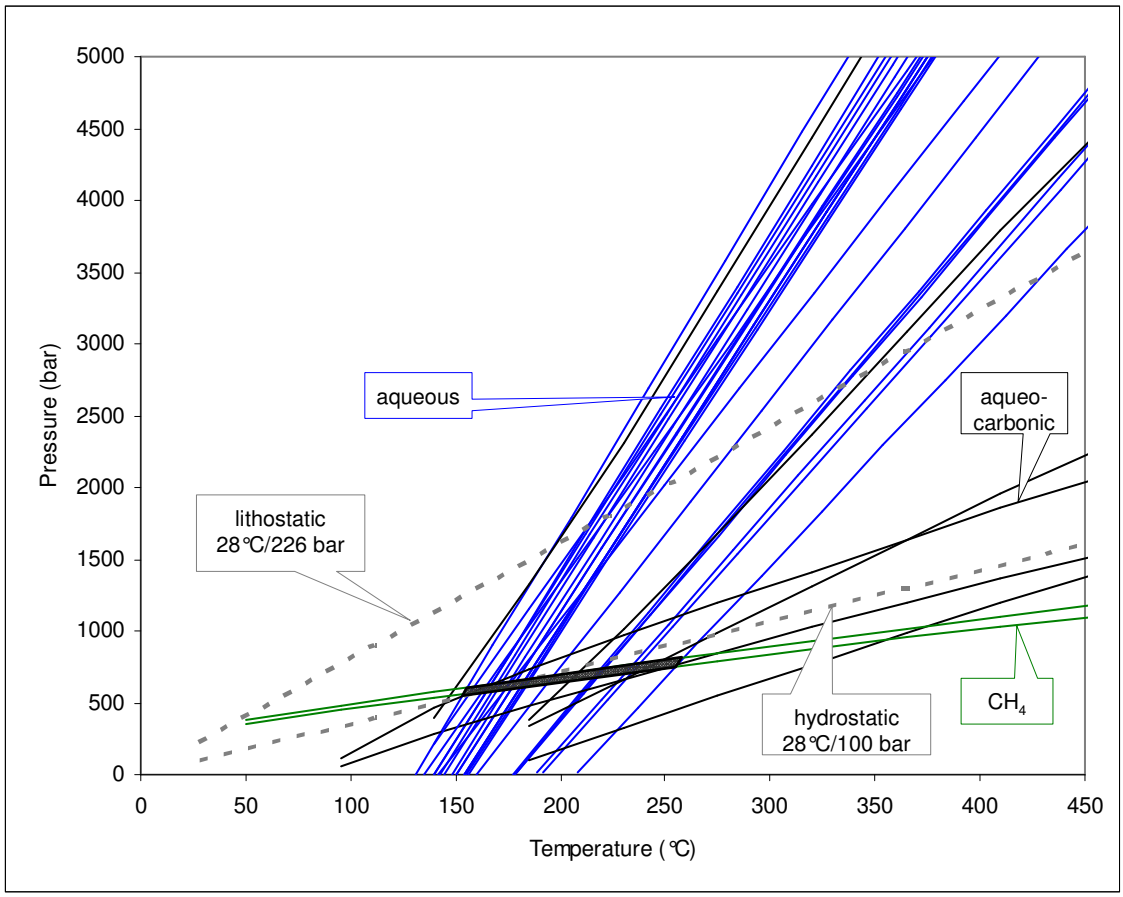

Figure 10.4. Isochores for early orogenic fluids of the Chambishi and Nchanga deposits with indicated present-day lithostatic and hydrostatic gradients of 28°C/ 226 bar and 28°C/ 100 bar respectively shown in dashed grey. Isochores for aqueous inclusions are indicated as blue lines, aqueo-carbonic inclusions are shown in solid black lines, with methane inclusions as green lines. The shaded area shows the area of intersection between CH_4 isochores and aqueous isochores.

10.4 Late orogenic fluids

Late orogenic fluids are different from both generations of earlier fluids in terms of composition, temperature and pressure. These fluids contain a diverse range of dissolved constituents and have minimum trapping temperatures that are significantly higher than

fluids trapped during the early stages of basin evolution. Four main fluid types were detected at the Mufulira, Nchanga, and Nkana mines all of which are believed to have been trapped during orogenesis. These fluids are hosted in quartz ± anhydrite veins which crosscut the stratiform copper orebodies at Mufulira. At Nkana, inclusions were hosted in quartz-K-feldspar veins which crosscut weakly developed mineral banding within which clusters of disseminated chalcopyrite were remobilised during late silicification. Late orogenic fluids were also seen at the Nchanga deposit at grain boundary junctions in an arkosic unit in the footwall to mineralisation. Here, inclusions were either re-filled during metamorphism, or secondary inclusions were trapped during the cracking and annealing of the host quartz.

10.4.1 NaCl - saturated, Ca - Mg - K brine

Evidence of this fluid type was found only at the Nchanga deposit and represents only a small percentage of fluid inclusion types. These liquid-vapour-solid inclusions contain solid halite phases which are not interpreted as daughter minerals since melting of halite occurs at higher temperatures than vapour homogenisation to the liquid phase. These inclusions are typically small and were initially believed to have formed early during basin development because of their small sizes and their location in the centres of quartz grains from the arkosic footwall sediments at Nchanga. However, their partial homogenisation temperatures of ~240°C to the vapour phase seem relatively high compared to other early basinal fluids found during this study, and these inclusions are now considered to form part of late orogenic fluids that circulated the basin during this later stage.

The irregular shapes of these inclusions together with varying liquid-vapour ratios of other inclusions in the same fluid inclusion assemblage suggest that these inclusions were initially trapped during the early stages of basin evolution, but then underwent a higher temperature overprint during orogenesis – they are regarded as re-filled and modified inclusions.

10.4.2 $MgCl_2$ - NaCl ± $CaCl_2$ brine

This fluid type was detected at the Nkana deposit and is characterized by minimum trapping temperatures ranging between 98 and 400 °C. The spread in salinities of this fluid (from low to moderate) probably indicates that trapping of these inclusions occurred during the heating of an early orogenic $MgCl_2$ - NaCl fluid with addition of a $CaCl_2$ fluid at higher temperatures (Figure 7.4).

10.4.3 NaCl - $CaCO_3$ - saturated brines with N_2

Solid hematite crystals were enclosed in inclusions during fluid trapping at Mufulira at temperatures between 329 - 379 °C. The aqueous phases of these inclusions are enriched in NaCl-$CaCO_3$, which at room temperature is evidenced by halite and calcite crystals.

The depressed eutectic melting temperatures of these inclusions suggests the presence of LiCl, $CaBr_2$, $FeCl_2$, $FeCl_3$ and $ZnCl_2$, with nitrogen as the dominant vapour phase constituent. These fluids are the hottest fluids found during this study and contain the highest salinities. The majority of these inclusions contain solid calcite crystals, and therefore indicate an equilibrium state between the fluid and host rock at the time of trapping. In addition to the presence of calcite, some inclusions also contain hematite, which was sourced from an oxidised host rock and are not interpreted as daughter crystals precipitating from the fluid. Late orogenic fluids must therefore, have been oxidising at neutral-to-alkaline conditions where the pH must have been greater than 5 (Figure 10.5). A fluid in equilibrium with a host rock at such Eh-pH conditions coincides with the oxic meteoric and marine waters described in Chapter 1, where copper- and cobalt hydroxides and -oxides are dominant.

The presence of an oxidised NaCl-saturated fluid provides a solution to the question of higher metal concentrations in late orogenic fluids and their role as mineralising agents. The high temperature, orogenic component of Copperbelt basinal fluids may have added to their oxidised and increasingly alkaline nature since silica and alkali enrichment in fluids is characteristic of metamorphic fluids (Azimov and Bushmin, 2007).

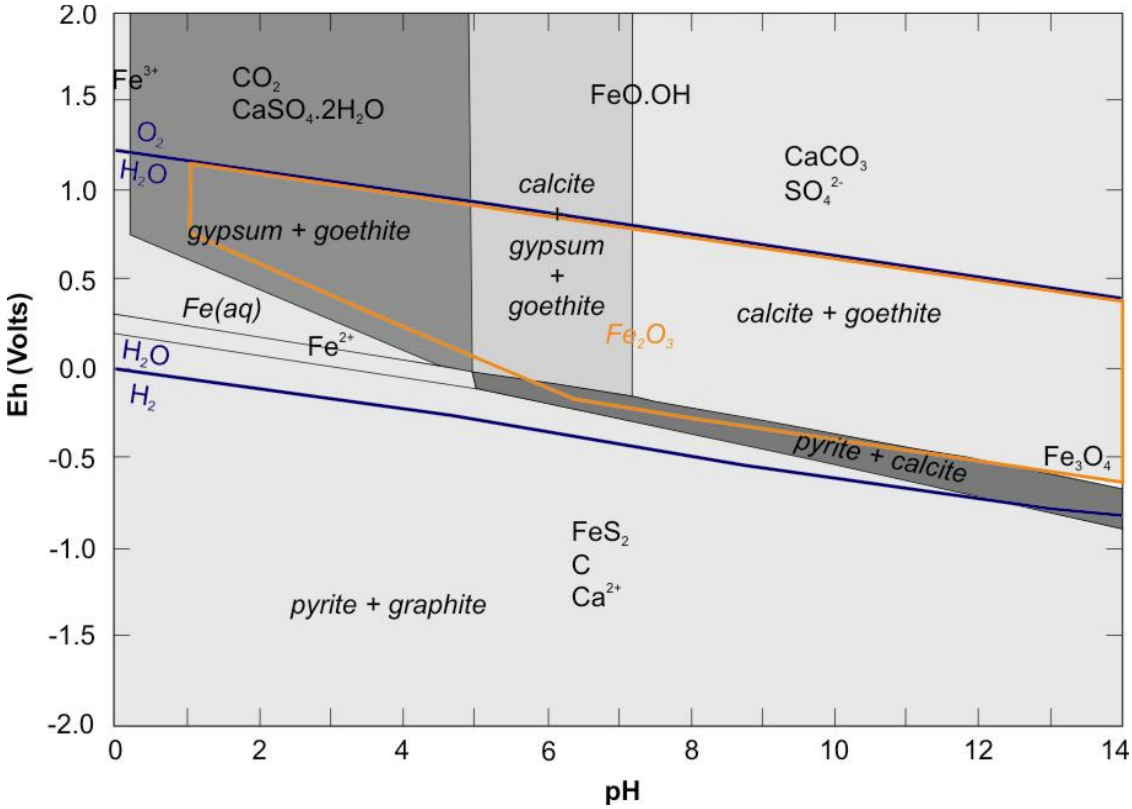

Figure 10.5. Reduction potential - pH diagram showing the stability fields of minerals in the C-Ca-Fe-S-H_2O system, and stability field for hematite in orange at 25•C, and 1atm (modified after Geological Survey of Japan, 2005 and Vink, 1996).

10.4.4 Low salinity $CaCl_2$ - $MgCl_2$ - H_2O ± CO_2 - CH_4 fluid

An aqueous, gas-rich $CaCl_2$ - $MgCl_2$ fluid of low salinity is present at Mufulira – this fluid also contains some CO_2 ± CH_4 dissolved in the liquid phase and occurs adjacent to the majority of halite-saturated high temperature fluids at the same locality. This low salinity $CaCl_2$ - $MgCl_2$ - H_2O ± CO_2 - CH_4 fluid was trapped in secondary late trails and, may either indicative of meteoric waters, possibly circulating within the basin after peak metamorphic activity, or derived from metamorphic fluids.

10.4.5 Late orogenic fluid summary and trapping conditions

Late orogenic fluids in the Katangan Basin are recognized as modified metamorphic fluids that were trapped at high temperatures and fluid pressures and are markedly distinct in composition, temperature, and pressure from earlier fluids. Notably, these late fluids are enriched in metals and contain the highest Pb and Cu contents of all three fluid types. Moreover, late orogenic fluids are saturated in salts, were hot and contain solid

hematite crystals suggesting the trapping of saline, high temperature, oxidised brines. Hematitic sandstone is documented in the Roan Group by Jackson *et al*., (2003), where the hematite is regarded as secondary and derived directly from lower Roan sediments by hot fluids circulating within the sediments during metamorphism. Temperatures of these fluids became progressively hotter with ongoing metamorphism and these fluids were able to dissolve more salts at higher temperatures. Evaporite beds supplied abundant salts to these increasingly hot and saline fluids as the basin matured. In addition to high trapping temperatures and high salinities, late orogenic fluids also contain 200-500 times more Sr than modern seawater, which supports an evaporite-derived origin for the abundant and diverse metal cations in this fluid type. Metal concentrations are all elevated during late orogenic times, and the highest ranges of copper, cobalt, zinc, lead and silver are found in late orogenic fluids.

Fluid pressures may be calculated from inclusion data by using (a) the vapour pressure of the fluid at homogenisation temperatures, (b) intersection of isochores and independent geothermometers, (c) intersection of fluid isochores of coeval fluids, (d) and the dissolution of solid phases such as halite where halite dissolution occurs at higher temperatures than partial homogenisation of the vapour phase (Shepherd *et al*., 1985). Late orogenic fluid inclusions show dissolution of the halite daughter minerals at lower temperatures than homogenisation of the inclusions, therefore cancelling out the last mentioned method of determining fluid pressures. Intersecting isochores of coeval fluids is not a viable option in this case to determine fluid pressures since late orogenic fluids are dominantly composed of aqueous and aqueous-solid inclusions with no purely carbonic fluid available with a sufficiently alternative slope.

Isochores of late orogenic aqueous (± NaCl saturated) and aqueous-nitrogen fluid inclusions were constructed for data from the Nkana, Nchanga, and Mufulira deposits (Figure 10.6). In the absence of an independent geothermometer, and in the absence of partly miscible fluids to constrain the pressure from microthermometry (Roedder and Bodnar, 1980), present day lithostatic and hydrostatic thermobaric gradients of 28 °C/ 226 bar and 28°C / 100 bar (Goldstein, 2001) were used in order to obtain the pressure corrected trapping conditions of fluid inclusions.

If the assumption is made that purely hydrostatic pressure conditions prevailed then late orogenic inclusions would have been trapped at temperatures between 180 - 530 °C corresponding to pressures between 570 - 1790 bar. However, under lithostatic or near-lithostatic pressure conditions, the intersection of lithostatic pressure gradients with the lower lithostatic gradient results in minimum temperature and pressure estimations at 240°C and 1750 bar. The upper intercept of the present day lithostatic gradient yields an

estimation of 525 °C at 4000 bar pressure.

Late orogenic fluids were probably trapped under lithostatic pressure conditions, corresponding to a depth of ~6.6 km. Trapping of late orogenic fluids at such depths corresponds to geothermal gradients between 27 and 78 °C/km for the minimum and maximum temperature range. A geothermal gradient of 78 °C/km would require an additional heat source, possibly related to later granitic intrusions, and higher peak metamorphic conditions than those applicable in the Copperbelt region.

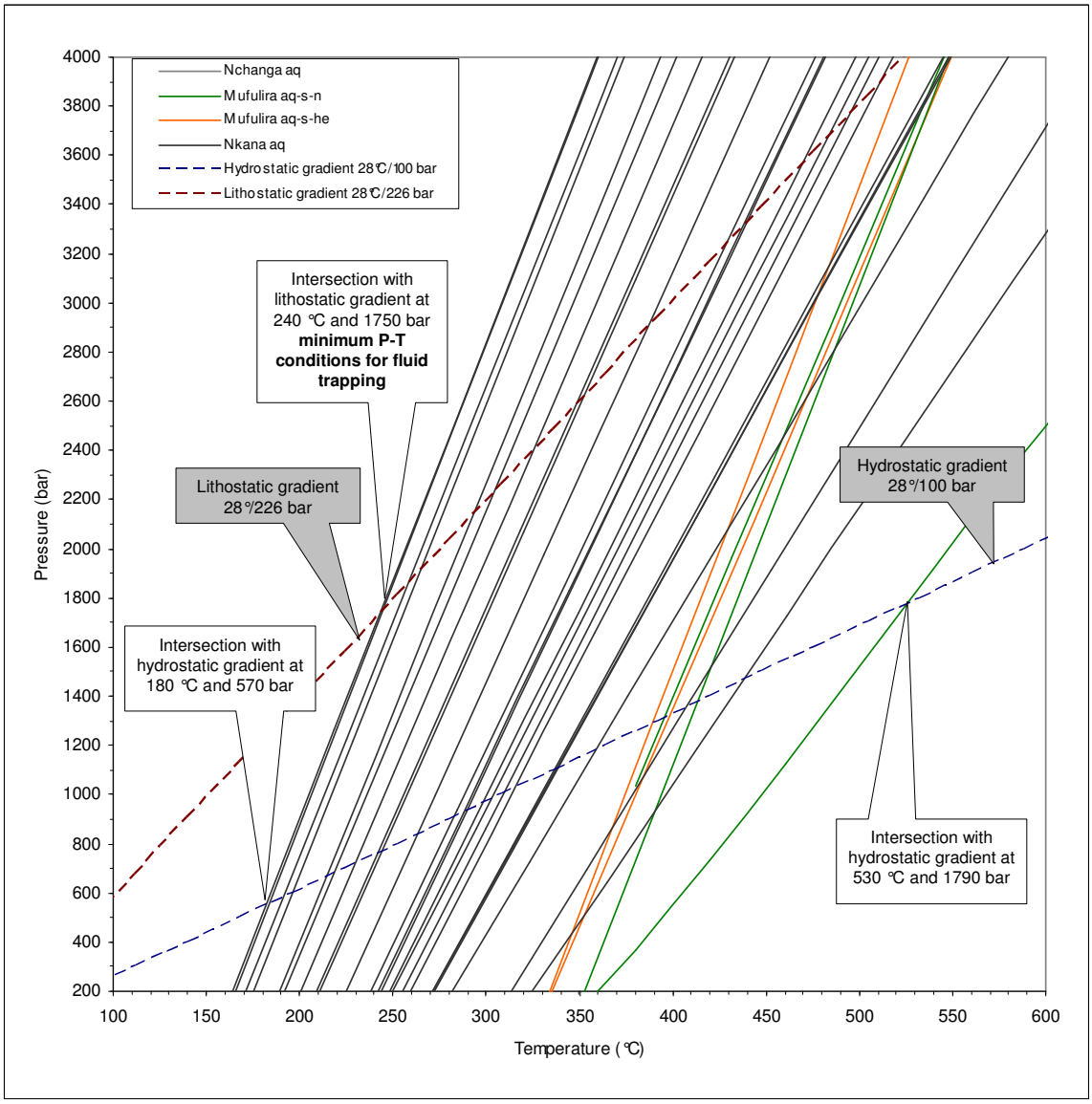

Figure 10.6. Constructed isochors for late orogenic fluids at the Mufulira, Nchanga, and Nkana deposits.

10.5 Reconstruction of trapping conditions of fluids of the Zambian Copperbelt and implications for mineralisation

Early generation fluid inclusions trapped in the Chambishi area provide evidence for the nature of basinal fluids that immediately postdate stratiform Cu-Co mineralisation. Chambishi offers a unique view into the early stages of fluid evolution in the Copperbelt and records the earliest fluids studied to date in the Zambian Copperbelt.

These fluids comprise moderate salinities at low temperatures (Figure 10.7) and are implicated in the early remobilisation of stratiform copper mineralisation. Copper complexes may have originally been transported in moderately oxidised brines that encountered black carbonaceous shales (e.g. in the Chambishi area). These black carbonaceous shales would have acted as a reducing agent, in addition to also supplying reduced sulphur in the form of S^{2-} from pyrite, with resultant copper sulphide precipitation. Progressive sediment burial during diagenesis and the progressive heating of connate fluids result in a trend from an early moderate salinity fluid to a higher temperature higher-salinity fluid. With continuing metamorphism, devolatilization reactions result in the production of a fluid of lower salinity, but at higher temperatures.

Previous P-T estimates for mineralising fluids by Kamona (1993), Richards *et al*. (1988a) and Speiser *et al*. (1995) are relevant to this discussion (Figure 10.8). The data of Kamona (1993) constrain the characteristics of epigenetic carbonate-hosted Pb-Zn mineralising fluids at Kabwe, a mineralisation style that postdates stratiform copper mineralisation. These fluids possibly correspond to the early orogenic fluids of this study. The data of Speiser *et al*. (1995) show the elevated pressure and temperature ranges for conditions associated with epigenetic iron-oxide-copper-gold mineralisation to the northwest of the Copperbelt. This epigenetic-hydrothermal vein style mineralisation (dated at ~503 - 512 Ma, Torrealday *et al*., 2000) also postdates earlier stratiform copper mineralization and is considered coeval with the peak of regional metamorphism in the Lufilian arc (Rainaud *et al*., 2005b).

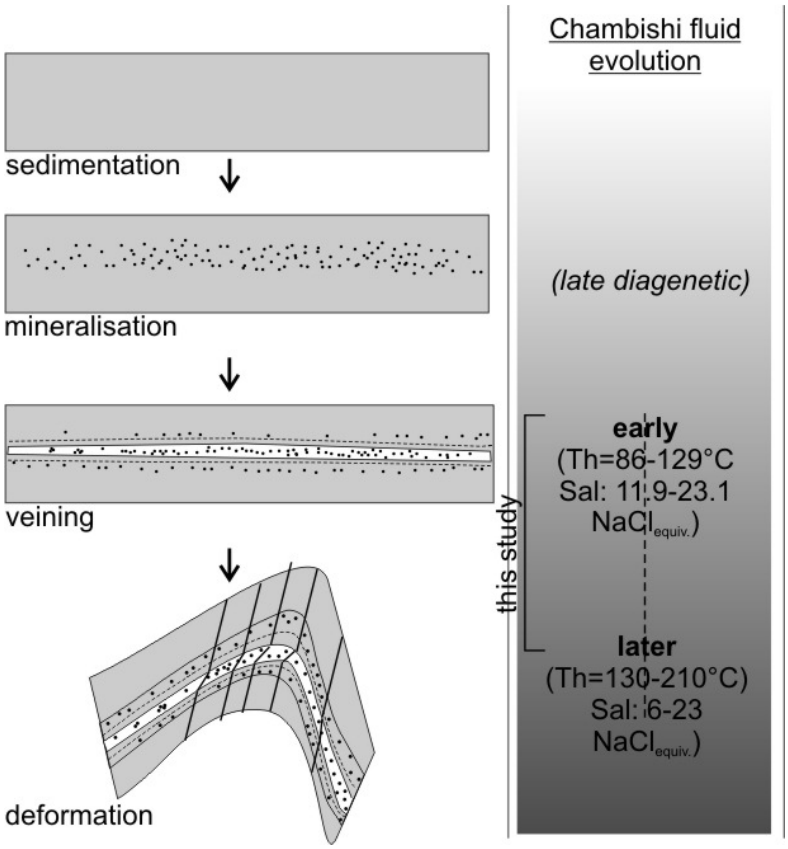

Figure 10.7. Schematic diagram showing the trapping of early basinal fluids in the Chambishi basin. Subsequent maturation of the basin results in the formation of fluids of variable compositions and higher trapping temperatures.

Similarly, the data of Richards *et al*. (1988a) constrain the P-T conditions prevalent during late hydrothermal veining and alteration at the Musoshi deposit in the DRC. This event of hydrothermal alteration, dated at ~514Ma (Richards *et al*., 1988b), is also related to peak Lufilian metamorphism and postdates stratiform copper mineralisation. The temperatures attained by Richards *et al*. (1988a) also exceed those obtained during this study of basinal and early orogenic fluids. These fluids correspond in temperature to late orogenic fluids found during this study. McGowan (2003) calculated entrapment temperatures of mineralising fluids at Nchanga of 220 to 310 °C at lithostatic pressures of ~ 1200 bar. Nchanga fluids correspond to the early orogenic fluids found during this study.

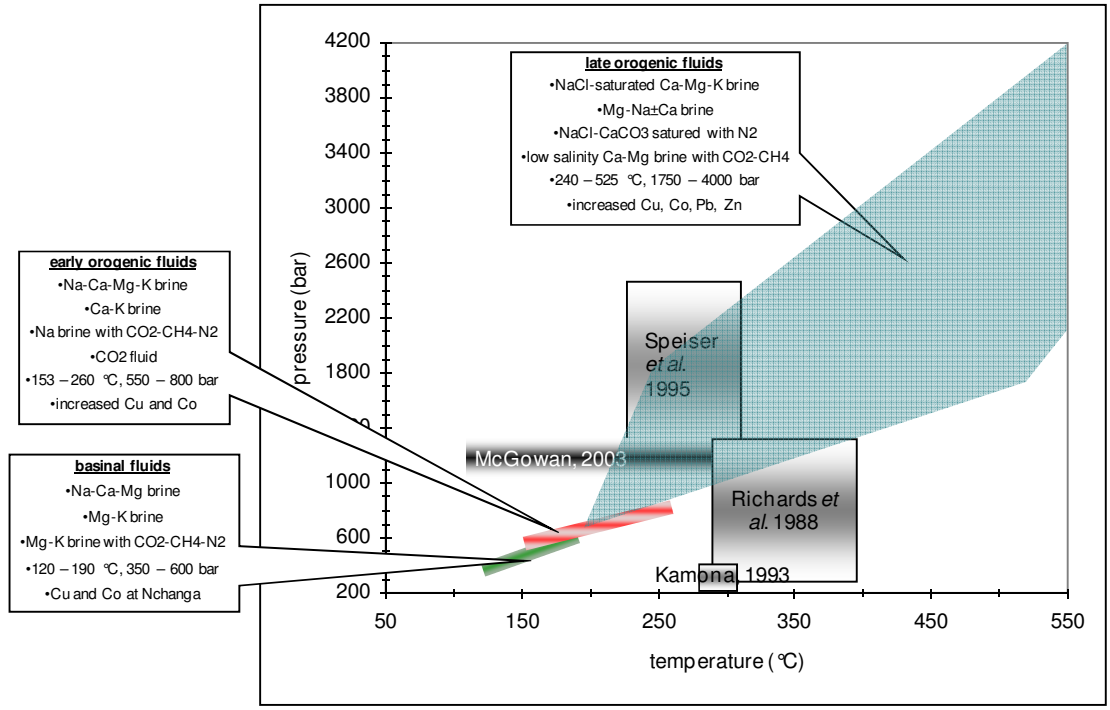

Figure 10.8. Range of trapping conditions for basinal, early-, and late orogenic fluids of the Copperbelt obtained during this study and compared to other authors.

Copper mineralisation is viewed as a multi-stage hydrothermal event, or as several pulses of a single prolonged fluid flow event. The terminal stages of diagenetic stratiform copper mineralisation occurred under near hydrostatic pressure conditions. Fluid flow may have been triggered from the release of pore fluids during basinal compaction.

Copper-bearing brines were transported in moderately oxidised brines, and mineralisation occurred due to the interaction of these oxidised fluids with more reduced horizons such as the widespread shale at the base of the Roan Group or fluids derived there from.

Sulphur is also supplied from the pyrite in the black shale. This early diagenetic mineralisation forms a constituent of the overall mineralised Katangan Supergroup in Zambia, and is by means of reduction of SO_4^{2-} when oxidised fluids meet a reducing agent in the shales. Fluids circulating within the basin after this initial diagenetic mineralising event were trapped at ~350 - 600 bar and temperatures between 120 - 190 °C (Figure 10.9a).

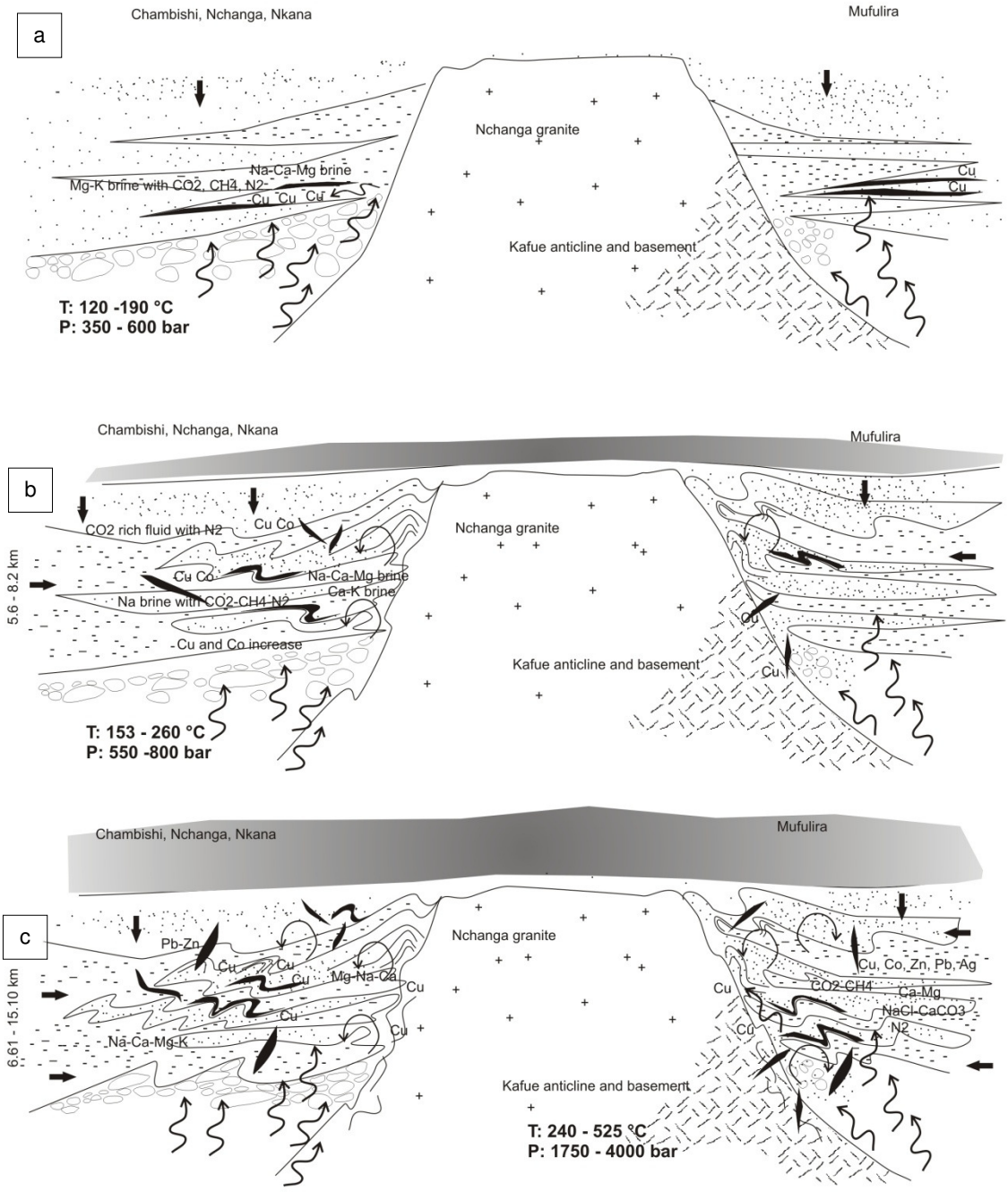

Figure 10.9. Simplified schematic with view to the northwest, showing the envisaged fluid history of the Copperbelt in the Nchanga, Konkola, Chambishi, Nkana and Mufulira areas: (a) prior to metamorphism, during basinal compaction, (b) during early orogenesis, (c) during late orogenic peak metamorphic times. Arrows indicate fluid flow in the host sediments; short, solid arrows indicate the pressure directions, ranging from vertical pressures due to sedimentary loading, and horizontal pressures exerted by regional metamorphic compression.

Pressures are mostly attributed to sedimentary loading and compaction of the basin. These fluids show moderate concentrations of copper and cobalt in the presence of Na, Mg, K, and Ca brines in the deposits on the southwest flank of the Kafue anticline.

During the onset of metamorphism, fluids were trapped at temperatures of 153 - 260°C and pressures between 550 - 800 bar at depths of around 5.6 – 8.2 km hydrostatic pressure gradient (Figure 10.9b). The temperature of the basin increases with the onset of metamorphism, but when considering the ranges in P-T conditions, it becomes clear that the initial effect of metamorphism is more thermal than pressure-related. The presence of abundant methane found during this study in early orogenic fluids may be implicated in the local epigenetic mineralisation at Nchanga where thermochemical (non-bacterial) sulphate reduction is believed to be the chief ore precipitating mechanism in late mineralisation (McGowan, 2003), following the irreversible reaction :-

$$CH_4 + 2H^+ + (SO_4)^{2-} \rightarrow H_2S + CO_2 + 2H_2O$$

H_2S produced during this reaction is a necessary catalyst for the sulphate reduction and precipitation of copper sulphides (Ohmoto and Goldhaber, 1997). At temperatures below 150°C, the kinetics of this reaction are dependant on pH, fO_2, and constrained activities of SO_4^{2-} and reducing agents, but at temperatures above 150°C, sulphate reduction by H_2S occurs easily (Ohmoto and Lasaga, 1982).

Early orogenic fluids are slightly depleted in Pb and Zn compared to earlier and later fluids, but show increasing Na and Cu concentrations relative to earlier basinal fluids. Localised pressure differences within the basin may have driven fluid circulation. Increasing pressures would have focused fluids along rheologically contrasted units such as the contact between the host sediments and the basement. Fluids may also have scavenged metals from the sediments at this time due to increased metal solubilities at higher temperatures.

With progressive metamorphism, fluids circulating within the basin become progressively heated and equilibrated with the surrounding metamorphic rocks and minerals (Figure 10.9c). Accordingly, these fluids become enriched in metals that were deposited earlier during stratiform mineralisation, effectively remobilising these early precipitates and upgrading existing orebodies. Salinities are also seen to increase significantly in these modified metamorphic fluids. As temperatures and pressures increase during orogenesis, fluid circulation is enhanced by temperature gradients and deformation, which probably lead to access of evaporitic horizons higher up in the sequence, which in turn would be the source for saline constituents. Late orogenic fluids

show trapping at temperatures between 240 - 525 °C at a minimum pressure of 1750 bar and indicate peak metamorphic conditions and consist of modified oxidized brines.

Interestingly, metal content increases consistently over the progressive evolution of the basin, with the latest fluids carrying significant amounts of Pb, Zn, Cu, Co, and Sr. The latest fluids also contain the highest salinities of all three fluid types and indicate the prolonged presence and equilibration of these fluids with the host rock. Later fluids are also more oxidised compared to earlier basinal fluids. A key to the widespread and paragenetically complex nature of the Copperbelt ores may be related to the longevity of fluid flow and the progressive ability of fluids to transport metals.

The marked increase in Pb and Zn in later fluids may be relevant to the formation of regional epigenetic Pb-Zn deposits further afield of the Copperbelt, such as at Kabwe and Kipushi. The late orogenic fluids seen in the Copperbelt compare favourably with mineralising fluids of the epigenetic Pb-Zn Kabwe deposit (Kamona, 1993) in terms of metal composition, temperature (300°C) and moderate salinities.

As fluids continue to circulate within the basin at increasing temperatures and pressures due to increasing metamorphic grades, metals are scavenged from early stratiform copper mineralisation, present in the basin. Early stratiform mineralisation is followed by continuing fluid circulation in the basin and metals are scavenged by hotter fluids which continue to act as mineralising agents.

The complex nature of fluid evolution in the Copperbelt is evidenced from the array of fluid types encountered during this study. This in turn accords with the paragenetically complex nature of the Copperbelt ores and the widespread extent of mineralisation. The presence of several mineralisation pulses may be the controlling factor which distinguishes the Central African Copperbelt as a world class deposit.

Reference List

Allan M.M., Yardley B.W.D., Forbes L.J., Shmulovich K.I., Banks D.A., Shepherd T.J., 2005. Validation of LA-ICP-MS fluid inclusion analysis with synthetic fluid inclusions. *American Mineralogist*, 90, 1767-1775.

Andersen T., Burke E.A.J., Austrheim H., 1989. Nitrogen-bearing, aqueous fluid inclusions in some eclogites from the Western Gneiss Region of the Norwegian Caledonides. *Contributions to Mineralogy and Petrology*, 103, 153-165.

Annels A.E., 1984. The geotectonic environment of Zambia copper-cobalt mineralization. *Journal of the Geological Society of London*, 141, 279-289.

Annels A.E., 1989. Ore genesis in the Zambian Copperbelt, with particular reference to the northern sector of the Chambishi basin. In: Boyle R.W., Brown A.C., Jefferson C.W., Jowett E.C., Kirkham R.V. (eds.), Sediment-hosted stratiform copper deposits, Geological Association of Canada Special Paper 36, 427-452.

Annels A.E., and Simmonds J.R., 1984. Cobalt in the Zambian Copperbelt. *Precambrian Research*, 25, 75-98.

Annels A.E., Vaughan D.J., Craig J.R., 1983. Conditions of ore mineral formation in certain Zambian Copperbelt deposits with special reference to the role of cobalt. *Mineralium Deposita*, 18, 71-88.

Armstrong R.A., Robb L.J., Master S., Kruger F.J., Mumba P.A.C.C., 1999. New U-Pb age constraints on the Katanga Sequence, Central African Copperbelt. *Journal of African Earth Sciences*, 28(4A), 6-7.

Armstrong R.A., Master S., Robb L.J., 2005. Geochronology of the Nchanga Granite, and constraints on the maximum age of the Katanga Supergroup, Zambian Copperbelt. *Journal of African Earth Sciences*, 42, 32-40.

Audéoud D., 1982. Les minéralisations uranifères et leur environnement à Kamoto, Kambove et Shinkolobwe (Shaba, Zaïre) pétrographie, géochimie et inclusions fluides. These - Doctorat de troisième cycle, Centre de Recherches sur la Géologie de l'Uranium, Nancy I, et, L'Université Claude Bernard – Lyon I, 212p.

Audétat A., Günther D., Heinrich C.A., 1998. Formation of a Magmatic-Hydrothermal Ore Deposit: Insights with LA-ICP-MS Analysis of Fluid Inclusions. *Science*, 279, 5359, 2091-2094.

Azimov P.Y., and Bushmin S.A., 2007. Solubility of minerals of metamorphic and metasomatic rocks in hydrothermal solutions of varying acidity: Thermodynamic modelling at 400-800°C and 1-5kbar. *Journal of Geochemistry International*, 45, 12, 1210-1234.

Bakker R.J., 1997. Clathrates: Computer programs to calculate fluid inclusion *V-X* properties using clathrate melting temperatures. *Computers & Geosciences*, 23(1), 1-18.

Bakker R.J., 1999. Adaption of the Bowers and Helgeson (1983) equation of state to the H_2O-CO_2 - CH_4 -N_2 -NaCl system. *Chemical Geology*, 154, 225-236.

Bakker R.J., 2003. Package *FLUIDS* 1. Computer programs for analysis of fluid inclusion data and for modelling bulk fluid properties. *Chemical Geology*, 194, 3-23.

Bakker R.J., and Thiéry R., 1994. Application of clathrates to fluid inclusion studies. In De Vivo, B. and Frezzotti, M.L. (eds.) Short Course of the Working Group (IMA) Fluid inclusions in minerals: Methods and Applications. Pontignano, Sienna, 1-4 September, 191-230.

Banks D.A., Boyce A.J., Samson I.M., 2002. Constraints on the origins of fluids forming Irish Zn-Pb-Ba deposits: evidence from the composition of fluid inclusions. *Economic Geology*, 97,

471-480.

Banks D.A., Gleeson S.A., Green R., 2000. Determination of the origin of salinity in granite-related fluids: evidence from chlorine isotopes in fluid inclusions. *Journal of Geochemical Exploration*, 69-70, 309-312.

Barker A.J., Bennett D.G., Boyce A.J., Fallick A.E., 2000. Retrogression by deep infiltration of meteoric fluids into thrust zones during late orogenic rapid unroofing. *Journal of Metamorphic Geology*, 18, 3, 307-318.

Bartholomé P., Evrard P., Katekesha F., Lopez-Ruiz J., Ngongo M., 1973. Diagenetic Ore-forming Processes at Kamoto, Katanga, Republic of the Congo. In: Amstutz G.C. and Bernard A.J. (eds.), Ores in Sediments. Springer-Verlag, Berlin, 21-41.

Bateman A.M., 1930. The ores of the Northern Rhodesia copper belt. *Economic Geology*, 25, 365-419.

Binda P.L., 1975. Detrital bornite grains in the Late Precambrian B graywackes of Mufulira, Zambia. *Mineralium Deposita*, 10, 179-186.

Binda P.L., 1994. Stratigraphy of Zambian Copperbelt orebodies. *Journal of African Earth Sciences*, 19, 4, 251-264.

Binda P.L. and Mulgrew J.R., 1974. Stratigraphy of copper occurrences in the Zambian Copperbelt. In: Gisements stratiformes et provinces cuprifères. (Bartholomé P. ed). Centenaire Société Géologique de Belgique, Liége, 215-233.

Binda P.L. and Porada H., 1995. Observations on the Katangan breccias of Zambia. In: Late Proterozoic belts in Central and Southwest Africa (M. Wendorff and L. Tack eds.), Museé royal de l"Afrique Centrale, Tervuren, Belgigue, *Annales Sciences Géologiques*, 101, 49-62.

Bodiselitsch B., Koeberl C., Master S., Reimold W.U., 2005. Estimating duration and intensity of Neoproterozoic snowball glaciations from Ir anomalies. *Science*, 308, (5719), 239-242.

Bodnar R.J. 1983. A method of calculating fluid inclusion volumes based on vapor bubble diameters and P-V-T-X properties of inclusion fluids. *Economic Geology*, 78**,** 535-542.

Bodnar R.J., 1993. Revised equation and table for determining the freezing point depression of H_2O-NaCl solutions. *Geochimica et Cosmochimica Acta*, 57, 683-684.

Bodnar R.J., 1994. Philosophy of fluid inclusion analysis. In De Vivo, B. and Frezzotti, M.L. (eds.) Short Course of the Working Group (IMA) Fluid inclusions in minerals: Methods and Applications. Pontignano, Sienna, 1-4 September, 1-6.

Bodnar R.J., Burnham C.W., Sterner S.M., 1985. Synthetic fluid inclusions in natural quartz. III. Determination of phase equilibrium properties in the system H_2O-NaCl to 1000 °C and 1500 bar. *Geochimica et Cosmochimica Acta*, 49, 1861-1873.

Bodnar R.J. and Vityk M.O. 1994. Interpretation of microthermometric data for H_2O-NaCl fluid inclusions. In De Vivo, B. and Frezzotti, M.L. (eds.) Short Course of the Working Group (IMA) Fluid inclusions in minerals: Methods and Applications. Pontignano, Sienna, 1-4 September, 117-130.

Boiron M.-C., and Dubessy J., 1994. Determination of fluid inclusion compositions: Microanalytical techniques. In De Vivo, B. and Frezzotti, M.L. (eds.) Short Course of the Working Group (IMA) Fluid inclusions in minerals: Methods and Applications. Pontignano, Sienna, 1-4 September, 45-72.

Boiron M.C., Essarraj S., Sellier E., Cathelineau M., Lespinasse M., Poty B. 1992. Identification of fluid inclusions in relation to their host microstructural domains in quartz by cathodoluminescence. *Geochimica et Cosmochimica Acta*, 56, 175-185.

Borovikov A.A., Gushchina L.N., Borisenko A.S., 2001. Specific features of $FeCl_2$ and $FeCl_3$ solutions behaviour at low temperatures (cryometry of fluid inclusions). In: F. Noronha, A. Dória and A. Guedes (eds.) XVI ECROFI European Current Research on Fluid Inclusions, Porto, 2001, Abstract volume, 61-63.

Borthwick J. and Harmon R.S., 1982. A note regarding ClF_3 as an alternative to BrF_5 for oxygen isotope analysis. *Geochimica et Cosmochimica Acta*, 46, 1665-1668.

Brandt R.T., Burton C.C.J., Maree S.C., Woakes M.E., 1961. Mufulira. In: The geology of the Northern Rhodesian Copperbelt, (ed. F. Mendelsohn), Macdonald, London, 411-461.

Brown A.C., 2006. Refinements for footwall red-bed diagenesis in the sediment-hosted stratiform copper deposits model. Economic Geology (Scientific Communications), 100, 763-771.

Brown, P.E. and Lamb, W.M. 1986. Mixing of H_2O-CO_2 in fluid inclusions; geobarometry and Archean Gold deposits. *Geochimica et Cosmochimica Acta*, vol. 50, pp. 847-852.

Brown, P E. and Lamb, W.M. 1989. P-V-T properties of fluids in the system H_2O + CO_2 + NaCl: New graphical presentations and implications for fluid inclusion studies. *Geochimica et Cosmochimica Acta*, v. 53, pp. 1209-1221.

Burke E.A.J., 2001. Raman microspectrometry of fluid inclusions. Lithos, 55, 139-158.

Burruss R.C., 1981. Analysis of phase equilibria in C-O-H-S fluid inclusions. In: L. Hollister and M.L. Crawford (eds.), Short Course in Fluid Inclusions: Applications to Petrology, Mineralogical Association of Canada, Calgary, 39-73.

Cahen L. and Snelling N.J., 1984. The geochronology and evolution of Africa, Claredon Press, Oxford, 512p.

Cailteux J.L.H., 1983. Le “Roan” shabien dans la région de Kambove (Shaba, Zaïre). PhD thèse, Université de Liège.

Cailteux J., 2003. Proterozoic sedimentary-hosted base-metal deposits of Western Gondwana. Conference and field workshop, Lubumbashi, 223p.

Cailteux J., Binda P.L., Katekesha W.M., Kampunzu A.B., Intiomale M.M., Kapenda D., Kaunda C., Ngongo K., Tshiauka T., Wendorff M., 1994. Lithostratigraphical correlation of the Neoproterozoic Roan Supergroup from Shaba (Zaire) and Zambia, in the central African copper-cobalt metallogenic province. *Journal of African Earth Sciences*, 19, 4, 265-278.

Cailteux J.L.H., Kampunzu A.B., Lerouge C., Kaputo A.K., Milesi J.P., 2005a. Genesis of sediment-hosted stratiform copper-cobalt deposits, Central African Copperbelt. *Journal of African Earth Sciences*, 42, 134-158.

Cailteux J.L.H., Kampunzu A.B.H., Batumike M.J., 2005b. Lithostratigraphic position and petrographic characteristics of R.A.T. (Roches Argilo-Talqueuses) Subgroup, Neoproterozoic Katangan Belt (Congo). *Journal of African Earth Sciences*, 42, 82-94.

Carpenter A.B., 1978. Origin and chemical evolution of brines in sedimentary basins. Oklahoma Geological Survey Circular, 79, 60-77.

Clarke Jr., S.P., 1966. Handbook of Physical Constants. *Geological Society of America Memoir*, 97, 587p.

Clayton R.N., and Mayeda T.K., 1963. The use of bromine pentafluoride in the extraction of oxygen

from oxides and silicates for isotopic analysis. *Geochimica et Cosmochimica Acta*, 27, 43-52.

Coplan T.B., and Hanshaw B.B., 1973. Ultrafiltration by a compacted clay membrane. I. Oxygen and hydrogen isotopic fractionation. *Geochimica et Cosmochimica Acta*, 37, 2295-2310.

Coplen T.B., Kendall C., Hopple J., 1983. Comparison of stable isotope reference samples. *Nature*, 302, 236-238.

Costantino M and Rice S.F., 1991. Supercritical phase separation in H_2O-N_2 mixtures. *Journal of Phyisical Chemistry*, 95, 9034-9036.

Craig H., 1961. Isotopic variations in meteoric waters. *Science*, 133, 1702-1703.

Cressie N.A.C., 1990. The origins of Kriging. *Mathematical Geology*, 22, 239-252.

Cunningham M.J., 1986. Copper-cobalt mineralisation in the northern portion of the Chambishi Basin, Zambia. Unpublised PhD thesis, University College, Cardiff.

Davis D.W., Lowenstein T.K., Spencer R.J., 1994. Melting behavior of fluid inclusions in laboratory-grown halite crystals in the systems NaCl-H_2O, NaCl-KCl-H_2O, NaCl-$MgCl_2$-H_2O, and NaCl-$CaCl_2$-H_2O. *Geochimica et Cosmochimica Acta*, 54, 591-601.

Daly M.C., Chakroborty S.K., Kasolo P., Musiza M., Mumba P., Naidu B., Namateba C., Ngambi O., Coward M.P., 1984. The Lufilian Arc and Irumide Belt of Zambia: results of a geotraverse across their intersection. *Journal of African Earth Sciences*, 2, 311-318.

Darnley A.G., 1960. Petrology of some Rhodesian Copperbelt orebodies and associated rocks: *Transactions of the Institution of Mining and Metallurgy*, 69, 137-172.

Deer W.A., Howie R.A., and Zussman J., 1992. An introduction to the rock-forming minerals. Second Edition, Pentice Hall, England, 696p.

Delhal J., 1991. Situation géochronologique 1990 du Précambrien du Sud-Kasai et de l'Ouest-Shaba. Musée royal d'Afrique centrale, Tervuren, Annual report, 1990, 119-125.

Deltombe E. and Pourbaix M., 1980. Cobalt, Section 12.2. In: Pourbaix M. (ed.), Atlas of electrochemical equilibria in aqueous solutions. National Association of Corrosion Engineers, Houston, Texas, U.S.A. CEBELCOR (Ed.) Brussels. 322-329.

De Magnée I., and François A., 1988. The origin of the Kipushi (Cu, Zn, Pb) deposit in direct relation with a Proterozoic salt diapir, Copperbelt of Central Africa, Shaba, Republic of Zaire. In: G.H. Friedrich et al. (eds.), Base metal sulfide deposits, Berlin, Springer-Verlag, 74-93.

Derome D., 2002. Evolution et origine des saumures dans les basins protérozoïques au voisinage de la discordance socle/couverture. L'exemple de l'environnement des gisements d'uranium associés aux bassins Kombolgie (Australie) et Athabasca (Canada). Doctoral thesis, Université Henri Poincaré, Nancy I, CREGU, Nancy, France, 265 pp.

Dewaele S., Muchez Ph., Vets J., Fernandex-Alonzo M., Tack L., 2006a. Multiphase origin of the Cu-Co ore deposits in the western part of the Lufilian fold-and-thrust belt, Katanga (Democratic Republic of the Congo). *Journal of African Earth Sciences*, 46, 455-469.

Dewaele S., Muchez P., Heijlen W., Boutwood A., Lemmon T., Tyler R., 2006b. Reconstruction of the hydrothermal history of the Cu-Ag vein-type mineralization at Dikulushi, Kundelungu foreland, Katanga, D.R. Congo. *Journal of Geochemical Exploration*, 89, 376-379.

De Zoubov, N., Vanleugenhaghe C., and Pourbaix M., 1980. *Copper, Section 14.1*. In: Pourbaix M. (ed.), Atlas of electrochemical equilibria in aqueous solutions. National Association of

Corrosion Engineers, Houston, Texas, U.S.A. CEBELCOR (ed.) Brussels. 384-392.

Diamond L.W., 1994. Introduction to phase relations of CO_2-H_2O fluid inclusions. In De Vivo, B. and Frezzotti, M.L. (eds.) Short Course of the Working Group (IMA) Fluid inclusions in minerals: Methods and Applications. Pontignano, Sienna, 1-4 September, 131-158.

Diamond L.W., 1996. Isochoric paths in immiscible fluids and the interpretation of multicomponent fluid inclusions. *Geochimica et Cosmochimica Acta*, 60, 20, 3825 - 3834.

Diamond L.W., 2001. Review of the systematics of CO_2-H_2O fluid inclusions. *Lithos*, 55, 69-99.

Diamond L. W. 2003. Chapter 5. Introduction to gas-bearing, aqueous fluid inclusions. In: *Fluid Inclusions: Analysis and Interpretation* (I. Samson, A. Anderson, D. Marshall, eds.), Mineralogical Association of Canada Short Course Series Vol. 32.

Diederix D., 1977. The geology of the Nchanga Mining Licence Area. Unpublished Company Report, Nchanga Consolidated Copper Mines Limited Chingola Division, 59p.

Dubessy J., Audeoud D., Wilkins R., Kosztolanyi C., 1982. The use of the Raman microprobe MOLE in the determination of the electrolytes dissolved in the aqueous phase of fluid inclusions. *Chemical Geology*, 37, 137-150.

Dubessy J., Derome D., Sausse J., 2003. Numerical modeling of fluid mixings in the H_2O-NaCl system application to the North Caramal U prospect (Australia). *Chemical Geology*, 194, 25-39.

Dubessy J., Lhomme T., Boiron M.-C., Rull F., 2002. Determination of chlorinity in aqueous fluids using Raman Spectroscopy of the stretching band of water at room temperature : Application to fluid inclusions. *Applied Spectroscopy*, 56, 1, 99-106.

Dubessy J., Poty B., Ramboz C., 1989. Advances in the C-O-H-N-S fluid geochemistry based on micro-Raman spectroscopic analysis of fluid inclusions. *European Journal of Mineralogy*, 1, 517-534.

El Desouky H., Muchez P., Dewaele S., Boutwood A., Tyler R., 2008a. Postorogenic origin of the stratiform Cu mineralization at Lufukwe, Lufilian Foreland, Democratic Republic of Congo. *Economic Geology*, 103, 555-582.

El Desouky H., Muchez P., Tyler R., 2008b. The sandstone-hosted stratiform copper mineralization at Mwitapile and its relation to the mineralization at Lufukwe, Lufilian foreland, Democratic Republic of Congo. *Ore Geology Reviews*, 34, 4, 561-579.

Fleischer V.D., Garlick W.G., Haldane R., 1976. Geology of the Zambian Copperbelt; Chapter 6. In: K.H. Wolf (ed.), Handbook of strata-bound and stratiform ore deposits – II Regional studies and specific deposits, Vol. 6, Amsterdam, The Netherlands, 223-352.

François A., 1974. Stratigraphie, tectonique et minéralisations dans l'Arc cuprifère du Shaba (République du Zaïre). In: Bartholomé P. (ed.). Gisements stratiformes et provinces cuprifères. Centenaire de la Société Géologique de Belgique, Liège, 79-101.

François A., 1995. Problèmes relatifs au Katanguien du Shaba. In: M. Wendorff and L. Tack (eds.), Late Proterozoic Belts in Central and Southwest Africa. Annales Sciences Géologiques Musée Royal de l'Afrique Centrale, Tervuren, Belgique, 101, 1-20.

Garlick W.G., 1953. Reflections on prospecting and ore genesis in Northern Rhodesia. *Transactions of the Institution of Mining and Metallurgy*, London, 63, 9-20.

Garlick W.G., 1961a. Ore genesis: The syngenetic theory. In: The geology of the Northern Rhodesian Copperbelt, (ed. F. Mendelsohn), Macdonald, London, 146-165.

Garlick W.G., 1961b. General Geology, Muva System. In: The geology of the Northern Rhodesian Copperbelt, (ed. F. Mendelsohn), Macdonald, London, 21-30.

Garlick W.G., 1961c. Structural evolution of the Copperbelt. In: The geology of the Northern Rhodesian Copperbelt, (ed. F. Mendelsohn), Macdonald, London, 89-105.

Garlick W.G., 1961d. Chambishi-Nkana Basin. In: F. Mendelsohn (ed.), The geology of the Northern Rhodesian Copperbelt. MacDonald, London, 281-342.

Garlick W.G., 1989. Genetic interpretation from ore relations to algal reefs in Zambia and Zaire. In: Sediment-hosted stratiform copper deposits, (eds. R.W. Boyle, A.C. Brown, C.W. Jefferson, E.C. Jowett, R.V. Kirkham), Geological Association of Canada Special Paper 36, 471-498.

Garlick W.G. and Brummer J.J., 1951. The age of the granites of the Northern Rhodesian Copperbelt. *Economic Geology*, 46, 478-497.

Garlick W.G. and Fleischer V.D., 1972. Sedimentary environment of Zambian copper deposition. *Geologie en Mijnbouw*, 51, 3, 277-298.

Garven G. and Raffensperger J.P., 1997. Hydrogeology and geochemistry of ore genesis in sedimentary basins. In: Geochemistry of hydrothermal ore deposits (ed. H.L. Barnes), John Wiley & Sons, New York, (3rd edition), 125 - 189.

Geological Survey of Japan, 2005. Atlas of Eh - pH diagrams. Intercomparison of thermodynamic databases. Geological Survey of Japan, Open File Report No. 419, National Institute of Advanced Industrial Science and Technology, Takeno, 285pp.

Goldstein R.H., 2001. Fluid inclusions in sedimentary and diagenetic systems. *Lithos*, 55, 159-193.

Goldstein R.H. and Reynolds T.J., 1994. Systematics of fluid inclusions in diagenetic minerals. SEPM (Society for Sedimentary Geology) Short Course, 31, 199p.

Gray A., 1930. The correlation of the ore-bearing sediments of the Katanga and Rhodesian copper belt. *Economic Geology*, 25, 783-804.

Gray A., 1932. The Mufulira copper deposit, Northern Rhodesia. *Economic Geology*, 27, 315-343.

Greyling L.N., Robb L.J., Master S., Boiron M.C., Yao, Y., 2005. The nature of early basinal fluids in the Zambian Copperbelt: A case study from the Chambishi deposit. *Journal of African Earth Sciences*, 42, 159-172.

Günther D. Frischknecht R., Heinrich C.A., Kahlert H.J., 1997. Capabilities of an Argon Fluoride 193 nm Excimer laser for laser ablation inductively coupled plasma mass spectrometry microanalysis of geological materials. *Journal of Analytical Atomic Spectrometry*, 12, 939-944.

Günther D., Audétat A., Frischknecht R., Heinrich C.A., 1998. Quantitative analysis of major, minor and trace elements in fluid inclusions using laser ablation-inductively coupled plasma mass spectrometry. *Journal of Analytical Atomic Spectrometry*, 13, 263-270.

Hanson R.E., Wardlaw M.S., Wilson T.J., Mwale G., 1993. U-Pb zircon ages from the Hook Granite Massif and Mwembeshi dislocation: constraints on Pan-African deformation, plutonism, and transcurrent shearing in central Zambia. *Precambrian Research*, 63, 189-209.

Hardie L.A. and Eugster H.P., 1970. The evolution of closed-basin brines. Mineralogical Society of America, Special Paper, 3, 273-290.

Harris C. and Erlank A.J., 1992. The production of large-volume, low delta ^{18}O rhyolites rifting of Africa and Antarctica; the Lebombo Monocline, Southern Africa. *Geochimica et*

Cosmochimica Acta, 56, 3561-3570.

Harris C., Johnstone W.P., Phillips D., 2002. Petrogenesis of the Mesozoic Sistefjell syenite intrusion, Dronning Maud Land, Antarctica and surrounding low-δ^{18} O lavas. *South African Journal of Geology*, 105, 205-226.

Harris C., Pronost J.J.M., Ashwal L.D., Cawthorn G., 2005. Oxygen and hydrogen isotope stratigraphy of the Rustenburg Layered Suite, Bushveld Complex: Constraints on crustal contamination. *Journal of Petrology*, 46 (3), 579-601.

Heijlen W., Muchez Ph., Banks, D.A., 2001. Origin and evolution of high salinity, Zn-Pb minearlising fluids in the Variscides of Belgium. *Mineralium Deposita*, 36, 165-176.

Heine G.W., 1986. A controlled study of some two-dimensional interpolation methods. *COGS Computer Contributions*, 3, 2, 60-72.

Hoefs, J., 1997. Stable isotope geochemistry (4th ed.) Springer, Berlin, 201p.

Hollister L.S. and Burress R.C., 1976. Phase equilibria in fluid inclusions from the Khtada Lake metamorphic complex. *Geochimica et Cosmochimica Acta*, 40, 163-175.

Horita J., Wesolowski D. J., Cole D.R., 1993. The activity-composition relationship of oxygen and hydrogen isotopes in aqueous solutions. I. Vapor-liquid water equilibrium of single salt solutions from 50 to 100 °C. *Geochimica et Cosmochimica Acta*, 57, 2797-2817.

Hitzman M., Kirkham R., Broughton D., Thorson J., Selley D., 2005. The sediment-hosted stratiform copper ore system. *Economic Geology 100th Anniversary Volume*, 609-642.

Huizenga J.-M., 2001. Thermodynamic modelling of C-O-H fluids. *Lithos*, 55, 101-114.

Huizenga J.M., and Touret J.L.R., 1999. Fluid inclusions in shear zones: The case of the Umwindsi shear zone in the Harare-Shamva-Bindura greenstone belt, NE Zimbabwe. *European Journal of Mineralogy*, 11, 1079-1090.

Jackson M.P.A, Warin O.N., Woad G.M., Hudec M.R., 2003. Neoproterozoic allochthonous salt tectonics during the Lufilian orogeny in the Katangan Copperbelt, central Africa. *Geological Society of America Bulletin*, 115, 3, 314-330.

Jordaan J., 1961. Nkana. In: F. Mendelsohn (ed.), The geology of the Northern Rhodesian Copperbelt. MacDonald, London, 297-328.

John T., Schenk V., Mezger K., Tembo F., 2004. Timing and PT evolution of whiteschist metamorphism in the Lufilian Arc-Zambezi Belt Orogen (Zambia): Implications for the assembly of Gondwana. *Journal of Geology*, 112, 71-90.

Journel A.G. and Huijbreghts C., 1978. Mining Geostatistics, Academic Press, 600pp.

Jowett E.C. 1989. Effects of continental rifting on the location and genesis of stratiform copper-silver deposits. In: Sediment-hosted stratiform copper deposits, (eds. R.W. Boyle, A.C. Brown, C.W. Jefferson, E.C. Jowett, R.V. Kirkham), Geological Association of Canada Special Paper 36, 53-66.

Kamona A.F., 1993. The Carbonate-hosted Kabwe Pb-Zn Deposit, Central Zambia. PhD thesis, Mitteilungen zur Mineralogie und Lagerstättenlehre, RWTH Aachen, 207p.

Kampunzu A.B., Cailteux J.L.H., Moine B., Loris H.N.B.T., 2005. Geochemical characterisation, provenance, source and depositional environment of 'Roches Argilo-Talqueses (RAT) and Mines Subgroups sedimentary rocks in the Neoproterozoic Katangan Belt (Congo): Lithostatigraphic implications. *Journal of African Earth Sciences*, 42, 119-133.

Kampunzu A.B., and Cailteux J.L.H.,

Kampunzu A.B., Wendorff M., Kruger F.J., Intiomale M.M., 1998. Pb isotopic ages of sediment-hosted Pb-Zn mineralisation in the Neoproterozoic Copperbelt of Zambia and Democratic Republic of Congo (ex-Zaire): re-evaluation and implications. *Chronique de la Recherche Minière*, 530, 55-61.

Kelly W.C. and Nishioka G.K., 1985. Precambrian oil inclusions in late veins and the role of hydrocarbons in copper mineralization at White Pine, Michigan. Geology, 13, 334-337.

Key R.M., Liyungu A.K., Njamu F.M., Somwe V., Banda J., Mosley P.M., Armstrong R.A., 2001. The western end of the Lufilian arc in NW Zambia and its potential for copper deposits. *Journal of African Earth Sciences*, 33, 503-528.

Killops S.D., and Killops V.J., 1993. An introduction to organic geochemistry. Longman Geochemistry Series, USA, 265p.

Kirkham R.V., 1989. Distribution, settings, and genesis of sediment-hosted stratiform copper deposits. In: Boyle R.W., Brown A.C., Jefferson C.W., Jowett E.C., Kirkham R.V. (eds.), Sediment-hosted stratiform copper deposits, Geological Association of Canada Special Paper 36, p. 3-38.

Kvenvolden K.A., and Roedder E., 1971. Fluid inclusions in quartz crystals from South-west Africa. *Geochimica et Cosmochimica Acta*, 35, 1209-1229.

Lapidus D.F., 1990. Dictionary of Geology. (eds. I. Winstanley). Collins, London, 565p.

Lefebvre J.J., 1978. Le Groupe de Mwashya megacycloteme terminal du Roan (Shaba, Zaire Sud-Oriental): l'approche stratigraphique et étude de l'environnement sédimentaire. *Annales de la Société géologique de Belgique*, 101, 209-225.

Leroy J., 1979. Contribution a l'étalonnage de la pression interne des inclusions fluides lors de leur décrépitation. Bulletin de Mineralogy., 120, 584-593.

Lerman A., 1970. Chemical equilibria and evolution of chloride brines. Mineralogical Society of America, Special Paper, 3, 291-306.

Ligang Z., Jingxiu L., Huanbo Z., Zhensheng C., 1989. Oxygen isotope fractionation in the quartz-water-salt system. *Economic Geology*, 84, 1643-1650.

Linke W.F., 1965. Solubilities, inorganic and metal-compounds. Vol. II, American Chemical Society, 1914p.

Marshall D.J., 1988. Cathodoluminescence of geological materials. Unwin Hyman, Boston, Massachusetts, 146p.

Master S., Rainaud C., Armstrong R.A., Phillps D., Robb L.J., 2002. Contributions to the geology and mineralization of the Central African Copperbelt: II. Neoproterozoic deposition of the Katanga Supergroup with implications for regional and global correlations. Geocongress-IAGOD Joint Meeting. Extended Abstracts (CD-ROM), Windhoek, Nambia, 5pp.

Master S., Rainaud C., Armstrong R.A., Phillips D., Robb L.J., 2005. Provenance ages of the Neoproterozoic Katanga Supergroup (Central African Copperbelt), with implications for basin evolution. *Journal of African Earth Sciences*, 42, 41-60.

Matsuhisa Y., Goldsmith J.R., Clayton R.N., 1979. Oxygen isotopic fractionation in the system quartz-albite-anorthite-water. *Geochimica et Cosmochimica Acta*, 43, 1131-1140.

Mauk J.L., Kelly W.C., van der Pluijm B.A., Seasor R.W., 1992. Relations between deformation and sediment-hosted copper mineralization: evidence from the White Pine part of the Midcontinent rift system. *Geology*, 20, 427 - 430.

Mavrogenes J.A., and Bodnar R.J., 1994. Hydrogen movement into and out of fluid inclusions in quartz: experimental evidence and geologic implications. *Geochimica et Cosmochimica Acta*, 58, 141-148.

Mbendi (2005). http://www.mbendi.co.za/indy/ming/cppr/af/zr/p0005.htm

McGowan R.R., 2003. The origin of the Nchanga copper-cobalt deposits of the Zambian Copperbelt. Unpublished PhD thesis, University of Southampton, 204p.

McGowan R.R., Roberts S., Foster R.P., Boyce A.J., Coller D., 2003. Origin of the copper-cobalt deposits of the Zambian Copperbelt: an epigenetic view from Nchanga. *Geology*, 31, 6, 497-500.

McGowan R.R., Roberts S., Boyce A.J., 2006. Origin of the Nchanga copper-cobalt deposits of the Zambian Copperbelt. *Mineralium Deposita*, 40, 617-638.

McKinnon D.M., and Smit N.J., 1961. Nchanga. In: Mendelsohn F. (ed.), The geology of the Northern Rhodesian Copperbelt. MacDonald, London, 234-274.

Mendelsohn F., 1961a. Katanga system. In: Mendelsohn F. (ed.), The geology of the Northern Rhodesian Copperbelt. MacDonald, London, 41-54.

Mendelsohn 1961b. Metamorphism. In: Mendelsohn F. (ed.), The geology of the Northern Rhodesian Copperbelt. MacDonald, London, 106-116.

Mendelsohn 1961c. Ore deposits. In: Mendelsohn F. (ed.), The geology of the Northern Rhodesian Copperbelt. MacDonald, London, 117-129.

Mernagh T.P. and Wilde A.R., 1989. The use of the later Raman microprobe for the determination of salinity in fluid inclusions. *Geochimica et Cosmochimica Acta*, 53, 765-771.

Muchez Ph., Vanderhaeghen P., El Desouky H., Schneider J., Boyce, A., Dewaele S., Cailteux J., 2008. Anhydrite pseudomorphs and the origin of stratiform Cu-Co ores in the Katangan Copperbelt (Democratic Republic of Congo). *Mineralium Deposita*, 43, 575-589.

Oakes C.S., Bodnar R.J., Simonson J.M., 1990. The system NaCl-$CaCl_2$-H_2O: I. The ice liquidus at 1 atm. total pressure. *Geochimica et Cosmochimica Acta*, 54, 603-610.

Ohba T., Kazahaya K., Matsuo S., 1995. Diffusional ^{18}O loss from inclusion water in a natural hydrothermal quartz form the Kaneuchi tungsten deposit, Japan. *Geochimica et Cosmochimica Acta*, 59, 14, 3039-3047.

Ohmoto H., and Goldhaber M.B., 1997. Sulphur and carbon isotopes. In: Barnes H.L. (ed.). Geochemistry of hydrothermal ore deposits. John Wiley and Sons, 517 - 611.

Ohmoto H. and Lasaga A.C., 1982. Kinetics of reactions between aqueous sulfates and sulfides in hydrothermal systems. *Geochimica et Cosmochimica Acta*, 46, 1727 - 1745.

Oliver M.A., 1990. Kriging: A method of interpolation for Geographical Information Systems. *International Journal of Geographic Information Systems*, 4, 313-332.

Pagel M., Barbin V., Blanc P., Ohnenstetter D. (eds.) 2000. Cathodoluminescence in Geosciences. Springer. Berlin. 514p.

Pirmolin J., 1970. Inclusions fluids dans la dolomite du Gisement stratiforme de Kamoto (Katanga Occidental). *Annales de la Société Géologique de Beligique* T.93, 397-406.

Porada H., 1989. Pan-African rifting and orogenesis in southern to Equatorial Africa and Eastern Brazil. *Precambrian Research*, 44, 103-136.

Rainaud C., Master S., Robb L.J., 1999. A fertile Palaeoproterozoic magmatic arc beneath the Central African Copperbelt. In: C.J. Stanley et al. (eds), Mineral Deposits: Processes to

Processing . Proceedings of the Fifth Biennial SGA Meeting and the Tenth Quadrennial IAGOD symposium, London, 22-25 August 1999, 1427-1430.

Rainaud C., Armstrong R.A., Master S., Robb L.J., Mumba P.A.C.C, 2002. Contributions to the geology and mineralization of the Central African Copperbelt: I. Nature and geochronology of the pre-Katangan basement. Geocongress-IAGOD Joint Meeting. Extended Abstracts (CD-ROM), Windhoek, Nambia, 5pp.

Rainaud C., Master S., Armstrong R.A., Robb L.J., 2003. A cryptic Mesoarchaean terrane in the basement to the Central African Copperbelt. *Journal of the Geological Society*, London 160, 11-14.

Rainaud C., Master S., Armstrong R.A., Robb L.J. 2005a. Geochronology and nature of the Palaeoproterozoic basement in the Central African Copperbelt (Zambia and the Democratic Republic of Congo), with regional implications. *Journal of African Earth Sciences*, 42, 1-31.

Rainaud C., Master S., Armstrong R.A., Phillips D., Robb L.J. 2005b. Monazite U-Pb dating and 40Ar-39Ar thermochronology of metamorphic events in the Central African Copperbelt during the Pan-African Lufilian Orogeny. *Journal of African Earth Sciences*, 42, 183-199.

Raybold J.G., 1978. Tectonic controls on Proterozoic stratiform copper mineralization. *Transactions of the Institution of Mining and Metallurgy*, 87, B79-B86.

Rice A.H.N., Halverson G.P., Hoffman P.F., 2003. Three for the Neoproterozoic: Sturtian, Marinoan and Varangerian glaciations. *Geophysical Research Abstracts*, 5, 11425.

Richards J.P., Krogh T.E., Spooner E.T.C., 1988a. Fluid inclusion characteristics and U-Pb Rutile age of late hydrothermal alteration and veining at the Musoshi stratiform copper deposit, Central African Copper Belt, Zaire. *Economic Geology*, 83, 118-139.

Richards J.P., Cumming G.L., Kristic D., Wagner P.A., Spooner E.T.C., 1988b. Pb isotope constraints on the age of sulphide ore deposition and U-Pb age of late uraninite veining at the Musoshi stratiform copper deposit, Central African Copperbelt, Zaire. *Economic Geology*, 83, 724-741.

Rickard D.T., 1974. Low temperature copper geochemistry: Gitological aspects. In: Bartholomé P. (ed.). Gisements stratiformes et provinces cuprifères. Centenaire de la Société Géologique de Belgique, Liège, 1-34.

Ridley J., 1993. The relations between mean rock stress and fluid flow in the crust: with reference to vein- and lode-style gold deposits. *Ore Geology Reviews*, 8, 23-37.

Ripley E.M., and Ohmoto H., 1977. Oxygen and hydrogen isotopic studies of ore deposition and metamorphism at the Raul mine, Peru. Geochimica et Cosmochimica Acta, 43, 1633-1643.

Robb L.J., 2005. Introduction to ore-forming processes. Blackwell Publishing, Oxford, UK, 373p.

Robb L.J., Master S., Armstrong R., Rainaud C., Greyling L., 2003. Timing of Cu-Co and Pb-Zn mineralization in the Central African Copperbelt: a link to Neoproterozoic glaciations? Transactions of the Institute of Mining and Metallurgy, 112, 2, 164-166.

Robert M., 1956. Géologie et géographie du Katanga - L'étude des ressources et de la mise en valeur. Hayez, Bruxelles, 620p.

Roedder E., 1972. Composition of fluid inclusions. US Geological Survey Professional Paper, 440JJ. 164p.

Roedder E., 1984. Fluid inclusions. *Reviews in Mineralogy*, 12, Mineralogical Society of America, 646p.

Roedder E., and Bodnar R.J., 1980. Geological pressure determinations form fluid inclusion studies. *Annual Reviews of Earth and Planetary Sciences*, 8, 263-301.

Rosasco G.J., and Roedder E., 1979. Application of a new Raman microprobe spectrometer to non-destructive analysis of sulfate and other ions in individual phases in fluid inclusions in minerals. *Geochimica et Cosmochimica Acta*, 43, 1907-1915.

Rose A.W., 1976. The effect of cuprous chloride complexes in the origin of red bed copper and related deposits. Economic Geology, 71, 1036-1048.

Rose A.W., 1989. Mobility of copper and other heavy metals in sedimentary environments. In: Boyle R.W., Brown A.C., Jefferson C.W., Jowett E.C., Kirkham R.V. (eds.), Sediment-hosted stratiform copper deposits, Geological Association of Canada Special Paper 36, 97-110.

Royle A.G., Clausen F.L., Frederiksen P., 1986. Practical Universal Kriging and Automatic Contouring. *Geoprocessing*, 1, 377-394.

Rye R.O., and O'Neil, J.R., 1968. The O^{18} content of water in primary fluid inclusions from Providencia, north-central Mexico. *Economic Geology*, 63, 232-238.

Sawyer E.W., and Robin P.-Y.F., 1986. The subsolidus segregation of layer-parallel quartz-feldspar veins in greenschist to upper amphibolites facies metasediments. *Journal of Metamorphic Geology*, 4, 237-260.

Schiffries C.M., 1989. Liquid-absent aqueous fluid inclusions and phase equilibria in the system $CaCl_2$-$NaCl_2$-H_2O. *Geochimica et Cosmochimca Acta*, 54, 611-619.

Schneider J., Melcher F., Brauns M., 2007. Concordant ages for the giant Kipushi base metal deposit (DR Congo) from direct Rb-Sr and Re-Os dating of sulfides. *Mineralium Deposita*, 42, 791-797.

Schneiderhöhn H., 1932. The geology of the Copperbelt, Northern Rhodesia. Mining Magazine, London, 46, 241-245.

Schwellnus J.E.G., 1961. Bancroft. In: Mendelsohn F. (ed.), The geology of the Northern Rhodesian Copperbelt. MacDonald, London, 214-234.

Selley D., Broughton D., Scott R., Hitzman M., Bull S., Large R., McGoldrick P., Croaker M., Pollington N., Barra F., 2005. A new look at the geology of the Zambian Copperbelt. In: J.W. Hedenquist, J.F.H. Thompson, R.J. Goldfarb, J.P. Richards (eds.), *Economic Geology 100th Anniversary Volume*, 100, 965-1000.

Seward T.M. and Barnes H.L., 1997. Metal transport by hydrothermal ore fluids. In: Geochemistry of hydrothermal ore deposits (ed. H.L. Barnes), John Wiley & Sons, New York, (3rd edition), 435 - 486.

Shepherd T.J., Rankin A.H., Alderton D.H.M., 1985. A practical guide to fluid inclusion studies. Blackie, Glasgow, 235p.

Shepherd T.J., and Chenery S.R., 1995. Laser ablation ICP-MS elemental analysis of individual fluid inclusions: an evaluation study. Geochimica et Cosmochimica Acta, 59, 19, 3997-4007.

Simon K., 2001. Does δD from fluid inclusion in quartz reflect the original hydrothermal fluid? *Chemical Geology*, 177, 483-495.

Speiser A., Hein U.F., Porada H., 1995. The Kansanshi copper mine (Solwezi area, northwestern Zambia): Geology, wall-rock alteration and fluid inclusions. Pasava J., Kribek B., and Zak K. (eds)., Mineral Deposits: From their origin to their environmental impacts, A.A. Balkema, Rotterdam, 389-392.

Sterner S.M. and Bodnar R.J., 1991. Synthetic fluid inclusions. X: Experimental determination of P – V – T – X properties in the CO_2 – H_2O system to 6 kbar and 700 °C. *American Journal of Science*, 291, 1-54.

Sterner S.M., Hall D.L., Bodnar R.J., 1988. Synthetic fluid inclusions. V. Solubility relations in the system NaCl-KCl-H_2O under vapour-saturated conditions. *Geochimica et Cosmochimica. Acta*, 52, 989-1006.

Sweeney M., 1987. The use of fluid inclusion geochemistry in determining the origin of veins, examples from the Zambian Copperbelt. Zambian Journal of Applied Earth Sciences 1, 18-28.

Sweeney M.A., and Binda P.L., 1994. Some constraints on the formation of the Zambian Copperbelt deposits. *Journal of African Earth Sciences*, 19, 4, 303-313.

Sweeney M.A., Binda P.L., Vaughan D.J., 1991. Genesis of the ores of the Zambian Copperbelt. *Ore Geology Reviews*, 6, 51-96.

Taylor, H.P., (1997). O and H isotope relationships in hydrothermal mineral deposits. In: H.L. Barnes (ed.), Geochemistry of Hydrothermal Ore Deposits. John Wiley and Sons, 229-302.

Thiéry R., Van den Kerkhof A.M., Dubessy J., 1994. υX properties of CO2-CH4-N2 fluid inclusions: modelling for T < 31 °C and P < 400 bars. *European Journal of Mineralogy*, 6, 47-55.

Torrealday H.I., Hitzman M.W., Stein H.J., Markey R.J., Armstrong R., Broughton D., 2000. Re-Os and U-Pb dating of the vein-hosted mineralization at the Kansanshi copper deposit, northern Zambia. *Economic Geology*, 95, 1165-1170.

Touret J.L.R., 1994. Fluid inclusions in sedimentary and digenetic environments. In De Vivo, B. and Frezzotti, M.L. (eds.) Short Course of the Working Group (IMA) Fluid inclusions in minerals: Methods and Applications. Pontignano, Sienna, 1-4 September, 251 - 269.

Touret J.L.R., 2001. Fluids in metamorphic rocks. *Lithos*, 55, 1-25.

Turekian K.K., 1968. Oceans (Foundations of Earth Science). Prentice-Hall, 120p.

Ulrich T., Günther D., Heinrich C.A., 2001. The evolution of a porphyry Cu-Au deposit based on LA-ICP-MS analysis of fluid inclusions: Bajo de la Alumbrera, Argentina. *Economic Geology*, 96, 1743-1774.

Unrug R., 1988. Mineralization controls and source of metals in the Lufilian fold belt, Shaba (Zaire), Zambia and Angola. *Economic Geology*, 83, 1247-1258.

Van den Kerkhof A.M., 1990. Isochoric phase diagrams in the systems CO_2 - CH_4 and CO_2 - N_2: Application to fluid inclusions. *Geochimica et Cosmochimica Acta*, 54 (3), 621-629.

Van den Kerkhof A.M., and Hein U.F., 2001. Fluid inclusion petrography. *Lithos*, 55, 27-47.

Van den Kerkhof A., and Thiéry R., 2001. Carbonic inclusions. *Lithos*, 55, 49-68.

Van den Kerkhof F. and Thiéry R., 1994. Phase transitions and density calculation in the CO2-CH4-N2 system. In De Vivo, B. and Frezzotti, M.L. (eds.) Short Course of the Working Group (IMA) Fluid inclusions in minerals: Methods and Applications. Pontignano, Sienna, 1-4 September, 171-190.

Van Hinsberg M.G.E., Verbrugge R., Schouten J.A., 1993. High temperature – high pressure experiments on H_2O-N_2. *Fluid Phase Equilibria*, 88, 115-121.

Vennemann T.W. and O'Neil J.R., 1993. A simple and inexpensive method of hydrogen isotope and water analyses of minerals and rocks based on zinc reagent. *Chemical Geology* (Isotope Geosci), 103, 227-234.

Vennemann T.W. and Smith H.S., 1990. The rate and temperature of reaction of ClF_3 with silicate minerals, and their revelance to oxygen isotope analysis. *Chemical Geology*, 86, 83-88.

Vink B.W., 1996. Stability relations of antimony and arsenic compounds in the light of revised and extended Eh-pH diagrams. *Chemical Geology*, 130, 21-30.

Vityk M.O., Krouse H.R., Demihov Y.N., 1993. Preservation of $\delta^{18}O$ values of fluid inclusion water in quartz over geological time in an epithermal environment: Beregov deposit, Transcarpathia, Ukraine. *Earth and Planetary Science Letters*, 119, 561-568.

Wakefield J., 1978. Samba: a deformed porphyry-type copper deposit in the basement of the Zambian Copperbelt. *Transactions of the Institution of Mining and Metallurgy*, 87, B43-B52.

Walraven F., and Rumvegeri B., 1983. Implications of whole-rock Pb-Pb and zircon evaporation dates for the early metamorphic history of the Kasai craton, Southern Zaire. *Journal of African Earth Sciences*, 16, 395-404.

Wendorff M., 2000a. Revision of the stratigraphic position of the "Roches Argilo-talqueuses" (R.A.T.) in the Neoproterozoic Katangan Belt, south Congo. *Journal of African Earth Sciences*, 30, 717-726.

Wendorff M., 2000b. New elements and implications of tectonic stratigraphy within the foreland of the Pan-African Katangan belt, central Africa. *Journal of African Earth Sciences*, 30, 87.

Wendorff M., 2002. Stratigraphic position of Cu-Co mineralized allochthonous megablocks in foreland successions of the Katangan external fold-thrust region: new criteria for mineral exploration. 11th IAGOD Symposium and Geocongress 2002, Extended Abstracts on CD-ROM, Geological Survey of Nambia, Windhoek, Namibia, 6pp.

Wendorff M., 2003. Stratigraphy of the Fungurume Group – evolving foreland basin succession in the Lufilian fold-thrust belt, Neoproterozoic-Lower Palaeozoic, Democratic Republic of Congo. *South African Journal of Geology*, 106, 17-34.

Wendorff M., 2005. Evolution of Neoproterozoic-Lower Palaeozoic Lufulian arch, Central Africa: a new model based on syntectonic conglomerates. *Journal of the Geological Society*, London, 162, 5-8.

West I., 1973. Vanished evaporites – significance of strontium minerals. *Journal of Sedimentary Petrology*, 43,1, 278-279.

Williams-Jones A.E., and Samson I.M., 1990. Theoretical estimation of halite solubility in the system NaCl - $CaCl_2$ - H_2O: applications to fluid inclusions. *Canadian Mineralogist*, 28, 299-304.

Wilkins R.W.T., 1979. Formation, modification and destruction of fluid inclusions. Notes for fluid inclusion workshop. Dept. Geol., La Trobe University, La Trobe, Bundoora, Victoria, Australia, Feb, 1979.

White S., 1973. Dislocations and bubbles in vein quartz. Nature, Phys. Sci., 243, 11-14.

Wood S.A., 1998. Calculation of activity-activity and log fO_2 – pH diagrams. *Reviews in Economic*

Geology, 10, 81-96.

Yardley B.W.D., 2005. Metal concentrations in crustal fluids and their relationship to ore formation. *Economic Geology, 100th Anniversary Special Paper,* 100, 4, 613-632.

Zhang Y.F., and Frantz J.D., 1987. Determination of the homogenisation temperatures and densities of supercritical fluids in the system NaCl - KCl - $CaCl_2$ - H_2O using synthetic fluid inclusions. *Chemical Geology*, 64, 335-350.

Appendix I

List of Samples

- Chambishi
- Nchanga
- Mufulira
- Nkana
- Konkola

Chambishi deposit samples

Sample	Description
Open Pit	
CBS-os1	Ore shale and quartz-sulfide (Ccp, Bn)-carbonate (dolomite) veins along boundary
CBS-os2	Grey ore shale
CBS-os3	Grey/green ore shale with disseminated sulfides (Cp, Bn, Py) along micro-scale layers
CBS-qz1	Lateral secretion quartz vein with disseminated sulfides (Cp, Bn) in ore shale
CBS-qz2	Lateral secretion quartz vein with disseminated sulfides (Cp, Bn) in ore shale
CBS-qz3	Lateral secretion quartz vein with disseminated sulfides (Cp, Bn) in ore shale
CBS-qz4	Lateral secretion quartz vein with disseminated sulfides (Cp, Bn) in ore shale
CBS-qz5	Lateral secretion quartz vein with disseminated sulfides (Cp, Bn) in ore shale
CBS-qz6	Lateral secretion quartz vein with disseminated sulfides (Cp, Bn) in ore shale
CBS-qz7	Lateral secretion quartz vein with disseminated sulfides (Cp, Bn) in ore shale
CBS-qz8	Lateral secretion quartz vein with disseminated sulfides (Cp, Bn) in ore shale
CBS-qz9	Lateral secretion quartz vein with disseminated sulfides (Cp, Bn) in ore shale
CBS-qz10	Lateral secretion quartz vein with disseminated sulfides (Cp, Bn) in ore shale
CBS-qz11	Lateral secretion quartz vein with disseminated sulfides (Cp, Bn) in ore shale
CBS-qz12	Lateral secretion quartz vein with disseminated sulfides (Cp, Bn) in ore shale
CBS-qz13	Lateral secretion quartz vein with disseminated sulfides (Cp, Bn) in ore shale
CHM-1	Ore Shale (not in situ) found at same locality as samples 2-4.
CHM-2	Quartz-vein with some mineralisation. Strike (strata): 257°, dip direction: 181°, cleavage: 20° into south, dip of quartz vein: 90°. Samples A and B are of quartz vein.
CHM-3	Host around quartz vein immediately to right of vein. Looking west (270°) in open pit. Fold.
CHM-4	Mineralised ore shale
CHM-5A	Ore shale with bedding parallel quartz, bornite, and malachite. Dip 21° in 157° direction, strike 261°
CHM-5B	Ore shale with bedding parallel quartz, bornite, and malachite. Dip 21° in 157° direction, strike 261°
CHM-5C	Ore shale with bedding parallel quartz, bornite, and malachite. Dip 21° in 157° direction, strike 261°
CHM-5D	Ore shale with bedding parallel quartz, bornite, and malachite. Dip 21° in 157° direction, strike 261°
CHM-6	Bornite and quartz in host (sample not in situ?)
CHM-7A	Quartz-(calcite?) vein bedding parallel in Hangingwall sediments. Not mineralised: hangingwall directly above Ore Shale
CHM-7B	Quartz-(calcite?) vein bedding parallel in Hangingwall sediments. Not mineralised: hangingwall directly above Ore Shale
CHM-7C	Quartz-(calcite?) vein bedding parallel in Hangingwall sediments. Not mineralised: hangingwall directly above Ore Shale
CHM-8A	Bornite in siltstone "Ore Shale" host. Picked up in E-N-E part of pit
CHM-8B	Bornite in siltstone "Ore Shale" host. Picked up in E-N-E part of pit
CHM-9	Bornite with alteration in siltstone "Ore Shale" host. Picked up in E-N-E part of pit.
Drill Core (Kalulushi)	
RCB1A-1	Quartz vein with associated intergrown pyrite, drill core 623.40 - 623.45m
RCB2-1	Quartz vein with malachite staining, drill core 90.35 - 90.40m
RCB2-4	Quartz vein with pyrite, drill core 105.30 - 105.37m
RCB2-8	Finely laminated, drill core 525.20 - 525.25m
RCB2-9	Pyrite in quartz in silty-arenitic unit. Minor calcite around pyrite. drill core 527.83 - 527.90m
RCB2-10	Quartz with one grain of ccp in well-sorted qtz-arenite, anhydrite. drill core 572.70 - 572.74m
RCB2-11	Anhydrite-carbonate, drill core 930.84 - 930.64m
NN75-1	Anhydrite-carbonate in quartzose dolomite, drill core 570.45 - 570.54m
NN75-2	Anhydrite replacing siltstone-greenschist, drill core 625.70 - 625.76m
NN75-3	Anhydrite lined by black hydrocarbons in dewatering texture, drill core 772.94 - 773.0m
NN75-4	Anhydrite-carbonate-quartz vein in greenschist metasediments, drill core 869.60 - 869.74m

Chambishi – samples

	Figure II.2.1. Lateral secretion quartz vein from the Chambishi open pit where pre-tectonic and syn-tectonic fluids were sampled from primary and secondary fluid inclusions
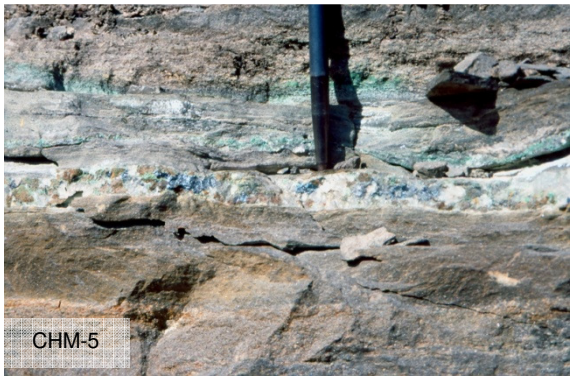	Figure II.2.2. Bedding-parallel quartz vein in the hangingwall sediments of the Chambishi open pit. These samples yielded mostly secondary fluid inclusion planes which were interpreted as representative of syn-tectonic fluids.
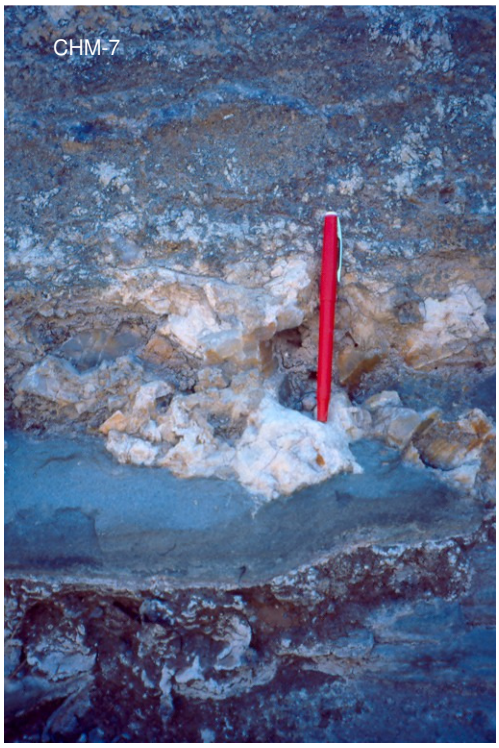	Figure II.2.3. Quartz-carbonate vein in the hangingwall sediments in the Chambishi open pit where syn-tectonic fluids were sampled in primary and secondary fluid inclusions.

Nchanga deposits samples

Sample	Description
Nchanga Open Pit	
NOP1	Lower Banded Shale with pyrite disseminations parallel to laminations. Very carbonaceous, black carbon/hydrocarbons. Not mineralised. Lower OreBody.
NOP2	Lower Banded Shale with pyrite disseminated parallel to bedding.
NOP3	Transition Arkose. Lower OreBody, mineralised with malachite, azurite (maybe chalcocite?)
NOP4	Arkose, unmineralised, authigenic quartz
NOP5	Pink Quartzite with underlying Shale Marker (SM). Unmineralised
NOP6	Pink Quartzite. No apparent mineralisation, but may contain some disseminated chalcocite: see with thin section.
NOP7	Pink Quartzite. Mineralised with malachite.
NOP8	Banded Sandstone Upper (BSSU). Cupriferous mica (vermiculite?). Syn-tectonic quartz vein in schist. Foliation bends around qtz.
NOP9	BSSU. Vermiculite & quartz, ?fold
NOP10	BSSU. Mineralised, but extremely incompetent. Strong schistose foliation. Quartz grains present within schistose foliation.
NOP11	Mineralised TFQ (The Feldspathic Quartzite). Carrollite, bornite, malachite most commonly presented here in disseminated quantities in well sorted arenitic quartzite.
NOP12	Mineralised TFQ, mostly with malachite, but bornite is present in disseminated clusters (sparsely populated). Clean orthoquartzite.
NOP13	Matrix and pebbles above Nchanga Granite unconformity.
NOP14A-I	Orientated samples of vein quartz of sub-vertical quartz veins in Pink Quartzite. Veins are average 30cm thick. Quartz veins are restricted to Pink Quartzite, and becomes terminated by the overlying BSSU and underlying SM.
NOP15	Pink Quartzite, unmineralised (maybe some disseminated chalcocite). Directly adjacent to quartz vein sampled in NOP14.
NOP16	Mineralised TFQ, with disseminated carrollite, bornite, chalcopyrite parallel to possible original bedding planes. Fluids probably travelled along bedding planes during infiltration.
NOP17	Quartz vein in TFQ with remobilised bornite.
NOP18	Disseminated bornite in TFQ.
NOP19	Disseminated bornite clusters in TFQ.
NOP20	Quartz vein in TFQ, with remolised bornite. The contact between the vein and host TFQ is not distinct/sharp. Fluid seemingly percolates through TFQ along preferred original bedding planes.
NOP21	Bornite & carrollite as 'vein' or bedding parallel thick disseminations in TFQ. Bedding is barely visible in TFQ, but mineralisation shows parallel orientation.
NOP22	Carrollite focussed parallel along bedding planes in coarser grained quartzite grains. Fluid pathway easier to follow along coarser, more permeable layers in the TFQ. Disseminated mineralisation, also present in finer grained areas, but focus of carrollite in coarser qtz-grains areas.
NOP23	Carrollite disseminated in TFQ, + chalcopyrite
NOP24	Course-grained bornite in quartz infilling in TFQ. Silica-rich fluid seemed to have percolated through TFQ and remobilised? Mineralisation already present into concentrated areas.
NOP25	Bornite in TFQ. Disseminated clusters

Nchanga deposits samples (continue)

NCG-gr1	Grey coarse-grained biotite granite
NCG-os1	Black ore shale containing disseminated sulfides (py) from lower ore bed
NCG-os2	Black ore shale without visible disseminated sulfides (py) from lower ore bed
NCG-os3	Black ore shale without visible disseminated sulfides (py) from lower ore bed
NCG-os4	Black ore shale containing disseminated sulfides (py) from lower ore bed
NCG-os5	Black ore shale containing disseminated sulfides (py) from lower ore bed
NCG-os6	Black ore shale containing disseminated sulfides (py) from lower ore bed
NCG-dy1	Lamprophyre dyke
NCG-dy2	Lamprophyre dyke
NCG-dk3	Lamprophyre dyke
NCG-dy4	Lamprophyre dyke
NCG-dy5	Lamprophyre dyke
NCG-dy6	Lamprophyre dyke
NCG-tfq1	Quartzite containing disseminated sulfides (azurite, malachite) in upper ore bed
NCG-tfq2	Quartzite containing disseminated sulfides (azurite, malachite) in upper ore bed
NCG-tfq3	Quartzite containing disseminated sulfides (azurite, malachite) in upper ore bed
NCG-mq1	Mica-quartz from the shear zone ore bed, smoke and white quartz
NCG-mq2	Mica-quartz from the shear zone ore bed, smoke and white quartz
NCG-mq3	Mica-quartz from the shear zone ore bed, smoke and white quartz
NCG-mq4	Mica-quartz from the shear zone ore bed, smoke and white quartz
NCG-mq5	Mica-quartz from the shear zone ore bed, smoke and white quartz
NCG-mq6	Mica-quartz from the shear zone ore bed, smoke and white quartz (BSS)
NCG-mq7	Mica-quartz from the shear zone ore bed, smoke and white quartz (BSS)
NCG-mq8	Mica-quartz from the shear zone ore bed, smoke and white quartz (BSS)
NCG-mq9	Mica-quartz from the shear zone ore bed, smoke and white quartz (BSS)
NCG-mq10	Mica-quartz from the shear zone ore bed, smoke and white quartz (BSS)
NCG-mq11	Mica-quartz from the shear zone ore bed, smoke and white quartz (BSS). Euhedral qtz.
Nchanga underground, 'C' Shaft	
NCH-1	Quartz vein, Footwall Arkose 2120ft level, location: 2420 8E 9B #27
NCH-2	quartz vein crosscutting the Footwall Arkose. 2420 8E 9B FR13
NCH-3	Footwall Arkose, samples A and B. 2420 8E 10B FR14
NCH-4	Chalcocite in Transition Zone (LOB), samples A, B, and C 2420 8E 10B FR14
NCH-5	Azurite and minor chalcopyrite in Transition Zone. 2420 8E 10B FR14
NCH-6	Transition with cuprite & malachite, samples A, B, and C, 1820 10E 13B scraper drift
NCH-7	Transition mineralised with malachite. 1820 10E 13B FR5
NCH-8A	Lower Banded Shale (ore) with massive chalcopyrite, malachite, cuprite. 1820 10E 13B FR5
NCH-8B	Lower Banded Shale (ore) with massive chalcopyrite, malachite, cuprite.
NCH-9	Arkose ore 1820 10E 13B FR5
NCH-10	Arkose Footwall waste 1970 10E 4B FR5
NCH-11	Arkose ore 1970 10E 7A FR24
Nchanga underground, Chingola B portal	
CNB-1	Footwall Arkose just below mineralised Arkose (Lower Orebody)
CNB-2	Quartz vein with crysocolla in the qtz. Qtz-vein is bedding parallel and croscutting.
CNB-3.1	Chalcocite & quartz vein, Panel 5
CNB-3.2	Chalcocite & quartz vein, Panel 5
CNB-4	Chalcocite & quartz vein, Panel 5
CNB-5	Chalcocite & quartz vein, Panel 5
CNB-6	Crosscutting quartz vein with associated crysocolla. Panel 5, incline position
CNB-7	Crosscutting quartz vein with associated crysocolla. Panel 5, incline position
CNB-8	Crosscutting quartz vein with malachite & crysocolla, Panel 5, incline position

Nchanga deposits samples (continue)

535m level	
CNB-9	Crosscutitng quartz vein, strike: 279°, dip 74°, direction: 215° Panel 5, SD4 position
CNB-10	Quartz vein mostly parallel to bedding, also disseminated, sediments strike: 351°, dip: 10°, direction: 272° Malachite & crysocolla around qtz. Panel 5, SD4 position
CNB-11	Quartz vein mostly parallel to bedding, also disseminated, sediments strike: 351°, dip: 10°, direction: 272° Malachite & crysocolla around qtz. Panel 5, SD4 position
CNB-12A	Quartz vein mostly parallel to bedding, also disseminated, sediments strike: 351°, dip: 10°, direction: 272° Malachite & crysocolla around qtz. Panel 5, SD4 position
CNB-12B	Quartz vein mostly parallel to bedding, also disseminated, sediments strike: 351°, dip: 10°, direction: 272°
CNB-13	Quartz vein mostly parallel to bedding, also disseminated, sediments strike: 351°, dip: 10°, direction: 272° Malachite & crysocolla around qtz. Panel 5, SD4 position
CNB-14	Malachite-quartz, strike: 350° Panel 5, SD4 position
CNB-15	Chalcocite vein crosscutting the Arkose, strike of vein: 276°, dip: varies~70-90°, direction: 5° Panel 5, SD4 position
Drill Core	
NCG-781a	TFQ, redox boundary
NCG-781b	TFQ, redox boundary
NCG-781c	Dolomite, redox boundary
NCG-781d	Dolomite, redox boundary
NCG-781d	Ore shale, redox boundary
L128-1	White quartz veins, not mineralized, 43 m. Oblique Luano core. Through Footwall.
L128-2	White quartz veins, not mineralized, 98.3 m. Oblique Luano core, through Footwall
L128-3	White quartz veins, not mineralized, 159.5 m. Oblique Luano core, through Footwall
L128-4	White quartz veins, not mineralized, 171.9 m. Oblique Luano core, through Footwall
L128-5	White quartz veins, not mineralized, 172 m. Oblique Luano core, through Footwall
L128-6	White quartz veins, not mineralized, 217.8 m. Oblique Luano core, through Footwall

Mufulira deposit samples

Sample	Description
Mufulira underground: 7 Shaft (main shaft), 13 July 2001, 1140mLevel - 1240mLevel	
MUF-1	52C Mining Drive, 1140mL.Bedding parallel chalcopyrite & qtz & anhydrite vein in Footwall Quartzite of C-orebody. Samples strike: 299°, direction 40°N
MUF-2	52C Mining Drive, 1140mL.Bedding parallel chalcopyrite & qtz & anhydrite vein in Footwall Quartzite of C-orebody. Samples strike: 299°, direction 40°N
MUF-3	52C Mining Drive, 1140mL.Bedding parallel chalcopyrite & qtz & anhydrite vein in Footwall Quartzite of C-orebody. Samples strike: 299°, direction 40°N
MUF-4	Crosscutting qtz-ccp-carbonate vein in Lufubu Basement, same location as MUF1-3. Samples strike: 291°, vein angle: 53°
MUF-5 A	Disseminated mineralisation in Lufubu Basement near contact with greywacke, same location as MUF-4. Gradational contact between Lufubu and C-orebody-greywacke
MUF-5 B	Disseminated mineralisation in Lufubu Basement near contact with greywacke, same location as MUF-4
MUF-6	Disseminated mineralisation in Lufubu Basement near contact with greywacke, same location as MUF-4. Gradational contact between Lufubu and C-orebody-greywacke
MUF-7A	1240mL, 56-57 Crosscut North. Crosscutting qtz-anhydrite veins in Lufubu Basement just below contact betw. Basement and seds. Strike of samples: 22°, direction 291°.
MUF-7B	1240mL, 56-57 Crosscut North. Crosscutting qtz-anhydrite veins in Lufubu Basement just below contact betw. Basement and seds. Strike of samples: 22°, direction 291°.
MUF7-C	1240mL, 56-57 Crosscut North. Crosscutting qtz-anhydrite veins in Lufubu Basement just below contact betw. Basement and seds. Strike of samples: 22°, direction 291°.
MUF7-D	1240mL, 56-57 Crosscut North. Crosscutting qtz-anhydrite veins in Lufubu Basement just below contact betw. Basement and seds. Strike of samples: 22°, direction 291°.
MUF7-E	1240mL, 56-57 Crosscut North. Crosscutting qtz-anhydrite veins in Lufubu Basement just below contact betw. Basement and seds. Strike of samples: 22°, direction 291°.
MUF7-F	1240mL, 56-57 Crosscut North. Crosscutting qtz-anhydrite veins in Lufubu Basement just below contact betw. Basement and seds. Strike of samples: 22°, direction 291°.
MUF-7G	1240mL, 56-57 Crosscut North. Crosscutting qtz-anhydrite veins in Lufubu Basement just below contact betw. Basement and seds. Strike of samples: 22°, direction 291°.
MUF-7H	1240mL, 56-57 Crosscut North. Crosscutting qtz-anhydrite veins in Lufubu Basement just below contact betw. Basement and seds. Strike of samples: 22°, direction 291°.
MUF-8A	Bornite-ccp vein in A-orebody in greywacke, 54.5 Crosscut North, 1240mL Also disseminated ccp-bornite present. Strike of samples: 43°
MUF-8B	Bornite-ccp vein in A-orebody in greywacke, 54.5 Crosscut North, 1240mL Also disseminated ccp-bornite present. Strike of samples: 43°
MUF-8C	Chalcopyrite. Bornite-ccp vein in A-orebody in greywacke, 54.5 Crosscut North, 1240mL Also disseminated ccp-bornite present. Strike of samples: 43°
MUF-8D	Chalcopyrite. Bornite-ccp vein in A-orebody in greywacke, 54.5 Crosscut North, 1240mL Also disseminated ccp-bornite present. Strike of samples: 43°
MUF-8E	Chalcopyrite. Bornite-ccp vein in A-orebody in greywacke, 54.5 Crosscut North, 1240mL Also disseminated ccp-bornite present. Strike of samples: 43°. Intergrown quartz.
MUF-8F	Chalcopyrite picked up close to MUF-8A and B locations, with quartz intergrown. Quartz-ccp precipitating simultaneous in host in large disseminations. Ccp also disseminates finely through host.
MUF-9A	Chalcopyrite. Bornite-ccp vein in A-orebody in greywacke, 54.5 Crosscut North, 1240mL Also disseminated ccp-bornite present. Strike of samples: 43°. Quartz intergrown.
MUF-9B	Chalcopyrite. Bornite-ccp vein in A-orebody in greywacke, 54.5 Crosscut North, 1240mL Also disseminated ccp-bornite present. Strike of samples: 43°. Quartz intergrown.
MUF-9C	Chalcopyrite. Bornite-ccp vein in A-orebody in greywacke, 54.5 Crosscut North, 1240mL Also disseminated ccp-bornite present. Strike of samples: 43°. Quartz intergrown.

Nkana deposit samples

Sample	Description
Drill core (synclinorium)	
NS4-1	Qz-Carb-epidote veinlet (1 cm) crosscutting ore shale, from 12.9 to 12.95 m
NS4-2A	Deformed Carb-Cp-Py-Po veinlets crosscutting ore shale, from 19.48 to 19.56 m
NS4-2B	Deformed Carb-Cp-Py-Po veinlets crosscutting ore shale, from 19.56 to 19.62 m
NS4-3	Disseminated Cp in carbonate, carbon shale altered to carbonate, from 22.55 to 22.65 m
NS4-4A	Qtz-phlogopite alteration with disseminated ccp mineralisation from 25.13 to 25.20 m
NS4-4B	Qz-phlogopite alteration with Cp mineralization from 25.20 to 25.29 m
NS4-5A	Qz-carb vein crossccutting ore shale from 27.7 to 27.79 m
NS4-5B	Disseminated Cp in ore shale and Cp veinlets (1-2 mm) crosscutting ore shale, from 27.79 to 27.84 m
NS4-5C	Disseminated Cp in ore shale and Cp veinlets (1-2 mm) crosscutting ore shale, from 27.84 to 27.89 m
NS4-6	Cp-carb veins (<1 mm to 5 mm) crosscutting ore shale, from 31.15 to 31.28 m
NS4-7	Ccp-qtz-carbonate vein crosscutting ore shale, from 33.53 to 33.61 m. Ccp is disseminated through qtz.
NS4-8	Cp-qz-carb vein (>7 cm) crosscutting ore shale, from 38.14 to 38.22 m
NS4-9	Deformed bedding cut by Cp vein (1 mm to 1 cm), from 41.58 to 41.75 m
NS4-10A	Dissiminated scapolite and Cp veinlets (<4 mm) in carbonitized ore shale, from 44.3 to 44.43 m
NS4-10B	Dissiminated scapolite and Cp veinlets (<4 mm) in carbonitized ore shale, from 44.43 to 44.57 m
NS4-11	Dissiminated Cp-Po-Kf-scapolite in TFQ, from 47.76 to 47.91 m
NS4-12	Dissiminated Cp-Bornite in TFQ, from 50.51 to 50.67 m
NS4-13	Qz-Kf-Cp vein croscutting altered ore shale, from 52.65 to 52.75 m
NS4-14	Cp-phlogopite-carb-Kf vein, from 59.41 to 59.56 m
NS4-15	Euhedral qtz in quartzite? With bornite-phlogopite filling in between qtz crystals, from 65.4 to 65.45 m
NS4-16	Qz-bornite vein, from 68.9 to 68.95 m
NS4-17A	Anhydrite-qz vein, from 72.21 to 72.26 m
NS4-17B	Anhydrite-qz vein, from 72.26 to 72.36 m
NS4-17C	Anhydrite-qz-bornite-epidote vein, from 72.46 to 72.54.
NS4-17D	Anhydrite-qz-bornite-epidote vein, from 72.45 to 72.55.
NS4-18	Anhydrite-qz-bornite-chalcocite-epidote, 73.60 to 73.70m.
NS4-19A	qz-Kfeldsp-epidote-chalcocite (too small for sections)
NS4-19B	qz-Kfeldsp-epidote-chalcocite. From 85.23 to 85.38m.
NS4-20A	A-D: 94.37 to 94.67m. Qz-mica-disseminated chalcocite
NS4-20B	K-feldsp-mica-bornite-qz
NS4-20C	K-feldsp-mica (phlogopite)-disseminated bornite, chalcocite
NS4-20D	K-feldp-mica-qz-epidote
NS4-21	99.53 to 99.65m. Qz, tremolite/tourmaline
NS4-22A	Kfelsp-qz. A-E: 99.95 to 100.3m.
NS4-22B	Kfelsp-qz.
NS4-22C	Kfeldsp-qz. Later stage qz-vein cut feldsp.
NS4-22D	Kfeldsp-qz
NS4-22E	Kfeldsp-qz
NS4-23	Qz-calcite-ccp-phlogopite, alteration, 212.3 to 212.45m. Ccp disseminates through host. Disseminated qtz infiltration
NS4-24A	Qz-ccp-phlogopite A - B: 212.73 to 212.87m.
NS4-24B	Qz-ccp-phlogopite
NS4-25	213.70 to 213.81m. Alteration, qz-phlogopite-ccp
NS4-26A	Altered Ore Shale with qz-ccp veins parllell to foliation. A-D: 220.28 to 220.66m.
NS4-26B	Qz-carbonate-ccp veins in Ore Shale. Ccp-qz-carbonate parallel to foliation & crosscutting
NS4-26C	Qz-carbonate-ccp veins in Ore Shale. Ccp-qz-carbonate parallel to foliation & crosscutting
NS4-26D	Qz-ccp in Ore Shale
NS4-27A	Qz-ccp in Ore Shale. A-C: 315.50 to 315.92m
NS4-27B	Qz-massive ccp vein
NS4-27C	Qz-massive ccp-vein in Ore Shale, alteration of Ore Shale
NS4-28A	Carbonate-qz-Kfeldsp, disseminated ccp, with host. 316.97 to 317.20m
NS4-28B	Carbonate-qz-Kfeldsp
NS4-28C	Carbonate-qz-Kfeldsp, later stage ccp vein in qz.
NK-1	Handsample K-feldsp-sid-pyrite-Fo
Road cut	
KAF-1A	Quartz veins in Lufubu Schist. Taken at Kafue Bridge on the road to Mufulira from Kitwe.
KAF-1B	Quartz veins in Lufubu Schist. Taken at Kafue Bridge on the road to Mufulira from Kitwe.

Konkola deposit samples

Sample	Description
Ventilation Shaft 3B drill core, logged from intersection with "Muliashi Porphyry"	
VS3B-1	quartz vein, from 81.6m to 81.7m
VS3B-2	quartz vein with feldspar, 82.7 to 82.8 m
VS3B-3	quartz-calcite vein, from 84.65 to 84.80 m. Vein is 23 cm thick
VS3B-4	quartz-Kfeldsp vein, from 90.50 to 90.60 m
VS3B-5	quartz-calcite vein, impregnating the host, no clear contact. From 94.70 to 94.80m
VS3B-6	ferroan (pink) calcite vein in porphyritic-gneissic texture of rounded porphyroblastic feldspars. 99.20 to 99.25m.
VS3B-7	quartz vein in leucocratic porphyry, no foliation. From 319.47 to 319.54m.
VS3B-8	Possible replacement texture of vein in porphyry. 354.85 to 354.93m.
VS3B-9	quartz vein in leucocratic finegrained plag (check). From 362.0 to 362.1m
VS3B-10	quartz+calcite vein in porphyry with biotite/phlogopite, feldspars. From 367.96 to 368.0m
VS3B-11	quartz-calcite vein in biotite schisotose matrix with feldspars. From 395.0 to 395.1m. Schistose appearance.
VS3B-12	from 461.6 to 461.8m. Quartz vein in leucocratic-greenish schisty fabric. Quartz-feldspar vein.
VS3B-13	quartz-feldsp vein with dark mineral. From 462.0 to 462.1m. The boudaries between the vein and host are not distinct.
VS3B-14	from 489.10 to 489.12 m. Quartz-calcite(ferroan) vein in porphyritic texture.
VS3B-15	Quartz vein in granite/feldspar. Black tourmaline needles and chlorite present. From 506.60 to 506.75 m.
VS3B-16	Quartz-feldspar vein in porphyritic texture defined by chlorite mica/biotite/phologopite matrix. Tourmaline. From 514.50 to 514.70 m
VS3B-17	from 723.88 to 724.0 m. Quartz vein in schist. Porphyritic texture, with weakly developed foliation. "lamprophyre" present from 785-797 m depth. Appears more like a biotite schist.
VS3B-18	from 821.30 to 821.40 m. Quartz vein in pink granite-porphyry.
Underground No. 1 Shaft	
KON 1	Mineralised qtz vein in quartzite. Reduction spot visible in qtzite
Underground No.3 Shaft	
KK1	1850ft level, 1750mW, bedding parallel quartz vein in Footwall sandstone. Dip: 25°,dipdirection 30°, sample strike:350°
KK2	1850ft level, 1750mW, bedding parallel quartz vein in Footwall sandstone. Dip: 25°,dipdirection 30°, sample strike:350°
KK3	1850ft level, 1750mW, bedding parallel quartz vein in Footwall sandstone. Dip: 25°,dipdirection 30°, sample strike:350°
KK4	Porous Conglomerate immediately above unconformity with granite. Dip = 10°, direction: 270°, stike: 340°
KK5A	Unit B in Ore Shale, 1850ft level, 2150mW. Close to nose. Malachite and maybe bornite.
KK5B	Unit B in Ore Shale, 1850ft level, 2150mW. Close to nose. Malachite and maybe bornite.
KK6A	Quartz vein parallel to bedding in Unit D of Ore Shale. General strike of samples: 350°, dip of strata varies to ~10°, dipdirection: 30°
KK6B	Quartz vein parallel to bedding in Unit D of Ore Shale. General strike of samples: 350°, dip of strata varies to ~10°, dipdirection: 30°
KK7	Chalcopyrite picked up in rubble at KK6 location.
KK8A	In nose, strike of samples: 30°, looking into 300°. Ore shale with bedding parallel quartz-bornite-ccp-chalcocite-feldspar vein.
KK8B	In nose, strike of samples: 30°, looking into 300°. Ore shale with bedding parallel quartz-bornite-ccp-chalcocite-feldspar vein.
KK9A	Quartz vein bedding parallel in Ore shale, strike of samples: 350°
KK9B	Chips of sample KK9A
KK10A	725mW, Unit C of Ore Shale. Mineralisation in dolomite.Dipdirection: 270°, dip ~15°, strike:~350°
KK10B	725mW, Unit C of Ore Shale. Mineralisation in dolomite.Dipdirection: 270°, dip ~15°, strike:~350°
KK10C	725mW, Unit C of Ore Shale. Mineralisation in dolomite.Dipdirection: 270°, dip ~15°, strike:~350°
KK11A	764mW, Crosscutting feldsp-quartz vein in dolomite layering in Unit B of Ore Shale, close to the top. At 75° to KK12.
KK11B	764mW, Crosscutting feldsp-quartz vein in dolomite layering in Unit B of Ore Shale, close to the top. At 75° to KK12.
KK12A	764mW, Dolomite layering in Unit B or Ore Shale close to top of unit. Ore Shale is not mineralised. Dip of layering: 50°, dipdirection: 340°, strike:~351°
KK12B	764mW, Dolomite layering in Unit B or Ore Shale close to top of unit. Ore Shale is not mineralised. Dip of layering: 50°, dipdirection: 340°, strike:~351°
KK12C	764mW, Dolomite layering in Unit B or Ore Shale close to top of unit. Ore Shale is not mineralised. Dip of layering: 50°, dipdirection: 340°, strike:~351°
KK13	3800mW, 1850ft level. Chalcocite-qtz-feldsp vein in Geological Footwall, on contact between Footwall and Unit A of Ore Shale.
KK14	OCB7, 4150mW, 1850ft level, strike of vein in Unit C of Ore Shale: 340°, dip:20°, dipdirection: 260°, vein is bedding parallel but also deviates and crosscuts layering.
KK15	Quartz-bornite-calcite vein bedding parallel to Ore Shale (siltstone). Not clearly mineralised, some CCP disseminated, chalcocite
KK16A	Samples strike: 350°, dip: 260°, same location as KK15. Crosscutting quartz vein in Unit C of Ore Shale. Vein terminates in above and below beds to silty Ore Shale.
KK16B	Samples strike: 350°, dip: 260°, same location as KK15. Crosscutting quartz vein in Unit C of Ore Shale. Vein terminates in above and below beds to silty Ore Shale.
KK16C	Samples strike: 350°, dip: 260°, same location as KK15. Crosscutting quartz vein in Unit C of Ore Shale. Vein terminates in above and below beds to silty Ore Shale.
KK16D	Samples strike: 350°, dip: 260°, same location as KK15. Crosscutting quartz vein in Unit C of Ore Shale. Vein terminates in above and below beds to silty Ore Shale.
Drill core	
SS12	From 319.16 to 319.25, length 0.1m Super Shaft, Footwall Quartzite
SS18	From 525.98 to 526.80, length: 0.1m, Super Shaft, Footwall Quartzite

Appendix II

LASER ABLATION INDUCTIVELY COUPLED PLASMA MASS SPECTROMETRY

- LA-ICP-MS WEIGHT RATIOS
- ABSOLUTE CONCENTRATIONS : LA-ICP-MS

AII-1 Absolute elemental concentration of LA-ICP-MS weight ratios

Elements analysed: Na, Mg, K, Co, Cu, Zn, Sr, Ag, Pb

Sum of weight ratios for elements analysed: 1.48404657

For inclusions with e.g., 13.5 wt.% NaCl equivalent determined from microthermometry:

135,000 ppm NaCl equiv.

Total cation concentration: Salinity (ppm NaCl equiv.) x 0.394[1]

Na (ppm) = total cation concentration / total cation weight ratios

Mg (ppm) = Na (ppm) x Mg weight ratio

[1] Molecular weight of Na: 23.0
NaCl: 58.4
Conversion factor of Na in NaCl is 0.394

AII-2 LA-ICP-MS weight ratios and ppm concentrations

H_2 -method

		weight ratios									*ppm*				
Sample	**Flinc #**	**Na**	**Ca**	**Mn**	**Fe**	**Ba**	**Total wt ratios**	**Salinity (wt.%NaClequiv)**	**Salinity**	**Total cations**	**Na**	**Ca**	**Mn**	**Fe**	**Ba**
Lw															
CBSqz3A	(2)1	1	0.087	0.003	0.020		1.110	21.68	216,800	85,419.20	76926	6723	240	1530	
	(2)a	1	0.123		0.019	0.001	1.143	21.4	214,000	84,316.00	73787	9042		1398	90
	(2)b	1	0.054	0.004	0.020		1.078	21.4	214,000	84,316.00	78209	4229	277	1600	
	(2)c	1	0.096	0.001	0.025	0.002	1.125	21.4	214,000	84,316.00	74937	7229	103	1903	144
	(2)d	1		0.002	0.018	0.001	1.021	21.4	214,000	84,316.00	82543		185	1505	84
	(2)e	1	0.142	0.003		0.001	1.146	21.4	214,000	84,316.00	73571	10455	219		71
	(2)f	1				0.002	1.002	21.4	214,000	84,316.00	84149				167
	(4)10	1	0.110	0.003		0.001	1.113	23.18	231,800	91,329.20	82027	8991	233		78
	(4)a	1		0.001	0.014	0.001	1.016	23.18	231,800	91,329.20	89851		107	1260	111
	(4)b	1	0.141			0.001	1.142	23.18	231,800	91,329.20	79974	11260			95
	(4)c	1	0.148	0.004	0.017	0.001	1.169	23.18	231,800	91,329.20	78127	11524	280	1338	60
	(2)g														
	(2)h	1	0.128				1.128	20	200,000	78,800.00	69864	8936			
	(2)i	1	0.104			0.001	1.105	20	200,000	78,800.00	71313	7417			70
	(2)j							20	200,000	78,800.00					
	(6)7	1		0.005			1.005	20.6	206,000	81,164.00	80779		385		
	(6)6	1	0.096	0.002	0.011	0.001	1.109	21.11	211,100	83,173.40	74985	7208	113	826	40
	(6)4	1	0.051			0.001	1.051	20.45	204,500	80,573.00	76627	3883			63
	(6)3	1	0.069				1.069	21.54	215,400	84,867.60	79406	5462			
	Mean	*1*	*0.104*	*0.003*	*0.018*	*0.001*		*21.47*	*214722.2222*	*84,600.56*	*78063*	*7874*	*214*	*1420*	*89*
	StDev	*0*	*0.032*	*0.001*	*0.004*	*0.000*		*1.09*	*10896.38664*	*4,293.18*	*4991*	*2460*	*90*	*309*	*36*
	RSD	*0*	*31.270*	*41.974*	*23.799*	*37.998*									

		weight ratios									*ppm*				
Sample	**Flinc #**	**Na**	**Ca**	**Mn**	**Fe**	**Ba**	**Total wt ratios**	**Salinity (wt.%NaClequiv)**	**Salinity**	**Total cations**	**Na**	**Ca**	**Mn**	**Fe**	**Ba**
CBSqz3A	(6)2	1	0.507	0.034	1.433	0.007	2.981	5.26	52,600	20,724.40	6953	3528	234	9960	48
	(6)1	1	1.077	2.794	4.074	0.033	8.977	5.26	52,600	20,724.40	2309	2486	6450	9405	75
								5.26	*52600*	*20724.4*	*4631*	*3007*	*3342*	*9683*	*62*
								0	*0*	*0*	*3284*	*737*		*393*	*19*
Lc-w (±s)															
NCGmq9d	(1)1	1	0.069	0.007	0.071	0.007	1.154	vap			0	0	0	0	0
	(1)7	1	0.950	0.010	0.928	0.015	2.903	vap			0	0	0	0	0
Lc															
NCGmq9d	(1)2	1	0.334	0.010	0.147	0.026	1.518	vap			0	0	0	0	0
	(1)9	1	0.477		0.291	0.025	1.792	vap			0	0	0	0	0
	(1)12	1	0.324	0.021	0.239		1.585	vap			0	0	0	0	0
	(1)a	1	0.246		0.094	0.019	1.359	vap			0	0	0	0	0
	Mean	*1*	*0.345*	*0.016*	*0.193*	*0.023*									
	StDev	*0*	*0.096*	*0.008*	*0.089*	*0.004*									
	RSD	*0*	*27.841*	*50.249*	*45.917*	*17.027*									
NCGmq9e	(1)a	1	0.116		0.271		1.387	vap			0	0	0	0	0
	(1)b	1	0.997	0.051			2.048	vap			0	0	0	0	0
	(1)c	1		0.040		0.004	1.044	vap			0	0	0	0	0
	(1)d	1	0.704	0.036			1.740	vap			0	0	0	0	0
	(1)e	1		0.053		0.002	1.055	vap			0	0	0	0	0
	(1)f	1	0.483	0.065			1.548	vap			0	0	0	0	0
	(1)g	1				0.004	1.004	vap			0	0	0	0	0
	Mean	*1*	*0.575*	*0.049*	*0.271*	*0.003*									
	StDev	*0*	*0.371*	*0.011*		*0.001*									
	RSD	*0*	*64.614*	*22.778*		*34.824*									

		weight ratios									*ppm*				
Sample	**Flinc #**	**Na**	**Ca**	**Mn**	**Fe**	**Ba**	**Total wt ratios**	**Salinity (wt.%NaClequiv)**	**Salinity**	**Total cations**	**Na**	**Ca**	**Mn**	**Fe**	**Ba**
Lw±s±he-(n)															
Muf 7H-A	(1)1	1	0.641	0.225			1.866	25	250,000	98,500.00	52790	33823	11887	0	0
	(1)a	1	0.362	0.207	0.214		1.782	40	400,000	157,600.00	88432	32015	18266	18888	0
	(1)b	1			0.519		1.519	40	400,000	157,600.00	103769	0	0	53831	0
	Mean	*1*	*0.501*	*0.216*	*0.366*			*35*							
	StDev	*0*	*0.197*	*0.013*	*0.216*										
	RSD	*0*	*39.305*	*6.099*	*58.930*										

			weight ratios														ppm							
Sample	**Flinc #**	**Na**	**Mg**	**K**	**Co**	**Cu**	**Zn**	**Sr**	**Ag**	**Pb**	**Mn**	**Total wt ratios**	**Salinity (wt% NaCl)**	**Salinity (ppm)**	**Total cations ppm**	**Na**	**Mg**	**K**	**Co**	**Cu**	**Zn**	**Sr**	**Ag**	**Pb**	**Mn**
Lw-(n)																									
CBSqz7B-A	(2)46	1			0.0001	0.0005			0.0000	0.0002		1.00	vap												
	(2)f	1	0.0318	0.2357	0.0002			0.0004	0.0002	0.0008		1.27	vap												
	(2)42	1	0.0275	0.1909	0.0002	0.0020	0.0014	0.0003	0.0003	0.0001		1.22	12.85	128,500	50,629.00	41,407	1,138	7,905	7	84	57	14	12	6	
	(2)43	1	0.0245	0.1551	0.0001	0.0006	0.0011	0.0003	0.0000	0.0003		1.18	12.85	128,500	50,629.00	42,833	1,050	6,643	3	26	45	11	2	15	
	(2)g	1	0.0140		0.0001	0.0016	0.0019	0.0004		0.0005		1.02	12.85	128,500	50,629.00	49,707	696		4	80	95	21		26	
	(2)h	1		0.2396	0.0002	0.0024			0.0002			1.24	12.85	128,500	50,629.00	40,752		9,765	6	97			9		
	(2)i	1		0.1683	0.0002			0.0005		0.0013		1.17	12.85	128,500	50,629.00	43,261		7,279	9			22		58	
	(2)48	1		0.1947								1.19	15.47	154,700	60,951.80	51,019		9,932							
	(2)47												13.51	135,100	53,229.40										
	(2)j	1			0.0001		0.0026	0.0002	0.0004			1.00	13.51	135,100	53,229.40	53,062			3		137	9	19		
	(2)k	1		0.2006								1.20	13.51	135,100	53,229.40	44,338		8,892							
	Mean	*1*	*0.0245*	*0.1978*	*0.0001*	*0.0014*	*0.0017*	*0.0003*	*0.0002*	*0.0006*			*13.36*			*45,797*	*962*	*8,403*	*5*	*72*	*83*	*15*	*11*	*26*	
	Stdev	*0*	*0.0076*	*0.0315*	*0.0001*	*0.0008*	*0.0007*	*0.0001*	*0.0001*	*0.0005*															
	RSD	*0*	*31.0358*	*15.9144*	*49.7318*	*58.4023*	*38.4672*	*34.1511*	*68.1437*	*81.6916*						*4,742*	*234*	*1,345*	*3*	*31*	*41*	*6*	*7*	*23*	
Lw		**Na**	**Mg**	**K**	**Co**	**Cu**	**Zn**	**Sr**	**Ag**	**Pb**															
CBSqz3A	(6)8	1	0.1356	0.1652	0.0002			0.0055				1.31	18.22	182,200	71,786.80	54,948	7,449	9,077	10			303			
	(6)9	1			0.0000				0.0001			1.00													
	(4)a	1		0.2131			0.0081	0.0063	0.0004			1.23	23.00	230,000	90,620.00	73,803		15,725			598	464	30		
	(4)3	1		0.1319			0.0048	0.0044	0.0001	0.0015		1.14	23.18	231,800	91,329.20	79,923		10,540			384	354	4	122	
	(4)4	1	0.1604				0.0096	0.0063				1.18	23.18	231,800	91,329.20	77,644	12,453				744	489			
	(4)b	1			0.0001	0.0025						1.00	23.00	230,000	90,620.00	90,380			12	228					
	(4)6	1						0.0075				1.01	23.00	230,000	90,620.00	89,948						672			
	(4)c	1			0.0000			0.0031	0.0001	0.0010		1.00	23.00	230,000	90,620.00	90,235			3			278	10	94	
	(4)8	1		0.1376		0.0034		0.0048				1.15	23.00	230,000	90,620.00	79,092		10,879		269		380			
	(4)d	1	0.0852	0.1161	0.0001	0.0021	0.0068	0.0041		0.0025		1.22	23.00	230,000	90,620.00	74,459	6,347	8,648	4	159	509	307		188	
	(4)e	1	0.0772	0.1578	0.0000	0.0010	0.0045		0.0002	0.0013		1.24	23.00	230,000	90,620.00	72,960	5,635	11,512	3	74	328	0	17	92	
	(4)f	1						0.0039				1.00	23.00	230,000	90,620.00	90,265						355			
	(4)g												23.00	230,000	90,620.00										
	(4)h	1		0.1329			0.0035	0.0061		0.0014		1.14	23.00	230,000	90,620.00	79,217		10,529			278	484		112	
	(4)i	1						0.0059				1.01	23.00	230,000	90,620.00	90,087						533			
	(4)j	1		0.1303	0.0001	0.0013	0.0082	0.0049		0.0030		1.15	23.00	230,000	90,620.00	78,949		10,290	5	101	651	388		235	
	(4)k	1	0.1600		0.0002							1.16	23.00	230,000	90,620.00	78,113	12,495		12						
	(4)l	1	0.1265		0.0000	0.0011		0.0051	0.0003	0.0019		1.13	23.00	230,000	90,620.00	79,850	10,098		2	87		410	21	151	
	(4)m	1		0.1752		0.0039		0.0043				1.18	23.18	231,800	91,329.20	77,178		13,519		304		328			
	(4)n	1	0.1458	0.2049			0.0029	0.0034		0.0030		1.36	23.18	231,800	91,329.20	67,154	9,792	13,762			192	228		201	
	(4)o	1		0.2124		0.0030	0.0044	0.0054				1.23	23.18	231,800	91,329.20	74,538		15,834		225	330	402			
	(4)p	1		0.1397		0.0036						1.14	23.18	231,800	91,329.20	79,886		11,156		287					
	(4)q	1			0.0001			0.0044				1.00	23.18	231,800	91,329.20	90,929			5			396			
	(4)r	1		0.1427	0.0001	0.0046		0.0043				1.15	23.18	231,800	91,329.20	79,292		11,318	10	365		343			
	(4)s	1						0.0054				1.01	23.18	231,800	91,329.20	90,836						493			
	(4)t	1			0.0000	0.0022			0.0005			1.00	23.18	231,800	91,329.20	91,078			4	198			50		
	(4)u	1						0.0040				1.00	23.18	231,800	91,329.20	90,968						361			
	(4)va	1	0.1113		0.0000	0.0017		0.0038	0.0007	0.0030		1.12	23.18	231,800	91,329.20	81,502	9,070		2	139		310	61	246	
	(4)v	1	0.0795	0.1374	0.0001			0.0057	0.0003	0.0022		1.23	23.18	231,800	91,329.20	74,546	5,924	10,240	6			424	23	167	
	(4)w	1	0.1856	0.1420	0.0001	0.0012	0.0069	0.0047	0.0001	0.0018		1.34	23.18	231,800	91,329.20	68,041	12,625	9,660	6	83	471	320	5	119	
	(4)x												23.18	231,800	91,329.20										
	(4)y	1		0.1260	0.0001		0.0061	0.0039		0.0027		1.14	23.18	231,800	91,329.20	80,207		10,107	4		485	310		215	
	Mean	*1*	*0.1267*	*0.1541*	*0.0001*	*0.0024*	*0.0060*	*0.0049*	*0.0003*	*0.0021*			*22.94*			*80,208*	*9,189*	*11,425*	*6*	*194*	*452*	*373*	*25*	*162*	
	Stdev	*0*	*0.0377*	*0.0314*	*0.0000*	*0.0012*	*0.0021*	*0.0011*	*0.0002*	*0.0007*						*8,729*	*2,769*	*2,168*	*3*	*95*	*168*	*123*	*20*	*55*	
	RSD	*0*	*29.7445*	*20.4014*	*63.0674*	*48.8186*	*35.8454*	*21.8124*	*82.1071*	*34.2603*															

			weight ratios													ppm									
Sample	**Flinc #**	**Na**	**Mg**	**K**	**Co**	**Cu**	**Zn**	**Sr**	**Ag**	**Pb**	**Mn**	**Total wt ratios**	**Salinity (wt% NaCl)**	**Salinity (ppm)**	**Total cations ppm**	**Na**	**Mg**	**K**	**Co**	**Cu**	**Zn**	**Sr**	**Ag**	**Pb**	**Mn**
NOP8B-A (3)n	(3)n	1		0.1377	0.0102			0.0078		0.0004		1.16	8.57	85,700	33,765.80	29,204		4,023	298			228		13	
	(3)o	1		0.2230	0.0054	0.0079		0.0079	0.0031			1.25	8.57	85,700	33,765.80	27,070		6,036	148	214		214	83		
	(3)p	1						0.0105				1.01	8.57	85,700	33,765.80	33,415						351			
	(3)m	1	0.2065		0.0012	0.0224	0.0137					1.24	8.57	85,700	33,765.80	27,147	5,606		34	608	371				
	(3)j	1				0.0145		0.0092				1.02	8.57	85,700	33,765.80	32,982				479		305			
	(3)l	1		0.1170	0.0096	0.0193	0.0027	0.0115		0.0037		1.16	8.57	85,700	33,765.80	29,016		3,394	278	561	78	333		106	
	(3)f												8.57	85,700	33,765.80										
	(3)g	1		0.2591	0.0104	0.0075			0.0028	0.0047		1.28	8.57	85,700	33,765.80	26,288		6,811	273	198			73	122	
	(3)h	1						0.0126		0.0048		1.02	8.57	85,700	33,765.80	33,188						417		161	
	(3)i	1	0.4333	0.1278	0.0067	0.0084	0.0090		0.0006			1.59	8.57	85,700	33,765.80	21,293	9,226	2,721	142	179	192		14		
	(3)d	1			0.0076	0.0266		0.0144	0.0013	0.0053		1.06	8.57	85,700	33,765.80	31,999			242	852		461	43	169	
	(3)e	1	0.3443	0.1134				0.0091	0.0004	0.0032		1.47	8.57	85,700	33,765.80	22,964	7,907	2,603				209	8	73	
	Mean	*1*	*0.3280*	*0.1630*	*0.0073*	*0.0152*	*0.0084*	*0.0104*	*0.0016*	*0.0037*			*8.57*			*28,597*	*7,580*	*4,265*	*202*	*441*	*213*	*315*	*44*	*107*	
	Stdev	*0*	*0.1143*	*0.0621*	*0.0033*	*0.0077*	*0.0055*	*0.0023*	*0.0012*	*0.0018*						*4,129*	*1,832*	*1,765*	*97*	*255*	*148*	*94*	*34*	*58*	
	RSD	*0*	*34.8325*	*38.1076*	*44.6811*	*50.6524*	*65.2266*	*22.4040*	*75.1016*	*47.9071*															
															0.00										
NS47b-A (2)1	(2)1	1		0.1703	0.0002			0.0021	0.0048			1.18			0.00	0	0	0	0	0	0	0	0	0	0
	(2)2	1		0.1988	0.0001	0.0054	0.0052	0.0013		0.0010		1.21			0.00	0	0	0	0	0	0	0	0	0	0
	(1)1	1	0.1934	0.3622				0.0013	0.0034	0.0022		1.56			0.00	0	0	0	0	0	0	0	0	0	0
	(1)2	1	0.1338	0.3109	0.0000	0.0012	0.0038	0.0009	0.0001	0.0013		1.45			0.00	0	0	0	0	0	0	0	0	0	0
	(1)3	1	0.2090	0.2269	0.0002	0.0082	0.0055	0.0024	0.0016			1.45			0.00	0	0	0	0	0	0	0	0	0	0
	(1)3 cont	1										1.00			0.00	0	0	0	0	0	0	0	0	0	0
	(1)4	1		0.3568				0.0010		0.0047		1.36			0.00	0	0	0	0	0	0	0	0	0	0
	Mean	*1*	*0.1787*	*0.2710*	*0.0001*	*0.0049*	*0.0048*	*0.0015*	*0.0025*	*0.0023*																
	Stdev	*0*	*0.0397*	*0.0832*	*0.0001*	*0.0035*	*0.0009*	*0.0006*	*0.0020*	*0.0017*																
	RSD		*22.2182*	*30.6864*	*55.1356*	*71.0530*	*18.8395*	*41.7055*	*82.6476*	*71.9891*																
Lw-c															0.00										
CBSqz3By	(4)2	1		0.2113		0.0481				0.0060		1.27	13.50	135,000	53,190.00	42,035		8,881		2,022				252	
	(4)1	1		0.2023	0.0037		0.0330					1.24	13.50	135,000	53,190.00	42,929		8,684	160		1,418				
	(4)4	1	0.0136	0.0201			0.0036		0.0001	0.0005		1.04	13.50	135,000	53,190.00	51,252	700	1,028			182		4	24	
	(4)5	1			0.0015	0.0070						1.01	13.50	135,000	53,190.00	52,740			81	370					
	(4)9	1	0.0144						0.0001			1.01	13.50	135,000	53,190.00	52,434	754						3		
	(4)10	1	0.2195	0.2108	0.0008	0.0147	0.0284	0.0020		0.0079		1.48	13.50	135,000	53,190.00	35,841	7,867	7,554	28	525	1,016	73		285	
	(4)a	1				0.0453		0.0004	0.0009			1.05	13.50	135,000	53,190.00	50,818				2,303		22	48		
	(4)b	1	0.1421	0.0845		0.0024	0.0069	0.0016	0.0006	0.0077		1.25	13.50	135,000	53,190.00	42,696	6,069	3,606		101	296	66	27	328	
	(4)c												13.50	135,000	53,190.00										
	(4)d	1	0.0412	0.0716		0.0014	0.0063	0.0010	0.0004	0.0060		1.13	13.50	135,000	53,190.00	47,156	1,942	3,377		67	297	49	18	285	
	(4)7	1	0.1455				0.0141	0.0001				1.16	13.50	135,000	53,190.00	45,868	6,672				644	6			
	(4)6	1		0.0577			0.0264		0.0004	0.0052		1.09	13.50	135,000	53,190.00	48,817		2,815			1,287		20	252	
	(4)11	1	0.1770			0.0018	0.0045		0.0004	0.0029		1.19	13.50	135,000	53,190.00	44,827	7,932			82	203		16	130	
	(4)13	1						0.0040	0.0004			1.00	13.50	135,000	53,190.00	52,959						211	19		
	Mean	*1*	*0.1076*	*0.1226*	*0.0020*	*0.0172*	*0.0154*	*0.0015*	*0.0004*	*0.0052*			*13.50*			46,952	4,562	5,135	90	781	668	71	19	222	
	Stdev	*0*	*0.0836*	*0.0824*	*0.0015*	*0.0207*	*0.0120*	*0.0014*	*0.0003*	*0.0027*						5,198	3,299	3,166	66		507		14	107	
	RSD		*77.6450*	*67.2463*	*75.6720*	*119.8493*	*78.1999*	*91.0569*	*71.2170*	*51.4906*															
CBSqz3A	(6)13	1																							
	(6)a	1																							
	(6)b	1	0.1425	0.0820			0.0069	0.0016	0.0004	0.0050		1.24			0.00	0	0	0	0	0	0	0	0	0	
	(6)c	1		0.0979				0.0048				1.10			0.00	0	0	0	0	0	0	0	0	0	
	(6)12	1	0.0277	0.1916	0.0001	0.0004	0.0038	0.0053	0.0002	0.0020		1.23			0.00	0	0	0	0	0	0	0	0	0	
	(6)d	1		0.1510		0.0001		0.0047	0.0000	0.0046		1.16			0.00	0	0	0	0	0	0	0	0	0	

			weight ratios													ppm								
Sample	**Flinc #**	**Na**	**Mg**	**K**	**Co**	**Cu**	**Zn**	**Sr**	**Ag**	**Pb**	**Mn**	**Total wt ratios**	**Salinity (wt% NaCl)**	**Salinity (ppm)**	**Total cations ppm**	**Na**	**Mg**	**K**	**Co**	**Cu**	**Zn**	**Sr**	**Ag**	**Pb**	**Mn**
	(6)e	1			0.0006							1.00			0.00	0	0	0	0	0	0	0	0	0	
	(6)f	1	0.1263	0.2002	0.0009	0.0002		0.0076	0.0005	0.0081		1.34			0.00	0	0	0	0	0	0	0	0	0	
	(6)g	1	0.0454	0.0866		0.0002	0.0027	0.0065	0.0002	0.0023		1.14			0.00	0	0	0	0	0	0	0	0	0	
	(4)2	1	0.0376	0.1379			0.0035	0.0073		0.0011		1.19			0.00	0	0	0	0	0	0	0	0	0	
	Mean	*1*	*0.0759*	*0.1353*	*0.0005*	*0.0002*	*0.0042*	*0.0054*	*0.0003*	*0.0038*															
	Stdev	*0*	*0.0541*	*0.0487*	*0.0004*	*0.0001*	*0.0019*	*0.0021*	*0.0002*	*0.0026*															
	RSD		*71.2188*	*36.0076*	*81.8017*	*54.6667*	*43.9818*	*38.1546*	*72.9906*	*67.5287*															
CHM7B-A	(1)5	1											18.96	189,600	74,702.40										
	(1)1	1	0.1990			0.0011			0.0002			1.20	18.13	181,300	71,432.20	59,506	11,844			68			14		
	(1)11	1		0.3141		0.0002	0.0034		0.0001	0.0004		1.32	16.71	167,100	65,837.40	49,943		15,688		11	172		5	18	
	(1)9	1	0.0760	0.1741	0.0000	0.0006	0.0037	0.0038		0.0006		1.26	19.21	192,100	75,687.40	60,125	4,570	10,467	2	36	224	225		38	
	(1)12	1	0.0546	0.2051	0.0001			0.0014	0.0001			1.26	19.21	192,100	75,687.40	60,009	3,278	12,308	4			82	7		
	(1)13	1	0.1540	0.1945	0.0000	0.0007		0.0020	0.0004			1.35	18.96	189,600	74,702.40	55,265	8,513	10,751	1	36		113	23		
	(1)a	1					0.0013	0.0030		0.0004		1.00	18.96	189,600	74,702.40	74,358					96	221		26	
	(1)b	1	0.0532		0.0004			0.0026				1.06	18.96	189,600	74,702.40	70,730	3,762		26			185			
	(1)c	1	0.1416		0.0001	0.0017		0.0014	0.0003			1.15	18.96	189,600	74,702.40	65,232	9,239		8	110		91	23		
	Mean	*1*	*0.1131*	*0.2220*	*0.0001*	*0.0009*	*0.0028*	*0.0024*	*0.0002*	*0.0005*			*18.67*			*61,896*	*6,868*	*12,304*	*8*	*52*	*164*	*153*	*14*	*28*	
	Stdev	*0*	*0.0604*	*0.0628*	*0.0001*	*0.0006*	*0.0013*	*0.0009*	*0.0001*	*0.0002*						*7,962*	*3,490*	*2,397*	*10*	*38*	*64*	*65*	*8*	*10*	
	RSD		*53.4356*	*28.2806*	*116.4111*	*65.3004*	*47.0524*	*39.7600*	*56.3875*	*36.2217*															
CHM7B-A +s	(1)2	1	0.0882			0.0005	0.0015	0.0027				1.09	27.00	270,000	106,380.00	97,337	8,584			53	148	258			
Lw-c±s															0.00										
NOP16A	(3)7	1	0.7326	1.0146	0.0185	0.0513	0.0171	0.0136	0.0002	0.0059		2.85			0.00	0	0	0	0	0	0	0	0	0	0
															0.00										
															0.00										
Lc-w (±s)															0.00										
CBSqz3A	(6)10	1	0.6157	0.0129		0.0035	0.0034	0.0003	0.0046	0.0152		1.66	23.76	237,600	93,614.40	56,543	34,811	727	0	201	191	18	263	862	0
															0.00										
															0.00										
															0.00										
															0.00										
NOP16A	(1)1	1			0.0003	0.0108	0.0235		0.0001	0.0099		1.04	24.00	240,000	94,560.00	90,515			27	976	2,131		13	897	
	(1)a												24.00	240,000	94,560.00										
	(1)4	1					0.0822	0.0063				1.09	24.00	240,000	94,560.00	86,872					7,143	545			
	(1)2	1			0.0003		0.0387					1.04	24.00	240,000	94,560.00	91,015			23		3,522				
	(1)3	1	0.0535	0.0702	0.0001	0.0078		0.0012		0.0008		1.13	24.00	240,000	94,560.00	83,412	4,461	5,857	7	654		103		66	
	Mean	*1*	*0.0535*	*0.0702*	*0.0002*	*0.0093*	*0.0482*	*0.0038*	*0.0001*	*0.0054*			*23.96*			*87,953*	*4,461*	*5,857*	*19*	*815*	*4,266*	*324*	*13*	*482*	
	Stdev	*0*			*0.0001*	*0.0021*	*0.0305*	*0.0036*		*0.0064*						*3,546*			*11*	*228*	*2,588*	*313*		*588*	
	RSD				*54.5769*	*22.3948*	*63.2600*	*95.0820*		*120.4172*															
Lm															0.00										
CBSqz7B-A	(1)1	1						0.0004	0.0000	0.0003		1.00	vap		0.00	0	0	0	0	0	0	0	0	0	0
	(1)7	1	0.2412	0.2165	0.0014	0.0221	0.0181	0.0007	0.0005			1.50	vap		0.00	0	0	0	0	0	0	0	0	0	0
	(1)20	1					0.0611	0.0009				1.06	vap		0.00	0	0	0	0	0	0	0	0	0	0
	(1)6												vap		0.00										
	(1)28	1			0.0074			0.0013				1.01	vap		0.00	0	0	0	0	0	0	0	0	0	0
	(1)32	1	0.0810				0.0721			0.0113		1.16	vap		0.00	0	0	0	0	0	0	0	0	0	0
	(1)35	1			0.0024							1.00	vap		0.00	0	0	0	0	0	0	0	0	0	0
	(1)38	1	0.2299		0.0003		0.0101	0.0004		0.0110		1.25	vap		0.00	0	0	0	0	0	0	0	0	0	0
	(1)a	1		0.2009			0.0370	0.0011		0.0094		1.25	vap		0.00	0	0	0	0	0	0	0	0	0	0
	(1)b	1			0.0025							1.00	vap		0.00	0	0	0	0	0	0	0	0	0	0

			weight ratios													ppm								
Sample	**Flinc #**	**Na**	**Mg**	**K**	**Co**	**Cu**	**Zn**	**Sr**	**Ag**	**Pb**	**Mn**	**Total wt ratios**	**Salinity (wt% NaCl)**	**Salinity (ppm)**	**Total cations ppm**	**Na**	**Mg**	**K**	**Co**	**Cu**	**Zn**	**Sr**	**Ag**	**Pb**	**Mn**
	(1)41	1	0.0214	0.2963		0.0023		0.0005		0.0006		1.32	vap		0.00	0	0	0	0	0	0	0	0	0	0
	(1)c	1	0.2029	0.1954			0.0282	0.0006	0.0008	0.0099		1.44	vap		0.00	0	0	0	0	0	0	0	0	0	0
	(1)d	1	0.1878	0.1510	0.0002	0.0097		0.0002	0.0001			1.35	vap		0.00	0	0	0	0	0	0	0	0	0	0
	(1)e	1		0.2082		0.0049	0.0280	0.0002	0.0005	0.0007		1.24	vap		0.00	0	0	0	0	0	0	0	0	0	0
	Mean	*1*	*0.1607*	*0.2114*	*0.0023*	*0.0097*	*0.0364*	*0.0006*	*0.0004*	*0.0062*															
	Stdev	*0*	*0.0889*	*0.0474*	*0.0027*	*0.0088*	*0.0225*	*0.0004*	*0.0003*	*0.0053*															
	RSD		*55.3402*	*22.4446*	*113.4324*	*89.8449*	*61.9416*	*58.8896*	*77.0720*	*86.3355*															
Vm											Mn				0.00										
NOP8B-A	(1)2	1		0.4464		0.0175	0.0845			0.0084	0.066	1.62			0.00	0	0	0	0	0	0	0	0	0	0
	(1)3	1									0.455	1.46			0.00	0	0	0	0	0	0	0	0	0	0
	(1)9	1								0.0285	1.467	2.50			0.00	0	0	0	0	0	0	0	0	0	0
	(1)b	1								0.0122	0.340	1.35			0.00	0	0	0	0	0	0	0	0	0	0
	(1)29	1					0.0990			0.0330	0.499	1.63			0.00	0	0	0	0	0	0	0	0	0	0
	(1)28	1					0.0886		0.0377			1.13			0.00	0	0	0	0	0	0	0	0	0	0
	(1)d										1.739	1.74			0.00	0	0	0	0	0	0	0	0	0	0
	Mean	*1*		*0.4464*		*0.0175*	*0.0907*		*0.0377*	*0.0205*	*0.761*														
	Stdev	*0*					*0.0075*			*0.0120*	*0.675*														
	RSD	*0*					*8.2219*			*58.7029*	*88.659*														
Lc															0.00										
NCGmq9d	(1)a	1	0.7305	0.3950	0.0017	0.0094		0.0021		0.0125		2.15	vap		0.00	0	0	0	0	0	0	0	0	0	0
	(1)b	1	0.9422	0.6216	0.0007	0.0255			0.0027	0.0180		2.61	vap		0.00	0	0	0	0	0	0	0	0	0	0
	(1)c	1		0.5968		0.0100			0.0072			1.61	vap		0.00	0	0	0	0	0	0	0	0	0	0
	(1)d	1	0.5804	0.5368	0.0010	0.0029	0.0693	0.0040	0.0003	0.0080		2.20	vap		0.00	0	0	0	0	0	0	0	0	0	0
	(1)e	1	0.3111		0.0013			0.0074		0.0114		1.33	vap		0.00	0	0	0	0	0	0	0	0	0	0
	(1)f	1			0.0036	0.0163			0.0008	0.0236		1.04	vap		0.00	0	0	0	0	0	0	0	0	0	0
	(1)g	1			0.0030	0.0203			0.0035	0.0265		1.05	vap		0.00	0	0	0	0	0	0	0	0	0	0
	(1)h	1	0.3232	0.1699	0.0010	0.0058	0.0257	0.0059		0.0152		1.55	vap		0.00	0	0	0	0	0	0	0	0	0	0
	(1)i	1	0.7132			0.0154		0.0098		0.0220		1.76	vap		0.00	0	0	0	0	0	0	0	0	0	0
	(1)j	1				0.0020		0.0077		0.0089		1.02	vap		0.00	0	0	0	0	0	0	0	0	0	0
	(1)k	1			0.0035	0.0168			0.0021	0.0246		1.05	vap		0.00	0	0	0	0	0	0	0	0	0	0
	(1)l	1	0.4775		0.0006	0.0084	0.0495	0.0059	0.0005	0.0082		1.55	vap		0.00	0	0	0	0	0	0	0	0	0	0
	(1)m	1							0.0027			1.00	vap		0.00	0	0	0	0	0	0	0	0	0	0
	(1)n	1	0.6476									1.65	vap		0.00	0	0	0	0	0	0	0	0	0	0
	(1)o	1	0.5034					0.0089				1.51	vap		0.00	0	0	0	0	0	0	0	0	0	0
	(1)p	1		0.2229	0.0001	0.0014	0.0115	0.0091		0.0132		1.26	vap		0.00	0	0	0	0	0	0	0	0	0	0
	Mean	*1*	*0.5810*	*0.4238*	*0.0017*	*0.0112*	*0.0390*	*0.0067*	*0.0025*	*0.0160*															
	Stdev	*0*	*0.2033*	*0.1937*	*0.0013*	*0.0077*	*0.0256*	*0.0025*	*0.0022*	*0.0067*															
	RSD		*34.9942*	*45.6910*	*76.7396*	*68.9518*	*65.6359*	*37.5770*	*89.9479*	*42.1241*															
Lw-s-(n)																									
Muf 7H-A	(2)p	1		0.1062	0.0000	0.0002	0.0203	0.0481	0.0001	0.0495		1.22	40.00	400,000	157,600.00	128,715		13,667	1	21	2,611	6,191	16	6,378	
	(2)q	1	0.0931	0.2717	0.0000	0.0021		0.0598	0.0003	0.0773		1.50	40.00	400,000	157,600.00	104,774	9,757	28,462	4	215		6,260	33	8,095	
	(2)j	1						0.0190				1.02	24.00	240,000	94,560.00	92,800						1,760			
	Mean	*1*	*0.0931*	*0.1889*	*0.0000*	*0.0011*	*0.0203*	*0.0423*	*0.0002*	*0.0634*						*108,763*	*9,757*	*21,064*	*3*	*118*	*2,611*	*4,737*	*25*	*7,236*	
	Stdev	*0*		*0.1170*	*0.0000*	*0.0013*		*0.0210*	*0.0001*	*0.0196*						*18,287*		*10,462*	*2*	*137*		*2,578*	*12*	*1,214*	
	RSD			*61.9352*	*91.1868*	*120.6518*		*49.6877*	*59.8481*	*30.9047*															
he	(2)g	1	0.5036	0.8005	0.0050	0.0839				0.1874		2.58	24.00	240,000	94,560.00	36,648	18,456	29,335	182	3,074				6,867	
he	(2)h	1	0.0072	0.0926	0.0001	0.0054	0.0096	0.0019		0.0080		1.12	24.00	240,000	94,560.00	84,065	602	7,785	12	456	810	159		671	
he	(2)e	1	0.0041	0.1331			0.0063	0.0171	0.0008	0.0049		1.17	24.00	240,000	94,560.00	81,071	334	10,794			512	1,389	64	395	
he	(2)f	1				0.1508			0.0986	0.3317		1.58	24.00	240,000	94,560.00	59,807				9,017			5,899	19,836	

			weight ratios													**ppm**									
Sample	**Flinc #**	**Na**	**Mg**	**K**	**Co**	**Cu**	**Zn**	**Sr**	**Ag**	**Pb**	**Mn**	**Total wt ratios**	**Salinity (wt% NaCl)**	**Salinity (ppm)**	**Total cations ppm**	**Na**	**Mg**	**K**	**Co**	**Cu**	**Zn**	**Sr**	**Ag**	**Pb**	**Mn**
he	(2)c	1	0.0038	0.0175		0.0013	0.0031			0.0038		1.03	24.00	240,000	94,560.00	91,851	350	1,607		118	281			352	
he	(2)d	1	0.0030	0.1354		0.0021	0.0117	0.0380	0.0003	0.0084		1.20	24.00	240,000	94,560.00	78,881	239	10,678		162	920	2,994	20	665	
he	(2)a	1	0.0879	0.4373	0.0002	0.0093	0.0841	0.0379	0.0165	0.0562		1.73	24.00	240,000	94,560.00	54,679	4,805	23,913	12	508	4,596	2,074	901	3,072	
he	(2)b	1	0.2820	0.1658		0.0123		0.0476	0.0006	0.0596		1.57	24.00	240,000	94,560.00	60,309	17,009	9,996		741		2,872	38	3,596	
he	(2)2	1	0.0385	0.9386	0.0003	0.0042	0.1017	0.1162	0.0313	0.1765		2.41	40.00	400,000	157,600.00	65,469	2,521	61,447	19	275	6,655	7,609	2,048	11,557	
he	(2)n	1	0.0272	0.1186	0.0002	0.0051	0.0139	0.0178	0.0008	0.0195		1.20	24.00	240,000	94,560.00	78,601	2,140	9,323	13	397	1,092	1,402	60	1,533	
he	(2)o	1	0.0393	0.3740	0.0004	0.0083	0.0367	0.0125	0.0006	0.0321		1.50	24.00	240,000	94,560.00	62,875	2,474	23,514	27	522	2,305	785	38	2,019	
he	(2)k	1	0.4318		0.0201	0.2876		0.0415	0.0126	0.1957		1.99	24.00	240,000	94,560.00	47,532	20,524		958	13,672		1,974	597	9,303	
he	(2)l	1	0.1347		0.0028	0.0987	0.0304	0.0167	0.0080	0.0922		1.38	24.00	240,000	94,560.00	68,348	9,209		193	6,744	2,081	1,140	545	6,299	
he	(2)m	1	0.7399		0.0170	0.3567		0.0128	0.0157	0.1596		2.30	24.00	240,000	94,560.00	41,083	30,395		698	14,655		526	646	6,557	
he	(2)i	1				0.3050		0.0599	0.1145	0.2892		1.77	24.00	240,000	94,560.00	53,467				16,309		3,202	6,119	15,463	
	Mean	*1*	*0.1772*	*0.3213*	*0.0051*	*0.0950*	*0.0330*	*0.0350*	*0.0250*	*0.1083*			*25.07*			*64,312*	*8,389*	*18,839*	*235*	*4,761*	*2,139*	*2,177*	*1,415*	*5,879*	
	Stdev	*0*	*0.2396*	*0.3174*	*0.0078*	*0.1290*	*0.0359*	*0.0309*	*0.0394*	*0.1084*						*16,254*	*9,940*	*17,296*	*350*	*6,128*	*2,148*	*1,972*	*2,222*	*5,940*	
	RSD		*135.2234*	*98.7764*	*152.7203*	*135.7677*	*108.6657*	*88.1982*	*157.3637*	*100.0649*															
	Mean	*1*	*0.1163*	*0.3401*	*0.0014*	*0.0336*	*0.0361*	*0.0431*	*0.0247*	*0.0929*															
	Stdev	*0*	*0.1830*	*0.3505*	*0.0024*	*0.0548*	*0.0444*	*0.0395*	*0.0383*	*0.1148*															
	RSD		*157.3537*	*103.0637*	*169.2834*	*162.7928*	*123.2094*	*91.5413*	*155.1113*	*123.5026*															
Lw-s											**Mn**														
NOP20A	(1)1	1		0.2508			0.0357		0.0017	0.0155	0.019	1.32	27.00	270,000	106,380.00	80,434	0	20,171	0	0	2,869	0	138	1,243	1,526
	(1)4	1							0.0051	0.0532	0.034	1.09	27.00	270,000	106,380.00	97,385	0	0	0	0	0	0	493	5,183	3,319
Lw-s-c																									
NOP16A	(2)5	1	0.2407	0.2242	0.0003	0.0056	0.0254	0.0115	0.0004	0.0136		1.52			0.00	0	0	0	0	0	0	0	0	0	0
	(2)6	1						0.0133				1.01			0.00	0	0	0	0	0	0	0	0	0	0
Lw-s																									
Muf 7D	(1)1	1		0.2518	0.0003	0.0033	0.0149	0.0198		0.0096		1.30	40.00	400,000	157,600.00	121,259		30,528	38	405	1,802	2,406		1,162	
	(1)2	1					0.0247			0.0571		1.08	40.00	400,000	157,600.00	145,689					3,593			8,318	
	(1)3	1	0.0158	0.1780	0.0002	0.0032	0.0242	0.0116	0.0000	0.0209		1.25	40.00	400,000	157,600.00	125,682	1,985	22,369	23	404	3,047	1,453	4	2,633	
													40.00	400,000	157,600.00										
	(1)4	1			0.0000	0.0021		0.0325	0.0000	0.0518		1.09	40.00	400,000	157,600.00	145,045			5	312		4,714	4	7,520	
	(1)5	1	0.0036	0.1709	0.0001	0.0014	0.0204	0.0104		0.0141		1.22	40.00	400,000	157,600.00	129,105	465	22,059	7	181	2,630	1,338		1,814	
	(1)6	1	0.0039	0.2837	0.0001	0.0030	0.0189	0.0139	0.0000	0.0228		1.35	40.00	400,000	157,600.00	117,058	457	33,209	17	353	2,209	1,629	3	2,664	
	(1)7												40.00	400,000	157,600.00										
	(1)8	1	0.0071	0.0953	0.0003	0.0029	0.0144	0.0059	0.0000	0.0187		1.14	40.00	400,000	157,600.00	137,688	975	13,127	36	400	1,985	813	2	2,573	
	(1)9	1	0.0031	0.1798	0.0001	0.0034	0.0121	0.0068	0.0000	0.0094		1.21	40.00	400,000	157,600.00	129,747	404	23,323	10	444	1,571	880	3	1,218	
	(1)10	1							0.0001			1.00	40.00	400,000	157,600.00	157,591							9		
	(1)11	1	0.0392						0.0001	0.0676		1.11	40.00	400,000	157,600.00	142,389	5,576						7	9,628	
	(1)12	1							0.0001			1.00	40.00	400,000	157,600.00	157,587							13		
	(1)13	1			0.0000				0.0001			1.00	40.00	400,000	157,600.00	157,587			3				10		
	Mean	*1*	*0.0121*	*0.1932*	*0.0001*	*0.0028*	*0.0185*	*0.0144*	*0.0000*	*0.0302*			*40.00*			*138,869*	*1,644*	*24,103*	*17*	*357*	*2,405*	*1,890*	*6*	*4,170*	
	Stdev	*0*	*0.0141*	*0.0665*	*0.0001*	*0.0007*	*0.0049*	*0.0092*	*0.0000*	*0.0223*						*14,422*	*2,018*	*7,106*	*14*	*88*	*724*	*1,353*	*4*	*3,330*	
	RSD		*116.2673*	*34.4112*	*79.2246*	*26.5983*	*26.5983*	*64.1057*	*51.8195*	*73.8477*															

Appendix III

SULPHIDES: SELECTED SEM SPECTRA

- Chambishi
- Nchanga

AIII-1 SEM analyses of selected sulphides from the Chambishi deposit

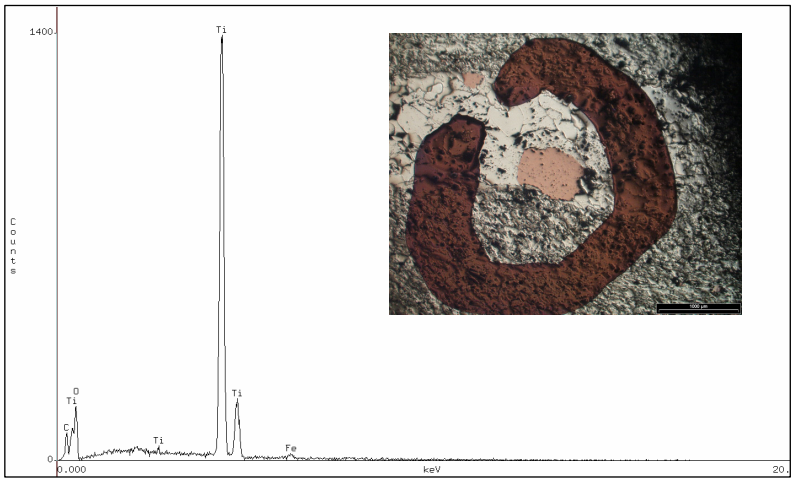

CHM 1. Rutile present in bornite.

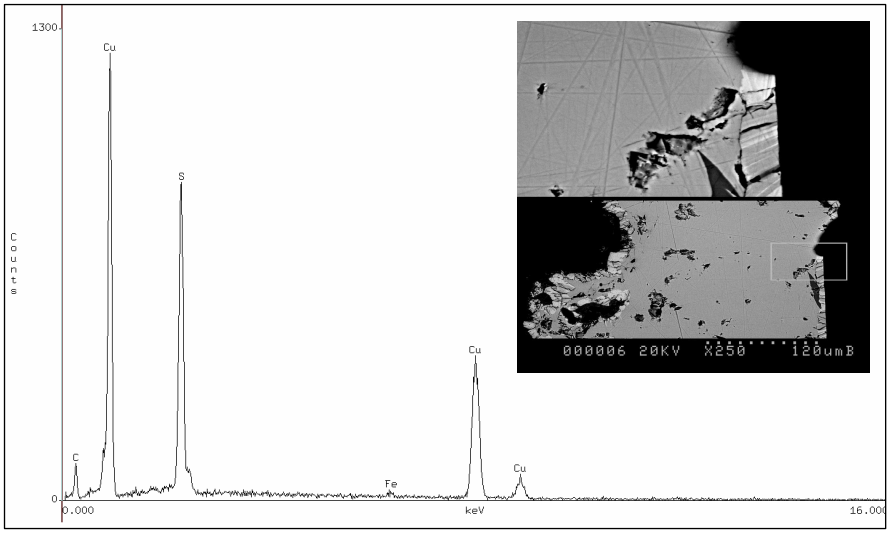

CHM8B. Alternating digenite and covelline bands.

AIII-2 SEM analyses of selected sulphides from the Nchanga deposit

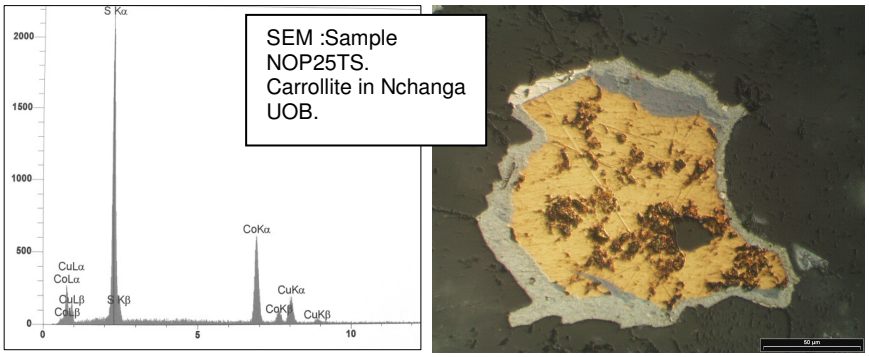

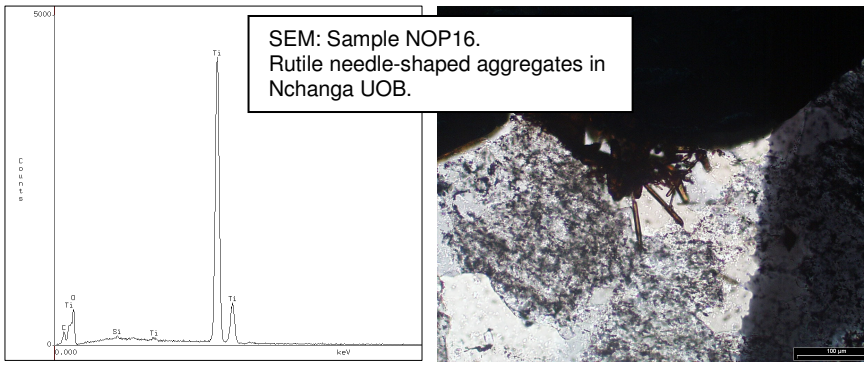

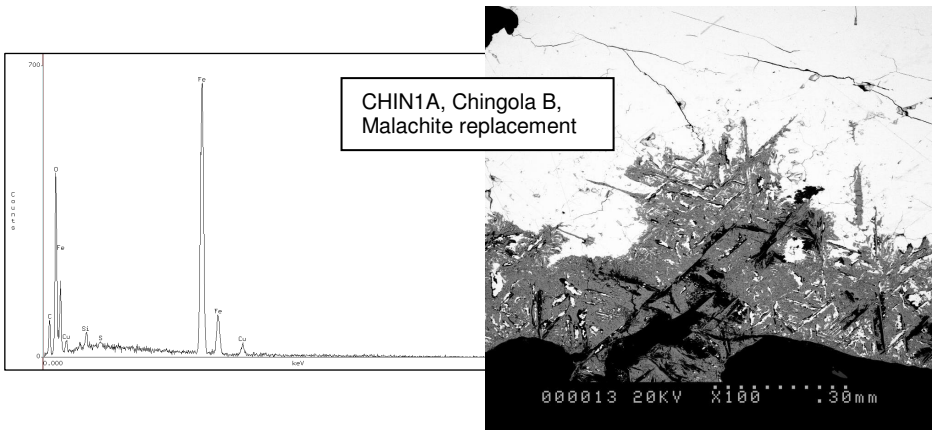

Appendix IV

PUBLICATIONS AND ABSTRACTS

- SEG Global Exploration 2002
- 11th Quadrennial IAGOD Symposium & Geocongress 2002
- RAU MINSA SAS-SEG Base Metal Symposium 2003
- Trans. Inst. Min. Met., 2003, 112, 2, 164-166
- Geoscience Africa 2004
- Journal of African Earth Sciences, 2005, 42, 159-172
- MDSG London 2006

Society of Economic Geologists Global Exploration 2002 Integrated Methods for Discovery, April 14-16, Denver, Colorado, USA. Poster presentation.

PRELIMINARY FLUID INCLUSION RESULTS FROM MINERALISED VEINS IN THE ZAMBIAN COPPERBELT

L.N. Greyling, Y. Yao, L.J. Robb, S. Master

Economic Geology Research Institute, School of Geosciences, University of the Witwatersrand, Private Bag 3, WITS, 2050, Johannesburg, South Africa. Tel: +27 11 717 6556, Fax: +27 11 339 1697, Email: greylin@science.pg.wits.ac.za

Stratiform Cu-Co ores in the Central African Copperbelt are hosted by the Neoproterozoic meta-sediments of the Katangan Sequence in the Democratic Republic of Congo and Zambia. In addition, the Katangan metallogenic province also hosts a variety of epigenetic ores such as the U-(Cu-Co-Ni-Mo) deposits at Shinkolobwe, Zn-Pb-Cu-Ge-Ga deposits at Kipushi and Kabwe, and the Cu-Au deposits at Kansanshi.

Theories on mineralisation in the Central African Copperbelt range from syngenetic-diagenetic to epigenetic. Given the scale and complexity of mineralisation styles in the Copperbelt, metallogenesis in the region is best viewed in a polygenetic framework. In order to document the fluid characteristics (P-T-X-V) and to model the regional fluid evolution and relevance to post-sedimentation mineralisation events, a research project has been set up to focus on the detailed fluid inclusion characteristics in vein quartz from the Nchanga, Nkana, Chambishi, Konkola, and Mufulira deposits. In addition, anhydrite from the Nkana and Chambishi deposits were also sampled.

Initial studies are aimed at the late stage (Pan African?) veins and associated epigenetic mineralisation. This approach is adopted in order to differentiate late fluids characteristics from the earlier diagenetic/connate fluid species associated with stratiform mineralisation. Sampling to date includes non-mineralised quartz veins, as well as quartz veins mineralised with bornite, chalcopyrite, carrollite, and malachite. The veins occur in crosscutting- and bedding parallel fashion related to the host sediments, and are representative of successive tectonic episodes during the basin evolution: (1) pre-tectonic in terms of the deformation and folding, with lateral secretion of mineralisation into the vein, (2) syn-tectonic quartz veins present along a mineralised décollement plane, and (3) post-tectonic. Fluids preserved within the vein quartz in both the pre- and post-tectonic settings are characterised by H_2O-NaCl-CO_2±N_2 (as indicated by microthermometry and Raman microspectrometry), while NaCl-saturated carbonic brine compositions are indicative of fluids representative of the syn-tectonic setting. Although components of the late stage epigenetic mineralisation are clearly related to the remobilisation and re-precipitation of early stratiform ores, it is apparent that epigenetic ores also reflect new phases of fluid flow related to discrete Pan African tectonic intervals.

CONTRIBUTIONS TO THE GEOLOGY AND MINERALISATION OF THE CENTRAL AFRICAN COPPERBELT: III - NATURE OF METAMORPHIC AND EPIGENETIC FLUIDS

L.N. Greyling, Y. Yao, L.J. Robb & S. Master

Economic Geology Research Institute – Hugh Allsopp Laboratory,
School of Geosciences, University of the Witwatersrand, South Africa,
e-mail: greylin@science.pg.wits.ac.za

SYNOPSIS

Preliminary fluid inclusion results indicate the presence of aqueous-carbonic fluid species in pre-deformation fluids, and aqueous fluid species in syn-tectonic, and post-deformational fluids. Fluid inclusion microthermometry and Raman spectrometry of quartz veins in the Chambishi open pit indicate the presence of H_2O-NaCl-CO_2±CH_4 fluids, with Th = 130-160°C, and salinities at 23 wt.% NaCl equiv. Syn-tectonic fluids from the Nchanga open pit show H_2O-NaCl compositions. Two end-member fluids are present in post-deformational veins in the Nkana deposit, namely (a) a low-salinity (8-14 wt.% NaCl equiv.) and high Th of 300-400°C; and (b) high salinity (14-23 wt.% NaCl equiv.) and low Th of 100-150°C.

INTRODUCTION

Theories on the origin and primary mineralisation mechanism of the Neoproterozoic stratiform Cu-Co ores in the Central African Copperbelt range from syngenetic-diagenetic (Schneiderhöhn, 1931, Garlick, 1961, Sweeney & Binda, 1994) to epigenetic (Jackson, 1932). In an attempt, therefore, to quantify the role of various mineralising mechanisms, late fluid characteristics are compared to earlier diagenetic/connate fluid species associated with stratiform mineralisation. A detailed fluid inclusion study will document of the regional fluid characteristics (P-T-X-V) and aid in the modelling of the regional fluid evolution and relevance to post sedimentation mineralising events. This study focuses on the fluids trapped in vein quartz from the Nchanga, Nkana, Chambishi, Konkola, and Mufulira deposits, with the initial emphasis on late stage veins associated epigenetic (remobilised?) mineralisation. This paper is a summary of preliminary results of fluid inclusion microthermometry in vein quartz from various geological settings.

GEOLOGICAL SETTING

Stratiform Cu-Co ores are hosted in the Neoproterozoic Katangan Sequence on the border between the Democratic Republic of the Congo and Zambia (Fig. 1). The ores occur mostly in the Ore Shale, but are also found in overlying feldspathic quartzites, and wackes. The Katangan Sequence is divided in Zambia into the Roan Supergroup, Lower Kundelungu, and Upper Kundelungu Supergroups (Fig. 2). The sediments of the Katangan Sequence were metamorphosed and deformed to greenschist and amphibolite facies during the Lufilian orogeny at ca. 600 - 500 Ma (John et al., 2002).

PREVIOUS FLUID INCLUSION STUDIES

Pirmolin (1970) described the presence of several solid phases in fluid inclusions from a unmineralised cherty dolomite layer of the Mines Group of the Roan Supergroup in the Democratic Republic of Congo, and concluded that mineralising solutions reached temperatures of ~200°C at salinities of ~40 wt.% NaCl equiv.

Fluid inclusions, hosted in crosscutting vein quartz through the Ore Shale from Konkola Mine, showed post-trapping alteration features (e.g. leakage and annealing), which lead Sweeney (1987) to conclude that these veins had undergone at least one post-formational tectono-thermal event. He found that inclusions of the same vein system showed varying fluid chemistry at different stratigraphic horizons, and identified the presence of hydrocarbon inclusions in several samples.

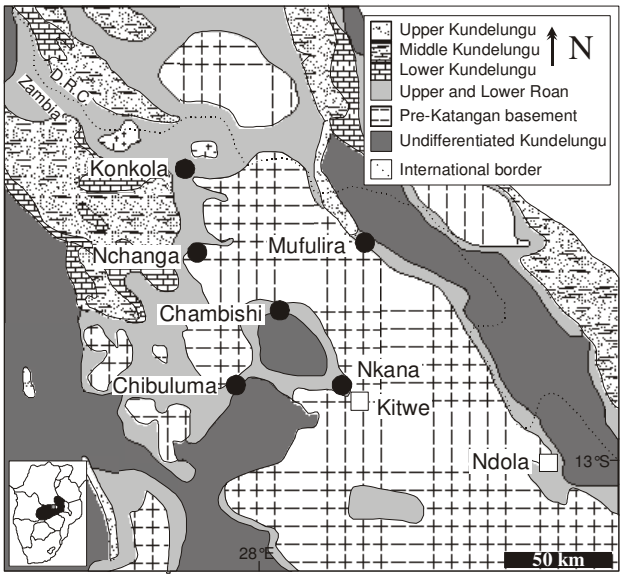

Fig. 1. Geological map of the Copperbelt in the Democratic Republic of Congo and Zambia.

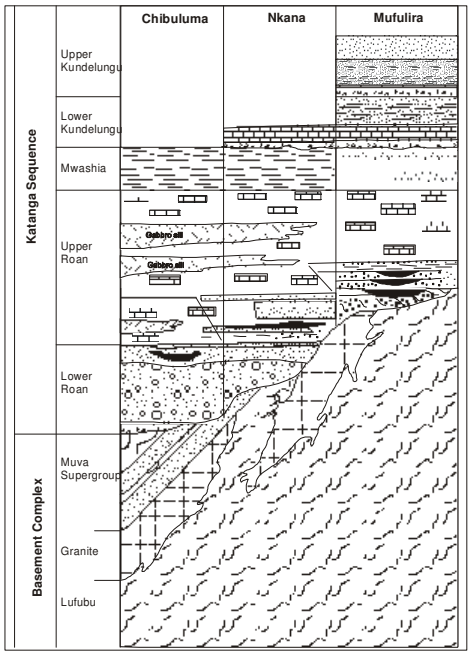

Fig. 2. Generalised stratigraphic profile of the Chibuluma, Nkana, and Mufulira deposits (after Fleischer et al., 1976).

This author also related the varying fluid chemistry to corresponding diagenetic changes in the different lithologies during basin evolution, and concluded that the veins formed by lateral migration of fluids during late diagenetic dewatering at temperatures of ~120°C.

Richards et al. (1988) indicated the presence of a halite-saturated fluid at temperatures of ~397°C in veins from the Musoshi copper deposit (D.R.C.), where late hydrothermal veining caused extensive footwall- and ore shale- alteration. Fluids were composed of approximately 39 wt.% NaCl, 15 wt.% KCl, and minor amounts of CO_2. It is concluded that the hydrothermal alteration event post-dated the stratiform copper mineralisation, causing modification of existing sulphide textures. The event may have been linked to compressional deformation and metamorphism during the Lufulian orogeny (Richards et al., 1987).

Epithermal mineralisation at the Kansanshi Copper Mine (Solwezi area, northwestern Zambia) was studied by Speiser et al. (1995), where vein mineralisation is related to hydrothermal alteration of the host rocks. Six fluid inclusion types were documented from the copper-quartz veins, and showed that epigenetic mineralisation precipitated from Na-Ca-Cl-H_2O-CO_2-(CH_4) brines. Ore formation pressures and temperatures correspond to 1.2 – 2.5 kbar and 230 – 310 °C respectively. Copper mineralisation post-dated host rock metamorphism, with crustal extension leading to increased heat flow and related hydrothermal fluid activity.

FLUID INCLUSIONS

Non-mineralised and mineralised (chalcocite-bornite-chalcopyrite-carrollite-malachite) quartz veins from the Chambishi, Nkana, Nchanga, Konkola, and Mufulira deposits in the Zambian Copperbelt are both discordant and bedding parallel and are representative of successive tectonic episodes during basin evolution. Samples in the Chambishi open pit were taken from quartz veins occurring bedding parallel to the Ore Shale (Fig. 3). Lateral secretion of mineralisation into the veins was noted with a refracted cleavage running through the quartz veins, indicating the emplacement of the quartz veins *prior to deformation and folding* of the mineralised sediments. Fluids in these samples show primary and secondary inclusions of H_2O-NaCl-CO_2±CH_4 compositions (Fig. 4), with a salinity of 23 wt.% NaCl equiv.

Quartz veins, occurring along the mineralised cupriferous vermiculite schist décollement plane in the Nchanga open pit, are representative of *syn-tectonic* fluids,and indicate the presence of H_2O-NaCl fluids in primary fluid inclusions. These NaCl-saturated solutions were heterogeneously trapped, as shown by the varying liquid-vapour-solid ratios.

Post-tectonic fluids were sampled from drill core through the Nkana synclinorium, from mineralised K-feldspar-quartz-biotite-anhydrite assemblage veins crosscutting host sediments. Primary and secondary inclusions from these veins show compositions of aqueous solutions (H_2O-NaCl) (Fig. 5). Initial microthermometric results show two possible end-member fluids: (A) low-salinity (8-14 wt.% NaCl equiv.) and high Th (300-400°C), and (B) high salinity (14-23 wt.% NaCl equiv.) and low Th (100-150°C) (Fig. 6).

Fig. 3. Lateral secretion vein in Ore Shale.

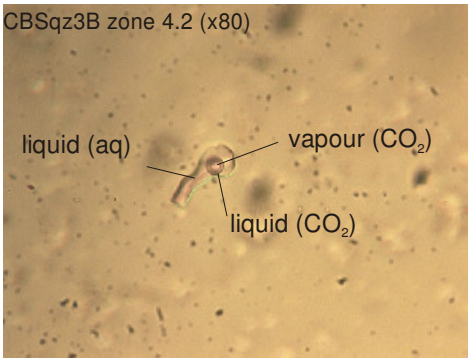

Fig. 4. Primary aqueous-carbonic fluid inclusion.

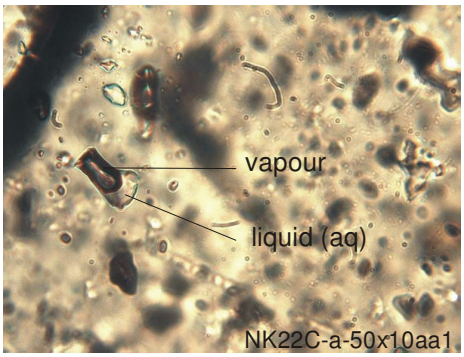

Fig. 5. Primary aqueous cluster inclusions.

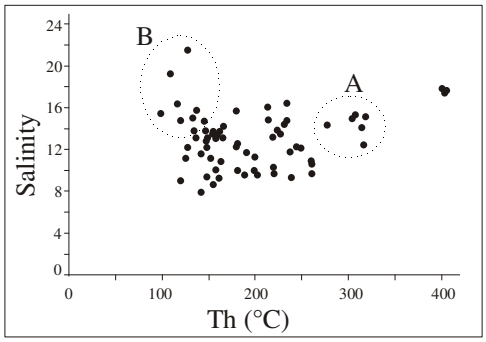

Fig. 6. Salinity (wt.% NaCl equiv.) vs. Th showing two end-member fluids.

DISCUSSION AND CONCLUSION

Initial studies of fluid inclusions, representative of various tectonic settings (pre-deformational, syn-tectonic, post-deformational), indicate the dominance of aqueous fluid species. Low temperature – high salinity fluids may be characteristic of basinal brines, which may correspond to early diagenetic stratiform mineralisation. High temperature – low salinity fluids are possibly derived from later regional metamorphic events, which are related to later stage remobilisation of mineralisation. It is suggested that stratiform Cu-Co mineralisation in the Zambian Copperbelt is resultant of multiple mineralisation events, involving diagenetic, metamorphic, and epigenetic processes.

ACKNOWLEDGEMENTS

Funding for this project is provided by the Economic Geology Research Institute, the University of the Witwatersrand and the National Research Foundation of South Africa. Anglo American (KCM), AVMIN, Non-Ferrous Metals Plc and First Quantum are thanked for providing access to the deposits.

REFERENCES

Fleischer V.D., Garlick W.G., Haldane R., (1976) Geology of the Zambian Copperbelt. In: K.H. Wolf (ed.) Handbook of strata-bound and stratiform ore deposits. II – Regional studies and specific deposits. Vol. 6, Cu, Zn, Pb, and Ag deposits. Elsevier, Amsterdam. p. 223-351.

John T., Schenk V., Scherer E., Mezger K., Haase K., Tembo F. (2002) Subduction and continental collision in the Lufulian Arc-Zambeai Belt orogen (Zambia): implications to the Gondwana assembly. Abstract Volume: 19th colloquium of African Geology, El Jadida, Morocco, 19-22 March 2002, p.188.

Pirmolin J., (1970) Inclusions fluids dans la dolomite du Gisement stratiforme de Kamoto (Katanga Occidental). Annales de la Société Géologique de Beligique, T. 93, p.397-406.

Richards J.P., Krogh T.E., Spooner E.T.C., (1988) Fluid inclusion characteristics and U-Pb Rutile ageof late hydrothermal alteration and veining at the Musoshi stratiform copper deposit, Central African Copper Belt, Zaire. Economic Geology, vol. 83, p.118-139.

Speiser A., Hein U.F., Porada H., (1995) The Kansanshi Copper Mine (Solwezi area, northwestern Zambia): Geology, wall-rock alteration and fluid inclusions. Mineral Deposits. Pasava, Kribek & Zak (eds), p. 389-392.

Sweeney M., (1987) The use of fluid inclusion geochemistry in determining the origin of veins, examples from the Zambian Copperbelt. Zambian Journal of Applied Earth Sciences, vol.1, p.18-28.

CONTRIBUTIONS TO THE GEOLOGY AND MINERALIZATION OF THE CENTRAL AFRICAN COPPERBELT: V. SPECULATIONS REGARDING THE 'SNOWBALL EARTH' AND REDOX CONTROLS ON STRATABOUND Cu-Co AND Pb-Zn MINERALIZATION

L. J. ROBB, S. MASTER, L. N. GREYLING,
Y. YAO & C. L. RAINAUD

Economic Geology Research Institute - Hugh Allsopp Laboratory,
School of Geosciences, University of the Witwatersrand, WITS 2050,
Johannesburg, South Africa.

SYNOPSIS

The major sediment-hosted Fe and Mn deposits of the world have formed by oxidative precipitation from ocean waters that are stratified in terms of redox state. There is mounting evidence that both Palaeoproterozoic Superior-type banded iron-formations and Neoproterozoic Rapitan-type iron ores formed in environments where fluctuations in redox states were influenced by global ice ages. Recent constraints on the age of the Katangan sequence in the Central African Copperbelt links much of its depositional history to the Cryogenian Period (850 to 650 Ma), during which time the Neoproterozoic 'Snowball Earth' occurred. This raises the question as to whether certain styles of stratiform sediment hosted copper (SSC) mineralization might also be genetically linked to the near-surface redox fluctuations that are associated with periods of global glaciation. Stratiform Cu-Co mineralization in the Copperbelt is early-to-late diagenetic in its timing and is suggested to be a product of the mixing of two fluids, one a pregnant oxidized solution and the other a reduced barren one. A source of reduced fluid might be compaction and diagenesis of sediments deposited during the global anoxia that accompanied the Sturtian/Chuos/Kaigas ice age at around 750 Ma. Fluids derived from such reduced sediments may also have been responsible for the formation of epigenetic Pb-Zn deposits hosted by cap carbonates. Our initial fluid inclusion studies indicate more than a single fluid population, although the relationship between fluids and the paragenetic sequence remains to be determined. Such a link needs to be tested by accurate age determinations of the stratabound mineralization events.

INTRODUCTION

The major sediment-hosted Fe and Mn deposits of the world have formed by oxidative precipitation from sea water that was stratified with respect to its redox state. Neoproterozoic Rapitan-type iron-formations formed in environments where fluctuations in near-surface redox states were influenced by two or more near-global ice ages, popularly referred to as the 'Snowball Earth' events (Hofmann & Schrag, 2000). There is mounting evidence that Palaeoproterozoic Superior-type banded iron-formations, as well as related bedded Mn ores, might also be related to a period of extensive low-latitude glaciation (Kirschvink et al., 2000). It is also intriguing to note that the Duitschland Formation of the Palaeoproterozoic Transvaal Supergroup is characterized by minor stratiform Cu deposits (Martini, 1979) hosted in limestones associated with diamictite units that are correlatable with the same low-latitude glaciogenic Makganyene diamictite with which the huge Fe and Mn ores of Griqualand West are linked (Bekker et al., 2001). Given that the solubilities of Cu, Co, Pb and Zn complexes in aqueous solution are redox sensitive, the question of environmental/climatic controls on the oxidative state of the near surface are perhaps also likely to be relevant to ore genetic considerations for the stratiform ores of the Central African Copperbelt. This is particularly so given the new constraints on the age of the Katangan sequence, a significant component of which was deposited during the Cryogenian Period (850 to 650 Ma).

RELEVANT GEOCHRONOLOGICAL CONSTRAINTS

We have recently provided U-Pb zircon geochronological constraints indicating that the Roan Group was deposited between 880 Ma (the age of the Nchanga granite and detrital zircons in the lower Roan sediments) and 760 Ma (a volcanic unit just below the Grand Conglomerat at the base of the Guba or Lower Kundelungu Supergroup; Key et al., 2001). A maximum age of the Upper Kundelungu (Plateau Group) sediments is provided by Ar-Ar ages of detrital muscovite of 565 Ma. The Katangan sequence was, therefore, deposited episodically over an extended period (>300 million years) of geological time. The two glacial diamictite units in the Katangan sequence, the Grand Conglomerat (GC) and Petit Conglomerat (PC) at the respective bases of the Lower and Upper Kundelungu Supergroups (now included in the Guba Group, Wendorff, 2001), are bracketed between 760 Ma and 580 Ma and are, therefore, possible correlatives of the Sturtian/Chuos/Kaigas (at circa 750 Ma) and the Marinoan/ Varangian/Numees (at circa 600 Ma) glaciogenic deposits that define the Snowball Earth freeze-over. The two glaciogenic horizons are characterized by cap carbonate units immediately overlying them. Magnetite- and haematite-rich BIF units (with minor Mn) below the GC in the Mwashya are correlated with similar iron formations in the Rapitan, Urucum, Damara and other sequences worldwide, which are a reflection of globally stratified oceans during the Cryogenian period. Evidence that the Mwashya sediments were deposited during the global ice ages comes from preliminary carbon isotope data, which show a negative excursion in del ^{13}C in the Mwashya, going to a minimum of –5 permil PDB in the Grand Conglomerat, and recovering to more positive values in the Kakontwe cap carbonates. The C isotope data permit a chemostratigraphic correlation between the Mwashya and Guba Groups, and other Neoproterozoic successions deposited during the Sturtian/Chuos glaciation.

There are few if any accurate age data constraining the timing of stratiform Cu-Co mineralization in the Copperbelt. A K-Ar age of 870±42 Ma (Cahen et al., 1984) for a microcline vein cutting stratiform ore is widely quoted, as is the range between 790 Ma and 750 Ma provided by Pb-Pb model ages for Pb-Zn mineralization from several deposits in the region (Kampunzu et al., 1999). However, Kamona et al. (1999) rejected the 3-stage “shale-curve” Pb-evolution model used by Kampunzu et al. (1999), and got ages of 680 Ma for Kabwe mineralization, and 456±18 Ma for Kipushi mineralization. Richards et al. (1988) provided a Pb-Pb model age of 645±15 Ma for Cu-Fe sulphides from the Musoshi Mine, a date interpreted as reflecting either primary ore deposition or Pb re-homogenization. Walraven and Chabu (1991) obtained a Pb model age of 823 Ma for Kinsenda copper sulphide mineralization. Given the long-lived depositional history of the Katangan sequences, it is clear that the concept of diagenetic mineralization is likely to be grossly diachronous and could itself have extended over an extended period of geological time. Diagenesis and related fluid flow in the lower Roan sediments were probably separated by more than 100 million years of time from those in the upper Mwashya and lower Kundelungu sequences.

NATURE OF STRATABOUND Cu-Co MINERALIZATION

Mineralization consists of disseminated copper and cobalt sulphide minerals (chalcocite, bornite, chalcopyrite, carrolite) occurring as dispersed grains, fracture fillings, near massive lenses and replacements of diagenetic pyrite, Fe-Ti detrital minerals and micaceous silicates. The sedimentary host rocks mainly form part of the lower Roan Supergroup and comprise a wide range of lithotypes, including basal continental clastics and aeolianites, shales and siltstones, evaporitic carbonates, dolomitic shales and stromatolitic bioherms. Much of the mineralization is linked to the ‘Ore Shale’, that was formed in a restricted marine or lacustrine environment, although many other sediment types are also mineralized. In at least one situation at Shituru Mine, stratiform mineralization is hosted by reduced volcaniclastic rocks in the Mwashya Group (Lefebvre, 1974). Unrug (1988) has emphasized the fact that stratiform Cu-Co mineralization is distributed throughout the Roan Supergroup but does not occur above the GC, into the Kundelungu sequences. Different scales of mineral zonation are evident in the district and, in general, there is metal segregation into Cu, Cu-Co and Pb-Zn rich zones.

NATURE OF Pb-Zn MINERALIZATION

Pb-Zn mineralization in the Katangan is epigenetic, and occurs in transgressive orebodies hosted in two different stratigraphic units. At Kabwe, Zambia, Pb-Zn-(V-Ga-Ge-Cd-Ag) mineralization in pipe-like bodies is hosted by carbonate rocks correlated with the Upper Roan Group. Highly saline (c. 30 wt.% eNaCl) fluid inclusions from Kabwe show homogenisation temperatures of 60 to 390°C (Kamona, 1993). At Kipushi, Kengere and Lombe in D. R. Congo, transgressive Zn-Pb-(Cu-Ga-Ge-Mo-As-Ag) mineralization occurring along faults and in breccia fill is hosted by the Kakontwe cap carbonate above the Grand Conglomerat. Kipushi fluids were reducing, since hydrocarbons ("shungite") are associated with the mineralization (Francotte & Jedwab, 1963), which was deposited at c. 300°C (T_h on fluid inclusions, Kapenda, unpubl. data, in Kampunzu et al., 1998).

REDOX BEHAVIOUR OF Cu, Co, Pb AND Zn

There is abundant geological evidence (e.g. replacement textures, reduction spheroids etc) to indicate that the formation of stratiform ores in the Copperbelt has been influenced by redox reactions involving electron transfer in an aqueous medium. The contrasting redox behaviour of metals such as Cu-Co, as well as Pb-Zn, can explain their segregation in such an environment and the development of metal zonation at a variety of scales. The higher the standard reduction potential (Eh_o) of a metal the more susceptible the species is to being reduced.

$Cu \leftrightarrow Cu^{2+} + 2e^-$	$Eh_o = +0.34V$
$Pb \leftrightarrow Pb^{2+} + 2e^-$	$Eh_o = -0.13V$
$Co \leftrightarrow Co^{2+} + 2e^-$	$Eh_o = -0.28V$
$Zn \leftrightarrow Zn^{2+} + 2e^-$	$Eh_o = -0.76V$

The contrasting characteristics of Cu and Co are illustrated in the redox reactions above and also illustrated in Figure 1. It is clear that progressive reduction will first result in the precipitation of Cu from an aqueous solution, followed under more reducing conditions by Co. Superposition of oxic and anoxic fluid fields on the Eh-pH diagram in Figure 1 shows that Cu and Co complexes are relatively soluble under oxic conditions but are less stable under reducing conditions.

The effects of mixing an oxidized, metal-charged fluid with a more reducing liquid such as an oilfield brine have been modelled by Metcalfe et al. (1994) who showed that addition of even a small proportion of the latter will, after only 5% mixing, dramatically change the redox state and promote the sequential precipitation of, first Cu, and then Pb and Zn (once all the Cu had effectively been stripped from solution Figure 2). Although data is not available for Co, the sequence is consistent with the paragenetic characteristics of SSC deposits in general.

GLOBAL ANOXIA AND THE FORMATION OF COPPERBELT STRATIFORM ORES?

Stratiform Cu-Co mineralization in the Copperbelt is generally regarded as being early-to-late diagenetic in its timing. Widely accepted models for the formation of SSC ores (Unrug, 1988; Jowett, 1986) envisage circulation of oxidized brines through porous continental (often aeolian) arenites that are themselves enriched in detritus from a metal fertile provenance. These fluids scavenge metals that have high solubilites in saline, oxidized and near neutral solutions (such as Cu, Co, U, Ni etc), with precipitation of metals occurring as they encounter environments where redox reactions take place (i.e. in the presence of diagenetic sulphides, organic rich sediments etc). Two scenarios exist, that are not mutually exclusive; (i) scavenging of metals by a *single oxidized fluid* passing through permeable strata with lateral precipitation of ores in the proximity of more reduced facies (Bechtel et al., 2002); or (ii) the mingling of *two fluids* in a single aquifer, one a pregnant oxidized solution and the other a reduced barren one (e.g., Bartholomé et al., 1972). Our initial fluid inclusion work suggests that the earliest fluids recorded (e.g. from Chambishi Mine) are characterized by low homogenization temperatures (T_h = 130 to 160°C) and constant high salinity (23 wt.% eNaCl; H_2O-NaCl-CO_2±CH_4) fluid

compositions that are potentially diagenetic in origin. Later syn- to post-orogenic fluids (e.g. Nchanga and Nkana Mines) are more diverse in composition and typically have higher homogenization temperatures.

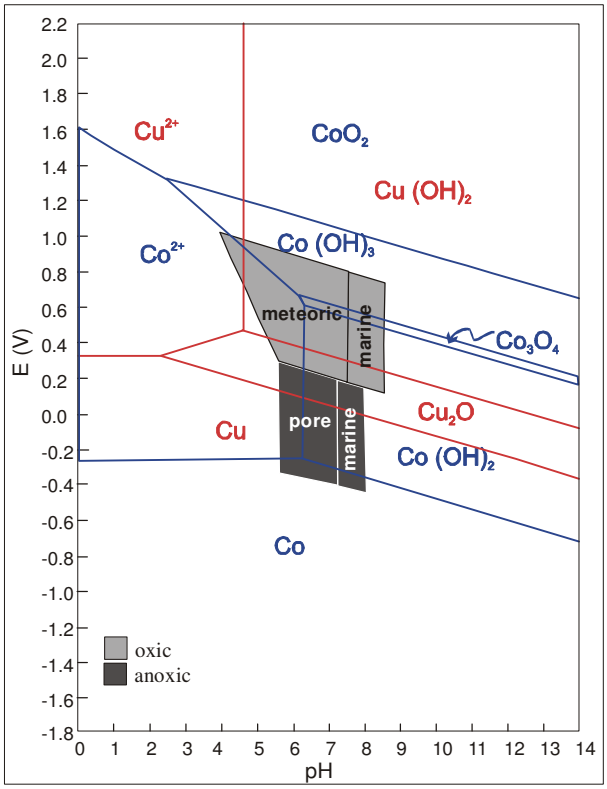

Figure 1: Potential - pH diagram for Cu and Co in the system Cu-Co-H_2O at 25°C (after de Zoubov et al., 1980, and Deltombe, 1980).

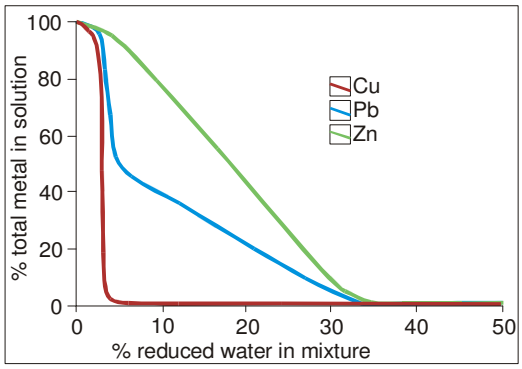

Figure 2: Fluid-rock equilibrium model showing the effect on Cu, Pb, and Zn solubility of mixing a reduced connate fluid with an oxidized metal-laden, diagenetic pore fluid (after Metcalfe et al., 1994).

In the ore genetic scenario involving the mixing of two fluids, the oxidised, metal-bearing fluid is generally thought to be a saline basin brine which became oxidising and chloride and sulphate enriched through reaction with red beds and evaporites. The reduced fluid is generally thought to be expelled into aquifers from the compaction of reduced organic-rich sediments. In the Katangan basin, oxidised brines could have evolved through reaction with the abundant evaporites in the upper Roan Group. We suggest that the

reduced fluids responsible for Pb-Zn mineralization, and for some of the Cu-Co mineralization in the two-fluid mixing model (e.g. at Shituru), could have been derived from the adundant black shales in the Mwashya Group, which were deposited during global anoxia coinciding with Snowball Earth conditions.

CONCLUSIONS

Although the conceptual notions regarding fluid mixing and metal deposition in SSC deposit environments are not new, they receive added credibility with respect to the Central African Copperbelt in the light of the new Cryogenian age constraints for Katangan deposition and preliminary fluid inclusion characteristics of ore bearing fluids. Confirmation of such a link with respect to the stratiform Cu-Co ores will need to be rigorously tested by obtaining accurate age determinations for the mineralization events.

REFERENCES

Bartholomé, P., Evrard, P., Katekesha, F., Lopez-Ruiz, J. & Ngongo, M. (1972) Diagenetic ore-forming processes at Kamoto, Katanga, Republic of the Congo. In: Amstutz, G. C. & Bernard, A. J. (Eds.), Ores in sediments. Springer, Berlin, 21-41.

Bechtel, A., Gratzer, R., Püttmann, W. & Oszczepalski, S. (2002). Geochemical characteristics across the oxic/anoxic interface (Rote Fäule front) within the Kupferschiefer of the Lubin-Sieroszowice mining district (SW Poland). Chemical Geology, 185, 9-31.

Bekker, A., Kaufman, A. J., Karhu, J. A., Beukes, N. J., Swart, Q. D., Coetzee, L. L. & Eriksson, K. A. (2001). Chemostratigraphy of the Palaeoproterozoic Duitschland Formation, South Africa: Implications for coupled climate change and carbon cycling. American Journal of Science, 301, 261-285.

De Zoubov, N., Vanleugenhaghe C., & Pourbaix M. (1980). *Copper, Section 14.1*. In: Pourbaix M. (Ed.), Atlas of electrochemical equilibria in aqueous solutions. National Association of Corrosion Engineers, Houston, Texas, U.S.A. CEBELCOR (ed.) Brussels. p. 384-392.

Deltombe E. & Pourbaix M. (1980). Cobalt, Section 12.2. In: Pourbaix M. (Ed.), Atlas of electrochemical equilibria in aqueous solutions. National Association of Corrosion Engineers, Houston, Texas, U.S.A. CEBELCOR (Ed.) Brussels. p. 322-329.

Cahen, L., Snelling., N. J., Delhal, J., Vail, J. R., Bonhomme, M. & Ledent, D. (1984). The Geochronology and Evolution of Africa. Clarendon, Oxford, 512 pp.

Francotte, J. & Jedwab, J. (1963). Traces d'organites (?) dans la Shungite de Kipushi. Bull. Soc. géol. Belg., 72, 393-400.

Hofmann, P. F. & Schrag, D. P. (2000). Snowball Earth. Scientific American, 282(1), January, 50-57.

Jowett, E. C. (1986). Genesis of Kupferschiefer Cu-Ag deposits by convective flow of Rotliegendes brines during Triassic rifting. Economic Geology, 81, 1823-1837.

Kamona, F. (1993). The carbonate-hosted Kabwe Pb-Zn deposit, Central Zambia. Ph.D. thesis, TU Aachen, Germany, Mitteilungen zur Mineralogie und Lagerstättenlehre, 44, 207 pp.

Kamona, F. Leveque, J., Friedrich, G. & Haack, U. (1999). Pb isotopes of the carbonate-hosted Kabwe, Tsumeb, and Kipushi Pb-Zn-Cu sulphide deposits in relation to Pan African orogenesis in the Damara-Lufilian Fold Belt of Central Africa. Mineralium Deposita, 34, 273 -283.

Kampunzu, A. B. & Cailteux, J. (1999). Tectonic evolution of the Lufilian Arc during the Pan-African orogenesis. Gondwana Research, 2(3), 401-421.

Kampunzu, A. B., Wendorff, M., Kruger. F. J. & Intiomale, M. M. (1998). Pb isotopic ages of sediment-hosted Zn-Pb mineralisation in the Neoproterozoic Copperbelt of Zambia and Democratic Republic of Congo (ex-Zaire): re-evaluation and implications. Chronique de la Recherche Minière, No. 530, 55-61.

Key, R. M., Liyungu, A. K., Njamu, F. M., Somwe, V., Banda, J., Mosley, P. N. & Armstrong, R. A. (2001). The Western arm of the Lufilian Arc, NW Zambia and its potential for copper mineralization. J. Afr. Earth Sci., 33 (3-4), 503-528.

Kirschvink, J. L., Gaidos, E. J., Bertani, L. E., Beukes, N. J., Gutzmer, J., Maepa, L. N. & Steinberger, R. E. (2000). The Paleoproterozoic Snowball Earth: extreme climatic and geochemical global change and its biological consequences. Proc. National Acad. Sci., 97, 1400-1405.

Lefebvre, J. J. (1974). Mineralisations cupro-cobaltiferes associées aux horizons pyroclastiques situés dans le faisceau supérieur de la Serie de Roan, à Shituru, Shaba, Zaire. In: Bartholomé, P. et al. (Eds.), Gisements stratiformes et provinces cuprifères. Soc. Géol. Belgique, Liège, 103-122.

Martini, J. E. J. (1979). A copper-bearing bed in the Pretoria Group in northeastern Transvaal. Geokongerss '77: Geol. Soc. S. Afr. Spec. Publ. 6, 65-72.

Metcalfe, R., Rochelle, C. A., Savage, D. & Higgo, J. W. (1994). Fluid-rock interactions during continental red bed diagenesis: implications for theoretical models of mineralization in sedimentary basins. In: Parnell, J. (Ed.), Geofluids: Origin, Migration and Evolution of Fluids in Sedimentary Basins, Geological Society Special Publication No. 78, 301-324.

Richards, J. P., Cumming, G. L., Krstic, D., Wagner, P. A. & Spooner, E. T. C. (1988). Pb isotope constraints on the age of sulfide ore deposition and U-Pb age of late uraninite veining at the Musoshi stratiform copper deposit, Central African Copper Belt, Zaire. Econ. Geol., 83, 724-741.

Unrug, R. (1988). Mineralization controls and source metals in the Lufulian Fold Belt, Shaba (Zaire), Zambia, and Angola. Economic Geology, 83, 1247-1258.

Walraven, F. & Chabu, M. (1991). Pb-isotope geochemistry of the Kipushi Zn-Pb-Cu ore deposit, southeastern Zaire. Abstr., 1st Int. Symp. Geology and Mineral Resources of the Central and Southern African Subcontinent, 15-25 August 1991, Geol. Dept., Univ. Lubumbashi, Zaire, 42-45.

Wendorff, M. (2001). New exploration criteria for 'megabreccia'-hosted Cu-Co deposits in the Katangan belt, central Africa. In: Piestrzynski, A. et al. (Eds.), Mineral Deposits at the Beginning of the 21st Century. Swets & Zeitlinger Publishers, Lisse, Netherlands, 19-22.

Rand Afrikaans University (PPM), Mineralogical Society of South Africa, South African Students - Society of Economic Geologists Symposium: Mineralogy and geochemistry of base metal deposits in Southern Africa – Implications for exploration and beneficiation, 23 September 2003

Fluid inclusion characteristics of the Copperbelt, and overview of Katangan geochoronology

Lynnette Greyling[1], Christine Rainaud[1], Laurence Robb[1], Michel Cathelineau[2], Marie-Christine Boiron[2], Yong Yao[1]

[1] *Economic Geology Research Institute, Private Bag 3, School of Geosciences, University of the Witwatersrand, 2050 WITS, South Africa*

[2] *CREGU, UMR G2R CNRS 7566, Faculté des Sciences, Université Henri-Poincaré, BP23, Vandoeuvre-Lés-Nancy Cedex, France*

INTRODUCTION

The stratiform ores of the Zambian and Democratic Republic of the Congo (DRC) Copperbelt are hosted by the metasediments of the Katangan sequence. This sedimentary succession overlies a Mesoarchaean to Neoproterozoic basement, which is composed of the metavolcanics of the Lufubu schists, the metasediments of the Muva Sequence, and various granitoids mainly intruding the Lufubu schists (Rainaud et al. 2003a,b; Armstrong et al. 2003). The Nchanga Granite is the youngest intrusion in the pre-Katangan basement and has been dated with certainty with the U-Pb SHRIMP technique at 877±11Ma (Armstrong et al. 2003).

Current lithostratigraphic practice in the DRC is to subdivide the Katanga Supergroup into the Roan, Nguba (ex-Lower Kundelungu) and Kundelungu (ex-Upper Kundelungu) Groups. Recently, Wendorff (2001; 2003a,b) has proposed a new lithostratigraphic scheme, in which the Katanga Supergroup is subdivided into the Roan, Guba and Kundelungu Groups, with two additional lithotectonic units, the Fungurume and Biano Groups, which were deposited syntectonically in a foreland basin during deformation of the earlier Katangan groups during the Pan-African Lufilian orogeny.

Age constraints on the deposition of this sedimentary sequence are still scarce. Detrital zircons from the Lower Roan yielded two groups of ages: one at around 2-1.8 Ga corresponding to the age of the Palaeoproterozoic basement, and another at around 880 Ma corresponding to the age of the Nchanga granite, therefore showing that the Katangan sedimentary sequence is younger that this intrusion. In western Zambia, volcanics within the Mwashya Subgroup (Nguba Group), have been dated at 760 ± 5 Ma, utilising SHRIMP U-Pb dating on zircons (Key et al., 2001). Recent dating by Barron et al. (2003) of two gabbroic bodies in the Solwezi area, NW Zambia, yielded ages of 745 ± 7.8 Ma and 752.6 ± 8.6 Ma, which are consistent with them being part of the extensional mafic magmatism associated with the Mwashya Subgroup (e.g., Kabengele et al., 2003).

To the southeast of the Mwinilunga (NW Zambia) area, strongly deformed and poorly differentiated Katangan rocks of the West Lunga Formation have been provisionally correlated with the Lower Kundelungu Supergroup (Liyungu et al., 2001), which corresponds to the upper part of the Nguba Group above the Grand Conglomerat (i.e., Muombe Subgroup of Wendorff, 2003a,b). One of the porphyritic lavas in this area has been dated with the SHRIMP (U/Pb on single zircons) at 735 ± 5 Ma (Armstrong, 2000;

Liyungu et al., 2001). Finally, detrital muscovites from Biano Group siltstones give a maximum $^{40}Ar/^{39}Ar$ age of sedimentation of 570 ± 5 Ma for this group.

MINERALIZATION

Mineralization in the Copperbelt is hosted mainly in shales (Luanshya, Nkana, Chambishi, Chingola, Chililabombwe, Musoshi) and arenites/arkoses (Mufulira, Bwana Mkubwa), of the lower part of the Roan Group. Subsequent metamorphic events (including the Pan African Lufulian orogeny) have led to the remobilisation of primary sulphides. The mineralization is present in the form of copper- (and locally cobalt-) sulphides. Major primary minerals include chalcopyrite, bornite, chalcocite, pyrite, ±carrollite and cobaltiferous pyrite. Secondary alteration minerals include covellite, digenite, tellurobismuthite, molybdenite, and uranium minerals as minor occurrences. Primary sulphide ores are leached and oxidised to copper carbonates (malachite, azurite), native copper, copper oxides (cuprite, tenorite), copper phosphates, copper silicates (chrysocolla), copper sulphates, cupriferous wad, and cupriferous micas (Notebaart & Vink, 1972).

FLUID INCLUSIONS

Fluid inclusion microthermometry and Raman spectroscopy were conducted on samples representing various tectonic settings from selected deposits in the Zambian Copperbelt. This has revealed the presence of diverse fluid types. The reader is referred to Table 1 for a list of properties of the following fluid types.

Authigenic quartz overgrowths

Primary fluid inclusions present in 'dust rims' between quartz grains of the metasediments of the Upper Ore Body at the Nchanga Mine revealed the presence of aqueous (w), and aqueous-carbonic (w-c) fluids generally with included halite daughter crystals (s). These inclusions are small in size, ranging from 6 to 15 µm in diameter.

Pre-tectonic quartz veins

Quartz veins intruded the mineralized metasediments of the Chambishi deposit before folding during metamorphism, as is indicated by field observations of cleavages running through the metasediments. Refracted cleavages are visible in the quartz veins. Mineralization from the sediments laterally secreted into the quartz veins which were subsequently folded together with the sediments. The veins are therefore representative of post-mineralising, pre-deformational fluids. These fluids are divided into three main types, namely aqueous (w), aqueous-carbonic (w-c), and methane-rich (m) inclusions. The aqueous fluids are low- to high salinity $CaCl_2$-NaCl±KCl brines.

Syn-tectonic quartz veins

Quartz veins, representative of pulses of syn-tectonic fluid introduction to the sediments during metamorphism, were sampled from the Chambishi, Nchanga, Nkana, and Mufulira deposits. The aqueous fluids inclusions (w) were found in samples from Nchanga, and correspond to low salinities. Aqueous-carbonic (w-c±s) fluids from Chambishi are relatively saline with CO_2, N_2, CH_4, $\pm C_2H_6$, and H_2. Aqueous-carbonic fluids sampled from Nchanga show CO_2 and N_2 in the volatile phases, with halite daughter minerals. Carbonic-rich inclusions (±w), and methane-rich (m) inclusions (with no H_2O) were also

identified. Aqueous inclusions from Nkana contain methane (w-m), whereas aqueous fluids from Mufulira are composed of N_2 in the volatile phases. The Mufulira inclusions are saturated with halite, and some inclusions also contain hematite (he) daughter minerals.

CONCLUSIONS

Microthermometry and Raman spectroscopy reveal the diverse nature of fluids representative of various tectonic settings. Fluid inclusions representative of syn-tectonic processes are more complex in compositions compared to earlier fluids. Fluid inclusions in the authigenic setting may be indicative of fluids preserved during diagenetic processes. However, subsequent fluid infiltration during metamorphic events may also have overprinted fluid inclusions, and/or trapped new inclusions in pre-existing porous zones in the sediments.

Table 1: Microthermometry and Raman analyses for fluid inclusions from three paragenetic settings of the Zambian Copperbelt (see text for explanation of abbreviations)

		Authigenic	***Pre-tectonic***	***Syn-tectonic***
deposit		Nchanga	Chambishi	Chambishi, Nchanga, Nkana, Mufulira
host mineral		quartzites	quartz veins	quartz veins
type		• w ±s • w-c ±s	• w • w-c • m	• w • w-c ±s • c ±w • m • w-n-s ±he
Tm ice (°C)	**w**	-15.7 to -3.1	-22.1 to -1.6	-7.1 to -6.0
	w-c	-25 to -17	-21.2 to -11.6	-24.0 to -6.4
volatile composition (mol%)		w-c ±s: CO_2: ~97 N_2 ~2.5 CH_4 ~ <0.3	w-c: CO_2: ~98.5 N_2: ~1.3 H_2S: ~<0.5 m: CH_4: ~93 N_2: ~6.5 C_2H_6: ~0.5	w-c ±s -Chambishi CO_2: 32-98 N_2: 1-47 CH_4: 0.3-35 H_2: 14 w-c ±s -Nchanga CO_2: ~97.5 N_2: ~2.5 c (±w) -Nchanga CO_2: ~97.5 N_2: ~2.5 m -Nchanga CH_4: 100 w-m-Nkana CH_4: 84 CO_2: 16 w-n-s ±he -Mufulira N_2: 100

ACKNOWLEDGEMENTS

The Society of Economic Geologists Foundation – Hugh E. McKinstry Fund and BHP Student Research Grant is thanked for contributing to the funding of this project.

REFERENCES

Armstrong, R.A., Master, S., Robb, L.J., Lobo-Guerrero, A. (2003). Geochronology of the Nchanga Granite, and constraints on the maximum age of the Katanga Supergroup, Zambian Copperbelt. J. Afr. Earth Sci. (submitted).

Armstrong, R.A. (2000). Ion microprobe (SHRIMP) dating of zircons from granites, granulites and volcanic samples from Zambia. Unpubl. Rep., ANU, PRISE Job No. A99-160, Canberra.

Barron, J.W., Broughton, D.W., Armstrong, R.A., Hitzman, M.W. (2003). Petrology, geochemistry and age of gabbroic bodies in the Solwezi area, northwestern Zambia. In: Contributions presented at the 3rd IGCP-450 Conference, Proterozoic Sediment-hosted Base Metal Deposits of Western Gondwana; Conference and Field Workshop Lubumbashi 2003, Lubumbashi, D.R. Congo, 75-77.

Kabengele, M., Mashala, T., Loris, N.B.T. (2003). Geochemistry of the Lower Mwashya pyroclastic rocks in the Likasi-Kambove area (D.R. Congo). In: Contributions presented at the 3rd IGCP-450 Conference, Proterozoic Sediment-hosted Base Metal Deposits of Western Gondwana; Conference and Field Workshop Lubumbashi 2003, Lubumbashi, D.R. Congo, 69-74.

Key, R. M., Liyungu, A. K., Njamu, F. M., Somwe, V., Banda, J., Mosley, P. N., Armstrong, R. A. (2001). The Western arm of the Lufilian Arc, NW Zambia and its potential for copper mineralization. J. Afr. Earth Sci., 33 (3-4), 503-528.

Liyungu, A. K., Mosley, P.N., Njamu, F.M., Banda, J. (2001). Geology of the Mwinilunga area. Rep. Geol. Surv. Zambia, 110, 36 pp.

Notebaart, C. W., and Vink, B. W. (1972). Ore minerals of the Zambian Copperbelt. *Geologie en Mijnbouw,* 51(3), 337-345.

Rainaud, C., Master, S., Armstrong, R.A., Robb, L.J., Mumba, P.A.C.C. (2003a). Nature and geochronology of the pre-Katangan basement in the Central African Copperbelt. J. Afr. Earth Sci. (submitted).

Rainaud, C., Master, S., Armstrong, R.A., Robb. L.J. (2003b). A cryptic Mesoarchaean terrane in the basement to the Central African Copperbelt. Journal of the Geological Society, London, 160, 11-14.

Wendorff, M. (2001). New exploration criteria for 'megabreccia'-hosted Cu-Co deposits in the Katangan belt, central Africa. In: Piestrzynski, A. et al. (Eds.), Mineral Deposits at the Beginning of the 21st Century. Swets & Zeitlinger Publishers, Lisse, Netherlands, pp. 19-22.

Wendorff, M. (2003a). Stratigraphy of the Fungurume Group- evolving foreland basin succession in the Lufilian fold-thrust belt, Neoproterozoic-Lower Palaeozoic, Democratic Republic of Congo. South African Journal of Geology, 106, 47-64.

Wendorff, M. (2003b). Conglomerates and sedimentary megabreccia (olistostrome) in Roan-Mwashya succession in Mufulira, Copperbelt of Zambia. In: Contributions presented at the 3rd IGCP-450 Conference, Proterozoic Sediment-hosted Base Metal Deposits of Western Gondwana; Conference and Field Workshop Lubumbashi 2003, Lubumbashi, D.R. Congo, 94-97.

Transactions of the Institute of Mining and Metallurgy, 2003, 112, 2, 164-166

TIMING OF Cu-Co and Pb-Zn MINERALIZATION IN THE CENTRAL AFRICAN COPPERBELT: A LINK TO NEOPROTEROZOIC GLACIATIONS?

Laurence Robb[1] Sharad Master[1], Richard Armstrong[2] ,
Christine Rainaud[1]and Lynnette Greyling[1]

1Economic Geology Research Institute-Hugh Allsopp Lab, School of Geosciences, University of the Witwatersrand, Johannesburg, SOUTH AFRICA (robblj@geosciences.wits.ac.za)
2 Research School of Earth Sciences, Australian National University, Canberra, ACT, AUSTRALIA (richard.armstrong@anu.edu.au).

Introduction:

Evidence for low-latitude continental glaciation is found in mid-and late Neoproterozoic successions worldwide. Global stratigraphic correlations are consistent with, but not yet proof of, two major phases of wide-spread glaciation, one mid-Neoproterozoic phase (often correlated with the 'Sturtian' event) at ca. 730 ± 15 Ma and a younger phase (generally referred to as the 'Marinoan') at ca. 580 ± 10 Ma. Rapitan type banded iron-formations are frequently associated with, but are not unique to, the earlier episode of glaciation. They point to stratified oceanic conditions in the Cryogenian Period in which ferric iron and silica were precipitated at a redox interface.

Age constraints:

We have recently provided geochronological constraints indicating that the Katangan sequences that host the vast stratiform Cu-Co and epigenetic Pb-Zn deposits of the Central African Copperbelt are midNeoproterozoic to Cambrian in age (Master et al., 2002). The lowermost Roan Group was deposited between 880 Ma (the age of the Nchanga granite and detrital zircons in the lower Roan sediments) and 760 Ma (a volcanic unit just below the Grand Conglomerat at the base of the Guba or Lower Kundelungu Supergroup; Key et al., 2001). A maximum age of the Upper Kundelungu (Plateau Group) sediments is provided by Ar-Ar ages from detrital muscovite of 565 Ma. The Katangan sequence was, therefore, deposited episodically over an extended period (about 300 million years) of geological time (Figure 1). The two glacial diamictite units in the Katangan sequence, the Grand Conglomerat (GC) and Petit Conglomerat (PC) at the respective bases of the Lower and Upper Kundelungu Supergroups (now included in the Guba Group, Wendorff, 2001), are bracketed between 760 Ma and 565 Ma and are, therefore, likely correlatives of the Sturtian and Marinoan glaciogenic deposits. The two glaciogenic horizons are characterized by cap carbonate units immediately overlying them. Magnetite- and haematite-rich BIF units (with minor Mn) below the GC in the Mwashya are correlated with similar iron formations in the Rapitan, Urucum, Damara and other sequences worldwide.

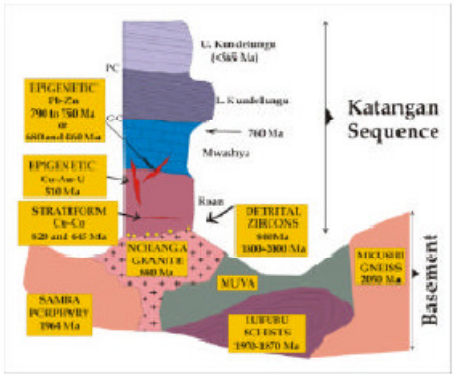

Figure 1. Simplified geological and age relationships in the Zambian portion of the Central African Copperbelt

Mineralization:

Stratiform mineralization in the Copperbelt consists of disseminated copper and cobalt sulphide minerals (chalcocite, bornite, chalcopyrite, carrolite) occurring as dispersed grains, fracture fillings, near massive lenses and replacements of diagenetic pyrite, Fe-Ti detrital minerals and micaceous silicates. The sedimentary host rocks mainly form part of the lower Roan Supergroup and comprise a wide range of lithotypes. Much of the mineralization is linked to the 'Ore Shale', that was formed in a restricted marine or lacustrine environment, although many other sediment types are also mineralized. In at least one situation at Shituru Mine, stratiform mineralization is hosted by reduced volcaniclastic rocks in the overlying Mwashya

Transactions of the Institute of Mining and Metallurgy, 2003, 112, 2, 164-166

Group. Unrug (1988) has emphasized the fact that stratiform Cu-Co mineralization is distributed throughout the Roan Supergroup but does not occur above the GC, into the Kundelungu sequences. Different scales of mineral zonation are evident in the district and, in general, there is metal segregation into Cu, Cu-Co and Pb-Zn rich zones. Pb-Zn mineralization in the Katangan is epigenetic, and occurs in transgressive orebodies hosted in two different stratigraphic units. At Kabwe, Zambia, Pb-Zn-(V-Ga-Ge-Cd-Ag) mineralization in pipe-like bodies is hosted by carbonate rocks correlated with the Upper Roan Group. At Kipushi, Kengere and Lombe in the DRC, transgressive Zn-Pb-(Cu-Ga-Ge-Mo-As-Ag) mineralization occurring along faults and in breccia fill is hosted by the Kakontwe cap carbonate above the GC. An interesting feature of many Pb-Zn deposits in Neoproterozoic sedimentary sequences, such as Kabwe in Zambia, Kipushi in the DRC and Skorpion in Namibia, as well as in other parts of the world such as Beltana in the Adelaidean of South Australia and Vazante in Brazil, is the presence, in addition to sphalerite, of non-sulphide zinc minerals (mainly willemite). Such mineralization is attributed to unusually high fO_2 and low fS_2 fugacities during first deformation of the host sediments, an event that at least in Africa and Brazil, occurred at about 680650 Ma (Large, 2001).

There are few if any accurate age data constraining the timing of either stratiform Cu-Co or epigenetic Pb-Zn mineralization in the Copperbelt. An age range of 790 Ma to 750 Ma is suggested by Pb-Pb model ages for Pb-Zn mineralization from several deposits in the region (Kampunzu et al., 1998). However, Kamona et al. (1999) reinterpreted these data and suggested ages of 680 Ma for Kabwe and 460 Ma for Kipushi mineralization. Richards et al. (1988) provided a Pb-Pb model age of 645±15 Ma for Cu-Fe sulphides from the Musoshi Mine, a date interpreted as reflecting either primary ore deposition or Pb re-homogenization. Walraven and Chabu (1994) obtained a Pb model age of 823 Ma for Kinsenda copper sulphide mineralization. Given the long-lived depositional and tectonic histories of the Katangan sequences, it is likely that mineralization was grossly diachronous, representing different episodes in the geological evolution of the region.

Metallogenesis and the Snowball Earth:

Ore genesis in stratiform sediment hosted copper (SSC) deposits is typically related to diagenetic processes where saline, oxidized, near-neutral connate waters scavenge redox-sensitive metals such as Cu, Co, U, Ni and Ag from sediments towards the base of a succession. Precipitation of these metals occurs when the pregnant solutions interact, either with another more reduced fluid, or with a reduced sediment higher up in the succession. Fluid inclusion studies in the Copperbelt indicate the presence of at least 2 distinct mineralizing solutions, which is consistent with a fluid mixing model for precipitation of metals over a long-lived paragenetic sequence. The onset of periodic intervals of anoxia related to near-global ice-ages (the 'Snowball Earth', Hoffman & Schrag, 2000) may have contributed to ore formation by providing basin-wide, but stratigraphically localized, reducing environments that controlled metal precipitation. The 'hot-house' rebound that characterized the aftermath of global glaciation may have been responsible for the highly oxidative conditions that resulted in the subsequent formation of widespread non-sulphide (willemite) mineralization in associated Pb-Zn deposits. It is conceivable that some of the secondary copper mineralization (malachite, chrysocolla etc) so characteristic of the Copperbelt might also be linked to this event, although much of it is undoubtedly much later. Re-Os isotope dating of stratiform sulphides from Nchanga, Chambishi and Mufulira mines in Zambia, currently in progress, will hopefully provide more accurate constraints on the timing of mineralization and shed light on its relationship to glaciogenic events in the basin.

References:

Hofmann, P. F. & Schrag, D. P. (2000) Scientific American, 282(1), 50-57.

Kamona, F. et al. (1999) Mineralium Deposita, 34, 273-283.

Kampunzu, A.B. et al. (1998) Chronique de la Recherche Minière, No 530, 55-61.

Key, R.M., et al. (2001). J. Afr. Earth Sci., 33 (3-4), 503-528.

Large, D. (2001) Erzmetall, 54(5), 264-274.

Master, S. et al. (2002) Extended Abstract, 11th Quad IAGOD Symposium and Geocongress 2002, Windhoek, CD-ROM.

Richards,J.P., et al. (1988) Econ. Geol., 83, 724-741.

Transactions of the Institute of Mining and Metallurgy, 2003, 112, 2, 164-166

Walraven, F. & Chabu, M. (1994) J. Afr. Earth Sci., 18(1), 73-82.

Unrug, R.(1988) Econ. Geol. 83, 1247-1258.

Wendorff, M. (2001) In: Piestrzynski, A. et al. (Eds.), Mineral Deposits at the Beginning of the 21st Century. Swets & Zeitlinger Publishers, Lisse, Netherlands, 19-22.

Geoscience Africa 2004, School of Geosciences, University of the Witwatersrand, 12-16 July 2004, Johannesburg, South Africa

LASER ABLATION ICP-MS OF FLUID INCLUSIONS OF THE CHAMBISHI DEPOSIT, ZAMBIAN COPPERBELT

L. N. Greyling[1], D. Banks[2], L. J. Robb[1], and Y.Yao[1]
[1] Economic Geology Research Institute, School of Geosciences, University of the Witwatersrand, (Private Bag 3, WITS 2050, South Africa, greylin@science.pg.wits.ac.za)
[2] School of Earth Sciences, University of Leeds, (Woodhouse Lane, Leeds LS2 9JT, UK)

Introduction: The Central African Copperbelt, located on the border between the Democratic Republic of the Congo and Zambia, is one of the largest stratiform copper districts in the world. Stratiform copper mineralisation is found in silty shale- and arenitic metasedimentary horizons of the lower Roan Group of the Katangan Supergroup. A fluid inclusion study is currently underway to decipher and describe the nature and role of fluids involved in the mineralisation process and subsequent metamorphism. This study concentrates on selected deposits in the Zambian Copperbelt, including Chambishi. One of the techniques employed during this study is that of laser ablation inductively coupled plasma mass spectrometry (LA-ICP-MS), which enables the quantification of single fluid inclusions [1].

Geological Setting: Mineralisation in the Chambishi deposit is in the form of chalcopyrite and bornite, with subsequent oxidation to malachite in the silty Ore Shale along the southwestern section of the Kafue anticline. Samples, representative of two distinct tectonic settings were selected from the Chambishi open pit, namely (1) a lateral secretion quartz vein, indicative of post-mineralisation conditions, corresponding to a pre-tectonic setting, and, (2) quartz veins representative of a post-mineralisation, syn-tectonic setting.

Fluid inclusions: Two main fluid types are found in pre-, and syn-tectonic veins, namely Lw, Lw-c (±s), (and Lc-w)*. In addition, monophase methane inclusions (Lm) were also identified from syn-tectonic samples. Pre-tectonic Lw inclusions are NaCl-$CaCl_2$ brines, with salinities grouped at ~7wt.% eNaCl, 12-17 wt.% eNaCl, and ~22 wt.% eNaCl. Syn-tectonic Lw inclusions are NaCl-$CaCl_2$ brines, with salinities ranging between 18-24 wt.% eNaCl. Total homogenization temperatures (to the liquid phase) for pre-tectonic inclusions are around 171°C, and around 146°C for syn-tectonic inclusions. Aqueous-carbonic pre- and syn-tectonic inclusions contain mainly CO_2 ($\pm N_2$) in the vapour phases, and 100%CH_4 in syn-tectonic vapour-rich inclusions.

Laser ablation ICP-MS: Fluid inclusions, ranging in size between 8-40µm were analysed (Fig. 1) using He and H_2 respectively in the collision cell, and referenced to the absolute concentration of Na estimated from microthermometry.

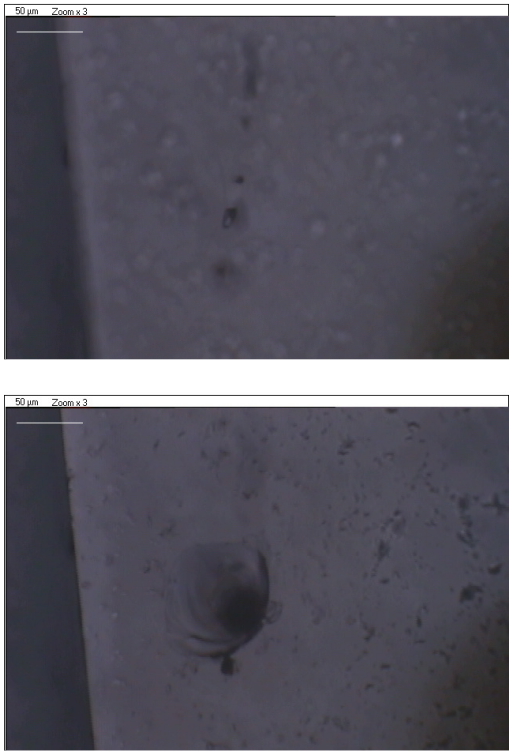

Fig. 1. An Lw-c type inclusion, from a syn-tectonic setting, before and after ablation, sample CBSqz3By.

Conclusions: LA-ICP mass spectrometry indicates the presence of K, Ca, Mn, Fe, ±Zn, ±Ag, ±Sr in fluid inclusions representative of pre- and syn-tectonic settings in the Chambishi deposit. The complex nature of fluid evolution

* Lw: Aqueous inclusions, total homogenisation to the liquid phase. Lw-c: aqueous-carbonic inclusions, with more than 50vol% aqueous component, homogenisation to the liquid phase .Lc-w: CO_2, N_2, CH_4, H_2S are the dominant components. (s):daughter minerals

in the Copperbelt is reflected in the presence of multiple generations of inclusions in most samples. A technique such as LA-ICP-MS provides a method to quantify elemental concentrations in individual inclusions.

References:

[1] Günther D., Audétat A., Frischknecht R., and Heinrich C.A. (1998) *J. of Anal. Atom. Spec*., 13, 263-270.

laser ablation	carbonic	tectonic setting	stratiform copper

Mineral Deposit Studies Group (MDSG) Annual Winter Meeting, Imperial College, Natural History Museum, 5-6 January 2006, London, UK

Fluids of the Zambian Copperbelt

L.N. Greyling*‡, L.J. Robb*, D.A. Banks†, S. Master*, Y. Yao*

** EGRI, School of Geosciences, University of the Witwatersrand, Private Bag 3, WITS, 2050, RSA*
(‡ present address: Shango Solutions, P.O. Box 2591, Cresta, 2118, South Africa, lynnette@shango.co.za, tel: +27 11 678 9731)
† School of Earth Sciences, University of Leeds, Woodhouse Lane, Leeds LS2 9JT, UK

Fluid inclusions were studied in samples of quartz veins and the meta-sediments of the Katanga Supergroup, in the Zambian Copperbelt. The sediment-hosted stratiform copper (+cobalt) deposits of the Central African Copperbelt have been extensively studied since the 1930's (e.g., Mendelsohn, 1961; Fleischer *et al.*, 1976 and references therein, Cailteux *et al.*, 1994), and occur in the Lufilian arc, spanning the border between the Democratic Republic of Congo and Zambia. This study considers the Chambishi, Nchanga, Mufulira, Konkola and Nkana deposits in the Zambian Copperbelt and constrains the regional fluid characteristics in terms of P-T-V-X conditions.

Fluid inclusion microthermometry, Raman microspectroscopy and laser ablation inductively coupled plasma mass spectroscopy (LA-ICP-MS) were among the methods used in order to achieve these objectives. Chronological constraints on a micro-scale facilitated the classification of distinct fluid populations in a tectonic framework. Notably, selected fluid inclusions from the Chambishi deposit were found to predate regional Lufilian metamorphism, and for the first time document the conditions prevalent in an early basin, immediately after basin-wide stratiform copper mineralisation (Greyling *et al.*, 2005). These early fluids consist of H_2O – NaCl ± $MgCl_2$ ± $CaCl_2$ brines with CO_2 ± CH_4 ± N_2 and indicate the presence of a low salinity and an intermediate salinity fluid.

Regional metamorphic fluids were sampled from all five deposits from inclusion trails identified in quartz grains in the lower Roan Group metasediments, and from isolated and trail inclusions in quartz veins. These later fluids consist of H_2O ± $CaCl_2$ ± NaCl ± KCl ± $MgCl_2$ brines with CO_2, ± CH_4 and ± N_2 and range in salinities from low to the highest at ~44 wt.% $NaCl_{equiv}$.

This study reveals the character of early basinal fluids and compares that to later fluids present during regional metamorphism.

References

Cailteux J., Binda P.L., Katekesha W.M., Kampunzu A.B., Intiomale M.M., Kapenda D., Kaunda C., Ngongo K., Tshiauka T., Wendorff M., 1994. Lithostratigraphical correlation of the Neoproterozoic Roan Supergroup from Shaba (Zaire) and Zambia, in the central African copper-cobalt metallogenic province. Journal of African Earth Sciences, 19, 4, 265-278.

Fleischer V.D., Garlick W.G., Haldane R., 1976. Geology of the Zambian Copperbelt; Chapter 6. In: K.H. Wolf (ed.), Handbook of strata-bound and stratiform ore deposits – II Regional studies and specific deposits, Vol. 6, Amsterdam, The Netherlands, 223-352.

Greyling L.N., Robb L.J., Master S., Boiron M.C., Yao Y., 2005. The nature of early basinal fluids in the Zambian Copperbelt: a case study from the Chambishi deposit. Journal of African Earth Sciences, 42, 159-172.

Mendelsohn F., 1961b. Metamorphism. In: Mendelsohn F. (ed.), The geology of the Northern Rhodesian Copperbelt. MacDonald, London, 106-116.

Available online at www.sciencedirect.com
SCIENCE DIRECT®
Journal of African Earth Sciences 42 (2005) 159–172
Journal of African Earth Sciences
www.elsevier.com/locate/jafrearsci

The nature of early basinal fluids in the Zambian Copperbelt: A case study from the Chambishi deposit

L.N. Greyling [a,*], L.J. Robb [a], S. Master [a], M.C. Boiron [b], Y. Yao [a]

[a] *Economic Geology Research Institute—Hugh Allsopp Laboratory, School of Geosciences, University of the Witwatersrand, Private Bag 3, 2050 WITS, Johannesburg, South Africa*
[b] *UMR CNRS G2R 7566 and CREGU, BP 23, 54501 Vandoeuvre les-Nancy Cedex, France*

Received 1 October 2004; accepted 1 April 2005
Available online 13 October 2005

Abstract

Fluid inclusions from a mineralised lateral secretion quartz vein in the Chambishi open pit in the Zambian Copperbelt represent fluids that immediately postdate stratiform copper mineralisation. Petrographic evidence indicates that this veinset predates deformation in the area. Fluid inclusion microthermometry and Raman spectroscopy of aqueous and aqueo-carbonic inclusions indicate the presence of an early saline H_2O–NaCl + $MgCl_2 \pm CaCl_2 \pm CO_2 \pm CH_4 \pm N_2$ fluid (11.9–23.1 wt.% $NaCl_{equiv}$) at homogenisation temperatures of 86–129 °C. Later fluids occur in fluid inclusion planes, and are linked to early metamorphism of the basin. These fluids are more varied in composition, and are aqueous, aqueo-carbonic, and pure methane inclusions. Aqueous and aqueo-carbonic inclusions are H_2O–NaCl $\pm$ $CaCl_2 \pm MgCl_2 \pm KCl \pm CO_2$, N_2, CH_4, H_2S fluids, with two salinity end-members, namely, a high salinity (18–23 wt.% $NaCl_{equiv}$)–lower temperature (~130–160 °C) fluid, and a lower salinity (~6 wt.% $NaCl_{equiv}$)–higher temperature (~140–210 °C) fluid. Later carbonic inclusion planes contain CH_4, with N_2 and C_2H_6. Later fluids are complex in composition, salinity, and homogenisation temperatures. These fluids are thought to be late-diagenetic fluids on the one hand, and an early (methane productive) metamorphic fluid on the other. Pressure and temperature conditions in the environment immediately after stratiform copper mineralisation were around 480–800 bar and 130–270 °C.

Keywords: Fluid inclusions; Zambian Copperbelt; Aqueo-carbonic; Deformation

1. Introduction

The Neoproterozoic stratiform Cu–Co ores of the Central African Copperbelt are hosted mainly by the Roan Group at the base of the Katanga Supergroup. This metallogenic province is situated on the border between Zambia and the Democratic Republic of the Congo (DRC), and is preserved in the Lufulian Arc (Fig. 1). Theories on the origin of mineralisation of these sediment-hosted stratiform copper deposits have ranged from syngenetic (Garlick, 1961; Fleischer, 1984; Sweeney and Binda, 1994) to epigenetic (Jackson, 1932; McGowan et al., 2003). However, recent models of ore deposition favour either early or late diagenesis (Robb, 2005). In addition, the presence of a variety of epigenetic ores such as the Cu–Au, U–(Cu–Co–Ni–Mo), and Zn–Pb–Cu–Ge–Ga deposits within the Katanga metallogenic province illustrates the scale and complexity of mineralisation styles. Therefore, regional metallogenesis is best viewed in a polygenetic framework. This paper describes the fluid inclusion character of quartz veins from the Chambishi deposit (Figs. 1 and 2). This forms part of a regional fluid study aimed at deciphering and documenting the characteristics and evolution of early fluids (late diagenetic), possibly associated with mineralisation, and late fluids (trapped during regional metamorphism postdating stratiform mineralisation).

* Corresponding author.
E-mail address: greylin@science.pg.wits.ac.za (L.N. Greyling).

1464-343X/$ - see front matter © 2005 Elsevier Ltd. All rights reserved.
doi:10.1016/j.jafrearsci.2005.08.002

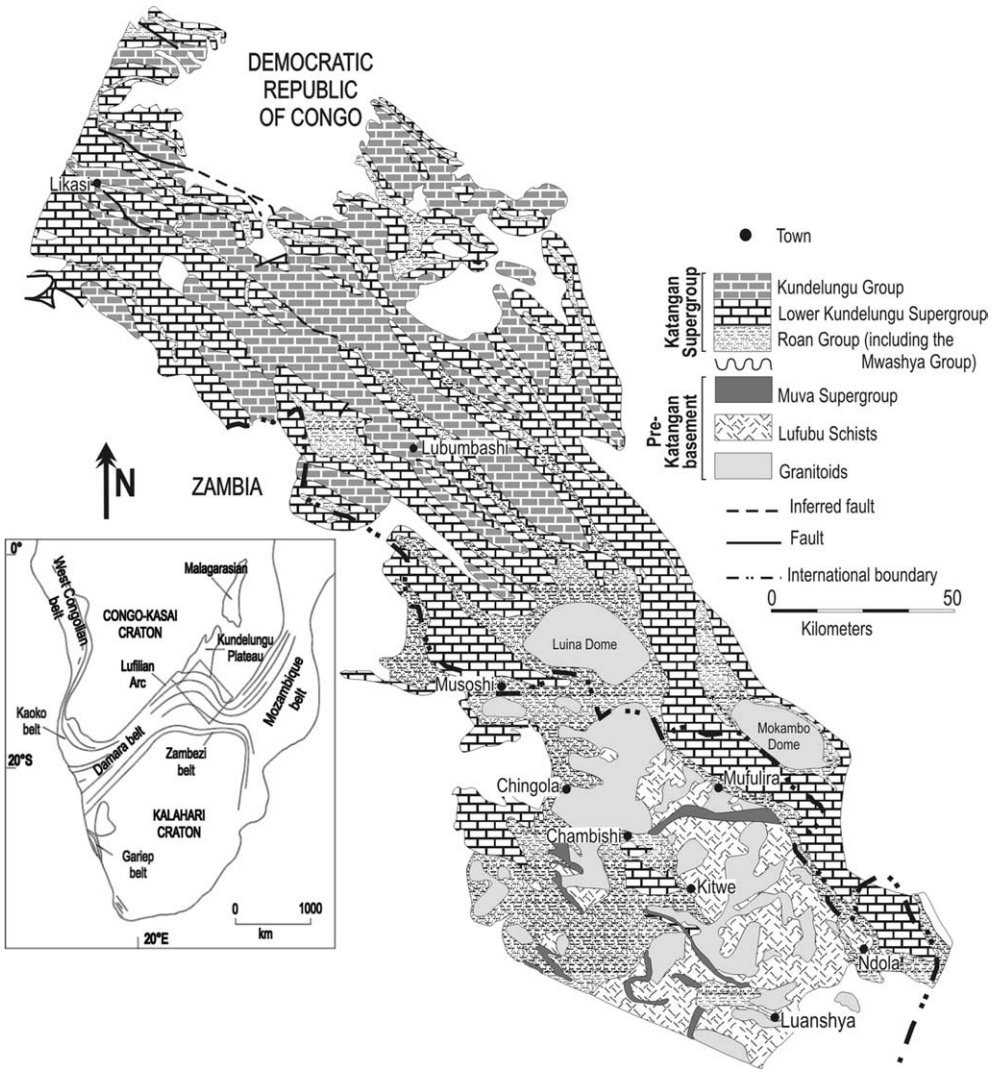

Fig. 1. General geology of the Central African Copperbelt, showing the location of the Chambishi deposit in Zambia (modified from François, 1974 and Rainaud et al., 2003).

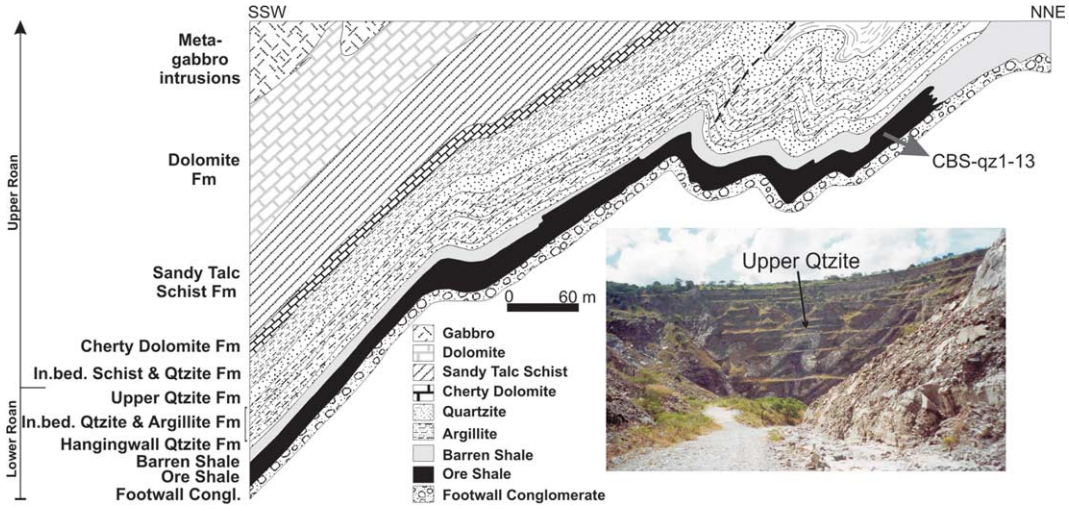

Fig. 2. Cross section of the Chambishi Main deposit (after Garlick, 1961), showing an asymmetrical fold in the now abandoned open pit. Regional thrusting occurred to the northeast as a result of compression during the Pan African Lufilian orogeny. The location of the samples for this study is indicated in the Ore Shale horizon.

2. Geological setting

2.1. Geology

The stratiform copper deposits of the Central African Copperbelt are hosted by the meta-sediments of the Neoproterozoic Katanga Supergroup (Fig. 1). The Katanga Supergroup unconformably overlies a basement comprised of an exposed Palaeoproterozoic calc-alkaline volcanic arc terrane (Rainaud et al., 1999), which in turn overlies a Mesoarchaean terrane (Rainaud et al., 2003). This basement is intruded by granitoids, which constrain the maximum age of Katangan sedimentation (Armstrong et al., 1999). The Katanga succession in Zambia is composed of the Roan, Mwashya, Nguba, and Kundelungu Groups, as specified by Wendorff (2003). Sedimentation of the Katanga in Zambia occurred between 880 Ma (Armstrong et al., 1999) and 620 Ma (Cahen et al., 1984), with the onset of deposition of the Roan Group siliciclastics (conglomerates, sandstones, and argillites) during rifting (Wendorff, 2003). Thus, the Roan Group non-conformably overlies the pre-Katanga basement in Zambia and southern DRC (Wendorff, 2003). The Roan Group is unconformably overlain by the Mwashya Group in the Kafue anticline region in Zambia. Two tillites are present in the Nguba Group, which is comprised of marine siliciclastics and carbonates. The base of the Nguba Group is indicated by the first tillite, the so-called Grand Conglomérat, which probably corresponds to the Sturtian glaciation (Robb et al., 2002; Robb, 2005).

The Katanga sediments were metamorphosed during the Lufilian orogenic event at ca. 600–500 Ma (John et al., 2002) to greenschist facies in the Zambian Copperbelt, and to amphibolite facies in the Solwezi area to the west of the Copperbelt, with a general decreasing in grade to the northeast, towards the DRC (Mendelsohn, 1961b). The Katanga meta-sediments are preserved in several basins (Konkola-, Chambishi-, Roan basins).

2.2. Regional stratiform copper mineralisation

Mineralisation in Zambia and the DRC is mainly hosted in the lower Roan Group, but minor occurrences of mineralisation are also found in the basement and in the dolomites of the Nguba Group. Ore minerals are mostly sulphides (including bornite, chalcocite, chalcopyrite, carrollite, and pyrite), and secondary oxides. Mineralisation in the lower Roan Group is hosted in two lithologies, namely, shales and quartzites and arkoses. Generally, the ore shale deposits are located along the west of the Kafue anticline (Fig. 1). The Ore Shale consists mostly of silty, micaceous (biotite or sericite ± muscovite), calcareous grains, with quartz, feldspar, Cu–Fe sulphides, chlorite and organic carbon. The thickness varies from 5 to 20 m, and sulphides are generally disseminated through the Ore Shale, with concentrations along bedding planes (Mendelsohn, 1961a). The sericitic quartzite-hosted deposits are found along the eastern flank of the Kafue anticline, in the Mufulira area (Fig. 1).

3. Previous fluid inclusion studies: Zambia and the DRC

Previous fluid inclusion studies in Zambia and the DRC include work by Pirmolin (1970), Sweeney (1987), Richards et al. (1988a), Speiser et al. (1995), and Kamona (1993). A summary of the main results is presented in Table 1, with the section below outlining the main findings of each of these studies.

- Pirmolin (1970) described fluid inclusions from an unmineralised cherty dolomite layer of the Mines Group of the Roan Supergroup at Kamoto, in the DRC, and concluded that solutions reached temperatures of ~200 °C at salinities of ~40 wt.% $NaCl_{equiv}$ at Kamoto.
- Crosscutting quartz veins at the Konkola and Chambishi Cu–Co deposits were studied by Sweeney (1987). These veins had undergone at least one post-formational tectono-thermal event. Scanning electron microscopy of decrepitated inclusion cavities showed the presence of Na, Al, Si, S, U, K, Ca, Fe, Cu, and Co, and KCl, NaCl daughter minerals. Gas analyses of decrepitated inclusions revealed the presence of CO_2, CH_4, and N_2. It was concluded that the veins formed by lateral migration of fluids during late diagenetic dewatering.
- Richards et al. (1988a) indicated the presence of a sylvite–halite-saturated fluid in quartz–hematite–rutile veins hosted in the footwall sediments of the Musoshi copper deposit (DRC), where late hydrothermal veining caused extensive footwall- and ore shale-alteration. Fluid inclusions were found to consist of NaCl, KCl ± CO_2. This hydrothermal event postdates stratiform copper mineralisation and is linked to compressional deformation and metamorphism during the Lufilian orogeny. They estimated the maximum homogenisation pressure at 1.2 kbar, which is the typical pressure for decrepitation of 12–13 μm size fluid inclusions in quartz (Leroy, 1979).
- Epigenetic iron-oxide–Cu–Au type mineralisation at the Kansanshi Copper Mine (Solwezi area, north-western Zambia) was studied by Speiser et al. (1995) and Speiser (1994). Hydrothermal veining at Kansanshi is connected with alteration of the host rocks, and mineralised (Cu–Mo–Fe) veins have been dated at ~503–511 Ma (Re–Os and U–Pb of molybdenite and monazite) by Torrealday et al. (1999). Mineralisation at the Kansanshi Mine may also correspond to mineralisation at the Shinkwelobwe Mine (Cu–U), which is dated at 602 Ma (U/Pb, Cahen et al., 1984). This style of mineralisation postdated host rock metamorphism.
- Kamona (1993) studied fluids from the epigenetic stratabound carbonate-hosted Pb–Zn Kabwe deposit, central Zambia. These epigenetic deposits are hosted by the Kabwe Dolomite Formation, where mineralising fluids were saline, ranging between 11 and 31 wt.% $NaCl_{equiv}$,

Table 1
Comparative results of previous fluid inclusion studies on Cu–Co and Pb–Zn deposits in the Central African Copperbelt

	Pirmolin (1970)	Sweeney (1987)	Richards et al. (1988)	Kamona (1993)	Speiser et al. (1995)	Kampunzu et al. (1998)
Area	Kamoto, DRC-Copperbelt	Konkola, Chambishi, Z-Copperbelt	Musoshi, DRC-Copperbelt	Kabwe, Central Zambia	Kansanshi, Solwezi, NW Zambia	Kipushi D.R.C.
Lithology	Mines Group, Roan	L. Roan Group	L. Roan Group	L. Kundelungu Group	?	?
Minerals	Cherty dolomite	Quartz veins	Quartz–hematite–uraninite veins	Dolomite	Quartz veins	?
Setting	Epigenetic stratiform Cu	Late diagenetic stratiform Cu	Epigenetic U–Pb hydrothermal	Epigenetic Pb–Zn	Epigenetic iron-oxide–Cu–Au	Epigenetic
Composition	~40 wt.% $NaCl_{equiv}$	H_2O, KCl, NaCl, CO_2, CH_4, N_2	H_2O, KCl–NaCl–$CaCl_2$–$FeCl_3$–CO_2, 39 wt.% NaCl, 15 wt.% KCl	11–31 wt.% $NaCl_{equiv}$	H_2O, NaCl–$CaCl_2$–CO_2–(CH_4)	?
P (kbar)	?	?	<1.2	0.09	1.2–2.5	?
Th (°C)	?	120	~397, ~275	257–305	230–310	Ca. 300

and T_h ranged between 257 and 305 °C, corresponding to ore deposition at 320 °C.

- Kampunzu et al. (1998) reported high homogenisation temperatures (300 °C) from fluid inclusions representative of mineralising fluids from the epigenetic sediment-hosted Pb–Zn Kipushi deposit. This style of mineralisation postdates stratiform copper mineralisation.

The work of Pirmolin (1970) and Sweeney (1987) is relevant to the present study. These data indicate that fluids circulated early during the basin evolution, and were saline with moderate homogenisation temperatures. The present study, however, provides information on a vein set in a mineralised setting, where the tectonic and paragenetic relationships are better constrained. Accordingly this study will add to existing knowledge of fluids that developed relatively early in the basin evolution.

4. The Chambishi copper deposit

Two deposits are identified in the Chambishi area, namely the Chambishi Main and the Chambishi West orebodies (Garlick, 1961; Garlick, 1976), where the Katanga meta-sediments unconformably overlie the 2050–1850 Ma basement comprising the granitoids and Lufubu schists (Master et al., 2005; Rainaud et al., 2005a). The Katanga meta-sediments are preserved along the northern rim of the Chambishi-Nkana basin, striking east–west, and dipping south at about 60° (Garlick, 1961). The Ore Shale Formation in this area consists of carbonaceous shale, argillaceous siltstones, and interbedded dolomite (Fig. 2). Disseminated copper (±cobalt) sulphide mineralisation is present within the Ore Shale Formation of the lower Roan Group (Fleischer, 1984). Zonation of chalcopyrite–bornite–chalcocite is present in the Ore Shale. The barren shale overlying the Ore Shale is mineralised with disseminated pyrite. Secondary malachite occurs as an oxidation product of primary sulphides.

A well-exposed area in the abandoned Chambishi open pit revealed a particularly interesting mineralised quartz vein whose relationship to stratiform mineralisation and deformation is clearly apparent (Fig. 3). The paragenetic sequence of events is:

- Deposition of the Ore Shale was followed by (late-diagenetic?) stratiform mineralisation of disseminated Cu-sulphides (chalcopyrite and bornite).
- Emplacement of a quartz vein parallel to bedding in the Ore Shale. This vein contains course-grained aggregates of chalcopyrite and bornite, which are partially oxidised to malachite. The shale immediately adjacent to the vein is devoid of mineralisation (Fig. 3(A)–(C)). Therefore, it is interpreted that this vein emplacement resulted in the lateral secretion of disseminated Cu-sulphide mineralisation from the host rock into the quartz vein, leaving a halo depleted of mineralisation immediately surrounding the vein (Fig. 3(A)).

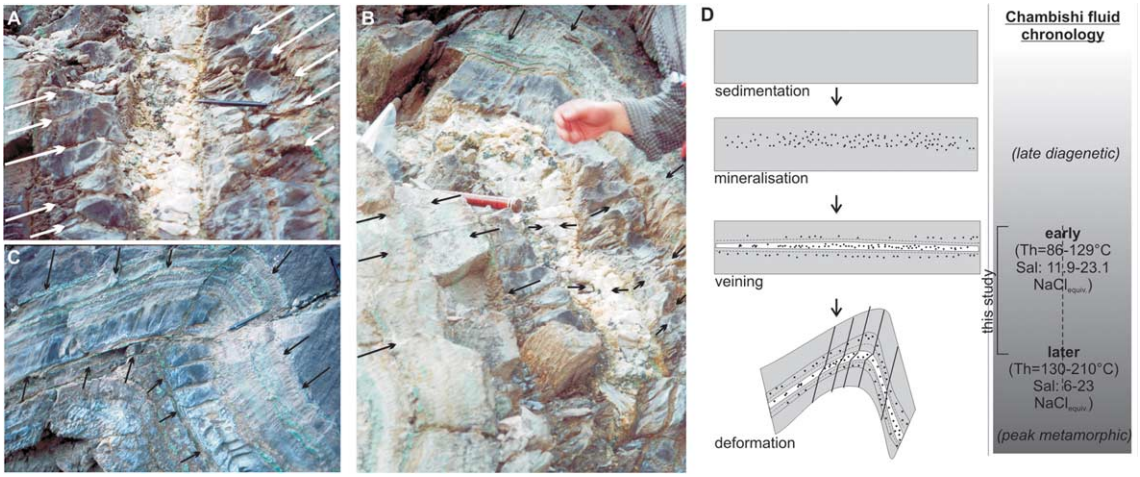

Fig. 3. Lateral secretion of primary copper mineralisation from the surrounding shale into a quartz vein, leaving a halo, depleted of mineralisation, surrounding the quartz vein in the Ore Shale horizon (A). The axial planar cleavage (B), produced during folding of the Ore Shale, is refracted by the intruding vein (C), which shows that introduction of the vein is prior to folding of the strata, but postdates stratiform mineralisation. (D) Simplified schematic illustrating the process of firstly sedimentation, followed by diagenetic mineralisation of disseminated Cu-sulphides, followed by the emplacement of a quartz vein bedding parallel to the shale, then finally, metamorphism and deformation resulting in the development of an axial planar cleavage through the host sediments. The cleavage is refracted through the quartz vein. Trapping of fluid inclusion types are chronologically illustrated. See text for further details.

- Deformation of both the sedimentary succession and the quartz vein during regional metamorphism imprinted an axial planar cleavage on the host rock, which is refracted in the quartz vein (Fig. 3(B) and (C)), clearly illustrating the presence of the quartz vein prior to deformation.

5. Chambishi fluid inclusions

5.1. Sample selection

Samples for the fluid inclusion study were selected from the above-mentioned quartz vein, hosted in the Ore Shale, illustrated in Fig. 3.

5.2. Methodology

Double polished wafers of ~200 μm thickness were used for the petrographic and microthermometric study. Microthermometry was performed on a Linkam TH600 stage connected to an Olympus Vanox binocular microscope. The accuracy of the measurements was of ±0.1 °C at low temperatures and ±2 °C at high temperatures. Inclusions were cooled to −170 °C and phase transitions were measured during heating. Estimation of the volumes of volatile phases at room temperature was done using the volumetric estimation chart of Roedder (1972). The gaseous molar fractions were determined using a Raman Labram Jobin-Yvon microspectrometer, with an ionised Ar laser (wavelength 514.5 nm) as excitation source. The laser was focused on the sample with an 80× objective lens.

Fluid inclusion types are defined according to the nomenclature used by Boiron et al. (1992). Inclusions are classified based on their final homogenisation ($T_h t$) behaviour (see Table 2), L: into the liquid phase, *V*: into the vapour phase, and presence of dominant aqueous (w) or carbonic (c) species (see Table 2 for explanation of abbreviations). Salinities for the aqueous inclusions were calculated from T_m (ice) using the equations in Bodnar and Vityk (1994). Salinities for aqueo-carbonic inclusions were calculated using degree of fill, T_h (CO_2) and T_m (clath) by using the equation of state in Bodnar (1983) and Brown and Lamb (1986, 1989) in the Linkam Scientific PVTX Software Modelling programme for Fluid Inclusions, V 2.1. Bulk densities of FIP's were calculated using the computer programme *Bulk*, version 01/03 (Bakker, 2003), and isochors were calculated and plotted using *Isochor* version 13/03/96 (Bakker, 1997) and *Isoc* version 01/03 (Bakker, 2003) utilizing the Bowers and Helgeson (1983) and Zhang and Frantz (1987) equations of state.

Table 2
Explanation of abbreviations used in microthermometric interpretations (from Goldstein and Reynolds, 1994; Boiron et al., 1992; Diamond, 2003)

$T_h t$	Temperature of final homogenisation
L	Homogenisation to the liquid phase
T_e	Eutectic temperature
T_m(hh)	Melting of hydrohalite
T_m(ice)	Final ice melting
$T_m(CO_2)$	Final melting of CO_2
T_m(cla)	Final melting of clathrate
$T_h(CO_2)$	Homogenization of the carbonic phase
c	Gaseous phases including CO_2, N_2, CH_4, H_2S
m	Methane dominantly present
FIPs	Fluid inclusion planes

5.3. Petrography

Certain minerals host fluid inclusions which become trapped either during, or subsequent to, crystal growth

(Goldstein and Reynolds, 1994). The relationship between individual inclusions, and amongst inclusions and growth zones, indicates the relative timing of entrapment. Based on petrographic observations, fluid inclusions and fluid inclusion assemblages may be identified as primary, secondary, or pseudo-secondary (Roedder, 1984; Goldstein and Reynolds, 1994). Assuming that no leaking or resetting has occurred during metamorphism in the Chambishi basin, earlier fluids (late diagenetic) are interpreted to exist either as isolated inclusions (as primary inclusions), or as inclusions occurring along poorly defined planes (as pseudo-secondary inclusions). Conversely, fluid inclusions in well-defined fluid inclusion planes (FIP's) have trapped fluids present during (and to some extent after) metamorphism, as secondary fluid inclusions.

Double polished quartz wafers in this study showed no growth zonation during optical microscopy or cathodoluminescence. However, a few small (<10 μm), isolated inclusions are interpreted to be of primary origin based on their isolated distribution among secondary fluid inclusion planes (FIP's) (Fig. 4(D), (E), (H) and (I)). These inclusions are interpreted of be representative of post-mineralising, pre-metamorphism fluids (see Fig. 3(D)). Secondary fluid inclusions form when fluid is trapped during healing of micro cracks, shear planes, or along twin planes or cleavage directions after crystal formation (Goldstein and

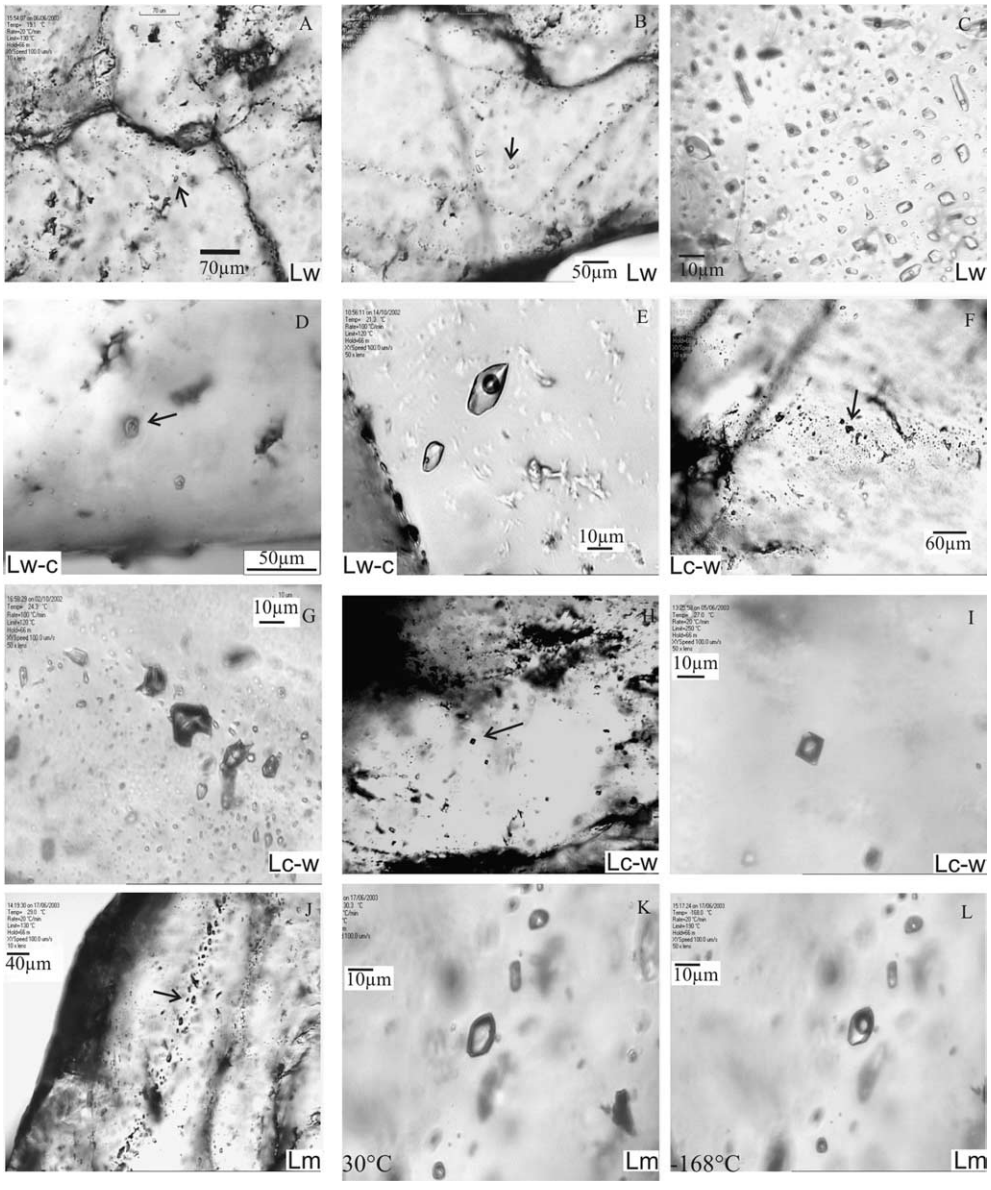

Fig. 4. Micrographs of typical fluid inclusion types in quartz. All images taken at room temperature, unless otherwise stated on the figure. (A) Isolated aqueous fluid inclusions (sample CBS-qz8A[1]9). (B) Isolated aqueous fluid inclusions (sample CBS-qz8A[1]2). (C) Secondary fluid inclusion planes (FIP's) of aqueous inclusions (CBS-qz3A[4]). (D) Isolated aqueo-carbonic inclusions (CBS-qz8A[1]3). (E) FIP's aqueo-carbonic inclusion (CBS-qz3By[4]1). (F) and (G) Secondary aqueo-carbonic trail fluid inclusions (CBS-qz6A[2]). (H) and (I) Isolated aqueo-carbonic inclusion with negative crystal shape (CBS-qz3A[6]10). (J) and (L) Secondary methane inclusions preserved in fluid inclusion planes (CBS-qz7BA[1]4).

Table 3
Results of microthermometry and Raman spectroscopy for all primary and secondary fluid inclusion types

Sample	FI	%Vap	Type	Microthermometry									Raman (mol%)					Bulk composition						
				T_e	T_m(hh)	T_m(ice)	T_h(tot)	Mode	$T_m(CO_2)$	$T_h(CO_2)$	Mode	T_m(cla)	CO_2	N_2	H_2S	CH_4	C_2H_6	H_2O	CO_2	N_2	CH_4	NaCl	ρ (g/cc)	$NaCl_{equiv}$
Isolated																								
Aqueous																								
Cbsqz8A	(1)1	10	Lw	−35	–	−21.1	Dec		–	–	–	–	–	–	–	–	–							23.1
Cbsqz8A	(1)2	10	Lw	−47	–	−21.1	129	L	–	–	–	–	–	–	–	–	–							23.1
Cbsqz8A	(1)5	20	Lw	<−25	−21	−12.3	–	–	–	–	–	–	–	–	–	–	–							16.2
Cbsqz8A	(1)6	10	Lw	∼−50	∼−21	−9.5	110	L	–	–	–	–	–	–	–	–	–							13.4
Cbsqz8A	(1)7	8	Lw	−50	∼−19	−9.5	109	L	–	–	–	–	–	–	–	–	–							13.4
Cbsqz8A	(1)8	10	Lw	−50	∼−19	−9.5	107	L	–	–	–	–	–	–	–	–	–							13.4
Cbsqz8A	(1)9	10	Lw	−45	∼−22	−13.6	126	L	–	–	–	–	–	–	–	–	–							17.4
Cbsqz8A	(1)10	10	Lw	−45	∼−22	−13.6	129	L	–	–	–	–	–	–	–	–	–							17.4
Cbsqz8A	(1)11	10	Lw	−45	∼−22	–	86	L	–	–	–	–	–	–	–	–	–							
Cbsqz8A	(2)1	10	Lw	∼−40	−22.4	−12.3	–		–	–	–	–	–	–	–	–	–							16.2
Aqueo–carbonic																								
Cbsqz3A	(6)2	10	Lw–c	−37	−20.8	–					–	2.0	98.5	⩽1		0.6		98.2	1.8			0.90		
Cbsqz3A	(6)10	60	Lc–w	–	–		–	–	−56.8	22.8	L	2	>98.5	1		⩽0.2		62.1	33.9	0.5	3.5	0.86		13.2
Cbsqz3A	(6)11	20	Lw–c–s	–	–	–	–	–	−57.9	23.9	L	2	99	⩽1				85.4	9.7	0.1	4.8	0.99		
Cbsqz3A	(6)12	20	Lw–c	–	–	–	–	–	−57.9	26.9	L	2.2	>99.5	⩽0.2	⩽0.2			85.7	9.6	0.03	4.7	0.98		12.9
Cbsqz8A	(1)3	25	Lw–c	–	–	–	>150	L	−57.0	11.8	L	3.0	98	⩽0.5		2		82.4	13	0.2	4.4	0.99		11.9
Cbsqz8A	(1)4	25	Lw–c	–	–	–	>150	L	–	15.0	L	3.0												11.9
Trails and fluid inclusion planes																								
Aqueous																								
Cbsqz3A	(2)1	10	Lw	−55	−22.3	−19.0	143	L	–	–	–	–	–	–	–	–	–							21.7
Cbsqz3A	(2)2	10	Lw	−51	−22.1	−18.6	148	L	–	–	–	–	–	–	–	–	–							21.4
Cbsqz3A	(2)3	10	Lw	−51	−22.1	−18.6	140	L	–	–	–	–	–	–	–	–	–							21.4
Cbsqz3A	(2)4	10	Lw	−53	−22.6	−14.6	150	L	–	–	–	–	–	–	–	–	–							18.3
Cbsqz3A	(2)5	10	Lw	−45	–	−15.4	150	L	–	–	–	–	–	–	–	–	–							19.0
Cbsqz3A	(4)1	10	Lw	−54	−22.9	−20.8	154	L	–	–	–	–	–	–	–	–	–							22.9
Cbsqz3A	(4)3	10	Lw	−54	−22.9	−21.2	145	L	–	–	–	–	–	–	–	–	–							23.2
Cbsqz3A	(4)4	10	Lw	−54	−23	−21.2	154	L	–	–	–	–	–	–	–	–	–							23.2
Cbsqz3A	(4)5	10	Lw	−55	−23.1	−21.2	156	L	–	–	–	–	–	–	–	–	–							23.2
Cbsqz3A	(4)9	10	Lw	−53	−22.5	−21.2	155	L	–	–	–	–	–	–	–	–	–							23.2
Cbsqz3A	(4)10	10	Lw	−53	−22.9	−21.2	154	L	–	–	–	–	–	–	–	–	–							23.2
Cbsqz3A	(6)0.1	10	Lw	−52	–	−18.9	131	L			–		–	–	–	–	–							21.6
Cbsqz3A	(6)1	10	Lw	−39	–	−3.2			–	–	–	–	–	–	–	–	–							5.3
Cbsqz3A	(6)3	10	Lw	−50	−22.3	−18.8					–		–	–	–	–	–							21.5
Cbsqz3A	(6)4	10	Lw	−53	−22.6	−17.3			–	–	–	–	–	–	–	–	–							20.4
Cbsqz3A	(6)5	10	Lw	−45	−22.6	−17.5			–	–	–	–	–	–	–	–	–							20.6
Cbsqz3A	(6)6	10	Lw	−54	−22.3	−18.2			–	–	–	–	–	–	–	–	–							21.1
Cbsqz3A	(6)7	10	Lw	−47		−17.5			–	–	–	–	–	–	–	–	–							20.6
Cbsqz3A	(6)8	10	Lw	−55	−21.8	−14.5	140	L	–	–	–	–	–	–	–	–	–							18.2
Cbsqz3Bx	(1)1	10	Lw	−25	–	−1.6	–	–	–	–	–	–	–	–	–	–	–							2.7
Cbsqz3Bx	(1)2	10	Lw	−23	–	−1.7	–	–	–	–	–	–	–	–	–	–	–							2.9
Cbsqz6A	(3)1	10	Lw	∼−41	–	−3.0	142	L	–	–	–	–	–	–	–	–	–							5.0
Cbsqz6A	(3)2	25	Lw	∼−26	–	−4.0	192	L	–	–	–	∼11	–	–	–	–	–							6.4

(*continued on next page*)

Table 3 (*continued*)

Sample	FI	%Vap	Type	Microthermometry									Raman (mol%)					Bulk composition						
				T_e	T_m(hh)	T_m(ice)	T_h(tot)	Mode	$T_m(CO_2)$	$T_h(CO_2)$	Mode	T_m(cla)	CO_2	N_2	H_2S	CH_4	C_2H_6	H_2O	CO_2	N_2	CH_4	NaCl	ρ (g/cc)	$NaCl_{equiv}$
Cbsqz6A	(3)3	15	Lw	~−29	–	−3.9	208	L	–	–	–	–	–	–	–	–	–							6.3
Cbsqz6A	(3)4	20	Lw	–	–	−4.0	189	L	–	–	–	~8	–	–	–	–	–							6.4
Cbsqz6A	(3)5	35	Lw	~−47	–	−4.8	160	L	–	–	–	–	–	–	–	–	–							7.6
Cbsqz6A	(3)6	25	Lw	–	–	−4.0	178	L	–	–	–	–	–	–	–	–	–							6.4
Cbsqz6A	(3)7	20	Lw										–	–	–	–	–							
Cbsqz6A	(3)8	20	Lw										–	–	–	–	–							
Cbsqz6A	(3)9	20	Lw	~−40	–	−4.1	179	L	–	–	–	–	–	–	–	–	–							6.6
Cbsqz6A	(3)10	20	Lw	~−39	–	−4.1	177	L	–	–	–	–	–	–	–	–	–							6.6
Aqueo-carbonic																								
Cbsqz3A	(4)2	10	Lw–c	−56	−22.9	−21.2	149	L	−57.9		–													
Cbsqz3By	(4)1	20	Lw–c	~−32	–	–	245	Dec	−57.2	29.4	L	7.5	98.2	1.5	⩽0.5	<0.1								4.8
Cbsqz3By	(4)2	10	Lw–c	–	–	−8.0	229	L	−57.2	30.0	L	5	99.5	<0.5	⩽0.2									9.0
Cbsqz3By	(4)3	20	Lw–c	−35		−9.6	229	L	−57.1	30.8	L	8.2												3.6
Cbsqz3By	(4)4	15	Lw–c	–	–	–	196	L	–	30.8	L	–												
Cbsqz3By	(4)5	40	Lw–c	–	–	–	>300	L	−56.9	30.8	V	–												
Cbsqz3By	(4)6	70	Lc–w	–	–	–	>300	V	−58.0	26.6	L	–	98.3	1.2	⩽0.5									
Cbsqz3By	(4)7	20	Lw–c	–	–	–	–	–	−58.0	30.8	L	–	98.2	1.3	⩽0.5	<0.1								
Cbsqz3By	(4)8	20	Lw–c	–	–	–	Dec	–	–	–	–	–												
Cbsqz3By	(4)9	50	Lw–c	–	–	−10.0	>300	L	–	28.3	V	–	>99.8		⩽0.2									
Cbsqz3By	(4)10	10	Lw–c	–	–	−9.0	189	L	–	27.9	L	~5												9.0
CHM7BA	(1)1	10	Lw–c	−51		−14.4				27.5	L	2.6	98.0	2.0		0.0		89.9	4.7	0.1	–	5.3	1.00	12.5
CHM7BA	(1)3	30	Lw–c	~−42	~−23.8	−21.0			−58.7	16.6	L	3.1	91.7	6.0		2.3		82.3	12.1	0.7	0.2	4.7	0.92	11.8
CHM7BA	(1)4	30	Lw–c	~−48	–	−23.8	Dec		−56.9	19.6	L	−0.4	98	1.7		0.3								16.0
CHM7BA	(1)5	10	Lw–c	–	–	–	179	L				1.1												
CHM7BA	(1)6	10	Lw–c	−44	~−23	−15.4	221	L				1.7												
CHM7BA	(1)7	10	Lw–(c)	~−40	–	−14.8	144	L																
CHM7BA	(1)8	10	Lw–(c)	−39	–	−15.7	150	L																
CHM7BA	(1)9	10	Lw–(c)	~−41	~−20	−15.7							32	47.5		6.5								
CHM7BA	(1)10	10	Lw–c	−46	~−21	−14.1	128	L																
CHM7BA	(1)11	15	Lw–(c)	−44	~−22	−12.8	211	L				−2.2	37	55.5		7.5								
CHM7BA	(1)12	10	Lw-(c)	−39	~−21	−15.7	214	L																
CHM7BA	(1)13	8	Lw-(c)	−42	~−21	−15.4	205	L																
CHM7BA	(1)14	10	Lw-(c)	−46	~−21	−15.7																		
CHM7BA	(1)15	10	Lw-(c)	−42	~−21	−15.5																		
CHM7BA	(1)16	10	Lw-(c)	–	–	−15.2																		
CHM7BA	(1)17	10	Lw-(c)	−41.3	~−21	−15.7																		
CHM7BA	(1)18	10	Lw-(c)	−39	–	−15.2																		
CHM7BA	(1)19	10	Lw-(c)	~−39	–	−13.0						5												
CHM7BA	(1)20	10	Lw-(c)	−35	–	−11.8						5												
Cbsqz6A	(2)2	90	Lc-w	–	–	–	–	–	−57.3	21.0	L	−2	98.2	1.3	⩽0.5			22.5	74.5	1.3		1.7	0.77	17.7
Cbsqz6A	(2)3	65	Lc-w	–	–	–	–	–	−57.1	27.5	L	–												
Cbsqz6A	(2)4	85	Lc-w	–	–	–	–	–	−57.5	27.5	L	–	98.2	1.3	⩽0.5			92.8	7.1	0.1		–	0.92	
Cbsqz6A	(2)5	75	Lc-w	–	–	–	–	–	−57.2	29.5	L	6.5	98.2	1.3	⩽0.5			57.5	40	0.6		1.9	0.62	6.6
Cbsqz6A	(2)6	75	Lc-w	–	–	–	–	–	−57.5	30.2	L	7.0	98.5	1.1	⩽0.5									5.8
Cbsqz6A	(2)7	90	Lc-w	–	–	–	–	–	−57.2	27.8	L	7.4	98.6	1.3	<0.1			27.2	71.1	0.9		0.8	0.67	5.1
Cbsqz6A	(2)8	70	Lc-w	–	–	–	–	–	−57.3	26.8	L	6.5	98.3	1.2	⩽0.5			56.3	41.4	0.5		1.8	0.77	6.6
Cbsqz6A	(2)9	80	Lc-w	–	–	–	–	–	–	27.9	L	–												
CHM7BA	(1)2	15	Lw-c-s	~−50		−16.2			−23.7		L	5.9	59	5.5		35.5	<0.1	90.9	2.9	0.1	0.7	5.4	0.94	19.6

Methane-dominated																			
Cbsqz7BA	(1)1	100	Lm	–	–	–	–	–	–	−88.1	L	–	nd	6.5		93	0.5		
Cbsqz7BA	(1)2	100	Lm	–	–	–	–	–	–	−87.8	L	–	–	–	–	–	–		
Cbsqz7BA	(1)3	100	Lm	–	–	–	–	–	–	−87.8	L	–	–	–	–	–	–		
Cbsqz7BA	(1)4	100	Lm	–	–	–	–	–	–	−87.7	L	–	–	–	–	–	–		
Cbsqz7BA	(1)5	100	Lm	–	–	–	–	–	–	−88.0	L	–	–	–	–	–	–		
Cbsqz7BA	(1)6	100	Lm	–	–	–	–	–	–	−87.9	L	–	–	–	–	–	–		
Cbsqz7BA	(1)7	100	Lm	–	–	–	–	–	–	–	–	–	nd	6.5		93	0.5		
Cbsqz7BA	(1)8	100	Lm	–	–	–	–	–	–	−87.9	L	–	nd	7		92	1		
Cbsqz7BA	(1)9	100	Lm	–	–	–	–	–	–	−87.9	L	–	–	–	–	–	–		
Cbsqz7BA	(1)10	100	Lm	–	–	–	–	–	–	−87.9	L	–	–	–	–	–	–		
Cbsqz7BA	(1)11	100	Lm	–	–	–	–	–	–	−87.9	L	–	–	–	–	–	–		
Cbsqz7BA	(1)12	100	Lm	–	–	–	–	–	–	−87.7	L	–	–	–	–	–	–		
Cbsqz7BA	(1)13	100	Lm	–	–	–	–	–	–	−87.7	L	–	–	–	–	–	–		
Cbsqz7BA	(1)14	100	Lm	–	–	–	–	–	–	−88.2	L	–	–	–	–	–	–		
Cbsqz7BA	(1)15	100	Lm	–	–	–	–	–	–	−88.2	L	–	–	–	–	–	–		
Cbsqz7BA	(1)16	100	Lm	–	–	–	–	–	–	−88.4	L	–	–	–	–	–	–		
Cbsqz7BA	(1)17	100	Lm	–	–	–	–	–	–	−88.6	L	–	–	–	–	–	–		
Cbsqz7BA	(1)18	100	Lm	–	–	–	–	–	–	−88.5	L	–	–	–	–	–	–		
Cbsqz7BA	(1)19	100	Lm	–	–	–	–	–	–	−88.5	L	–	–	–	–	–	–		
Cbsqz7BA	(1)20	100	Lm	–	–	–	–	–	–	−87.7	L	–	–	–	–	–	–		
Cbsqz7BA	(1)21	100	Lm	–	–	–	–	–	–	−87.7	L	–	–	–	–	–	–		
Cbsqz7BA	(1)22	100	Lm	–	–	–	–	–	–	−88.1	L	–	–	–	–	–	–		
Cbsqz7BA	(1)23	100	Lm	–	–	–	–	–	–	−88.2	L	–	–	–	–	–	–		
Cbsqz7BA	(1)24	100	Lm	–	–	–	–	–	–	−87.8	L	–	–	–	–	–	–		
Cbsqz7BA	(1)25	100	Lm	–	–	–	–	–	–	−88.3	L	–	–	–	–	–	–		
Cbsqz7BA	(1)26	100	Lm	–	–	–	–	–	–	−88.1	L	–	–	–	–	–	–		
Cbsqz7BA	(1)27	100	Lm	–	–	–	–	–	–	−88.2	L	–	–	–	–	–	–		
Cbsqz7BA	(1)28	100	Lm	–	–	–	–	–	–	–	–	–	nd	7		92.5	0.5		
Cbsqz7BA	(1)29	100	Lm	–	–	–	–	–	–	−88.2	L	–	–	–	–	–	–		
Cbsqz7BA	(1)30	100	Lm	–	–	–	–	–	–	−88.2	L	–	–	–	–	–	–		
Cbsqz7BA	(1)31	100	Lm	–	–	–	–	–	–	−88.1	L	–	–	–	–	–	–		
Cbsqz7BA	(1)32	100	Lm	–	–	–	–	–	–	−88.0	L	–	–	–	–	–	–		
Cbsqz7BA	(1)33	100	Lm	–	–	–	–	–	–	−88.4	L	–	–	–	–	–	–		
Cbsqz7BA	(1)34	100	Lm	–	–	–	–	–	–	−88.1	L	–	–	–	–	–	–		
Cbsqz7BA	(1)35	100	Lm	–	–	–	–	–	–	−88.1	L	–	–	–	–	–	–		
Cbsqz7BA	(1)36	100	Lm	–	–	–	–	–	–	−88.7	L	–	–	–	–	–	–		
Cbsqz7BA	(1)37	100	Lm	–	–	–	–	–	–	−87.9	L	–	–	–	–	–	–		
Cbsqz7BA	(1)38	100	Lm	–	–	–	–	–	–	−88.1	L	–	–	–	–	–	–		
Cbsqz7BA	(1)39	100	Lm	–	–	–	–	–	–	−88.2	L	–	–	–	–	–	–		
Cbsqz7BA	(1)40	100	Lm	–	–	–	–	–	–	−88.3	L	–	–	–	–	–	–		
Cbsqz7BA	(1)41	100	Lm	–	–	–	–	–	–	−86.5	L	–	–	–	–	–	–		

Reynolds, 1994). The majority of inclusions documented here are interpreted as secondary. Therefore, inclusions in trails and fluid inclusion planes have trapped later fluids, which also postdate mineralisation, but are coeval with deformation (Fig. 4(A)–(C), (G) and (J)–(L)). This study reports the characteristics of fluids trapped subsequent to mineralisation, and coeval with deformation of the Chambishi basin.

5.4. Fluid inclusion types

Fluid inclusions were found preserved as isolated occurrences, in trails and planes. The types were defined using the above mentioned nomenclature of Boiron et al. (1992). Selected representative data are presented in Table 3. The following types were identified:

5.4.1. Aqueous inclusions

Aqueous fluid inclusions are found as both isolated inclusions (Fig. 4(A) and (B)) and secondary planes (Fig. 4(C)). Initial melting of isolated inclusions at between −50 and −35 °C is interpreted to be eutectic melting. Eutectic melting temperatures of isolated inclusions indicate the presence of H_2O–NaCl + $MgCl_2$ ± $CaCl_2$ (Goldstein and Reynolds, 1994; Roedder, 1984). Isolated inclusions range in size between 12 and 30 μm diameter, with 8–20% vapour. Final ice melting temperatures (T_m(ice)) for isolated inclusions range from −9.5 to −21.1 °C (Fig. 5(A)), corresponding to salinities of between 13.4 and 23.1 wt.% $NaCl_{equiv}$. Final homogenisation (T_ht) was to the liquid phase ranging from 86 to 129 °C (Fig. 5(B)).

Aqueous fluid inclusions in trails and planes contain 10–35% vapour. Initial melting of aqueous phases, interpreted as eutectic melting (T_e), occurred between −55 and −23 °C, which corresponds to a composition of H_2O–NaCl ± $CaCl_2$ ± $MgCl_2$ ± KCl (Goldstein and Reynolds, 1994). T_m(ice) for FIP's show two groups, showing two fluids of different salinities, namely a low salinity group ranging between −1.6 and −4.8 °C, which corresponds to salinities of 2.7–7.6 wt.% $NaCl_{equiv}$, and a higher salinity group, with T_m(ice) varying between −14.5 and −21.2 °C, which indicates salinities of 18.2–23.3 wt.% $NaCl_{equiv}$ (Fig. 5(A)). Total homogenisation (T_ht) for FIP's was always to the liquid phase, between 131 and 208 °C (Fig. 5(B)).

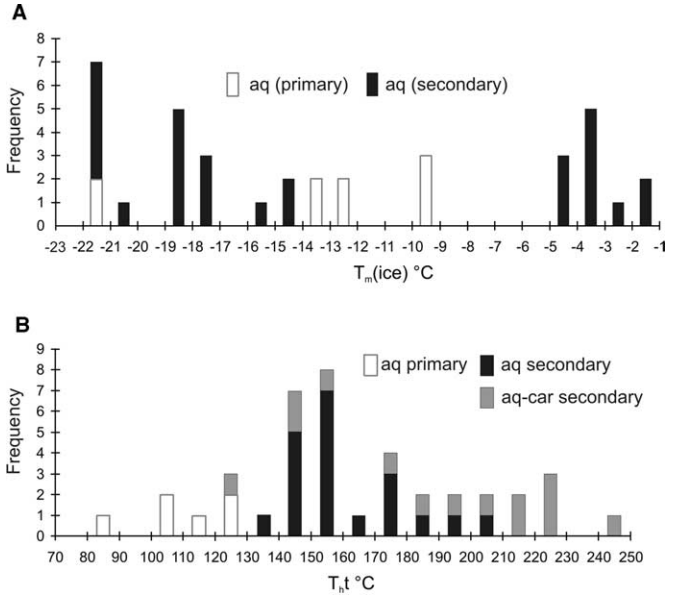

Fig. 5. (A) Histogram showing the distribution of the final ice melting temperatures ($T_m$ice) of aqueous isolated (primary) and trail (secondary) inclusions. (B) Histogram showing the final homogenisation temperature (T_ht in °C) distribution of all aqueous and aqueous carbonic inclusions.

5.4.2. Aqueo-carbonic inclusions

Several inclusions consist of mixed aqueous and non-aqueous phases. The non-aqueous components (carbonic) refer to CO_2, CH_4, C_2H_6, N_2 and H_2S. Isolated aqueo-carbonic inclusions (Fig. 4(D), (H) and (I)) range in size between 8 and 20 μm, with between 10% and 60% vapour. This inclusion type also occurs as secondary trails (Fig. 4(E)–(G)), with vapour phases ranging between 8 and 90 vol%. Melting of isolated inclusions containing carbonic phases (T_m (CO_2)) are between −56.8 and −57.9 °C, and between −58.7 and −56.9 °C for inclusions in FIP's (Fig. 6(A)). Homogenisation of the carbonic components

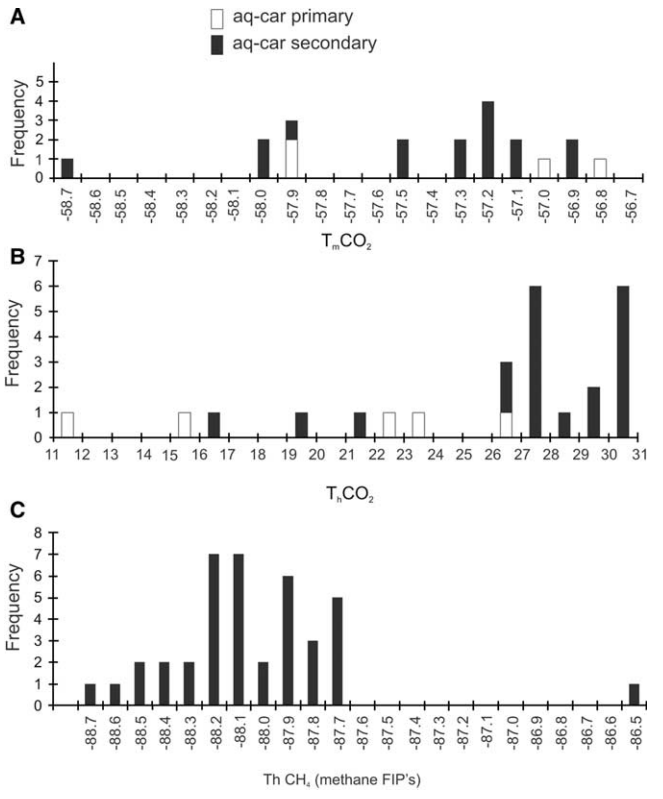

Fig. 6. (A) Histogram of melting of CO_2 temperatures (T_mCO_2) for all aqueous (aq) and aqueo-carbonic (aq-car) inclusions. (B) The distribution in temperatures of CO_2 homogenisation for all aqueous and aqueo-carbonic inclusions (T_hCO_2). Homogenisation was to the liquid phase. (C) Distribution of homogenisation temperatures (T_hCH_4) methane inclusions in fluid inclusion planes. Homogenisation for all inclusions was to the liquid phase.

(T_h (CO_2)) in isolated inclusions was to the liquid phase at between 11.8 and 26.9 °C, and between 16.6 and 30.8 °C for FIP's (Fig. 6(B)). Total homogenisation temperatures (T_ht) range between 128 and 245 °C for FIP's (Fig. 5(B)). Raman microspectrometry revealed the presence of possible magnesite ($MgCO_3$) in one isolated inclusion (CBSqz3A(6)11) with T_h (CO_2) = 23.9 °C. Carbonic phases of isolated inclusions consist of CO_2 (determined with Raman spectroscopy) ranging between 98 and >99.5 mol%, with N_2 and CH_4 comprising the remainder of the vapour. Carbonic phases in inclusions in FIP's contain between 32 and >99.8 mol% CO_2, <0.5–55.5 mol% N_2, 0.3–35.5 mol% CH_4, and <0.1 mol% H_2S (determined with Raman spectroscopy). Salinities for isolated inclusions range between 11.9 and 13.2 wt.% $NaCl_{equiv}$, and between 3.6 and 19.6 wt.% $NaCl_{equiv}$ in FIP's. Bulk densities range between 0.62 and 1.00 g/cm^3.

5.4.3. Methane-dominated inclusions

A distinctive population of fluid inclusion planes comprising numerous methane inclusions was identified, ranging in size between 7 and 16 μm (Fig. 4(J)–(L)). $T_h(CH_4)$ was to the liquid phase at between −88.7 and −86.5 °C (Fig. 6(C)). Raman spectroscopy indicated that they are methane-rich and contain between 6.5 and 7 mol% N_2 and between 0.5 and 1 mol% C_2H_6. These secondary inclusions are classified according to their phase behaviour as H1-type inclusions with homogenisation as the final phase transition (Van den Kerkhof, 1990).

6. Interpretation of Chambishi fluid types

6.1. Early fluids

Isolated fluid inclusions in the quartz vein are interpreted as primary inclusions, and therefore represent a fluid that circulated early in the basin history (Fig. 3(D)). Salinities of primary aqueous and aqueo-carbonic inclusions range between 11.9 and 23.1 wt% $NaCl_{equiv}$ (Fig. 7(A)), and final homogenisation temperatures range from 86 to 129 °C.

Low temperature–high-salinity aqueous fluids may result from dissolution of evaporites, or boiling of a lower salinity fluid. The effect of boiling, or effervescence, whereby the vapour of a high-density fluid is trapped as a low-density fluid (Roedder, 1984), was not observed in this study. The Katanga sequence hosts abundant evaporites in the upper Roan at Mufulira and Konkola, and within the lower Roan (Garlick, 1974). Therefore, the high salinities and low trapping temperatures of isolated aqueous fluid inclusions in this study are best explained by the dissolution of evaporites by circulating connate fluids. The presence of CO_2, and lesser amounts of N_2 and CH_4 in the earlier fluids, may be explained by the decomposition of higher hydrocarbon organic matter (Roedder, 1984) present within the Katanga sedimentary sequence.

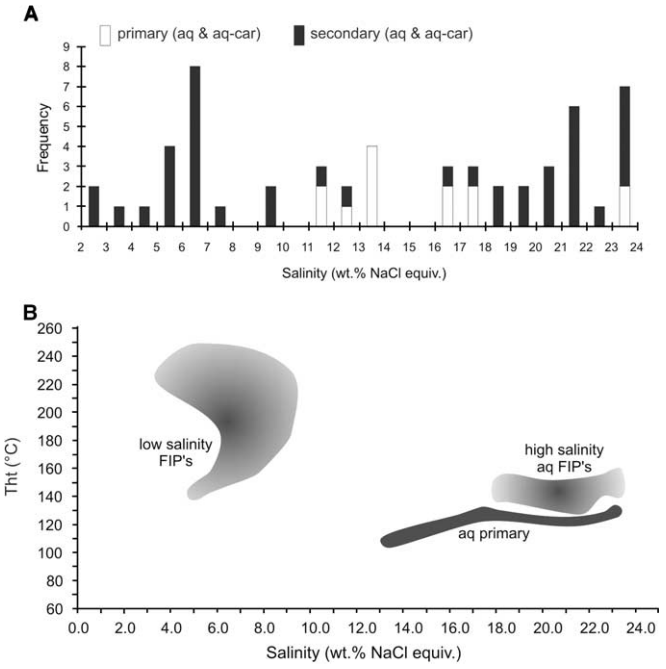

Fig. 7. (A) Frequency vs salinity (wt.% $NaCl_{equiv}$) for all aqueous and aqueous-carbonic inclusions from isolated and trail populations show a large spread. (B) Salinity (expressed in wt.% $NaCl_{equiv}$) vs homogenisation temperatures (T_ht) to the liquid phase for primary (black diamonds) and secondary (white squares) aqueous inclusions. Secondary fluid inclusions show two groups in terms of salinity, namely a low-salinity (~6 wt.% $NaCl_{equiv}$) higher temperature (~140–210 °C) group, and a high-salinity (~18–23 wt.% $NaCl_{equiv}$) lower temperature (~130–160 °C) group.

6.2. Later fluids

Secondary fluid inclusions are interpreted to represent fluids that circulated later in the basin history (Fig. 3(D)) and are characterised by two distinct salinity populations (Fig. 7), namely a low-salinity (~6 wt.% $NaCl_{equiv}$), higher temperature (~140–210 °C) group, and a high-salinity (~18–23 wt.% $NaCl_{equiv}$), lower temperature (~130–160 °C) group. The high-salinity group is considered to have formed from circulating basinal fluids that became increasingly saline and slightly hotter with progressive dissolution of evaporites. The presence of a later, low-salinity, hotter fluid still may best be explained by devolatilization reactions during the onset of Lufilian regional metamorphism. With increasing metamorphism, the average hydrocarbon molecular weight rapidly decreases to that of methane (Roedder, 1984), and may explain the presence of methane, increasingly present in secondary aqueo-carbonic inclusions, and also in methane-dominated fluid inclusion plane, where methane generally derived from the decomposition of hydrocarbon organic matter (Roedder, 1984; Killops and Killops, 1993).

7. Discussion and conclusions

Early fluids described in this study are fairly homogeneous in composition and show moderate to high salinities

(~12–23 wt.% $NaCl_{equiv}$). The quartz vein in which these early fluids are trapped contains a chalcopyrite–bornite assemblage that was derived from the stratiform mineralisation in the adjacent host rock. These early fluids are not directly implicated in stratiform copper mineralisation, but are however, implicated in the early remobilisation of stratiform mineralisation from the ore shale, and must have been present immediately after stratiform Cu–Co mineralisation in the basin. Fluids in this environment were trapped during the early stages along a prograde pressure–temperature P–T path.

Conversely, later fluids exhibit a range in salinities (~6–23 wt.% $NaCl_{equiv}$), compositions, and trapping temperatures, and occur in prominent fluid inclusion planes that are tentatively linked to the axial planar cleavage which is refracted in the quartz vein, linking fluids in these planes to metamorphism. Progressive sediment burial during diagenesis and the resultant heating of connate fluids is evident from Fig. 7(B), where an early high-salinity fluid evolves to a higher temperature high-salinity fluid. With continuing metamorphism, devolatilization reactions result in the production of a fluid of lower salinity, but at higher temperatures. Fluid inclusions in this particular quartz vein show the evolution of fluid trapping along a prograde P–T path.

Isochors plotted on a pressure–temperature diagram give an estimation of P–T conditions during fluid trapping (Roedder, 1984; Goldstein and Reynolds, 1994). Intersection of aqueous and carbonic isochors of homogeneously trapped inclusions constrains the range of P–T conditions applicable to the present study. Isochors for isolated aqueous inclusions were constructed for T_ht ranging between 107 and 129 °C, and for T_ht ranging between 131 and 208 °C for FIP's. Intersection of aqueous and carbonic isochors in this study constrains the pressure and temperature of fluid inclusion trapping to around 480–800 bar and 130–270 °C (Fig. 8). These data reconstruct the pressure and temperature conditions of the environment possibly associated with (and immediately postdating) stratiform copper mineralisation, prior to peak metamorphism.

Previous P–T estimates for mineralising fluids by Kamona (1993), Richards et al. (1988a) and Speiser et al. (1995) are also plotted on Fig. 8. The data by Kamona (1993) constrain the characteristics of epigenetic carbonate-hosted Pb–Zn mineralising fluids at Kabwe, a mineralisation style that postdates stratiform copper mineralisation. These fluids are hotter than those detected in the present study. The data by Speiser et al. (1995) show the elevated pressure and temperature ranges for conditions associated with epigenetic iron-oxide–copper–gold mineralisation to the northwest of the Copperbelt. This epigenetic-hydrothermal vein style mineralisation (dated at ~503–512 Ma, Torrealday et al., 1999) also postdates earlier stratiform copper mineralization and is considered coeval with the peak of regional metamorphism in the Lufilian arc (Rainaud et al., 2005b). Pressures and temperatures associated with this style of mineralisation are substantially higher than those documented in this study (Fig. 8). Similarly, the data from Richards et al. (1988a) constrain the P–T conditions prevalent during late hydrothermal veining at the Musoshi deposit in the DRC, associated with alteration. This event of hydrothermal alteration, dated at ~514 Ma (Richards et al., 1988b), is also related to peak Lufilian metamorphism and postdates stratiform copper mineralisation. The temperatures attained by Richards et al. (1988a) also exceed those obtained during this study. The present study therefore constrains for the first time the characteristics of a relatively low-temperature and pressure, late-diagenetic fluid that is interpreted to be associated with the terminal stages of stratiform copper mineralisation in terms of composition, salinity, pressure and temperature. This study also documents the nature of fluids that evolved subsequent to stratiform mineralisation, and which are associated with the onset of early deformation and metamorphism.

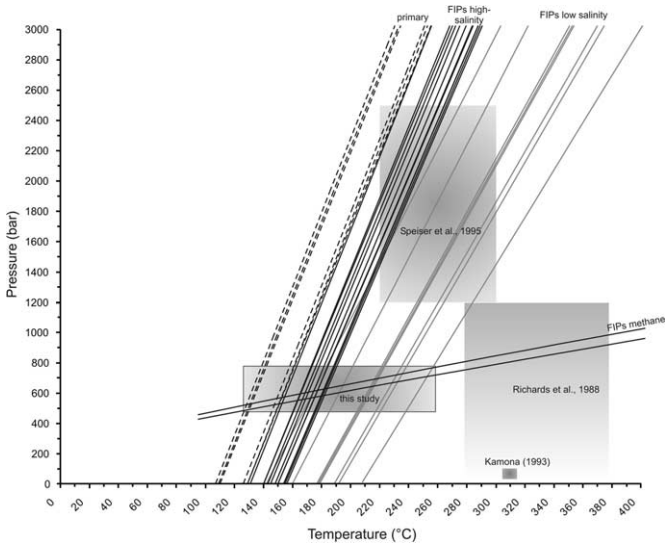

Fig. 8. Isochors of primary and secondary aqueous inclusions and methane FIP's. Isochors of primary aqueous inclusions are indicated as dashed lines. Isochors for high salinity FIP's are shown as solid black lines, and sold grey lines for low salinity FIPs. Isochors of methane FIP's are shown as solid black gently sloping lines. Intersection of the aqueous and carbonic (methane) isochors constrain a P–T region of ~480–800 bar and ~130–270 °C. Previous studies by Richards et al. (1988a), Speiser et al. (1995) and Kamona (1993) are shown. See text for further details.

Acknowledgements

Funding for this project is provided by the Economic Geology Research Institute, the National Research Foundation of South Africa, Centre National de la Recherche Scientifique (CNRS) and the French Embassy, South Africa, and a Hugh E. McKinstry Student Research Award from the Society of Economic Geologists Foundation. Non-Ferrous Metal Plc is thanked for providing access to the Chambishi open pit. Raman analyses were conducted by Thérèse Lhomme at G2R, UMR 7566, Université Henri Poincaré, Nancy, France. Constructive suggestions by Jan-Marten Huizenga and Sally Sutton are gratefully acknowledged.

References

Armstrong, R.A., Robb, L.J., Master, S., Kruger, F.J., Mumba, P.A.C.C., 1999. New U–Pb age constraints on the Katanga sequence, Central African Copperbelt. Journal of African Earth Sciences 28 (4A), 6–7.

Bakker, R.J., 1997. Clathrates: computer programs to calculate fluid inclusion *V–X* properties using clathrate melting temperatures. Computers and Geosciences 23 (1), 1–18.

Bakker, R.J., 2003. Package FLUIDS 1. Computer programs for analysis of fluid inclusion data and for modelling bulk fluid properties. Chemical Geology 194, 3–23.

Bodnar, R.J., 1983. A method of calculating fluid inclusion volumes based on vapor bubble diameters and P–V–T–X properties of inclusion fluids. Eonomic Geology 78, 535–542.

Bodnar, R.J., Vityk, M.O., 1994. Interpretation of microthermometric data for H_2O–NaCl fluid inclusions. In: De Vivo, B., Frezzotti, M.L. (Eds.), Short Course of the Working Group (IMA) Fluid Inclusions in Minerals: Methods and Applications. Virginia Tech, Blacksburg, pp. 117–130.

Boiron, M.C., Essarraj, S., Sellier, E., Cathelineau, M., Lespinasse, M., Poty, B., 1992. Identification of fluid inclusions in relation to their host microstructural domains in quartz by cathodoluminescence. Geochimica et Cosmochimica Acta 56, 175–185.

Bowers, T.S., Helgeson, H.C., 1983. Calculation of the thermodynamic and geochemical consequences of nonideal mixing in the system H_2O–CO_2–NaCl on phase relations in geological systems: equation of state for H_2O–CO_2–NaCl fluids at high pressures and temperatures. Geochimica et Cosmochimica Acta 47, 1247–1275.

Brown, P.E., Lamb, W.M., 1986. Mixing of H_2O–CO_2 in fluid inclusions; geobarometry and Archean Gold deposits. Geochimica et Cosmochimica Acta 50, 847–852.

Brown, P.E., Lamb, W.M., 1989. P–V–T properties of fluids in the system $H_2O + CO_2 + NaCl$: New graphical presentations and implications for fluid inclusion studies. Geochimica et Cosmochimica Acta 53, 1209–1221.

Cahen, L., Snelling, N.J., Delhal, J., Vail, J.R., Bonhomme, M., Ledent, D., 1984. The Geochronology and Evolution of Africa. Claredon Press, Oxford, 512p.

Diamond, L.W., 2003. Glossary: terms and symbols used in fluid inclusion studies. In: Samson, I., Anderson, A., Marshall, D. (Eds.), Fluid Inclusions: Analysis and Interpretation. Mineralogical Association of Canada Short Course, vol. 32, pp. 363–372.

Fleischer, V.D., 1984. Discovery, geology and genesis of copper–cobalt mineralisation at Chambishi Southeast prospect, Zambia. Precambrian Research 25 (1–3), 119–133.

François, A., 1974. Startigraphie tectonique et minéralisations dans l'Arc cuprifére du Shaba (République du Zaïre). In: Barthdolumé, P. (Ed.), Gisements stratiformes et provinces cupriféres. Société Géologique de Belgique, pp. 79–101.

Garlick, W.G., 1961. Chambishi-Nkana Basin. In: Mendelsohn, F. (Ed.), The Geology of the Northern Rhodesian Copperbelt. MacDonald, London, pp. 281–342.

Garlick, W.G., 1974. Depositional and diagenetic environment related to sulphide mineralization, Mufulira, Zambia—a discussion. Economic Geology 69, 1344–1351.

Garlick, W.G., 1976. Chambishi. In: Fleischer, V.D., Garlick, W.G., Haldane, R. (Eds.), Geology of the Zambian Copperbelt. In: Wolf, K.H. (Ed.), Handbook of strata-bound and stratiform ore deposits, vol. 6, pp. 249–256, Chapter 6.

Goldstein, R.H., Reynolds, T.J., 1994. Systematics of fluid inclusions in diagenetic minerals. Society for Sedimentary Geology Short Course 31, 199.

Jackson, G.C.A., 1932. The Geology of the N'Changa district, Northern Rhodesia. Quarterly Journal of the Geological Society of London 88, 443–515.

John, T., Schenk, V., Scherer, E., Mezger, K., Haase, K., Tembo, F., 2002. Subduction and continental collision in the Lufulian Arc-Zambezi Belt orogen (Zambia): implications to the Gondwana assembly. Abstract Volume: 19th colloquium of African Geology, El Jadida, Morocco, 19–22 March 2002, p. 188.

Kamona, A.F., 1993. The carbonate-hosted Kabwe Pb–Zn deposit, Central Zambia. Ph.D Thesis, Mitteilungen zur Mineralogie und Lagerstättenlehre, RWTH Aachen, p. 207.

Kampunzu, A.B., Wendorff, M., Kruger, F.J., Intiomale, M.M., 1998. Pb isotopic ages of sediment-hosted Pb–Zn mineralisation in the Neoproterozoic Copperbelt of Zambia and Democratic Republic of Congo (ex-Zaire): re-evaluation and implications. Chronique de la Recherche Minière 530, 55–61.

Killops, S.D., Killops, V.J., 1993. An introduction to organic geochemistry, Longman Geochemistry Series. USA, p. 265.

Leroy, J., 1979. Contribution à l'étallonage de la pression interne des inclusions fluids lors de leur décrépitation: bull. Minéralogie 102, 584–593.

Master, S., Rainaud, C., Armstrong, R.A., Phillips, D., Robb, L.J., 2005. Provenance ages of the Neoproterozoic Katanga Supergroup (Central African Copperbelt); with implications for basin evolution. Journal of African Earth Sciences, this issue, doi:10.1016/j.jafrearsci.2005.08.005.

McGowan, R.R., Roberts, S., Foster, R.P., Boyce, A.J., Coller, D., 2003. Origin of the copper–cobalt deposits of the Zambian Copperbelt: an epigenetic view from Nchanga. Geology 31 (6), 497–500.

Mendelsohn, F., 1961a. Katanga system. In: Mendelsohn, F. (Ed.), The Geology of the Northern Rhodesian Copperbelt. MacDonald, London, pp. 41–54.

Mendelsohn, F., 1961b. Metamorphism. In: Mendelsohn, F. (Ed.), The Geology of the Northern Rhodesian Copperbelt. MacDonald, London, pp. 106–116.

Pirmolin, J., 1970. Inclusions fluids dans la dolomite du Gisement stratiforme de Kamoto (Katanga Occidental). Annales de la Société Géologique de Beligique T 93, 397–406.

Rainaud, C., Master, S., Robb, L.J., 1999. A fertile Palaeoproterozoic magmatic arc beneath the Central African Copperbelt. In: Stanley, C.J. et al. (Eds.), Mineral deposits: processes to processing. Proceedings of the Fifth Biennial SGA Meeting and the Tenth Quadrennial IAGOD symposium, London, 22–25 August 1999, pp. 1427–1430.

Rainaud, C., Master, S., Armstrong, R.A., Robb, L.J., 2003. A cryptic Mesoarchaean terrane in the basement to the Central African Copperbelt. Journal of the Geological Society, London 160, 11–14.

Rainaud, C., Master, S., Armstrong, R.A., Robb, L.J., 2005a. Geochronology and nature of the Palaeoproterozoic basement in the Central African Copperbelt (Zambia and the Democratic Republic of Congo); with regional applications. Journal of African Earth Sciences, this issue, doi:10.1016/j.jafrearsci.2005.08.006.

Rainaud, C., Master, S., Armstrong, R.A., Phillips, D., Robb, L.J., 2005b. Monazite U–Pb dating and Ar^{40}/Ar^{39} thermochronology of metamorphic events in the Central African Copperbelt during the Pan African Lufilian orogeny. Journal of African Earth Sciences, this issue, doi:10.1016/j.jafrearsci.2005.08.007.

Richards, J.P., Krogh, T.E., Spooner, E.T.C., 1988a. Fluid inclusion characteristics and U–Pb Rutile age of late hydrothermal alteration and veining at the Musoshi stratiform copper deposit, Central African Copper Belt, Zaire. Economic Geology 83, 118–139.

Richards, J.P., Cumming, G.L., Kristic, D., Wagner, P.A., Spooner, E.T.C., 1988b. Pb isotope constraints on the age of sulphide ore deposition and U–Pb age of late uraninite veining at the Musoshi stratiform copper deposit, Central African Copper Belt, Zaire. Economic Geology 83, 724–741.

Robb, L., 2005. Introduction to Ore-forming Processes. Blackwell Publishing, Oxford, p. 373.

Robb, L.J., Master, S., Greyling, L., Yao, Y., Rainaud, C., 2002. Contributions to the geology and mineralization of the Central African Copperbelt: V. Speculations regarding the "Snowball Earth" and redox controls on stratabound Cu–Co and Pb–Zn mineralisation. In: Anhaeusser, C.R. (Ed.), Economic Geology Research Institute, Information Circular 362. University of the Witwatersrand, pp. 38–42.

Roedder, E., 1972. Composition of fluid inclusions. US Geological Survey Professional Paper, 440JJ, p. 164.

Roedder, E., 1984. Fluid inclusions. Reviews in Mineralogy, 12, Mineralogical Society of America, p. 646.

Speiser, A., 1994. Untersuchungen an Flüssigkeitseinschlüssen in Gangquarzen aus der Kansanshi Mine (Solwezi-Area, North-Western District, Zambia). Diplomarbeit Teil II, Institut für Geologie und Dynamik der Lithosphäre der Geord-Augaust-Universität zu Göttingen, p. 65.

Speiser, A., Hein, U.F., Porada, H., 1995. The Kansanshi copper mine (Solwezi area, northwestern Zambia): Geology, wall-rock alteration and fluid inclusions. In: Pasava, J., Kribek, B., Zak, K. (Eds.), Mineral Deposits: From their Origin to their Environmental Impacts. A.A. Balkema, Rotterdam, pp. 389–392.

Sweeney, M., 1987. The use of fluid inclusion geochemistry in determining the origin of veins, examples from the Zambian Copperbelt. Zambian Journal of Applied Earth Sciences 1, 18–28.

Sweeney, M.A., Binda, P.L., 1994. Some constraints on the formation of the Zambian Copperbelt deposits. Journal of African Earth Sciences 19 (4), 303–313.

Torrealday, H.I., Hitzman, M.W., Stein, H.J., Markey, R.J., Armstrong, R., Broughton, D., 1999. Re–Os and U–Pb dating of molybdenite from mineralized veins from the Kansanshi Copper Deposit, Zambia. In: Stanley C.J. et al. (Eds.), Mineral deposits: processes to processing. Proceedings of the Fifth Biennial SGA Meeting and the Tenth Quadrennial IAGOD symposium, London, 22–25 August 1999, pp. 1295–1297.

Van den Kerkhof, A.M., 1990. Isochoric phase diagrams in the systems CO_2–CH_4 and CO_2–N_2: application to fluid inclusions. Geochimica et Cosmochimica Acta 54 (3), 621–629.

Wendorff, M., 2003. Stratigraphy of the Fungurume Group—evolving foreland basin succession in the Lufilian fold-thrust belt, Neoproterozoic-Lower Palaeozoic, Democratic Republic of Congo. South African Journal of Geology 106, 17–34.

Zhang, Y.F., Frantz, J.D., 1987. Determination of the homogenisation temperatures and densities of supercritical fluids in the system NaCl–KCl–$CaCl_2$–H_2O using synthetic fluid inclusions. Chemical Geology 64, 335–350.